ECM1 Overexpression in Bladder Cancer

Rebecca Joy Ellerington

Submitted in accordance with the requirements for the degree of
Doctor of Philosophy

The University of Leeds

Faculty of Medicine and Health

March 2019

The candidate confirms that the work submitted is her own and that appropriate credit has been given where reference has been made to the work of others.

Acknowledgments

Undertaking this PhD has been both challenging and extremely rewarding. It would not have been possible without the support and guidance that I received from many people, and I would like to take this opportunity to acknowledge that support.

Firstly, I would like to extend an enormous thank you to both my supervisors. I would like to express my sincere gratitude to Dr Carolyn Hurst. You have always been on hand to offer your help and advice both in and out of the lab. Thank you for dedicating so much time and attention to me, I could not have imagined having a better supervisor for my PhD. I would also like to extend my thanks to Prof. Maggie Knowles, you are a fountain of knowledge and have always been willing to impart your wisdom.

I also owe a thank you to everyone past and present from Lab 5 for their guidance and patience. Each one of you have always being eager to offer your help. In particular I would like to thank Dr Julie Burns for training me in cell culture and virus work, you were always around to point me in the right direction in the lab. I am also grateful to Filomena Esteves and Emma Black for training me in immunohistochemistry, and to Marjorie Davison for donating the tivantinib for my project, and offering her advice and knowledge on the subject. Additionally, I would like to thank my fellow PhD students Rebecca Astley and Ben Hopkins for your encouragement and insightful comments which kept my morale up even in the most challenging moments.

A very heartfelt thank you goes to my Mum, Dad, Sarah and Peter for being the most supportive family I could wish for. You always encourage me to achieve my ambitions and offer your love and support in everything I do.

A final thanks goes to LICAP for funding my PhD.

Thank you everyone I couldn't have done it without you.

Abstract

Analysis of genome-wide mRNA expression data from 45 bladder cancer-derived cell lines revealed a Basal/Squamous subgroup exhibiting upregulation of extracellular matrix protein 1 (ECM1). Assessment of ECM1 at the mRNA and protein levels confirmed an ECM1-high subset of cell lines and primary tumours. Mucin 1 (MUC1) was also significantly upregulated in the ECM1-high subgroup. MUC1 expression was strongly correlation with ECM1 expression. Mining of publicly available microarray data showed significantly reduced overall survival in bladder cancer (BC) patients whose tumours expressed high levels of both ECM1 and MUC1.

ECM1 knockdown cell lines were established and *in vitro* phenotypic assays showed that ECM1 knockdown had an inhibitory effect on wound-healing ability. A previous study in breast cancer reported that ECM1 interacts with and stabilises epidermal growth factor receptor (EGFR) enhancing Ras/Raf/MEK/ERK signalling. A direct interaction between ECM1 and EGFR could not be confirmed in ECM1-high BC-derived cell lines. Treatment of knockdown cell lines with recombinant ECM1 indicated that ECM1 initiates activation of downstream effectors in the EGFR pathway. Comparison of ECM1 knockdown and control cell lines using a phospho-receptor tyrosine kinase array showed that activation of the MET receptor is also ECM1 dependent in ECM1-high cells. Differential gene expression and pathway analysis conducted on ECM1 knockdown and control cell lines revealed that ECM1 modulates the mRNA levels of several extracellular matrix genes and genes linked to a more aggressive Basal/Squamous phenotype including the EGFR ligand amphiregulin, keratins 5 and 6, and the transcription factor ELF5. Drug sensitivity experiments targeting EGFR and mesenchymal epithelial transition factor (MET) revealed partial resistance in the ECM1 high cell lines. Comparison of the inhibitors' effects on ECM1 KD and control cell lines indicated that high ECM1 expression alone was not influencing this lack of sensitivity and it is likely that there are multiple alternative mechanisms mediating survival in these cells.

Table of Contents

List of Tables

List of Figures

Abbreviations

3'UTR	Three prime untranslated region
5' LTR	Five prime long terminal repeat
AMC	Academic Medical Center
ampR	Ampicillin resistance gene
ANOVA	Analysis of variance
ARQ197	Tivantinib
Asn	Asparagine
BCL2	B-cell lymphoma 2
BTC	Betacellulin
cDNA	Complementary deoxyribonucleic acid
CDS	Coding DNA sequence
Chr	Chromosome
CIS	Carcinoma *in situ*
Co-IP	Co-immunoprecipitation
COSMIC	Catalogue of Somatic Mutations in Cancer
Cppt	Central polypurine tract
DMEM	Dulbecco's Modified Eagle's Medium
DNA	Deoxyribonucleic acid
dNTP	Deoxynucleotide triphosphate
DTSSP	3,3'-Dithiobis(sulfosuccinimidylpropionate
EC_{50}	Half the maximal effective concentration
ECM1	Extracellular matrix protein 1
EDTA	Ethylenediaminetetraacetic acid
ELF3	E74-like transcription factor 3
ELF5	E74-like transcription factor 5
EMT	Epithelial-to-mesenchymal transition
EPGN	Epigen
EPR	Epiregulin
ERBB1	Erythroblastic leukemia viral oncogene homolog 1 (also see EGFR)
ERBB2	erythroblastic leukemia viral oncogene homolog 2 (also see HER2)
ERBB3	Erythroblastic leukemia viral oncogene homolog 3 (also see HER3)
ERBB4	Erythroblastic leukemia viral oncogene homolog 4 (also see HER4)
ETS	Epithelium twenty-six family of transcription factors
F1 ori	F1 origin of replication
FFPE	Formalin-fixed paraffin-embedded
FGFR3	Fibroblast growth factor receptor 3
G1	Grade 1
G2	Grade 2
G3	Grade 3
GC	Gemcitabine and cisplatin
GEO	Gene Expression Omnibus
GO	Gene ontology
GSC	Genomic subtyping classifier
GU	Genomically unstable
HB-EGF	Heparin binding EGF like factor
HCC	Hepatocellular carcinoma
HER2	Human epidermal growth factor receptor 2 (also see ERBB2)
HER3	Human epidermal growth factor receptor 3 (also see ERBB3)
HER4	Human epidermal growth factor receptor 4 (also see ERBB4)
HGF	Hepatocyte growth factor
HGFR	Hepatocellular growth factor receptor(also see MET)
hPGK	Human phosphoglycerate kinase

HRP	Horseradish peroxidase
IC_{50}	The half maximal inhibitory concentration
IGF-IR	Type-1 insulin like growth factor receptor
IHC	Immunohistochemistry
INS-R	Insulin receptor
IP	Immunoprecipitation
JAK	Janus kinase
KLK	kallikrein-related peptidase
KRT	keratin
KRTDAP	Keratinocyte differentiation associated protein
LB	Lysogeny broth
LIMMA	Linear Model for Microarray Analysis
MCL1	Myeloid cell leukaemia protein 1
MEK	Mitogen-activated protein kinase kinase
MEM	Modified Eagle's Medium
MET	mesenchymal epithelial transition factor (also see HGFR)
MIBC	Muscle-invasive bladder cancer
ml	Milliliter
mM	Milimolar
MMP9	Matrix metallopeptidase 9
MPS	Milk powder solution
mRNA	Messenger ribonucleic acid
MUC1	Mucin 1
MVAC	Methotrexate, vinblastine, doxorubicin and cisplatin
NCBI	National Center for Biotechnology Information
NEB	New England Biolabs
ng	Nanogram
NGS	Next generation sequencing
NHP	Non-hairpin
NHU-Pool	Normal human urothelial pooled cell line
nm	Nanometer
nM	Nanomolar
NMIBC	Non-muscle-invasive bladder cancer
NSCLC	Non-small cell lung cancer
p53	Tumour protein 53
PBS	Phosphate-buffered saline
PCR	Polymerase chain reaction
PFA	Paraformaldehyde
phospho-RTK	Phospho-receptor tyrosine kinase
PI3K	phosphoinositide 3-kinase or phosphatidylinositol 3-kinase
PIC	Lentiviral preintegration complex
PIK3CA	Phosphatidylinositol 3-kinase gene
Psi	RNA packaging signal
PTEN	phosphatase and tensin homolog
PTHrP	Parathyroid hormone-related protein
pUC ori	pUC bacterial origin of replication
puroR	Puromycin resistance gene
qRT-PCR	Quantitative real time polymerase chain reaction
Raf	RAF proto-oncogene serine/threonine-protein kinase
Ras	Rat sarcoma protein
RIPA	Radioimmunoprecipitation assay buffer
RLT	RNeasy Lysis Buffer
RRE	Rev response element
RNA	Ribonucleic acid
rRNA	Ribosomal RNA

RT	Room temperature
RTK	Receptor tyrosine kinase
SAM	Significance analysis of microarrays
SCC	Squamous cell carcinoma
shRNA	Short-hairpin RNA
SIN/3' LTR 3'	Self-inactivating long terminal repeat
siRNA	Small interfering RNA
SNP	Single nucleotide polymorphisms
SPARC	Secreted protein acidic and cysteine rich
STAG2	Stromal antigen 2
Stat	Signal transducer and activator of transcription protein
TBE	Tris-Boric acid-EDTA buffer
TBS	Tris-Buffered Saline
TCA	Trichloroacetic acid
TCGA	The Cancer Genome Atlas
TERT	Telomerase reverse transcriptase
TGF-α	Transforming growth factor alpha
TI	Trypsin inhibitor
TMA	Tissue microarray
TNM	Tumour-node-metastasis
TP53	Tumour protein 53 gene
TV	Trypsin-versene (0.5%) with EDTA (0.02%) in PBS
TWIST1	Twist family BHLH transcription factor 1
UNC	University of North Carolina
UPK	Uroplakin
UroA	Urobasal A
UroB	Urobasal B
UWD	Urbach–Wiethe disease
VIM	Vimentin
WHO	World Health Organisation
w/v	Weight per volume
°C	Degrees Celsius
μg	Microgram
μl	Microliter
μm	Micrometer
μM	Micromolar

Chapter 1
Introduction

1.1 Bladder Cancer

1.1.1 Epidemiology

The normal bladder urothelium is a specialised transitional epithelium that acts as a physical blood-urine barrier [1]. This barrier consists of regenerative basal cells, intermediate cells, and large superficial hexagonal cells known as umbrella cells [1, 2]. Roughly 90% of primary bladder tumours diagnosed in the UK arise in the urothelium [3]. Each year 165,000 deaths attributed to the disease globally, and over 10,000 new cases of bladder cancer are diagnosed in the UK and making it the seventh most common cancer in the UK [4, 5].

Most cases of bladder cancer occur in people aged over 60 [5], and the disease is generally diagnosed following the appearance of visible blood in the urine (hematuria) or blood-traces found upon urine testing [5]. The disease is more prevalent in men compared to women with 75% of diagnoses occurring in males [6]. The reasons for this gender discrepancy are still being debated, but a number of explanations have been offered including the potential for sex steroid hormone regulation of the disease, and differences in exposure to risk factors [6].

1.1.2 Aetiology

The majority of bladder tumours are thought to develop following exposure to exogenous carcinogens which may enter the circulatory system through ingestion, inhalation or contact with the skin[7]. Risk factors include tobacco smoking and occupational exposure to aromatic amines and polycyclic hydrocarbons [7].

Smoking is the highest risk factor for bladder cancer development accounting for over 50% of all cases [7]. Tobacco contains numerous carcinogenic compounds such as aromatic amines that result in DNA damage [6]. A systematic review and meta-analysis of 83 studies showed a significant increase in relative risk of bladder cancer development for current, former and second-hand smokers compared to non-smokers, highlighting the strong association between bladder cancer development and tobacco [8].

Bladder cancer development is also associated with carcinogenic contact in an occupational setting. In 1981, it was estimated that 10% of all bladder cancer cases were directly related to workplace exposure to carcinogens [9]. More current estimates are nearer 5-7% with health and safety legislation most likely playing a key role in this reduction [7]. Recent reviews on the relative risk of developing bladder cancer and the associated mortality as a result of occupational exposure to carcinogens have highlighted that workers exposed to aromatic amines through involvement in rubber and plastic production, textile dying, and hairdressing are still at elevated risk and such exposure remains an important issue for public health [7]. Furthermore, exposure to aromatic amines as part of lifestyle choices such as regular hair dying could also increase risk [6].

1.1.3 Pathology and prognosis

Bladder cancer is a heterogenous malignant disease that has traditionally been divided into two main forms (muscle-invasive and non-muscle-invasive) based on their pathology, response to treatment and distinctive genetic backgrounds [10, 11]. Stage and grade of tumours is assessed by histological examination. The Tumour-Node-Metastasis system is used to describe the stage of tumours, which relates to the degree to which the tumour has invaded the tissue layers of the bladder (Figure 1-1)[12]. Tumours are further classified as low grade or high grade based on the 2004 World Health Organization (WHO) classification system [12], and Grade 1, 2, or 3 based on the 1973 WHO classification system[13]. Grading describes the degree of similarity between tumour cells and healthy tissue. Tumour cells that are well differentiated and bare high resemblance to healthy urothelial cells are low grade (Grade 1 or 2), while tumours that are poorly differentiated and bear little resemblance to healthy urothelium are high grade (Grade 2 or 3).

Approximately 70% of all newly diagnosed cases present as non-muscle-invasive bladder cancer (NMIBC)[14]. NMIBC consists of three pathological stages: Ta, T1 and Tis (Figure 1-1). The majority of non-muscle-invasive bladder cancers present as stage Ta with the tumour being confined to the urothelium or mucosa. These tumours are also mostly low grade [10]. Approximately 20% of cases are diagnosed as stage T1 where the tumour has invaded the subepithelial connective tissue or *lamina propria*, of which the majority are high grade. Carcinoma *in situ* (CIS or Tis)

is a high grade non-papillary lesion which lies flat to the urothelium. CIS accounts for 10% of cases and is thought to be a precursor of MIBC [10, 14]. Five-year survival in patients with NMIBC is good (>90%), although there is a high rate of disease recurrence (50-70%) [14] and 10–20% of cases initially diagnosed as NMIBC will progress to MIBC [14].

Approximately 25% of patients will present with muscle-invasive bladder cancer (MIBC) at diagnosis [14]. This muscle-invasive form encompasses tumours which have invaded the muscle wall or *muscularis propria* (stage T2 to T4) (Figure 1-1), and are typically high grade [10]. Although these tumours account for a lower proportion of cases than NMIBC, five-year survival rates are much poorer having been reported to be as low as 49% [15]. This is in part due to the increased progression and metastatic potential of these tumours [14] but also as a result of limited treatment options which consist of cisplatin-based chemotherapy and radical cystectomy [15].

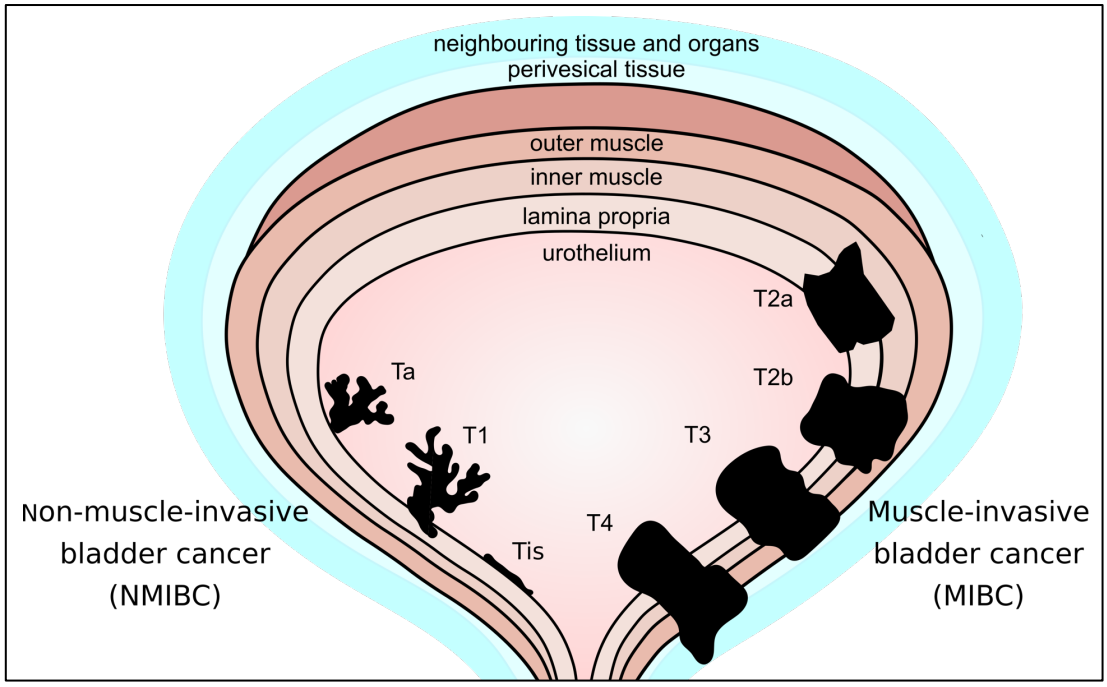

Figure 1-1: Bladder cancer staging.

The pathological staging of bladder cancer according to the World Health Organisation's Tumour-Node-Metastasis (TNM) staging system [12]. NMIBC consists of stages Tis, Ta and T1. MIBC consists of stages T2a, T2b, T3 and T4.

1.1.4 Treatment of bladder cancer

Treatment of NMIBC is dependent upon perceived risk of recurrence and progression, which is largely based on the stage and grade of the tumour [16]. Low grade non-invasive tumours are considered low-risk and are normally treated with intravesical mitomycin C following transurethral resection. High grade NMIBC, that is normally considered higher risk, is treated by transurethral resection, adjuvant chemotherapy and maintenance intravesical Bacillus Calmette–Guérin (BCG) [17]. It is challenging to predict which high grade non-invasive tumours will progress, thus it is a difficult choice to decide which patients require complete removal of the bladder and surrounding lymph nodes, known as radical cystectomy, and for which patients, tumour resection and BCG treatment may be sufficient [16]. Current recommendations call for radical cystectomy only if patients fail BCG treatment [16]. Ten-year survival rates are around 80% if cystectomy is performed prior to progression to MIBC, while 10-year survival rates in delayed cystectomy in patients who fail BCG is just 51% [18]. Radical cystectomy comes with the risks associated with major surgery and can lead to reduced quality of life for patients, thus many patients and clinicians are unwilling to choose this option unless it is deemed necessary [19].

Treatment of MIBC has remained largely unchanged for over 30 years and 5-year survival rates have remained static [20]. The limited treatment options consist mainly of radical cystectomy and complimentary neoadjuvant or adjuvant chemotherapy [15]. Chemotherapeutic options for MIBC are most often cisplatin-based, with patients receiving either methotrexate, vinblastine, doxorubicin and cisplatin (MVAC) or gemcitabine and cisplatin (GC) combination therapies [21].The major concern for MVAC therapy is toxicity, a problem augmented by the typically elderly patient profile which is often associated with numerous medical comorbidities [3]. In early studies, severe MVAC toxicity was seen with more than half of patients requiring hospitalisation for toxic complications as a direct result of treatment [22]. The most common side effects include a dramatic reduction in neutrophil levels resulting in complications due to infection, and significant ulceration of the digestive tract causing difficulty in eating and drinking [23]. Renal and cardiac toxicities as well as nausea can also be problematic [23]. MVAC is associated with a toxic death rate of 4% [24]. In the early 2000s, GC combination therapy was implemented for use in patients with bladder cancer [23]. While overall survival statistics of 14-15 months are comparable with MVAC, toxicity is much

lower [23]. Even though MVAC and GC are the standard regimens for MIBC, the best reported estimate of response rate to these cisplatin-based options in MIBC is 50% highlighting a need for new treatment options [21]. Furthermore, pre-screening to identify “non-responders” to cisplatin prior to treatment is difficult and there is an urgent need for predictive biomarkers that would allow identification of patients who require alternative regimens [21].

MIBC that initially respond well to treatment often progress later with half of patients who undergo chemotherapeutic treatment and radical cystectomy eventually dying as a direct result of disease recurrence or pre-existing metastatic disease [25]. Currently there are no effective second-line chemotherapeutic options for patients with paclitaxel, pemetrexed, docetaxel and vinflunine giving a median overall survival of just 5 months [26]. There has been increasing interest in immune intervention-based therapies for the treatment of MIBC which are aimed at initiating or enhancing a host immune response against the tumour [27, 28].

Immune based therapy is not a new concept in bladder cancer treatment. In the 1960s, intravesical BCG was demonstrated to be beneficial in the treatment of NMIBC as it was thought to initiate a local immune response [3]. BCG treatment is still used as the current standard of care for patients with high risk NMIBC [29]. As muscle-invasive tumours have a very high frequency of somatic mutations compared to other solid tumours, potentially leading to an increase in neoantigens, it is hoped that this may result in an increased sensitivity to immune checkpoint therapy drugs [27, 30]. Recently, the field of immune-based therapy for treatment of MIBC has focused mainly on a group of T-cell checkpoint inhibitors [3].

Currently five immune checkpoint inhibitors have been approved by the United States Food and Drug Administration (US-FDA) for first-line or second-line treatment of metastatic MIBC. These drugs include two monoclonal antibodies that target programmed death receptor-1 (PD-1) (pembrolizumab and nivolumab) and three that target its counterpart programmed death receptor ligand-1 (PD-L1) (atezolizumab, durvalumab, and avelumab) [25]. The interaction of the PD-1 receptor and its ligand suppresses the immune response, and in normal cells this is important in preventing an autoimmune response following infection [25]. In the context of cancer, PD-L1 is expressed by tumour cells and interacts with PD-1 presented by T-cells allowing the tumour cells to evade immune recognition. Drugs

that block this molecular interaction can therefore increase immune response resulting in tumour shrinkage [25].

Although these immune checkpoint drugs provide promise for the treatment of patients with MIBC who are “non-responders” to cisplatin, response rates have been reported to range from just 20 to 25% [3]. A significant challenge still lies in assigning the right therapeutic agent to each patient and identification of new biomarkers to predict patient response is still necessary. Molecular characterisation may help to provide insight into disease behaviour and be used to stratify patients into groups most likely to respond to therapeutic options. Improved understanding of the correlation between molecular and clinical features may therefore help to advance clinical management of the disease.

1.2 Genomic landscape of bladder cancer

Early studies of the genomic alterations in bladder cancer assessed somatic mutations in specific candidate genes including fibroblast growth factor receptor 3 (*FGFR3)*, phosphatidylinositol-4,5-bisphosphate 3-kinase catalytic subunit alpha (*PIK3CA),* cyclin dependent kinase inhibitor 2A *(CDKN2A)*, tumour protein 53 (*TP53)*, tuberous sclerosis complex subunit 1 (*TSC1)*, retinoblastoma protein 1 (*RB1)* and the rat sarcoma (RAS) gene family, loss of heterozygosity (LOH) and copy number alterations. Whole genome and whole exome sequencing studies have confirmed somatic mutations in these genes and have also identified alterations in new candidates including numerous chromatin modifier genes.

Low stage and grade bladder tumour genomes are very stable whereas MIBC genomes commonly contain numerous copy number alterations, rearrangements and high-level amplifications [31-35]. The genomes of stage T1 tumours show varying levels of complexity with some resembling Ta tumours and others resembling MIBC [33].

Loss of heterozygosity or copy number loss of chromosome 9 is the most common genomic alteration detected in bladder tumours. Copy number loss is found in approximately 50% of all tumours. Many studies have investigated potential candidate genes and several critical regions have been identified. A critical region on the p-arm is 9p21 containing the *CDKN2A* gene which encodes p16 and

p14ARF, two cell-cycle regulators that negatively regulate the RB and p53 pathways, respectively [10]. TSC1 is another tumour suppressor gene on 9q which has been reported to be biallelically inactivated in 12-16% of tumours and has a function in negative regulation of mTOR [36, 37].

Activating mutations in the fibroblast growth factor receptor 3 (*FGFR3*) gene are commonly detected in hotspot regions in exons 7, 10 and 15 and lead to constitutive activation of the receptor. The frequency of *FGFR3* mutation is ≥ 70% in stage Ta tumours, 10-45% in stage T1 tumours and 15% in muscle-invasive tumours [38]. Muscle-invasive bladder tumours exhibit upregulated FGFR3 protein expression in 40-50% of non-mutant cases [38]. *FGFR3* can be also be activated in 2-5% of cases by chromosomal translocation to generate fusion proteins, the most common of which is FGFR3-TACC3 [32, 39, 40]. Activating mutations in the RAS gene family (*HRAS*, *KRAS* and *NRAS)* occur in hotspot regions in approximately 10% of all tumours and are not associated with stage or grade. Mutual exclusivity of RAS and *FGFR3* mutations has been reported [41] and may reflect the involvement of both proteins in the activation of the RAS-MAPK pathway. The phosphatidylinositol-3 kinase (PI3K) pathway is also an important signalling pathway that is altered in bladder cancer. The p110α catalytic subunit (*PIK3CA*) gene is mutated in 40-50% of low grade, low stage Ta tumours and 20% of stage T1 and muscle-invasive tumours [42]. Activating point mutations are commonly located in the helical domain (E542K and E545K) and less frequently in the kinase domain (H1047R).

Telomerase reverse transcriptase (*TERT*) promoter mutations occur in 60-80% of all bladder tumours making them the most common genomic alteration in bladder cancer [43, 44]. It has been suggested that these mutations represent an early event in all urothelial cancers. These mutations commonly occur in two hotspots and are predicted to create binding sites for ETS/TCF transcription factors leading to increased transcriptional activity [45].

The tumour suppressor genes *TP53*, *RB1* and *CDKN2A* are commonly inactivated in muscle-invasive tumours and result in p53/cell-cycle alterations in approximately 89% of MIBC [32]. *TP53* is mutated in approximately 50% of all MIBC making it the most commonly mutated gene in these tumours [32]. In contrast, *TP53* mutation occurs in only 1% of low grade Ta tumours. A higher frequency of mutation occurs in T1 tumours and these mutations can co-occur with *FGFR3* mutations [46]. Deletion of the *RB1* gene region at 13q14 and loss of RB1 protein expression

occurs commonly in muscle-invasive tumours [10]. RB1 and p16 expression is inversely correlated in MIBC and is associated with poor prognosis [10].

Whole exome and whole genome sequencing studies in MIBC have revealed a high median somatic mutation rate per megabase (5.5 mutations/Mb) that is comparable to rates reported in melanoma and non-small cell lung cancer [47-49]. The mutation rates in NMIBC are much lower with rates of 1.64 (median) overall and 1.8 (median) non-synonymous mutations per megabase having been reported in two studies of stage Ta and Ta/T1 tumours, respectively [31, 50]. A major finding of these next-generation sequencing studies has been the discovery of frequent mutations in chromatin modifier (CM) genes including *KDM6A*, *KMT2A*, *KMT2C*, *KMT2D*, *CREBBP*, *EP300*, *ARID1A*, *ARID4A*, *ASXL1*, *ASXL2 and STAG2* [50-52]. CM mutations are present in tumours of all stages and grades, with the highest frequent in non-muscle-invasive bladder cancers [31, 50, 51]. Inactivating mutations are common in many of these genes, suggestive of a tumour suppressor function [32].

1.3 The role of receptor tyrosine kinases in bladder cancer

One finding of large-scale genomic studies has been the presence of various alterations in the genes encoding for receptor tyrosine kinases (RTKs). RTKs are a family of 58 cell surface receptors that are unified by their characteristic structure of an extracellular N-terminal domain, a transmembrane domain, and a cytoplasmic kinase domain. Upon activation by a ligand, conformational changes are induced resulting in the homo or hetero-dimerisation of two RTKs. Intrinsic kinase activity of the cytoplasmic domain of one receptor results in phosphorylation of specific residues on the cytoplasmic region of the other providing a scaffold to recruit effector proteins and thus activate downstream pathways including the RAS/RAF/MEK/ERK, PI3K/PTEN/AKT and JAK/STAT pathways [42]. The activation of these pathways ultimately leads to the transcriptional activation of genes involved in cell proliferation, cell migration, cell differentiation and decreased apoptosis.

Abnormal RTK activation is a common feature of many epithelial carcinomas including bladder cancers and is mediated by four main mechanisms: gain-of function mutations, genomic amplification, chromosomal rearrangements, and autocrine activation [47]. A number of key RTK subfamilies have been implicated in bladder cancer development and progression. For example, activating mutations in

the fibroblast growth factor receptor 3 (FGFR3) gene are common in low stage and grade tumours and overexpression of FGFR1 has been reported in a large proportion of tumours of all stages and grades [38, 53, 54]. The ERBB subfamily of RTKs also play an important role in bladder cancer. There have been several studies suggesting that epidermal growth factor receptor (EGFR) plays a key role in the development and progression of bladder cancer, with approximately half of all bladder tumours overexpressing the receptor [55-59]. There is also a significant association between EGFR expression and increased invasiveness of tumours and poorer survival for patients [reference]. Mesenchymal epithelial transition factor (MET), a receptor that normally plays a role in embryogenesis and wound-healing [60], has also been implicated in MIBC with increased MET signalling showing a strong correlation with increased metastatic potential and poor outcome for patients [59].

Constitutive and aberrant activation of pathways downstream of RTKs are important in bladder cancer. Activation of the RAS/RAF/MEK/ERK pathway by RTKs triggers a cascade of phosphorylation events involving downstream kinases leading to a multitude of physiological and pathological cellular processes such as growth, proliferation, differentiation, migration and apoptosis. Activating RAS mutations are seen in approximately 10% of all bladder tumours, and increased signalling via the RAS/RAF/MEK/ERK pathway has been associated with poorer prognosis for bladder cancer patients [32, 47-49]. Similarly, RTK activation may also trigger the activation of the PI3K/PTEN/AKT pathway. This is one of the most frequently dysregulated pathways in cancer and is thought to play a major role in bladder carcinogenesis with immunohistochemical studies demonstrating an increase in the level of phosphorylated AKT in up to 88% of bladder cancer cases [47-49].

1.4 Molecular subtypes of MIBC

Large-scale genome-wide studies of mRNA, microRNAs, DNA-methylation, copy number alterations and somatic mutations have enabled the identification of cancer subtypes [61-65]. The most widespread approach to cancer subtyping remains genome-wide gene expression profiling [65-68]. This approach has enabled the identification of molecular subtypes based on mRNA expression profiles in multiple cancer types including breast, lung, colorectal, pancreatic, leukaemia and bladder [66]. It is hoped that the classification of cancers into subtypes will ultimately aid the

identification of actionable drug targets and biomarkers to predict prognosis and response to therapy.

Over the past 20 years genome-wide gene expression profiling of breast cancer has led to the identification and extensive characterisation of four molecular subtypes termed luminal A, luminal B, HER2-enriched (HER2-E) and basal-like [69]. Collectively, these are known as the intrinsic subtypes of breast cancer and each exhibits differences in response to treatment, incidence and patient survival [69]. Subtyping of breast cancers provides both prognostic and predictive information that can be used to support information provided by traditional clinical parameters such as tumour size, histological stage and grade, and node status, to guide better informed treatment decisions for patients [70]. Several research groups are now working towards providing similar information for bladder cancer. A timeline of the main studies and the molecular subtypes described is shown in Figure 1-2.

In 2010, a research group from Lund University were the first to classify bladder tumours based on molecular data including genome-wide gene expression data [71]. They carried out hierarchical cluster analysis of gene expression data from 144 bladder tumours across all stages and grades, and combined this information with whole genome copy number data and mutational analysis data for 8 key genes for; fibroblast growth factor receptor 3 (*FGFR3),* phosphatidylinositol 3-kinase (*PIK3CA*), Kirsten rat sarcoma (*KRAS*), Harvey rat sarcoma (*HRAS*), neuroblastoma rat sarcoma (*NRAS*), tumour protein 53 (*TP53*), cyclin dependent kinase inhibitor 2A (*CDKN2A*) and tuberous sclerosis (*TSC1)* [71]. This identified 2 subgroups of bladder tumours which they termed MS1 and MS2. MS1 tumours had a high frequency of activating mutations in *FGFR3* and *PIK3CA* suggesting they are dependent on activation of receptors early on in signalling pathways [71]. Genomic instability was the most notable characteristic of tumours classified into the MS2 subtype, and while this group also had a high level of TP53 mutations and MDM2 amplification, genomic instability was independent of these traits [71]. They also found that the MS2 subtype could be further divided into two groups, one with no *TP53* impairment, and the other with *TP53* impairment and a significantly higher number of focal genomic amplifications [71].

In a subsequent study, the Lund group identified five major molecular subtypes of bladder tumours based on hierarchical cluster analysis of gene expression data from 308 urothelial cell carcinomas of all stages and grades [72]. The five subtypes

defined were urobasal A (UroA), urobasal B (UroB), genomically unstable (GU), squamous cell carcinoma-like (SCC-like) and “infiltrated”. UroA was identified as a group with good prognosis that mainly consisted of NMIBC of low pathological grade. This subtype was characterised by frequent *FGFR3* mutations and elevated levels of FGFR3, GATA binding protein 3 (*GATA3*), cyclin D1 (*CCND1*) and tumour protein 63 (*TP63*). The UroB subtype shared many similarities with the UroA subtype but were characterised by more frequent *TP53* mutation and increased expression of keratins 5, 13, 15 and 17. A high frequency of muscle-invasive bladder tumours (50%) were assigned to this subtype. The GU subtype also had a high number of muscle-invasive bladder tumours, with 40% of cases being muscle-invasive, and the group was described as ‘high risk’. This subtype was also characterised by frequent *TP53* mutation, high cyclin E1 (*CCNE*) and human epidermal growth factor receptor 2 (*HER2*) expression, and low keratin (*KRT*) expression. The majority of tumours classified as SCC-like showed squamous-cell differentiation. The SCC-subtype was characterised by expression of a number of keratins (4, 6A/B/C, 14 and 16) and also exhibited elevated expression of EGFR. The UroB and SCC-like subtypes had the poorest prognosis and the SCC-like was more commonly seen in females. The “infiltrated” subtype had a high level of immune cell infiltration and also expressed the epithelial-to-mesenchymal transition (EMT) associated genes Snail Family Transcriptional Repressor 1 (*SNAI1*) and Zinc Finger E-Box Binding Homeobox 1 (*ZEB1*).

The Lund group later expanded upon this study by using both global mRNA and extensive immunohistochemical analysis of 307 advanced bladder tumours (cystectomised) and defined five tumour-cell phenotypes characterised by the expression patterns of a specific set of markers [73]. Urobasal (CCND1+; FGFR3+; RB1+; CDKN2A-), genomically unstable (CCND1-; FGFR3-; RB1-; CDKN2A+), mesenchymal-like (VIM+; ZEB2+; EPCAM-; CDH1-), basal/SCC-like (KRT5+; KRT14+; GATA3-; FOXA1-), and small-cell/neuroendocrine-like (TUBB2B+; EPCAM+; CDH1-; GATA3-). The authors did however acknowledge that these subtypes require independent validation [73].

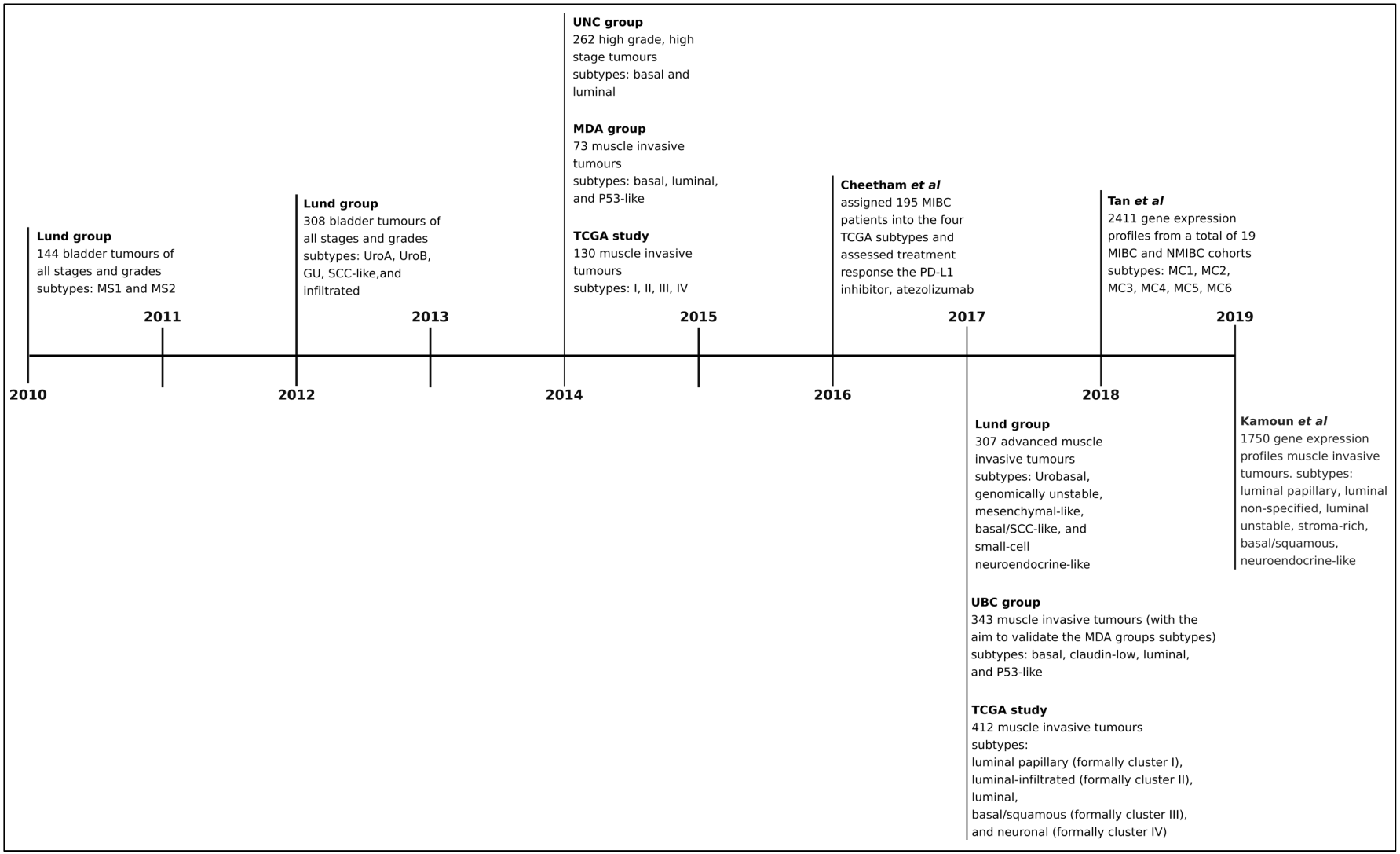

Figure 1-2: A timeline of bladder cancer subtyping studies since 2010.

In 2014, Damrauer *et al.* from the University of North Carolina (UNC) used consensus cluster analysis of genome-wide gene expression data for 262 high-grade muscle-invasive bladder tumours, and defined two molecular subtypes of MIBC that share similarities to the luminal and basal intrinsic subtypes of breast cancer [74]. Tumours in the luminal subgroup demonstrated largely papillary histology, and had upregulated expression of uroplakins, keratin 20, FGFR3, CDH1 and cell cycle genes such as CCND1. The basal subtype expressed markers similar to those seen in the basal layer of the urothelium [74], including upregulated keratins 5, 6B and 14, and upregulated CD44, suggestive of squamous metaplasia. The basal subtype had a much poorer survival rate compared to the luminal subtype [74]. They also identified a subgroup of the basal subtype which they labelled “Claudin-low” as it shared features reminiscent of a subset of breast tumours with the same name. This subgroup had low claudin expression and increased expression of EMT markers. No difference in overall or disease free survival was noted between the Claudin-low tumours and the other basal tumours.

These MIBC subtyping studies do not stand alone and comparisons between them reveal overlapping features. For example, the basal subtype identified by Damrauer *et al.* shows similarities to both the SCC-like and UroB subtypes defined by the Lund group. Although there is overlap in the studies’ findings, Damrauer *et al.* were the first to assign a breast cancer molecular subtyping system to bladder cancer which interestingly was found to hold clinical relevance. It is now widely accepted that MIBC subtypes can be broadly divided into basal and luminal tumours.

Luminal and basal subtypes of bladder cancer were also reported by a group from the MD Anderson (MDA) Cancer Center that identified three subgroups following whole genome mRNA expression profiling and unsupervised cluster analysis of a discovery cohort of 73 MIBC patient samples [75]. Two of these subtypes were termed basal and luminal as they shared gene expression features with their breast cancer namesakes. The MDA group also identified an intermediate subtype that, due to an upregulation of a gene expression signature associated with activated wild-type p53, was labelled p53-like [75]. Similar to the “infiltrated” subtype denoted by the Lund group, this p53-like subtype also had a high level of non-tumour cell infiltration, particularly of cancer-associated fibroblasts. The p53 subtype was also characterised by an enrichment of an extracellular matrix related gene expression signature [75]. The MDA group was the first to introduce the idea that molecular

subtypes could predict response to traditional neoadjuvant cisplatin-based chemotherapy (NAC) and demonstrated that patients with p53-like tumours had a lower response rate to NAC [75].

A group from the University of British Columbia (UBC) subsequently examined the concept of bladder cancer subtypes being used to predict response to NAC [76]. They aimed to validate the work of the MDA group using a larger cohort, and also sought to investigate the relationship between NAC resistance and other previously annotated subtypes [76]. They also proposed a subdivision of the UNC luminal subtype into luminal and luminal-infiltrated. The luminal-infiltrated subtype was seen to be similar in many aspects to the luminal subtype, but also had an increased immune-infiltration gene expression signature and was associated with a low response rate to NAC [76]. Division of the basal subtype into a basal subtype which may benefit from NAC and a claudin-low subtype which did not respond well to NAC was also proposed. The claudin-low subtype was characterised by an EMT phenotype, low PPARG expression and high activity of nuclear factor kappa light chain enhancer of activated B cells (NF-κB) [76]. While the molecular subtyping of MIBC has highlighted clinically relevant findings in relation to response to NAC, subtyping based on hierarchical clustering requires large cohorts of patients, which means it cannot be implemented on an individual patient basis in the clinic. In response to this, the UBC group trained a single-sample genomic subtyping classifier (GSC) in order to assign individual tumours to one of their four subtypes. Such an approach may be more applicable in a diagnostic setting [76].

One of the largest subtyping studies has come from The National Cancer Institute and National Human Genome Research Institute who have developed a multi-institutional collaboration known as The Cancer Genome Atlas (TCGA) Research Network. The TCGA has collected and analysed the molecular data for hundreds of tumour samples from 33 different cancer types including bladder cancer [77]. Initially, a study of 130 muscle invasive tumours was carried out by the TCGA in 2014, identifying four subtypes named clusters I-IV [47]. Clusters I and II were identified as luminal subgroups with high expression of GATA3 and FOXA1. Cluster I also exhibited mainly papillary histology similar to the luminal subtype identified by the UNC group. Cluster III was identified as a more basal-squamous subtype similar to the previously annotated basal subtypes of other research groups, and expressed high levels of keratins 5 and 14 which are also high in urothelial stem-like progenitor cells [47, 78]. The addition of non-coding RNA data to the analysis allowed the further

identification of a new subtype called cluster IV which expressed genes characteristic of epithelial-to-mesenchymal transition.

In 2017, the TCGA expanded upon their original study and reported data for a larger MIBC cohort consisting of 412 tumours [32]. This larger sample set enabled refinement of their original subtypes, and provided insights into prognosis and therapeutic response, with suggestions of which subtypes would benefit from FDA approved immune checkpoint inhibitors, or alternative more targeted therapeutic strategies. The five subgroups were named: luminal papillary, luminal-infiltrated, luminal, basal/squamous, and neuronal. The luminal-papillary, luminal-infiltrated and luminal subtypes all share features with the previously identified luminal subtype, expressing high levels of uroplakins, KRT20, GATA3 and forkhead box A1 (FOXA1), but each group also possesses some unique features. The luminal-papillary subset, for example, showed the best overall survival, and had a papillary morphology. *FGFR3* mutations and *FGFR3-TACC3* fusions were enriched in this subtype, and high expression of CDH1 and ERBB2 was also observed. The luminal-infiltrated subgroup had a strong mesenchymal expression signature and low tumour purity, and the luminal subtype had high expression of genes that are commonly expressed in terminally differentiated umbrella cells such as KRT20 and SNX31, and had extremely high expression of the uroplakins UPK1A and UPK2.

The molecular data and patient metadata collated from the TCGA studies have been made publicly available to aid research into diagnosis, treatment and preventative strategies for cancer. As a result, the focus of research regarding treatment of MIBC is now trending towards targeted therapies and away from traditional chemotherapeutics [77]. In the first study of its kind, a phase II trial of platinum-treated locally advanced MIBC adopted the TCGA classification approach to assign 195 patients into the four original subtypes (I-IV), and assessed the differences in treatment response to the monoclonal antibody atezolizumab that inhibits PD-L1 [79]. Analysis revealed a higher response in the luminal cluster II patients, suggesting that subtypes may independently predict response to new immune checkpoint inhibitors. This highlights the potential for the stratification of MIBC based on molecular subtypes as an effective approach for the allocation of therapeutic options. Further studies to elucidate the association between molecular subtypes of MIBC and response to immune checkpoint inhibitors are planned[28].

In order for this process to be adopted in the clinic it is important that a consensus on subtype classification is reached. While these studies have provided good groundwork in the identification of MIBC molecular subtypes, they have all been based on relatively small cohort sizes of between 100 and 500 samples. However over 5000 samples may be need in order to reliably detect mutations that occur in less than 2% of the samples [80]. Thus cohorts this large may also be required to detect rarer molecular subtypes. The increased ability to detect subtypes when using larger cohorts is highlighted by the TCGA studies which identified five subtypes when 412 samples were examined, compared to only four subtypes that were identified when the original 130 samples were examined.

In September 2018, a much larger study was conducted by a group from the National University of Singapore collating and analysing 2411 gene expression profiles from a total of 19 MIBC and NMIBC cohorts [81]. This study identified 6 major molecular subtypes (MC1-6) [81]. These subtypes were compared to previously annotated subtypes through analysis of key markers, cross referencing with existing subtype annotation, and re-performing consensus clustering on a subset of the bladder tumours using the most significantly altered genes and previously published subtype signatures [81]. This revealed that MC1-6 corresponded well with previously annotated subtypes. MC1 (also called Neural-like or NEURAL) is similar to the Lund group's small-cell/neuroendocrine-like subtype and the TCGA neuronal subtype. MC2 (also called Luminal-like or LUM) is similar to a NMIBC subtype known as class 3, identified by Hedegaard *et al.* [82]. MC3 (also called Papillary-like or PAP) is similar to the Lund group's urobasal subtype and the TCGA luminal-papillary subtype. MC4 (also called HER2-like or HER2L) is similar to Lund group's genomically unstable subtype and the TCGA luminal subtype. MC5 (also called squamous cell carcinoma-like or SCC) is similar to the Lund group's SCC-like subtype, the MD Anderson Cancer Center basal subtype and the TCGA basal-squamous subtype. MC6 (also called Mesenchymal-like or MES) is similar to the Lund group's "infiltrated" subtype, the MD Anderson Cancer Center p53-like subtype and the TCGA luminal-infiltrated.

Tan *et al.* also related this new subtyping information to potential therapeutic approaches [81]. In order to predict the treatment approaches best suited to each subtype, cell line drug response analysis was conducted using the UBC-40, a panel of 40 well characterised bladder tumour derived cell lines [83]. The 40 cell lines were assigned to each of the six subtypes. Subtypes were then correlated with the 50%

growth inhibitory concentration (GI50) for 25 different therapeutic compounds [81]. This revealed differing responses amongst subtypes. MES demonstrated the highest resistance to the majority of compounds compared to the other subgroups which was thought to be related to its stem-like features. The LUM subtype showed high resistance to the FGFR1 and FGFR3 inhibitor PD-173074. It was noted that while there were differences in levels of resistance to these therapeutic compounds, there was no clear association between the subtypes and sensitivity to any of the therapeutic compounds. This analysis was conducted on a limited number of cell lines, and does not represent a large-scale tumour screen, but it may still be useful as a preliminary analysis and provide information for future more in-depth and larger scale studies.

This large-scale study in principle could help a consensus on the molecular subtyping of bladder cancer to be reached and improve understanding of the clinical implications of such subtypes. However, the study of Tan *et al.* has been regarded as flawed, as the manner in which datasets were merged was problematic and internal validation was not systematically performed. This led to bias in the classification system. For example, the "MC1" or "neural" subtype comprised of 77% FFPE tumour samples compared to only 7% in the MC2 or luminal subtype [84].

In December of the same year a pre-print was released from an international collaboration known as 'The Bladder Cancer Molecular Taxonomy Group' who have undertaken a more robust study aimed at providing a consensus classification of MIBC subtypes based on 1750 transcriptome profiles of muscle-invasive tumours from six different studies[32, 74, 75, 85-87] (doi: http://doi.org/10.1101/488460). Six molecular subtypes were defined, which largely overlapped with previously annotated classifications. These subtypes were named: Luminal Papillary (LumP), Luminal Non-specified (LumNS), Luminal Unstable (LumU), Stroma-rich, Basal/Squamous (Ba/Sq) and Neuroendocrine(NE)-like.

The LumP accounted for nearly a quarter of the samples. The majority of tumours assigned to this group showed papillary morphology, and bared similarity the TCGA luminal papillary and Lund UroA subtypes. LumP was characterised by a high expression of FGFR3 and low expression of CDKN2A at the mRNA level, and had a high frequency of mutations to *FGFR3*, *KDM6A*, and *STAG2*. These features are also common in low stage (Ta - T1) non-muscle-invasive tumours, implying this group may have progressed from NMIBC. This group also had the best prognosis.

LumNS was a much smaller subset with just 8% of samples assigned to this subtype. Similar to the MDA luminal, UNC luminal, and Lund genomically unstable subtypes, this group showed high mRNA expression of PPARG and mutations to the *ELF3* gene. This subtype was also characterised by a high level of fibroblasts infiltrating the tumour, and had the worst prognosis of the three luminal subtypes. Fifteen percent of samples were assigned to the LumU subtype, similar to TCGA luminal subtype. This group was typically genomically unstable, and had a high mutational burden. This group had a high level of mutations to *TP53*, *ERCC2*, and had increased activation of the ERBB2/HER2. The Stroma-rich subtype was comprised of patients with both luminal and non-luminal tumours, and showed similar characteristics to TCGA luminal infiltrated and MDA p53-like subtypes. There were also tumours assigned to this group that had previously been assigned to the Lund group's mesenchymal-like, genomically unstable and Urobasal subtypes. The main characteristic of this subtype was the high level of non-tumour cell infiltration including B cells, smooth muscle, fibroblasts, and myofibroblasts. The Ba/Sq subtype was the largest with 35% of tumours assigned to this group. It was seen to be similar to the UNC basal, MDA basal, Lund basal-SCC-like, and TCGA basal-squamous subtypes, and showed high expression of EGFR, KRT14 and KRT5/6, and low expression of GATA3, FOX1A, and PPARG. This group also had a high level of *TP53* and *RB1* mutations, and showed squamous differentiation by histological assessment. The NE-like subtype by contrast was a very small subsete with just 3% of sample assigned to this group. It was similar to the TCGA neuronal and the Lund group small-cell/neuroendocrine-like subtypes, and was characterised by inactivating mutations to *TP53* and *RB1.* It is hoped that these consensus biological subtypes will be useful in treatment stratification, and the group also presented a single-patient classifier in order to enable application of this consensus classification system in the clinic.

1.5 Preceding work in our laboratory implicating ECM1 and MUC1 in a subgroup of MIBC

Cell line panels such as the UBC-40 represent a valuable resource for use as model systems in which to test therapeutic approaches [83, 88, 89]. It is essential that the molecular features of such cell line panels are fully characterised and that these characteristics faithfully reflect those present in the tumours from which they were

derived. Prior to the start of this study, our laboratory assembled a panel of 45 bladder tumour-derived cell lines and carried out genome-wide expression profiling in order to determine whether molecular subgroups were present within the (Hurst *et al*., unpublished data). This analysis will be discussed fully in Chapter 3. One of the subgroups identified exhibited unique features compared to previously annotated subtypes and was chosen for further study in the current project. This subgroup has Basal/Squamous features but also exhibits significant upregulation of a subset of 50 genes including extracellular matrix protein 1 (*ECM1*) and mucin 1 (*MUC1*).

1.6 ECM1

1.6.1 ECM1 in normal physiology

Extracellular matrix protein 1 (ECM1) is an 85kDa highly glycosylated protein [90]. It was first identified in 1994 as a secreted protein in a mouse osteogenic stromal cell line [91], and later in 1997 the human form of ECM1 was characterised [92]. The human *ECM1* gene maps to 1q21, adjacent to the epidermal differentiation complex, and encodes for a protein expressed mainly in the basal layers of the skin and specialised epithelia [91]. The normal physiological function of ECM1 is not fully understood, nor is the mechanism by which ECM1 exerts it's biological functions, however, it is thought to be important in embryo development and wound healing, as the protein is linked to angiogenesis [93, 94], cell differentiation including keratinocyte differentiation and endochondral ossification [95], and cell proliferation [96].

The ECM1 protein contains a 19 amino acid signalling peptide and four functional domains: a cysteine-free N-terminus, two tandem repeats, and a C-terminus [94] (Figure 1-3). The tandem repeat and C-terminus domains have a CC-(X_{7-10})C motif that may form protein double loops similar to those involved in protein–protein interactions seen in other molecules such as the serum albumin family of proteins and a protein known as Endo 16 calcium-binding protein expressed by sea urchins [92, 97, 98]. These similarities suggest that ECM1 may act in a similar manner by serving as a transporter protein or having the capability to bind growth and differentiation factors [94, 99]. Indeed, within the epidermal layers of the skin ECM1 has been noted to bind to several extracellular matrix proteins such as collagen

type IV, fibronectin, laminin 332, fibulin-1C/1D and MMP9 implying that ECM1 could have a role as an extracellular fixative important for maintaining the structural integrity of the skin [90]. This role has not been fully elucidated as *in vivo,* transgenic mice overexpressing ECM1a did not have significant changes in the structure of the epidermis [100].

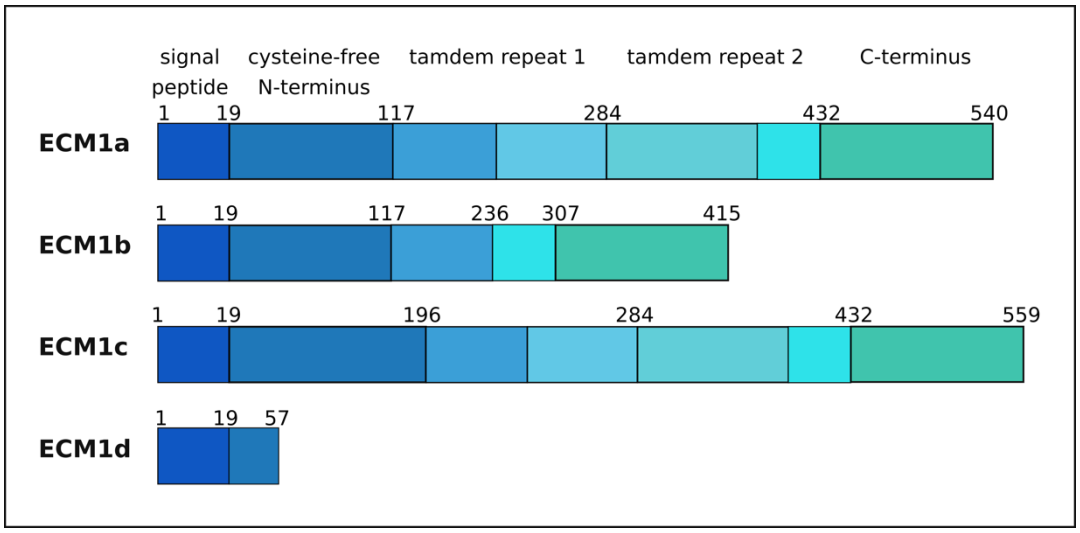

Figure 1-3: A schematic representation of the ECM1 protein slice variants and functional domains.
The figure has been created from information obtained from [93].

In addition to its involvement in extracellular matrix integrity, ECM1 has also been suggested to play other key roles as part of its normal physiological function. ECM1 may influence cell-type specific cell growth as it has been reported to stimulate epithelial cell proliferation [96, 101] and may inhibit chondrocyte proliferation [102]. Furthermore, ECM1 is thought to be involved in the regulation of endochondral bone and cartilage formation [94, 95, 103], and it has been noted to influence calcification of the extracellular matrix [102]. Gene expression analysis has suggested that ECM1 is a late-response, downstream molecule of parathyroid hormone-related protein (PTHrP) signalling which is an important pathway in the regulation of chondrogenesis [104].

The function of ECM1 may be splice variant dependent as there are four known splice variants of ECM1. ECM1a is the main isoform expressed in basal keratinocytes, dermal blood vessels and adnexal epithelia [105]. ECM1b is smaller

than ECM1a as it lacks the amino acid chain encoded by exon 7 and is found in the spinous and granular layers of the epidermis [105]. ECM1c is the largest isoform and is only found in the basal layer of the epidermis [94]. ECM1d is the smallest isoform consisting of just 57 amino acids, and has so far only been observed a fibroblast cell line *in vitro,* thus its biological importance *in vivo* is still unknown [106, 107]. While each variant has been observed in different tissue types, the potential differences in function have not yet been explored.

1.6.2 ECM1 in human disease

The normal function of ECM1 has in part been clarified by studies that have examined diseases associated with malfunctioning ECM1. In 1929 Urbach and Wiethe, a dermatologist and an otorhinolaryngologist respectively, first described an autosomal recessive condition known as Urbach–Wiethe disease (UWD) or lipoid proteinosis that was later shown to be caused by loss of function mutations in the *ECM1* gene [108, 109]. UWD is rare with only 300 reported cases since its discovery [110]. However it can significantly impact the quality of life for patients. Symptoms vary amongst sufferers but it is usually characterised by early childhood presentation of a hoarse voice due to a thickening of the vocal cords, and pox-like scars covering the skin. Later in the disease course, excessive thickening of the skin and mucous membranes develops, often presenting on the face and tonsils [111]. This can lead to complications such as breathing difficulties or blindness due to thickening of the skin around the eyes [110]. The dermatological nature of the condition implies ECM1 plays a crucial role in skin homeostasis. Furthermore, damage by minor physical trauma leads to severe scarring and blistering in patients hinting at a role for ECM1 in wound healing. Deposition of calcium in blood vessels can occur in patients resulting in ischemia, suggesting that calcium metabolism may also be influenced by ECM1 [110].

The chronic inflammatory skin disease known as lichen sclerosis has a similar clinical presentation to lipoid proteinosis and may also be associated with reduced ECM1 function. Autoantibodies against the ECM1 protein have been identified in the circulation of patients with this disease, substantiating the idea that ECM1 influences skin homeostasis [112].

ECM1 has also been linked to the chronic inflammatory diseases ulcerative colitis (UC) and Crohn's disease [102]. While the development and progression of these

conditions are multifaceted and include genetic, environmental and immunogenic factors, a significant association between a single nucleotide polymorphism (SNP) in the *ECM1* gene (rs3737240) and the development of the two conditions has been established [113]. However, the functional impact of this SNP has not yet been elucidated.

1.6.3 ECM1 in cancer

In contrast to the loss of ECM1 function in human diseases, high ECM1 expression has been reported in a number of carcinomas including thyroid, biliary, hepatocellular, laryngeal and breast [114, 115, 116 , 117]. While the precise nature of the role of ECM1 in carcinogenesis is not clear, it has been linked to a number of pro-carcinogenic pathways. The application of ECM1 to chorioallantoic membranes of chicken embryos was seen to promote new blood vessel growth (angiogenesis) on a level comparable to that seen when membranes are treated with vascular endothelial growth factor (VEGF) [93]. Angiogenesis is considered a turning point in tumour development, when previously slow growing and localised tumours may become more invasive with rapid growth [93]. Thus, it is possible that ECM1 contributes to tumour progression and metastasis by its involvement in this process. The role of ECM1 in angiogenesis may be attributed to its interactions with other proteins. For example, ECM1 has been reported to interact with the vascular regulator, perlecan [94]. This indicates a possible co-regulatory role for ECM1 in blood-vessel development.

ECM1 may also play a role in metastasis. A correlation between ECM1 and metastatic potential of hepatocellular carcinoma (HCC) was reported in 2011 [118] and in a later study a similar correlation was observed in laryngeal cancer [119]. ECM1 has also been shown to have a potential role in breast cancer metastasis, with breast cancer cell lines overexpressing ECM1 having increased rates of migration and invasion as seen by the transwell assay [120].

ECM1 may contribute to metastasis by its involvement in lymphatic vessel development (lymphangiogenesis) as ECM1 and vascular endothelial growth factor c (VEGF-c) have been seen to have a synergistic effect in promoting lymphangiogenesis in human breast cancer [121]. Further evidence that ECM1 is involved in the metastatic process comes from a positive correlation between matrix metallopeptidase 9 (MMP9) activity and ECM1 expression [122]. The proteolytic

activity of MMP9 causes degradation of many components of the extracellular matrix allowing tumours, no longer contained by an intact basement membrane, to invade surrounding tissues eventually leading to metastatic spread [122]. Furthermore, cleavage of collagen IV by MMP9 exposes a cryptic epitope that is known to increase angiogenesis [90] thus it is reasonable to propose that an interaction between ECM1 and MMP9 may not only lead to an increase in metastatic potential but may also promote angiogenesis. ECM1 has also been shown to influence cell proliferation [93, 122]. Increased proliferation rates have been demonstrated in both healthy endothelial cells transfected with recombinant ECM1 and breast cancer cell lines overexpressing ECM1 [93, 122].

Two proteins that have been reported to physically interact with ECM1 in breast cancer are EGFR and MUC1 [122]. EGFR, also known as ERBB1, is a member of the ERBB family of tyrosine kinase receptors which includes three other receptors ERBB2/HER2, ERBB3/HER3, and ERBB4/HER4 all of which are the products of the *c-erbB* oncogenes [55]. EGFR is encoded by the proto-oncogene c-*erb*B-1 located on chromosome 7 [123]. Like the other receptors of this family, EGFR has a highly conserved intracellular domain with several phosphorylation sites and kinase activity. EGFR also contains an extracellular ligand binding region which is less well conserved between members of the ERBB family of receptors. There are seven known ligands for EGFR: epidermal growth factor (EGF), transforming growth factor alpha (TGF- α), amphiregulin (AREG), heparin binding EGF like factor (HB-EGF), betacellulin (BTC) epiregulin (EPR), and epigen (EPGN) [55].

Upon activation by a ligand, conformational changes are induced resulting in the homo or hetero-dimerisation of two ERBB receptors [55]. Intrinsic kinase activity of one receptor in the dimer, phosphorylates specific residues present on the intracellular region of the other receptor [124, 125]. This provides a scaffold which can recruit effector proteins and activate downstream signalling pathways including the PI3K/PTEN/AKT, Ras/Raf/MEK/ERK, Src/FAK and JAK/Stat pathways [125, 126]. Pathway activation ultimately results in transcriptional activation of genes involved in cell proliferation, migration, differentiation and decreased apoptosis [127]. EGFR overactivation as a result of overexpression, mutation, decreased inhibition or increased ligand availability has been observed in a number of carcinomas and is often related to poorer survival [128]. Overexpression of EGFR has been described in a number of epithelial malignancies including lung, breast and colon cancer [55, 129-131].

There have been several studies suggesting that EGFR overexpression also plays an important role in the development and progression of bladder cancer [55-58]. Normal urothelium expresses relatively low levels of EGFR [132]. In contrast, approximately half of all bladder tumours overexpress EGFR [59] and there is a significant association between EGFR expression and prognostic factors including reduced differentiation and invasion of the *muscularis propria* [55]. EGFR overexpression has also been associated with poorer survival in patients [133] and with increased recurrence following adjuvant chemotherapy for the treatment of advanced MIBC [134]. EGFR-targeted agents have had limited success in current ongoing clinical trials due to acquired resistance [59]. The association between EGFR overexpression and cisplatin resistance has highlighted the potential need for kinase inhibitors or monoclonal antibody treatments targeting the receptor to be used in combination with cisplatin-based treatments [59].

1.6.4 MUC1

MUC1 is part of a family of proteins known as mucins [135]. These are large highly-branched, high molecular weight glycoproteins that fall into three categories: membrane-associated mucins, gel-forming-secreted mucins, and soluble-secreted mucins [136]. MUC1 is a membrane-associated mucin encoded by a gene mapping to 1q21 [135]. While MUC1 is typically expressed in basal epithelial cells, in the urothelium MUC1 is expressed only in the apical membranes of superficial umbrella cells where it not only acts as a physical barrier between the urine and urothelial cells [137] but also plays an important role in cell adhesion and morphogenetic signal transduction [136].

Changes in the gene expression, rate of synthesis, and glycosylation patterns of MUC1 have been reported during malignant transformation of epithelial cells [138]. These changes can lead to multiple pro-carcinogenic effects, for example, overexpression of MUC1 is associated with reduced cell-to-cell adhesion, which is associated with more metastatic and invasive tumours [139]. Furthermore, changes in glycosylation of the extracellular domain have been reported to impact host immune recognition of tumours through alterations to the immunogenic epitopes that are displayed [135]. High protein expression of MUC1 as determined by immunohistochemistry has shown that MUC1 is overexpressed in over 90% of breast carcinomas, and high expression has been associated with poorer prognosis

in a number of carcinomas including ovarian, lung, colon, and pancreatic carcinomas [140].

Several studies have associated altered MUC1 expression with bladder cancer. Expression of MUC1 is normally confined to umbrella cells in healthy tissue but in nearly 75% of bladder carcinomas moderate staining of MUC1 can also be observed in the basal and intermediate layers of the urothelium [135, 141]. High levels of MUC1 expression are associated with multifocality [142] and higher-grade tumours [143]. Despite links between altered MUC1 expression and the invasiveness of bladder tumours, there is no association between MUC1 expression and patient outcome [143] or pathological stage of bladder cancer [135]. The majority of muscle-invasive bladder tumours stain positively for MUC1, and changes in the level of glycosylation of MUC1 early in tumour formation may impact invasive potential of these tumours [135].

MUC1 has also been demonstrated to physically interact with EGFR [122, 144, 145]. Co-immunopreciptation experiments in a breast cancer cell line showed that MUC1 can physically interact with EGFR and HER3, and these interactions were increased in cells overexpressing ECM1 or in cells treated with recombinant ECM1 [122]. Moreover, this study also established a physical interaction between ECM1 and EGFR, and ECM1 was seen to increase the half-life of EGFR and HER3, implying that ECM1 stabilises these receptors both through direct interaction with EGFR, and the promotion of interactions between MUC1, EGFR and HER3 [122]. Galectin 3 (gal-3) has also been demonstrated to interact with MUC1 and facilitate EGFR-MUC1 interactions [122, 144], and high ECM1 expression has been correlated with increased gal-3 secretion and increases in protein expression levels of MUC1 [122]. The sum of these findings has led to the proposal of a membrane-embedded stable complex formed between ECM1, MUC1 and EGFR which may mediate trastuzumab-resistance in the breast cancer cell line BT-474 TR (Figure 1-4). This study also showed that siRNA knockdown of MUC1, gal-3 or ECM1 led to reduced p-EGFR and p-ERK expression, suggesting this complex may mediate signalling through the Ras/Raf/MEK/ERK pathway.

The suggestion of potential interactions between ECM1, MUC1 and EGFR in breast cancer is of particular interest to the current study. Many similarities exist between the molecular features of breast cancer and bladder cancer, as highlighted by molecular subtyping studies [72, 74, 75]. Upregulation of EGFR is characteristic of the

basal subtypes of both carcinomas [86] and EGFR levels are elevated in the Basal/Squamous subgroup of cell lines (subgroup 2) expressing high levels of ECM1 and MUC1. Investigation of the complex reported by Lee *et al.* (2014) in breast cancer is, therefore, worthy of further investigation in bladder cancer.

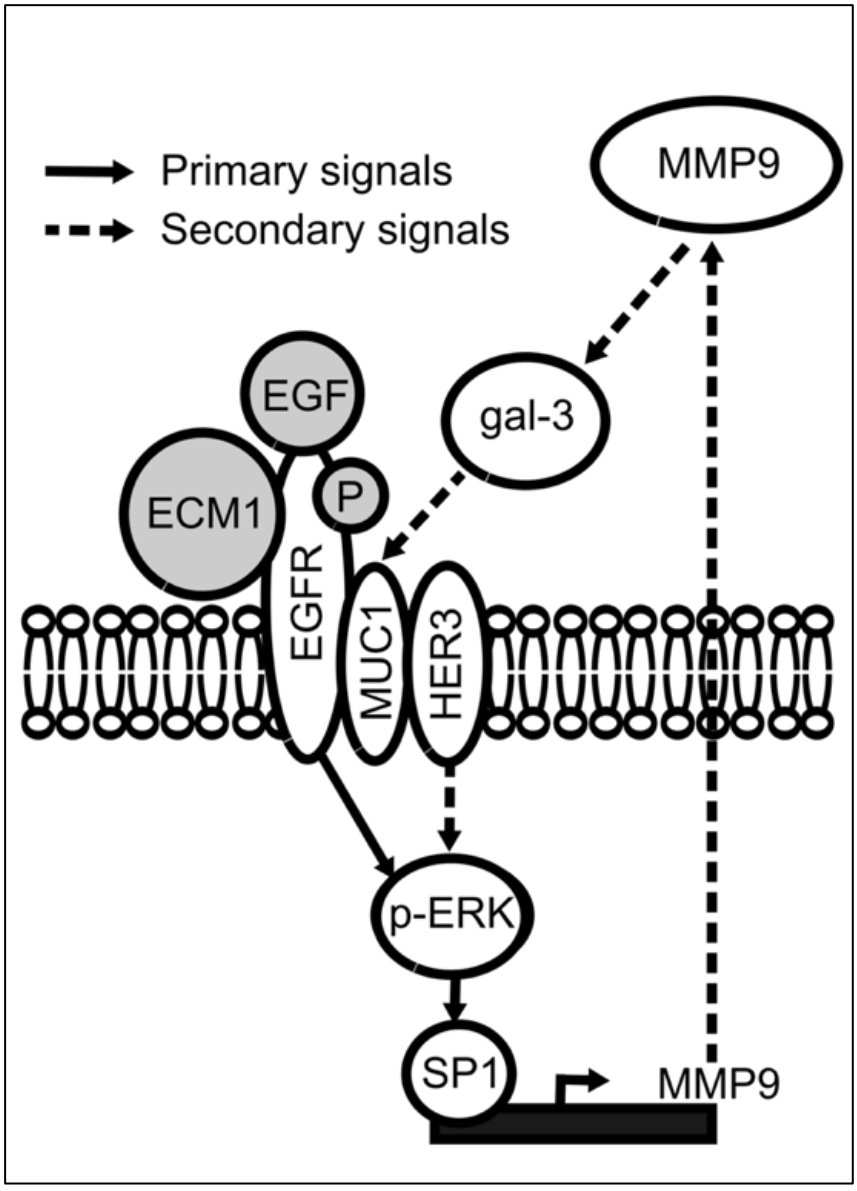

Figure 1-4: A proposed ECM1 complex in breast cancer.

A schematic model showing the proposed complex formed by ECM1, EGFR, MUC1 and HER3 and the potential interactions with gal-3, MMP9 and EGF [122].

1.7 Project Aims

- To validate the existence of a subset of ECM1-high and MUC1-high bladder tumour-derived cell lines.
- To evaluate ECM1 expression in primary tumours, and determine if there is an association between ECM1 expression and patient survival or metastatic potential of tumours.
- To identify a potential interaction between the ECM1 and EGFR proteins and evaluate the impact of ECM1 on the activation of the EGFR pathway.
- To investigate the phenotypic effects of ECM1 shRNA knockdown on cell growth, migration and wound healing capabilities of bladder tumour-derived cells.
- To investigate the potential impact of shRNA knockdown of ECM1 on the effectiveness of therapies targeting the EGFR pathway.

1.8 Hypotheses

- There is a relationship between ECM1 expression and an aggressive, metastatic phenotype of MIBC.
- ECM1 and MUC1 have a functional relationship in promoting this phenotype.
- ECM1 enhances EGFR signalling potentially through physical interaction.
- ECM1 influences resistance to EGFR inhibitors in MIBC.

Chapter 2
Materials and Methods

2.1 Gene expression profiling of bladder tumour-derived cell lines

Total RNA from 45 bladder tumour-derived cell lines was used for whole genome expression profiling that was performed prior to the start of this study (Hurst *et al.*, unpublished data). A pooled sample of normal human urothelial samples (NHU-Pool) was also used in gene expression profiling experiments, and refers to a pooled normal sample generated by mixing together total RNA from 3 different normal urothelial cell lines.

Total RNA was extracted from cultured cells using TRIZOL (Invitrogen, Paisley, UK) according to the manufacturer's instructions. RNA was DNase-treated and cleaned up using a Qiagen RNeasy Mini Kit (Qiagen, Crawley, UK) according to the manufacturer's instructions. Whole-genome expression profiling was performed using GeneChip Human Genome U133 Plus 2.0 Arrays (Affymetrix, Santa Clara, CA, USA).

2.2 Data Mining

Human gene expression data were mined using the publicly available R2 microarray analysis and visualisation platform (developed by Dr. Jan Koster in the Academic Medical Center (AMC) at the University of Amsterdam) that can be accessed at http://r2.amc.nl. This is a web-based interface for the statistical computing language 'R' which can be used to correlate the expression profile of a gene of interest in publicly available gene expression datasets. Expression profiles for 308 fresh-frozen urothelial carcinomas of all stages and grades [72], 116 formalin-fixed paraffin-embedded (FFPE) muscle-invasive bladder tumours [75], 142 fresh-frozen muscle-invasive tumours [75] and 412 fresh-frozen muscle-invasive bladder tumours [32] were examined. These datasets can also be accessed through the Gene Expression Omnibus (GEO) database at the National Center for Biotechnology Information (NCBI) website (GSE32894, GSE48276, GSE48075, and GSE97768 respectively). R2 was used to generate dendrograms by

hierarchical clustering of expression data from selected microarray datasets for all probes that detected ECM1. These were used to select IDs for patients with tumours overexpressing ECM1 so comparisons could be made to all other samples.

The data generated from TCGA study of 412 fresh-frozen muscle-invasive bladder tumours [32] were used to generate Kaplan–Meier survival plots in GraphPad Prism version 7.00 for Mac OS X (GraphPad Software, La Jolla California USA). Survival data was obtained from the Memorial Sloan Kettering Cancer Centre cBioPortal (www.cbioportal.org).

Based on R2 analysis, the IDs of samples identified as having high ECM1 expression in the Sjödhal [72] and the Choi [75] datasets were obtained. Using another online platform, GEO2R, genes differentially expressed between the two groups were determined using the Bioconductor Linear Model for Microarray Analysis (LIMMA) package. Stringency settings were applied to include only probes that had a fold change greater than 2 and a p value less than 0.05. Venn analysis was conducted using Partek® Genomics Suite® software and used to identify genes consistently upregulated in both datasets. These genes were analysed using MetaCore (Thomson Reuters) to determine the pathways that were most altered in ECM1-high tumours

2.3 Cell lines and tissue culture

Forty-five bladder tumour-derived cell lines were used in this study (Table 2-1). Cell culture was performed in a BioMAT class II laminar flow hood (MAT) under sterile conditions. In order to avoid contamination, the working surface of the hood was cleaned with 2% Trigene (Medichem) then 70% ethanol before and after each use. Cell density and cell morphology was observed routinely with a phase-contrast light microscope. Pictures were obtained using a Zeiss Axiovert 10 microscope with a Canon Powershot G6 7.1 Megapixel camera.

Cells were removed from liquid nitrogen storage and rapidly thawed in a water bath at 37 °C. Cells were recovered into 10 ml of growth medium appropriate for each cell line (Table 2-1) and pelleted by centrifugation at 1000 x g for 4 min. The formed cell pellet was re-suspended in 5 ml medium and transferred to 25 cm^2 vented

canted-neck cell culture flasks (Corning). All cell lines were grown under standard cell culture conditions in a humidified incubator (Sanyo) at 37 °C in 5% CO_2 in air in media outlined in Table 2-1.

Cells were routinely passaged once 90% confluence was reached. Medium was aspirated from cell flasks, and cells were rinsed once in phosphate-buffered saline (PBS). Cells were incubated in PBS containing 0.1 % ethylenediaminetetraacetic acid (EDTA) at 37 °C for 5 min after which the PBS-EDTA was subsequently aspirated and cells were incubated for 5 min in 0.5 ml 0.05% trypsin-versene - 0.02% EDTA in PBS (TV) (Sigma Aldrich) for a 25 cm^2 flask, or 1 ml TV for a 75 cm^2 flask, until cells became detached. Inhibition of TV was achieved by resuspension of the cells in 15 ml fresh media containing 10% serum and culturing was continued with a fraction of this cell suspension being transferred to a 75 cm^2 vented canted-neck cell culture flask (Corning) containing fresh medium. For cells cultured in media containing less than 10% serum, cells were resuspended in 10 ml media containing 1 ng/ml of trypsin inhibitor (TI) (Sigma). Cell suspensions were centrifuged at 1000 x g for 4 min and the formed cell pellet was resuspended in 10 ml medium. A fraction of this cell suspension was transferred to a 75 cm^2 flask containing fresh medium and cell culture was continued. Cells were cultured for no more than 10 passages from thawing. All LUCC cell lines were cultured in Corning Primaria vented canted-neck cell culture flasks which have a modified polystyrene surface (Corning).

2.4 Cell counting

For assays in which a specific number of cells per well was required, cells were counted prior to seeding in plates. Cells were harvested and a single cell suspension was produced as outlined in section 2.3. 100 µl of the cell suspension was then added to 10 ml ISOTON™ and cells were counted using a Beckman Coulter Z2 Cell and Particle Counter (Beckman Coulter). Counts were performed in triplicate and an average reading used.

Table 2-1: Media and supplements required for cell culture.

An overview of all cell lines used in the project and the medium and supplements they were cultured in. Standard cell culture conditions of 37 °C in 5% CO_2 in air were used for all cell lines.

Cell Lines	Media	Media Supplements
DSH1, JO'N, SD, SW-1710, RT112M, 5637, KU-19-19, JMSU-1, HCV 29	RPMI 1640 medium (Sigma)	10% fetal bovine serum (FBS) 1% L-glutamine (L-glut)
TCC-SUP, T24, CAL-29, UM-UC-3, VM-CUB1, VM-CUB2, VM-CUB3, 639V, 647V, SW-780, BFT905, BFT909	Dulbecco's Modified Eagle's Medium (DMEM) (Sigma)	10% FBS 1% L-glut
LUCC1, LUCC2, LUCC3, LUCC4, LUCC5, LUCC7	Nutrient mixture F12 (Ham) (Gibco)	1% FBS 1% Insulin-Transferrin-Selenium Hydrocortisone (1 μg/ml) 1% Non-essential amino acids Cholera toxin (30 ng/ml)
HT-1376, SCaBER, HT-1197, J82, MGH-U3	Modified Eagle's Medium (MEM) (Sigma)	10% FBS 1% L-glut 1% Non-Essential Amino Acids
RT4, BC3C	McCoy's 5A Modified Medium (Sigma)	10% FBS 1% L-glut
253J	50% Dulbecco's Modified Eagles's Medium (DMEM) (Sigma), 50% RPMI 1640 medium (Sigma)	5% FBS 1% L-glut
U-BLC1	66% Dulbecco's Modified Eagles's Medium (DMEM) (Sigma), 33% RPMI 1640 medium (Sigma)	5% FBS 1% L-glut
92-1, 94-10, 96-1, 97-7, 97-18, 97-1, 97-24	Nutrient mixture F12 (Ham) (Gibco)	1% FBS 1% Insulin-Transferrin-Selenium Hydrocortisone (1 μg/ml) 1% L-glut 1% Non-essential amino acids
LUCC6, LUCC8, TERT-B	Keratinocyte Growth Medium (Kit 2) (PromoCell)	1% FBS Bovine Pituitary Extract (4 μl/ml) Recombinant Human Epidermal Growth Factor (0.125 ng/ml)

2.5 Single cell cloning

In order to assess the heterogeneity of ECM1 expression in cell populations, cell lines cloned from a single cell were generated using the HT-1376 cell line. When 90% confluency was reached, cells were harvested from 75 cm^2 flasks as described (section 2.3) and counted using the Beckman Coulter Z2 Cell and Particle Counter (Beckman Coulter) as previously outlined (section 2.4). Cells were resuspended in media at a concentration of 1 cell per 100 μl. To each well of a 96-well plate (Corning), 100 μl of cell suspension was added and plates were incubated in a humidified incubator for 1 hour at 37 °C in 5% CO_2 in air to allow cells to attach. Each well was examined using phase-contrast light microscopy to confirm the presence of a single cell. The media in these wells was changed every 4 days. Once 90% confluency was reached, cells were detached as previously described (section 2.3) and resuspended in 1 ml fresh media. This cell suspension was then transferred to a single well of a 24-well plate (Corning) and cell culture continued with media being changed every 3-4 days. Cells were passaged when 90% confluency was reached, and all cells from each well were transferred into a single well of a 6-well plate (Corning). When 90% confluency was reached in the 6-well plate, cells were again passaged, this time into 25 cm^2 vented canted-neck cell culture flasks (Corning).

2.6 Total RNA extraction

Total RNA was extracted from the bladder tumour-derived cell lines when 70% confluency was reached. To each 75cm^2 flask, 350 µl of RNeasy Lysis Buffer (RLT) (Qiagen) containing 1% beta-mercaptoethanol was added and cells were incubated on ice for 1 min. A cell scraper was used to detach lysed cells from the flask surface and crude lysate was transferred to 1.5 ml microcentrifuge tubes and frozen at -80 °C for up to 3 months prior to total RNA extraction carried out using a Qiagen RNeasy kit (Qiagen).

Crude lysate was thawed on ice then one volume of 70% ethanol was added and the sample was transferred to an RNeasy MinElute spin column sitting in a collection tube. Samples were centrifuged for 15 s at 8000 x *g* in a microcentrifuge and flow through discarded. To each column, 350 µl of RW1 buffer was added and

samples were centrifuged for 15 s at 8000 x *g* in a microcentrifuge and flow through discarded. Two further washes were carried out using 500 µl RPE Buffer (Qiagen) each time with samples being centrifuged first at 8000 x *g* in a microcentrifuge for the first wash step then at 13,000 x *g* for 1 min in a microcentrifuge for the second wash step. Columns were then transferred to new collection tubes and centrifuged at 13,000 x *g* for 1 min to remove excess wash buffer and to dry the columns. The columns were then placed into a new 1.5ml microcentrifuge tubes and 30 µl RNase-free water was added. Columns were spun in a microcentrifuge at 13,000 x *g* for 1 min to elute the RNA. Total RNA was quantified using a Nanodrop 8000 UV-Vis spectrophotometer (LabTech) measuring light absorbance at a wavelength of 260 nm in order to determine the samples' concentrations and purity. RNA was stored at -80 °C for up to 1 year.

2.7 cDNA synthesis

First strand cDNA was synthesised using the Superscript™ II RT system (Invitrogen) according to the manufacturer's instructions. Reactions containing 10 µl total RNA (100 ng/µl stock), 1 µl random primers (250 ng/µl stock) and 1 µl dNTPs (10 mM stock) were mixed gently with a pipette and denatured in a heat-block at 65 °C for 5 min. Samples were placed immediately on ice. To each sample 4 µl 5x First Strand Buffer (Invitrogen), 2 µl DTT (0.1M stock) (Invitrogen), 40 U RNaseOUT™ (Invitrogen), and 200 U Superscript™ II RT (Invitrogen) were added. Reactions were incubated in a water bath at 42 °C for 50 min followed by a heat inactivation step at 70 °C for 15 min in a heat-block. cDNA was diluted 1 in 5 by addition of 80 µl of molecular biology grade water prior to storage at -80 °C. Samples were stored in 20 µl aliquots to avoid repeated freeze thawing.

2.8 qRT-PCR

Quantitative real time polymerase chain reaction (qRT-PCR) analysis of gene expression was carried out using Taqman Gene Expression Assays (Applied Biosystems). Template cDNA was synthesised as previously described (section 2.7). Reactions were carried out in a total volume of 20 µl containing 10 µl 2x TaqMan® Gene Expression Master Mix (Applied Biosystems), 1 µl Taqman™ gene

expression assay (ECM1 [H00189435_m1{; MUC1 [H001159357_m1]; or SDHA [H H00417200_m1]) (Applied Biosystems), 2 µl cDNA sample, and 7 µl molecular biology grade water. Two microliters of molecular biology grade water was used in place of cDNA for PCR negative controls. Expression was normalised relative to the expression of a succinate dehydrogenase complex flavoprotein subunit A (SDHA) control and measured relative to the NHU-pool sample (section 2.1). Reactions were performed in triplicate in 96-well optical plates (Applied Biosystems) and run on a QuantStudio 5 Real-Time PCR System (ThermoFisher Scientific) with cycling conditions set as follows: initial 2 min hold at 50 °C, followed by 95 °C for 10 min then 40 cycles of 95 °C for 15 s and 60 °C for 1 min.

2.9 DNA extraction and quantification

DNA was extracted using the QIAamp DNA mini kit (Qiagen) according to manufacturer's instructions. DNA was extracted from the bladder tumour derived cell lines when 70% confluency was reached. Medium was aspirated from one T75 flask and cells were washed twice with PBS. Cells were harvested with trypsin as outlined in section 2.3. Harvested cells were collected in a 1.5 ml microcentrifuge tube and centrifuged at 300 x *g* for 5 min to pellet cells. The cell pellet was resuspended in 200 µl PBS and 20 µl of proteinase K was added (Qiagen). To each sample, 200 µl of Buffer AL (Qiagen) and the samples were pulse-vortexed for 15 s to ensure a homogenous suspension was achieved prior to incubation in a heat-block at 56 °C for 10 min. Samples were briefly centrifuged and 200 µl of 100% ethanol added before they were pulse-vortexed for 15 s and briefly centrifuged. Samples were transferred to a QIAamp Mini spin column (Qiagen) placed in a 1 ml collection tube and centrifuged at 6000 x *g* for 1 min. The flow through was discarded and columns placed in new 2 ml collection tubes. To each collection tube, 500 µl of Buffer AW2 (Qiagen) was added and samples were centrifuged at 20, 000 x *g* for 3 min. The flow through was discarded and columns placed in a new 2 ml collection tubes before being centrifuged at 20,000 x *g* for 1 min. Columns were placed in 1.5 ml microcentrifuge tubes, and 200 µl of molecular biology grade water was added to each column. Samples were incubated for 1 min at room temperature (RT) prior to being centrifuged at 600 x *g* for 1 min. Columns were discarded, and the flow through containing purified DNA was quantified using a Nanodrop 8000 UV-Vis spectrophotometer (LabTech) measuring light absorbance at a wave length

of 260 nm in order to determine the samples' concentrations. DNA was stored at -80 °C until required.

2.10 Protein extraction and quantification

RIPA lysis buffer (1% Triton X-100, 1mM EDTA, 0.5% sodium deoxycholate, 0.1% SDS in PBS) was routinely used for the extraction of proteins for western blot analysis and coimmunoprecipitation. Cells were lysed when 70-90% confluence was reached. Medium was aspirated and cells were rinsed twice in cold PBS. Cells were lysed on ice by the addition of 250 µl RIPA buffer containing protease inhibitors (P8340; Sigma) and phosphatase inhibitors (P5726; Sigma). Crude lysates were transferred to 1.5 ml micro-centrifuge tubes and cleared by centrifugation at 13,000 rpm for 10 min at 4 °C.

Protein concentration was determined using the Bradford protein quantification assay (BioRad) according to manufacturer's instructions. 1x Bradford dye reagent (Biorad) was filtered through grade 1 Whatman® qualitative filter paper (Whatman). A set of protein standards containing 0, 0.2, 0.4, 0.6 and 0.8 mg/ml bovine serum albumin (BSA) (New England Biolabs) in PBS was prepared. Samples were prepared by adding 4 µl protein lysate to 16 µl of molecular biology grade water. To 20 µl of each standard and protein sample, 1 ml of filtered 1x Bradford dye reagent was added and samples were mixed gently with a pipette. Samples were transferred to 1 ml spectrophotometer cuvettes (Sigma) and absorbance was measured at 595 nm using a SmartSpec Plus spectrophotometer (BioRad). A standard curve was generated using the BSA standards and this was used to determine the protein concentrations of the samples based on their absorbance.

2.11 Western blotting

Protein lysates were extracted and quantified from cell lines as previously outlined (section 2.10). Samples were diluted to a concentration of 1.5 mg/ml in a total volume of 100 µl in PBS containing 1x SDS loading dye (50 mM TrisHCl pH6.8, 0.2% SDS, 6% glycerol, 0.01% bromophenol blue, and 10% beta-mercaptoethanol).

Twenty microliters of each protein sample (30 µg) was heated for 3 min at 100 °C before being loaded onto precast Any kD™ SDS-polyacrylamide gels (BioRad). Gels were run at 3 W per gel until the dye-front had just run off the bottom of the gel. Proteins were transferred to Trans-Blot® Turbo Midi Nitrocellulose membranes (BioRad) using the Trans-Blot Turbo Transfer System (BioRad) set on the high molecular weight program. Membranes were blocked using 4% w/v MPS in PBS containing 0.1%-Tween (PBS-T) for 30 min.

All primary antibodies used in this study are shown in Table 2-2. The primary antibodies were diluted in 2% MPS and incubated with the blots overnight at 4 °C. Blots were washed four times for 15 min in PBS-T. Horseradish peroxidase (HRP) conjugated secondary antibodies (Goat-Antimouse HRP, Abcam; Mouse-Antirabbit HRP, Southern Biotech) were added at 1:3000 in 2% MPS for 2 h at RT. The HRP labelled antibody was visualised by chemiluminescence using Luminata Forte Western HRP Substrate (Merk Millipore) and imaged with a ChemiDoc MP System and Image Lab Software (BioRad). Blots were stripped in 50 mM Tris pH7.5, 10 M urea at 55 °C for 50 min before re-probing with an anti-alpha tubulin (AbD Serotec) primary antibody as a loading control. Detection and visualisation was carried out as previously described.

Table 2-2: Primary antibodies used in western blot analysis.

An overview of the primary antibodies used in western blot analysis including the species from which they were derived, the manufacturing company and the concentration at which they were used.

Antibody name	Species	Company	Dilution factor	Type
Anti-ECM1 (C-12; sc-365946)	Mouse	Santa Cruz Biotechnology	1:2000	Polyclonal
Anti-MUC1 (C595; sc-59798)	Mouse	Santa Cruz Biotechnology	1:1000	Polyclonal
Anti-EGFR (A300-388-A)	Rabbit	Bethyl Laboratories	1:10,000	Monoclonal
Anti-phospho-EGFR (Tyr1068; D7A5)	Rabbit	Cell Signalling Technology	1:2000	Monoclonal
Anti-ERK (K-23; sc-94)	Rabbit	Santa Cruz Biotechnology	1:1000	Polyclonal
Anti-phospho-ERK (E4; Try204; Sc-7383)	Mouse	Santa Cruz Biotechnology	1:1000	Monoclonal
Anti-MET (4560)	Rabbit	Cell Signalling Technology	1:2000	Polyclonal
p-HGR R/c-MER (Y1234/Y1235; AF2480)	Rabbit	R&D Systems	1:2500	Polyclonal

2.12 Fixation of cell pellets for immunohistochemistry

When 80% confluence was reached in one T75 flask, cells were rinsed in PBS and detached from the flask using trypsin as outlined previously (section 2.3). Cells were re-suspended in 9 μl of the appropriate media and the cell suspension was transferred to a 15 ml falcon tube before centrifugation at 3000 rpm for 10 min at 4 °C. Media was aspirated and 5 ml of 4% formalin in PBS added to the pellet overnight at RT. Formalin was removed and discarded, and pellets were stored in 70% ethanol for up to 2 weeks. Pellets were removed intact from the falcon tubes, placed in histological cassettes (Simport), washed once in PBS, then stored in 70% ethanol prior to processing by Filomena Esteves in the core histology facility at the Leeds Institute of Medical Research. Processing was carried out using a Leica ASP200 Tissue Processor (Leica Biosystems) according to manufacturer's instructions. Specimens were dehydrated at 37 °C in a series of ethanol concentrations in water: 70% ethanol for 30 min; 80% ethanol for 30 min; 90% ethanol for 30 min; 95% ethanol for 30 min; 100% ethanol for 1h; 100% ethanol for 1h; and 100% ethanol for 1.5 h. Ethanol was then displaced from the samples using three separate incubations in xylene at 37 °C for 1 h, 1.5 h and 1.5 h, respectively. Specimens were infused with paraffin wax (CellPath Ltd) for 1 h at 65 °C a total of three times. Each sample was finally embedded in liquid paraffin wax (CellPath Ltd) heated to 60 °C, and once set, stored at RT until needed for sectioning.

2.13 Immunohistochemistry

Immunohistochemical (IHC) staining of FFPE tumour sections, cell pellets and tissue microarrays (TMAs) was carried out with the assistance of Filomena Esteves. Sections of paraffin embedded tumours were cut to 4 μm from formalin fixed paraffin embedded tissue blocks using a microtome (AS325 retraction; Thermo Shandon) and mounted onto Superfrost™ microscope slides. Previously sectioned TMAs were kindly gifted by Professor Martha Sanchez-Carbayo (University of the Basque Country, Spain). Slides were heated for 20 min at 70 °C then deparaffinised in 100% xylene (three times for 3 min each time), rehydrated in 100% ethanol (four times for 1 min each time) and finally washed once in water to remove excess ethanol.

Antigen retrieval was carried out to unmask epitopes in FFPE material. Slides were heated in a Menarini Antigen Retrieval Unit pressure cooker (Menarini Diagnostics) in 1x Access Revelation Buffer solution (Menarini Diagnostics) to 125 °C for 2 min. Slides were briefly washed in 1x Tris-Buffered Saline (TBS) Automation Wash Buffer (Menarini Diagnostics). Slides were then rinsed under running water before washing in TBS for 30 s and Menarini Wash Buffer (Menarini Diagnostics) for 30 s. Endogenous peroxidase and alkaline-phosphatase activity was blocked with 2 drops of Bloxall blocking solution (Vector Laboratories) for 10 min. Non-specific antigen binding was blocked by incubation in a 10% casein solution (Invitrogen) for 20 min.

The following primary antibodies were used: anti-ECM1 (C-12; sc-365946; Santa Cruz Biotechnology) and anti-MUC1 (C595; sc-59798; Santa Cruz) (Table 2-2). An IgG negative control was also used (Santa Cruz). Primary antibodies were diluted to 1:200 in antibody diluent (Invitrogen) and applied to slides for 1 h at RT. Slides were washed twice in 1x TBS automation wash buffer (Menarini Diagnostics). Post-primary HRP conjugation of antibodies was achieved using a Novocastra post-primary blocking kit (Leica Biosystems). Slides were incubated with 2 drops of post primary (rabbit anti-mouse IgG) reagent (Leica Biosystems) for 30 min, then washed twice in 1x TBS automation wash buffer (Menarini Diagnostics) for 5 min. Each slide was treated with 2 drops of polymer reagent (anti-rabbit Poly-HRP-IgG) (Leica Biosystems) to conjugate rabbit immunoglobulins to horseradish peroxidase. Slides were then washed twice in TBS for 5 min.

Detection was performed using DAB peroxidase substrate (Vector Laboratories). Two hundred microliters of ImmPACT™ DAB substrate was applied to each slide for 5 min. Each slide was transferred to a water reservoir for 5 min before counterstaining in haematoxylin for 30 s. Slides were then washed in running water for 1 min, Schotts water for 1 min, 100% ethanol once for 15 s, 100% ethanol once for 2 min and 100% ethanol twice for 3 min, and immersed in 100% xylene (three times for 3 min). Coverslips were mounted on the slides with DEPEX (Fisher Scientific UK Ltd) and slides were visualised using an Olympus Bx50 microscope (Olympus Optical Co.).

2.14 Immunofluorescence

Cells were grown on glass coverslips for use in immunofluorescence. Glass coverslips (Corning) were sterilised in 100% ethanol, air dried and placed in the centre of each well of a 6-well tissue-culture plate (Corning). When 80% confluence was reached, cells were detached from flasks and counted using the Beckman Coulter Z2 Cell and Particle Counter (Beckman Coulter) as previously outlined (section 2.4). 6 x 10^5 cells in a total volume of 2 ml of the appropriate medium were transferred to each individual well of a 6-well plate containing a coverslip. Cells were incubated overnight in a humidified incubator (Sanyo) at 37 °C in 5% CO_2 in air or until 70% confluency was reached.

Media was aspirated from the wells and cells were washed three times in PBS before fixation by the addition of 200 µl of 4% paraformaldehyde (PFA) for 20 min at RT. Cells were then permeabilised with 2 ml 0.1% Triton-X100 in PBS for 5 min at RT. Slides were then washed three times in PBS and non-specific antibody-binding sites blocked by incubating in 2 ml PBS containing 200 µl 0.1% MPS for 10 min.

The following primary antibodies were used: anti-ECM1 (C-12; sc-365946; Santa Cruz Biotechnology), anti-ECM1 (N17; sc-65086; Santa Cruz Biotechnology), anti-EGFR (199.12; AHR5072; Invitrogen), anti-EGFR (1005; sc-03; Santa Cruz Biotechnology), and anti-MUC1 (C595; sc-59798; Santa Cruz) (Table 2-2). Primary antibodies were prepared at a concentration of 1:100 in 0.1% milk powder solution (MPS) in PBS and centrifuged at 13,000 rpm for 5 min at RT to remove debris. Coverslips were removed from the wells and incubated with 200 µl of primary reagent, inverted on parafilm in a humidified chamber for 1 h RT, after which coverslips were returned to the 6-well dish and washed three times in PBS.

The following secondary reagents were used: Alexa Flour 488 goat anti-mouse IgG (H+L) (A11029; Thermo Fisher Scientific), Alexa Flour 594 goat anti-rabbit IgG (A11037; Thermo Fisher Scientific), Alexa Flour 594 chicken anti-goat IgG (A21468; Thermo Fisher Scientific), and TRITC-conjugated phalloidin and DAPI (FAK100 Actin Cytoskeleton / Focal Adhesion Staining Kit; Merck Millipore). Secondary reagents were prepared at a concentration of 1:500 in 0.1% MPS in PBS and centrifuged at 13,000 rpm for 5 min RT to remove debris. Coverslips were incubated with 200 µl of the appropriate secondary reagent, inverted on parafilm in a darkened humidified chamber for 1 h at RT. Coverslips were then returned to the

6-well dish and washed three times in PBS before being mounted on microscope slides with 50 µl Flouromount G (SouthernBiotech). Slides were left to set overnight and stored in the dark before viewing on an EVOS FL Cell Imaging System (Thermo Fisher Scientific).

2.15 Protein precipitation from media

Protein was extracted from cell media in order to determine if ECM1 was being secreted by the ECM1-high cell lines and to assess glycosylation state. When cells grown in a 75 cm^2 flask were 40% confluent, media was aspirated and replaced with serum free media. After 48 h media was collected from cells and 1.2 ml was transferred to a 1.5 ml micro-centrifuge tube and cleared of cell debris by centrifugation at 13,000 rpm for 10 min at 4 °C. The media was then passed through a 0.45 µm pore syringe filter (Corning) to remove any remaining cell debris. Two-hundred and fifty microliters of trichloroacetic acid (TCA) (100% W/V) was added to 1 ml of cleared media and samples were incubated at 4 °C for 10 min before being spun at 14,000 rpm for 5 min. The supernatant was removed and an acetone wash step conducted by adding 200 µl ice cold acetone, centrifuging at 14,000 rpm for 5 min, and removing and discarding the supernatant. This acetone wash step was repeated once more before the pellet was dried at 95 °C in a heat block for 10 min with the cap removed from the microcentrifuge tube. The dried pellet was either (1) re-suspended in 200 µl of 1x SDS loading dye in PBS, heated for five min at 90 °C and ECM1 protein expression analysed by western blotting as previously outlined or (2) was resuspended in 200 µl molecular biology grade water and vortexed for 5 min to resuspend prior to deglycosylation treatment (section 2.16).

2.16 Deglycosylation

Protein extracted from cultured media was isolated as outlined above. De-glycosylation of the secreted proteins was carried out using the GlycoProfile™ II Enzymatic In-solution N-Deglycosylation Kit (Sigma Aldrich) according to the manufacturer's instructions. In a 1.5 ml microcentrifuge tube, 90 µl of resuspended secreted protein or 90 µl of RNase B Standard Positive Control (Sigma Aldrich), were added to 5 µl Denaturant Solution (Sigma Aldrich) and vortexed briefly.

Samples were heated to 100 °C in a heat block for 10 min then allowed to cool to RT. To each sample, 5 μl 1x Reaction Buffer (Sigma Aldrich) was added and each sample was divided into two 50 μl aliquots. To one aliquot 5 μl (2.5 U) of PNG F Enzyme (Sigma Aldrich) was added, and to the second aliquot 5 μl of molecular biology grade water was added as an enzyme negative control. Samples were incubated in a water bath at 37 °C for 2 h, then heated to 100 °C for 10 min in a heat block to stop the reaction. Protein quantification was conducted using the Bradford protein quantification assay (BioRad) and ECM1 was analysed by western blotting as previously outlined.

2.17 Mutation screening and copy number analysis

In order to investigate potential molecular mechanisms associated with ECM1 over-expression, the *ECM1* gene was screened for the presence of somatic mutations and existing copy number data covering the region containing the *ECM1* gene was interrogated.

2.17.1 Mutation screening

Somatic mutations in the *ECM1* gene were examined in the Catalogue of Somatic Mutations in Cancer (COSMIC), an online database (http://cancer.sanger.ac.uk/cosmic) that holds information of somatic mutations in human cancers assembled from large-scale experiments such as The Cancer Genome Atlas (TCGA) and scientific literature. This identified potential mutational hotspot positions in 3 different exons that were deemed worthy of further investigation. Two mutations were found in COSMIC in two or more different tumour samples in exons 7 and 10 (hg19 coordinates: chr1:150483939 G>A, and chr1:150485894 C>T, respectively). A further two mutations were identified in COSMIC in exon 8 that were a single base pair apart (hg19 coordinates: chr1:150484937 G>A, and chr1:150484939 C>T).

The regions in exons 7, 8 and 10 of the *ECM1* gene containing the potential mutations of interest identified by interrogation of the COSMIC database were screened by PCR and direct sequencing. Primers were designed using Primer3 software (http://primer3.ut.ee/) [146]. The target specificity of each primer pair was

analysed using the online platform NCBI Primer-BLAST. Primers with the least ECM1 unspecific binding were selected. Primers were designed to include a minimum of 30 bases before and after the mutation site, and to give a total PCR product length of between 150 and 300 base pairs (b.p.). A list of the final primers selected can be found in Table 2-3.

PCR was performed in a volume of 25 µl containing 1x AmpliTaq Gold buffer, 2.5 mM $MgCl_2$, 0.2 mM dNTPs, 5 pmoles of each primer (Table 2-3), 2.5 U AmpliTaq Gold (Applied Biosystems) and 10 ng of template DNA extracted as previously described. The following cycle parameters were used: 95 °C for 5 min followed by 35 cycles of 95 °C for 30 s; 60 °C for 30 s; and 72 °C for 30 s. Samples were then incubated at 72 °C for 10 min and chilled to 4 °C. To check product length and efficiency of amplification gel electrophoresis was used. A gel was cast using 2% agarose (w/v) in 1x Tris-Boric acid-EDTA buffer (TBE) (BioRad) containing 0.25 µg/ml ethidium bromide (Severn Biotech Five microlitres of PCR product was mixed with 5 µl Gel loading dye (NEB) and loaded on the gel. Ten microliters of Quick-Load® 100 bp DNA Ladder (NEB) was also loaded as a reference to determine the molecular weights of the PCR products. The gel was electrophoresed in 1x TBE buffer at 90 V for 40 min and imaged using a Bio-Rad ChemiDoc MP.

PCR products were treated with Illustra ExoProStar 1-step (Fisher Scientific) to remove excess deoxyribonucleotide triphosphates and primers. One microliter of ExoProStar (GE Healthcare Life Scienes) was added to 2.5 µl of PCR product and incubated at 37 °C for 15 min before heat inactivation at 80 °C for 15 min. Sanger sequencing was carried out in 96-well PCR plates using the primers listed in Table 2-3 and a BigDye Terminator V1.1 Cycle Sequencing Kit (Applied Biosystems). Reactions contained 0.16 µM of primer (forward or reverse), 1 µl ExoProStar-treated PCR product, 0.25 µl 1x BigDye Terminator Ready Reaction Mix V1.1 (Life Technologies) and molecular biology grade water to give a total volume of 10 µl. The following cycle parameters were used: 96 °C for 1 min followed by 25 cycles of 96 °C for 10 s; 50 °C for 5 s; and 60 °C for 4 min.

Reactions were cleaned-up using precipitation by the addition of 1 µl sodium acetate (3 M) and 25 µl ice cold 100% ethanol and incubation at RT for 30 min. DNA was pelleted by centrifuging at 1800 x g for 1 min in a Beckman Allegra X12R benchtop centrifuge (Beckman Coulter) and the supernatant was discarded by

inverting the reaction plate. Pellets were washed in 70 μl of 70% ethanol and plates centrifuged at 1650 x g for 15 min at 8 °C. The plates were inverted to remove ethanol and pellets were air dried prior to resuspension in 15 μl HiDi™ formamide (Invitrogen Life Technologies). Prior to capillary electrophoresis on an ABI PRISM 3100 Genetic Analyzer (Applied Biosystems) samples were heated for 1 min at 95 °C and snap cooled on ice. Sequencing data was analysed using 4Peaks (A. Griekspoor and Tom Groothuis, mekentosj.com) and visual inspection of the electropherograms.

Table 2-3 Primers used for PCR and Sanger sequencing analysis of ECM1.

An overview of all primers used in PCR and mutational screening by Sanger sequencing of regions of exons 7, 8 and 10 of the *ECM1* gene.

Primer Name	Sequence (5' -> 3')	Melting temp (°C)	Expected product length (b.p.)
ECM1 Ex7 F1	CTGGGAGGAAGGCAGGAATG	68.1	186
ECM1 Ex7 R1	CTGGTAGTGTGGCTGGGGAG	67	
ECM1 Ex7 F2	GGAGGAAGGCAGGAATGTGG	68	247
ECM1 Ex7 R2	CAGGAGGGAAAGGCAGCTC	66.3	
ECM1 Ex8 F1	GAGAGAAGGGGCCAAGTGTC	65.1	297
ECM1 Ex8 R1	GTGGGGAAGGACTAGGCAAC	64.7	
ECM1 Ex8 F2	CTGTGACCGGGAGTATGCTG	60.1	198
ECM1 Ex8 R2	TGCTTGGTGAGAACTCTTTGGT	64.9	
ECM1 Ex10 F1	ACGTGGCTCTAGTGTCTGGA	62.6	169
ECM1 Ex10 R1	GTTCAGATGGGTGGGGCAG	68	

2.17.2 Copy number analysis

Whole genome copy number analysis was performed on a panel of 45 bladder tumour-derived cell lines prior to the start of this study using Genome-Wide Human SNP 6.0 Arrays (Affymetrix, Santa Clara, CA USA) (Hurst et al, unpublished data). Five hundred nanograms of DNA from each cell line was labelled and hybridised according to the array manufacturer's instructions. Data was analysed and viewed using Partek® Genomics Suite® software, version 6.6 (Partek Inc., St. Louis, MO, USA).

2.18 Analysis of ECM1 mRNA isoform expression

Analysis of ECM1 mRNA isoform expression was carried out in order to determine which ECM1 isoforms are expressed by the ECM1-high cell lines as well as an additional 4 bladder tumour derived cell lines not classified into the ECM1-high subtype, and a pooled normal human urothelial sample (NHU-Pool). Primers were designed using reference sequences for each isoform of ECM1 (ECM1a, ECM1b, and ECM1c) from The National Center for Biotechnology Information (NCBI) gene database (Appendix F). Using each isoform's individual NCBI reference sequence, genomic sequences were cross referenced with exon sequences as denoted on the Ensembl genome browser in order to identify differences between exonic and intronic regions in the different isoforms. This revealed that isoform ECM1b did not contain exon 7, and ECM1c had an extended form of exon 4. Using this information, candidate primers were designed using Primer3 software (http://primer3.ut.ee/) [146] that would generate products of differing sizes for each isoform. The target specificity of each primer pair was analysed using the online platform NCBI Primer-BLAST. Primers with the least ECM1 unspecific binding were selected. Details of these primers are given in Table 2-4.

PCR was performed using the selected primers and cDNA generated from total RNA as previously described (section 2.7). Reactions contained 1x Q5 Reaction Buffer (New England Biolabs, NEB), 200 µM dNTPs, 0.05 µM forward primer, 0.5 µM reverse primer, 1.25 U Q5 Hot Start High-Fidelity DNA Polymerase (NEB) and 1 µl cDNA sample in a total reaction volume of 25 µl made up with molecular biology grade water. One microliter of molecular biology grade water was used in place of cDNA for PCR negative controls. The following cycle parameters were used: 98 °C for 30 s followed by 30 cycles of 98 °C for 10 s; 58 °C for 30 s; and 72 °C for 30 s. Samples were then incubated at 72 °C for 2 min and chilled to 4 °C.

PCR products were analysed using gel electrophoresis to check product length and efficiency of amplification. Five microliters of PCR product was mixed with 5 µl of Gel loading dye (NEB) and loaded on a 2% agarose-TBE gel. The gel was electrophoresed in 1x TBE buffer at 90 V for 40 min and imaged using a Bio-Rad ChemiDoc MP.

Table 2-4: Primer pairs used to determine ECM1 isoform expression and the expected product size for each isoform.

Primer Pair	Primer Name	Sequence (5' -> 3')	T_m (ºC)	Exon location	Product Length (bp)		
					ECM1a	ECM1b	ECM1c
1	1F	GGATCACCCTGACTCCTCTC	58.75	3	130	130	211
	1R	CTTTTCAGCAGGGAGTTGGG	58.59	5			
2	2F	CCCCACCCCTATCCCGAA	60.04	3	0	0	144
	2R	GTGAGCAGCCCACCCTTT	59.88	4			
3	3F	CACAAACCGCCTAGAGTGTG	58.85	6	204	0	204
	3R	CCCGAGGAAATATCAGGCTG	57.82	7			
4	4F	CACAAACCGCCTAGAGTGTG	58.85	6	447	72	447
	4R	GCATACTCCCGGTCACAGTA	58.89	8			
5	5F	CCCAACTATGACCGGGACAT	59.16	8	136	136	136
	5R	GGGCAGTCATGTTGTGGATC	58.90	9			
6	6F	GCCTAGAGTGTGCCAAACTT	58.10	6	541	166	541
	6R	ATGTCCCGGTCATAGTTGGG	59.16	8			

2.19 Puromycin selection dose curves

The lowest concentration of puromycin required to kill 100% of cells was determined for each cell line chosen for ECM1 knockdown experiments (section 2.20). Cells were cultured as previously described and counted using the Beckman Coulter Z2 Cell and Particle Counter (Beckman Coulter). Cells were seeded at 250,000 cells per well in two 6 well dishes for each cell line, and cultured for 48 h before 2 ml of media containing puromycin was introduced across a range of concentrations (0, 0.1, 0.2, 0.3, 0.4, 0.5, 0.75, 1, 1.5, 2, or 3 μg/ml). Media containing puromycin was changed every 3 days. After 7 days cells were rinsed twice with PBS and 0.5 ml of methylene blue added to each well for 15 minutes. Plates were rinsed three times in water or until the water ran clear and were then dried upside down. Images were taken with a 13 megapixel autofocus camera (Huawei). The lowest concentration of puromycin that killed all of the cells was chosen as the selection dose for short hairpin RNA (shRNA) knockdown studies.

2.20 shRNA knockdown of ECM1

shRNA plasmid DNAs were purchased from Sigma Aldrich. shRNA sequences were cross referenced with ECM1a, ECM1b and ECM1c gene sequences obtained from NCBI and analysed using NCBI BLAST. Three plasmids targeting all three isoforms of ECM1 and predicted to have the least ECM1 unspecific binding were selected. Details of these shRNA plasmids can be found in Table 2-5 and a plasmid map of the vector can be found in Figure 2-1.

Table 2-5: shRNA constructs used for ECM1 knockdown.

The sequence for each shRNA used in the ECM1 knockdown studies, the regions they target, and their abbreviated names are shown. CDS refers to coding DNA sequence, 3'UTR refers to the three prime un-translated region.

Clone ID	Target Sequence (5' -> 3')	Vector	Region	Abbreviation in text
TRCN0000059575	CAACTGCTTCAACATCAATTA	pLKO.1	CDS	KD1
TRCN000037051	CTGAACACTCATTACACTAAA	pLKO.1	3'UTR	KD2
TRCN0000059576	CGCTGCTGTGACCTGCCATTA	pLKO.1	CDS	KD3

Glycerol stocks of shRNA plasmids were made using an Agilent General Cloning kit as per manufacturer's instructions. Two-hundred microliters of XL1-Blue Competent Cells (Agilent) were gently mixed with 1.85 µl β-Mercaptoethanol (1.42 M, Agilent) and left on ice for 10 min. Fifty microliters of the competent cells were added to 14 ml BD Falcon polypropylene round-bottom tubes and 20 ng shRNA plasmid (Sigma) was added before incubation on ice for 30 min. Cells were heat-shocked in a 42 °C water bath for 45 s before being placed immediately on ice for a further 2 min. Off ice, 500 µl Super Optimal broth with Catabolite repression (SOC) medium was added to each tube and samples were incubated at 37 °C for 45 min in a shaking incubator. Ten microliters of transformed cells were plated on 1.5% agar (w/v) plates in Lysogeny broth (LB)* (1% Tryptone (w/v); 1% NaCl (w/v); 0.5% yeast extract (w/v)) containing 1 µg/ml ampicillin that were prepared 12 h previously. Plates were incubated at 37 °C for 12 h.

Isolated colonies of transformed cells for each of the shRNAs were picked and used to inoculate 5 ml of LB containing 1 µg/ml ampicillin which was then incubated at 37 °C for 8 h in a shaking incubator. One millilitre of cell culture was added to 150 ml LB containing 1 µg/ml ampicillin and incubated for a further 12 h at 37 °C in a shaking incubator. The cell cultures were centrifuged at 6000 rpm for 20 min at 4 °C in a Beckman J2-21 floor model centrifuge (Beckman Coulter) and supernatant discarded. Plasmids were isolated from cell pellets a using PureYield™ Plasmid Maxiprep System (Promega) according to the manufacturer's instructions. Pellets were re-suspended in 12 ml of re-suspension buffer (Promega), before 12 ml of lysis buffer (Promega) was added. Cells were lysed for 2 min before 12 ml of neutralising buffer (Promega) was added and samples centrifuged at 14000 x *g* for 20 min at 21 °C. The supernatant was collected and purified by filtering through a PureYield™ Clearing Column (Promega). The flow through was added to a PureYield™ Maxi Binding Column (Promega) stacked on a vacuum manifold and maximum vacuum was applied. Twenty millilitres of Column Wash was added to the binding column and the vacuum applied until the membrane was dry. DNA was eluted into 1.5 ml microcentrifuge tubes by adding 1 ml of nuclease-free water to the binding column. DNA was quantified using a Nanodrop 8000 UV-Vis

* The acronym LB can also interpreted as Luria broth, Lennox broth, or Luria-Bertani medium, however I am using the term "Lysogeny broth" as originally intended by its creator Giuseppe Bertani [147].

spectrophotometer (LabTech) measuring light absorbance at a wavelength of 260 nm in order to obtain the samples' concentrations.

Cell lines from the ECM1-high subgroup were chosen for mRNA knockdown and functional studies. These cell lines were HT-1376, LUCC4, HT-1197 and 647V. Lentiviral particles containing the purified shRNA plasmids were synthesised in HEK 293-FT cells to transduce these cell lines. Briefly, in a 1.5 ml microcentrifuge tube, 750 μl opti-MEM medium, 1 μg PLKO.1 shRNA plasmid, 1 μg pCMV-dR8.2 dvpr packaging plasmid, 200 ng pCMV-VSV-G envelope plasmid and 8 μl TransIT-293 were mixed gently prior to incubation at RT for 30 min.

HEK 293-FT cells were cultured under standard conditions (section 2.3) and split into one 25 cm^2 flask for each transduction with ECM1 knockdown shRNAs or with one of the three control vectors representing a scramble control vector in which the shRNA does not target any known genes, or a non-hairpin (NHP) control which does not form a hairpin when transcribed (Sigma). Once 60% confluence was reached the lentiviral components described above were added to each flask and rocked gently for 1 minute to allow mixing. Cells were incubated overnight before the media was changed. Media was harvested at 24 h and 48 h and the harvests were pooled. Pooled media was filtered through a 0.45 μm pore syringe filter to remove cell debris, and divided into 1 ml aliquots. Aliquots were frozen at -80 °C until needed.

Cell lines to be transduced were cultured in 25 cm^2 flasks as previously outlined. Once 60% confluence was reached media was aspirated and 4 ml of media containing 1 ml shRNA lentivirus was added. The cell lines HT-1376, HT-1197, and 647V were incubated with lentivirus overnight before media containing virus was removed and fresh media was added to each flask. Cells were cultured for a further 24 h prior to puromycin selection. For the LUCC4 cell line, cells were incubated in media containing lentivirus for 5 h before virus was removed from the flasks and media was changed. Cells were incubated for 24 h in media without virus, before virus was re-introduced for a further 5 h. Cells were then incubated for 72 h in media containing no virus before puromycin selection.

Cells were incubated in media containing selection concentrations of puromycin as determined previously for 7 days or until all cells in the control flask that had not

been infected with virus were dead. After this, cells were maintained as previously outlined with the addition of maintenance concentrations of puromycin which were determined to be half that of the selection concentration. Cells were removed from puromycin for 24 h prior to lysate (protein or RNA) preparation.
in ECM1 overexpressing samples.

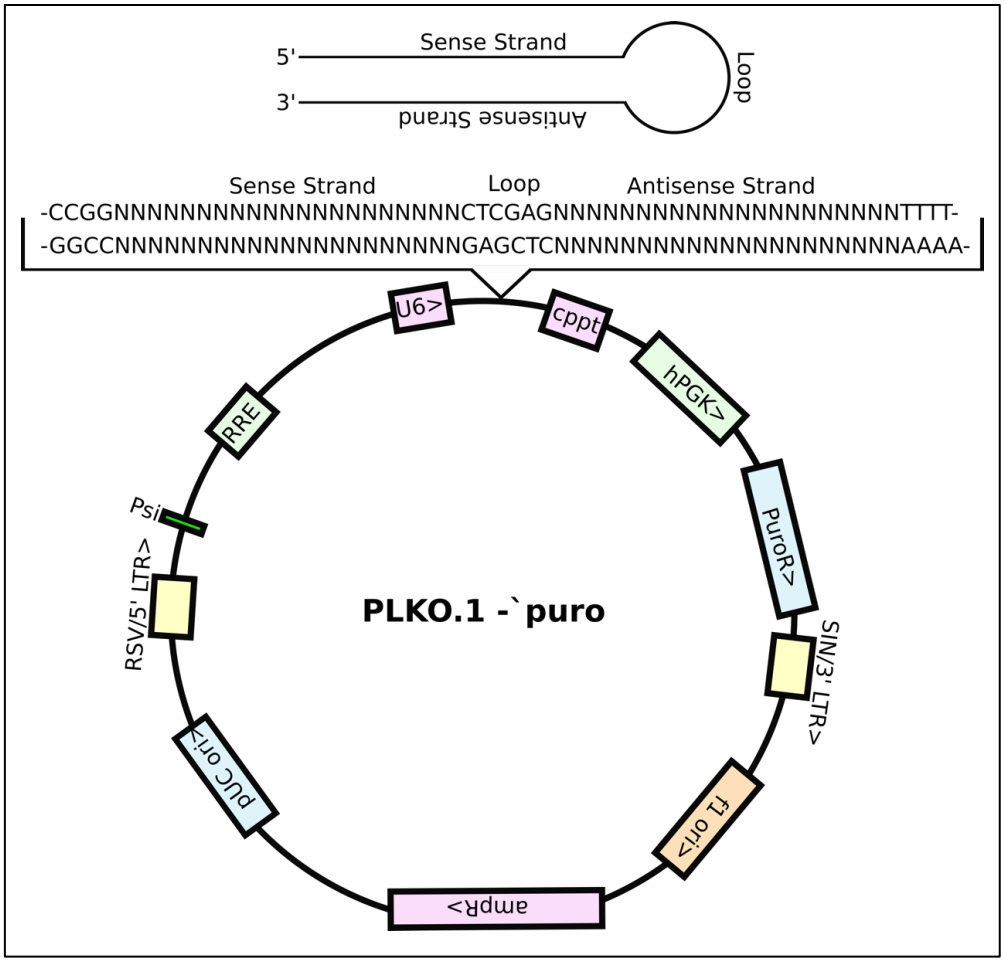

Figure 2-1: A schematic representation of the *pLKO.1* shRNA carrying vector used in this study.

As well as shRNA targeting ECM1 or controls, the following genes were also present in the plasmid: central polypurine tract (*cppt*) which improves transduction efficiency as it facilitates the lentiviral preintergration complex (*PIC*) import into the host cell's nucleus; human phosphoglyceratekinase (*hPGK*) eukaryotic promoter which drives transcription of the puromycin resistance gene (*puroR*) for selection of cells successfully transduced with the pLKO.1 plasmid; SIN/3' LTR 3' - self inactivating long terminal repeat; f1 origin (*f1 ori*) of replication; ampicillin resistance (*ampR*) gene for selection of the presence of the pLKO.1 plasmid in bacterial cells during the generation of glycerol stocks ; pUC bacterial origin of replication (*pUC ori*); 5' LTR - 5' long terminal repeat; Psi - RNA packaging signal; RRE - Rev response element; U6 promoter region that drives transcription and thus the generation of the shRNA transcripts by RNA polymerase III. This figure was adapted from "Mission RNAi: Vector Maps" (Sigma) retrieved 25.07.18 from: <https://www.sigmaaldrich.com/life-science/functional-genomics-and-rnai/shrna/library-information/vector-map.html>.

2.21 Growth curve

Cells were seeded at a density of 5 x 10^3 cells per well in 2 ml media in 6-well plates. Plates were incubated under standard conditions and media was changed every three days. Cells were counted on days 1, 4, 7, 10, 13, 16, 19 and 21 as previously outlined in section 2.4. Triplicate wells were plated for each cell line and readings were carried out in triplicate per well.

2.22 Wound healing assay

Cells were seeded in triplicate into 6-well plates at a cell density of 5 x 10^5 cells per well in 2 ml media appropriate for each cell line. Cells were incubated under standard conditions overnight or until 100% confluence was reached. Samples to be treated with recombinant ECM1 were seeded in triplicate into 6-well plates at a cell density of 4 x 10^5 cells per well in 2 ml media appropriate for each cell line. Cells were incubated under standard conditions for 8 h. Recombinant ECM1 (R&D Systems™: 3937-EC) was reconstituted in PBS to 100 μg/ml. Recombinant ECM1 was added to the samples at a final concentration of 100 ng/ml, 200 ng/ml, 300 ng/ml, 400 ng/ml, 500 ng/ml, 750 ng/ml, 1 μg/ml, or 2 μg/ml in 2 ml media appropriate for each cell line. Cells were incubated under standard conditions overnight when 100% confluence was reached. A sterile 30 µl pipette tip was used to create a cross patterned scratch in the confluent monolayer in each well. Images were captured using a Zeiss Axiovert 10 microscope with a Canon Powershot G6 7.1 Megapixel camera at 0 h, 24 h and 48 h. Plates were marked to ensure the images were captured across the same region of the scratch at each time point. Three images were taken per well.

Images were analysed using ImageJ software with the MRI wound healing macro add on to calculate wound area. Percentage differences in wound area over time were calculated as follows:

$$\frac{(wound\ area\ at\ 0\ h - \ wound\ area\ at\ 24\ h\ or\ 48\ h)}{wound\ area\ at\ 0\ h} \times 100$$

Ordinary one-way ANOVA with post analysis multiple comparisons was performed on the data to determine statistical significance between samples using GraphPad Prism 7.0 software.

2.23 Transwell assay

Falcon® Permeable Supports with 8.0 µm pore size transparent PET membranes (Corning) were placed in 24 well plates containing 500 µl serum-supplemented media appropriate to each cell line (Table 2-1) to act as a chemoattractant and encourage cell migration through the insert pores. Cells cultured in 75 cm^2 flasks were detached when 70% confluency was reached and counted as described in section 2.4. Cells were seeded into inserts at 5 x 10^4 cells per well in 200 µl serum free media and incubated in a humidified incubator (Sanyo) under standard conditions for 24 h.

Media was aspirated from both the wells and inserts, and each insert was washed once in PBS. A cotton swab was used to remove all cells from the interior surface of each insert and cells were fixed by the addition of 4% formalin. Plates were incubated at RT for 15 min to fix cells. Formalin was aspirated and inserts were washed twice in PBS. Inserts were incubated in 0.2% crystal violet in 2% ethanol for 10 min at RT. Inserts were airdried and viewed using phase-contrast light microscopy. Cells were counted from five random 1 mm^2 sections of the insert and an average reading taken.

2.24 Co-immunoprecipitation

SureBeads™ Protein G and Protein A Magnetic Beads (Biorad) were prepared according to the manufacturer's instructions. One hundred microliters of beads were transferred to 1.5 ml microcentrifuge tubes and washed three times in PBS-T by adding 200 µl PBS-T vortexing briefly, concentrating the beads using a magnet and removing the supernatant. One to two micrograms of antibody was diluted to a final volume of 200 µl with molecular biology grade water. Diluted antibodies were added to washed beads and then rotated at RT for 1 h. The following antibodies were used: anti-ECM1 (C-12; sc-365946; Santa Cruz Biotechnology), anti-EGFR (A300-388A, Bethyl Laboratories Inc.), anti-BAD (C-20, sc-943, Santa Cruz), and anti-Sv-

40 T Ag (sc-147, Santa Cruz). After 1 h tubes were removed from the tube rotator and the beads were concentrated using a magnet. The supernatant containing unbound antibody was removed and the beads were washed four times in PBS-T as previously described.

Cells were cultured to 70-90% confluence, medium was aspirated and cells were rinsed twice in ice cold PBS. If crosslinking was conducted, 10 ml of 1 mM 3,3'-Dithiobis(sulfosuccinimidylpropionate) (DTSSP) was added to each flask for 30 min, followed by a 15 min treatment with 1M Tris 7.5 pH to stop the reaction. Cells were rinsed once with ice cold PBS to remove traces of DTSSP and Tris. All cells were lysed on ice in RIPA buffer and quantified using the Bradford protein quantification assay (BioRad) as previously outlined (section 2.10).

One hundred microliters (300-500 µg) of protein lysate was added to the antibody-bound beads and samples were rotated at 4 °C overnight. Beads were magnetised and supernatant removed. Beads were washed four times in PBS-T. Forty microliters of 1x Laemmli buffer (Sigma) was added and beads where briefly vortexed before being incubated at 70 °C for 10 min to elute the bound protein. Beads were concentrated using a magnet and the supernatant containing immunoprecipitated (IP) protein was run on a western blot as previously outlined (section 2.11).

2.25 Phospho-RTK array analysis

Phosphoarray analysis was carried out using the Human Phospho-Receptor Tyrosine Kinase Array Kit (R&D Systems™) as per manufacturer's instructions. Cells were cultured to 70-90% confluence. For "serum-free" samples, samples were incubated in serum free media for 24 h prior to harvesting protein lysates. For ECM1-treated samples, samples were incubated in serum free media for 24 h and treated with 1 µg/ml recombinant ECM1 (R&D Systems™: 3937-EC) for 5 min prior to harvesting. Forty microliters of protease inhibitor (P8340; Sigma) was added to 2 ml of Lysis Buffer 17 (R&D Systems™). Medium was aspirated from the cells and 500 µl of Lysis Buffer 17 was added to each 75 cm^2 flask. Cells were incubated with the lysis buffer on ice on a rocking platform for 30 min. A cell scraper was used to detach lysed cells from the flask, and the crude lysate was transferred into a microcentrifuge tube and spun at 14,000 g for 5 min in a microcentrifuge to clear.

The supernatant was transferred into a new microcentrifuge tube on ice and quantified using the Bradford protein quantification assay (BioRad) as previously outlined (section 2.10).

All reagents were brought to RT prior to use and 2 ml of Array Buffer 1 (R&D Systems™) was added to each well of a four well array dish provided with the kit. Array membranes were incubated in Array Buffer 1 for 1 h on a rocking platform. 300 μg of total protein was prepared in a final volume of 1.5 ml with Array Buffer 1 (R&D Systems™). Array Buffer 1 was removed from the array dish, and membranes were incubated with protein lysates at 4 °C overnight on a platform rocker. Membranes were removed from the four well array dish and placed in individual plastic dishes with 20 ml of 1x Wash Buffer (R&D Systems™) and incubated for 10 min at RT on a rocking platform. The Wash Buffer was removed from each dish, and a further two wash steps were carried out in 1x Wash Buffer (R&D Systems™).

Anti-phospho-tyrosine HRP detection antibody (R&D Systems™) was diluted 1:10,000 in 1x Array Buffer 2 (R&D Systems™) and 2 ml added to each well of the four-well dish. Membranes were transferred to the four-well dish and incubated with the detection antibody for 2 h at RT on a rocking platform. The array membranes were removed from the four well array dish and placed in individual plastic dishes and washed three times in 20 ml of 1x Wash Buffer (R&D Systems™) as previously described.

The bound HRP labelled antibody was visualised by chemiluminescence using the Chemi Reagent Mix (R&D Systems™) and imaged with a ChemiDoc MP System. Images were analysed using Image J Software (SciJava).

2.26 Microarray analysis of ECM1 knockdown cells

Total RNA was harvested as previously outlined. RNA was treated to remove any contaminating DNA prior to analysis using the Affymetrix GeneChiP® Human Transcriptome Array 2.0. DNase reactions contained 6 μg of total RNA, 40 U RNase OUT™, 4 μl of 10x Digest buffer, and 3 U DNase 1, in a total volume of 36 μl made up with molecular biology grade water. Reactions were incubated at RT for 15 min before 4 μl of 25 mM EDTA was added to stop the reaction. The volume of

each sample was adjusted to 100 μl with molecular grade water prior to enzymatic clean-up using a Qiagen RNeasy kit (Qiagen) as follows. To each sample 350 µl buffer RLT (Qiagen) containing 1% beta-mercaptoethanol and 250 µl 100% ethanol were added to each sample. Samples were transferred to an RNeasy MinElute spin column sitting in a collection tube (Qiagen) and centrifuged for 30 s at 8000 x *g* and flow through discarded. Samples were washed by adding 500 µl RPE Buffer (Qiagen) to the columns and centrifuging at 8000 x *g* for 30s in a microcentrifuge. This wash step was repeated using another 500 µl RPE Buffer (Qiagen) but samples were spun at 13,000 x *g* for 2 min. Columns were then transferred to new collection tubes and centrifuged at 13,000 x *g* for 1 min to remove excess wash buffer and dry the columns. The columns were then placed into new 1.5ml collection tubes and 30 µl dH_2O added. Samples were spun in a microcentrifuge at 13,000 x *g* for 1 min to elute the RNA. RNA was quantified using a Nanodrop 8000 spectrophotometer measuring light absorbance at a wavelength of 260 nm.

The integrity of the RNA was also examined on a 2200 TapeStation (Agilent) using the RNA ScreenTape System according to manufacturer's instructions. Briefly, to a 0.2 ml PCR tube, 5 μl of RNA ScreenTape buffer (Agilent) and 1 μl of RNA or ScreenTape Ladder (Agilent) was added. Samples were heated to 72 °C for 3 min in a PCR block then immediately cooled on ice for 2 min before being analysed on a 2200 Tapestation (Agilent) system. An example of a TapeStation profile can be found in the Appendix J.

cDNA was synthesised and qRT-RCR was conducted as previously outlined (sections 2.7 and 2.8) to confirm levels of ECM1 prior to microarray analysis. Microarray analysis was conducted by Tepnel Pharma Services (Hologic). Reverse transcription and amplification of total RNA was conducted according to the manufacturer's instructions using the Affymetrix GeneChip® WT PLUS Reagent Kit. cDNA was quantified using optical density (Nanodrop), normalised and hybridised onto Affymetrix GeneChiP® Human Transcriptome Arrays 2.0 for 16 h at 45 °C. Microarrays were washed and stained according to manufacturer's instructions with the Affymetrix GeneChip® Hybridisation, Wash and Stain Kit on the Affymetrix Genechip® Fluidics Station 450 and scanned using an Affymetrix Genechip® 7G microarray scanner. Quality control was performed on the data using Affymetrix Expression Console Software.

The Bioconductor Linear Model for Microarray Analysis (LIMMA) package was used to determine genes differentially expressed between the ECM1 knockdown and control samples. These genes were analysed using MetaCore (Thomson Reuters) to determine altered pathways.

2.27 Drug treatments and CellTitre® Blue cell viability assay

Between 3000 and 7000 cells were plated in 100 μl media in each well of flat bottomed 96-well plate (Corning) in order to achieve 80% confluency in the untreated control at the end of the 7-day assay. For the LUCC4 cell line, Corning Primaria flat bottomed 96-well plates were used. Cells were incubated under standard conditions overnight. After 24 h media was aspirated from each well, and fresh media containing the appropriate concentration of erlotinib (Cayman Chemicals) and/or tivantinib (Selleckchem) was added in 0.1% DMSO. Five replicate wells were used for each concentration of drug. Media containing the appropriate drug concentration was changed after 72 h. After 110 h total incubation time, 20 μl of CellTitre-Blue warmed to 37 °C was added to each well and the plate was incubated in a humidified incubator (Sanyo) at 37 °C in 5% CO_2 in air for 2 h in the absence of light. Fluorescence was measured on a Berthold Mithras LB 940 Multimode microplate reader with excitation settings at 540 nanometres and emission at 590 nanometres. Wells containing media and no cells were used as a control to which readings were blanked, and results were normalised to wells containing cells treated with 0.1% DMSO but no drug. Dose response equations were calculated and curves were generated using GraphPad Prism® in order to determine IC_{50} values. Isobolograms were also generated using GraphPad Prism® in order to assess additive effects of combination treatment.

Chapter 3
Identification of a Basal/Squamous subgroup of bladder cancer cell lines with high ECM1 and MUC1 expression

3.1 Introduction

Muscle-invasive bladder cancer (MIBC) represents 25% of all bladder cancers and is a very heterogenous disease. MIBC accounts for the majority of patient deaths from bladder cancer and treatment for these patients has changed little over the past three decades. The standard of care remains platinum-based chemotherapy but response rates are less than 50% and relapse is common. Checkpoint immunotherapy was recently approved for second-line therapy in patients whose first-line chemotherapy has failed, but the reported overall response rates are modest, and robust predictive biomarkers are still currently lacking.

Several studies have assessed MIBC at the molecular level using transcriptome profiling of bladder tumours in order to define molecular subtypes that may facilitate the stratification of patients into more relevant prognostic and treatment groups, and improve treatment options by identifying new approaches to therapy [81]. Six main research groups have now described molecular subtypes of MIBC: Baylor [85], UNC [74], CIT-Curie [86], MDA [75], Lund [87] and TCGA [32]. A recent study by Kamoun *et al*. (manuscript in press), used a consensus subtyping system to unify the subtypes from these published MIBC molecular classification systems into six molecular classes of MIBC: Luminal Papillary, Luminal Non-specified, Luminal Unstable, Stroma-rich, Basal/Squamous and Neuroendocrine-like (doi: http://doi.org/10.1101/488460). The potential clinical utility of such molecular subtyping has also been highlighted by a limited number of studies that have related molecular stratification to chemotherapy and immunotherapy [75, 76, 79, 148].

A few studies have also profiled bladder tumour-derived cell line panels [83, 88, 89]. These cell line panels represent a valuable resource for use as model systems in which to test therapeutic approaches. Molecular profiling of such panels is essential in order to ensure that the molecular features of the cell lines are fully characterised and that these characteristics faithfully reflect those present in the tumours from which they were derived. Prior to the start of this study, our laboratory assembled a panel of 45 bladder tumour-derived cell lines and carried out genome-wide gene

expression analysis of this panel using GeneChip Human Genome U133 Plus 2.0 Arrays (Hurst *et al*., unpublished data). Several of these cell lines have not been included in the previous studies that have evaluated the presence of clinically relevant subgroups in bladder tumour-derived cell line panels and the data from our panel therefore represents a novel resource. Preliminary analysis of this expression data using non-negative matrix factorisation (NMF) analysis classified the cell lines into 5 molecular subgroups (subgroups 1-5) (Hurst *et al*., unpublished data). This background data is presented in the current Chapter along with further analysis of two genes, extracellular matrix protein 1 (ECM1) and mucin 1 (MUC1), which were amongst a subset of genes significantly upregulated in subgroup 2, a potential new subset of basal-squamous bladder cancers.

3.2 Results

3.2.1 Background data - Molecular subgroups of bladder tumour-derived cell lines

Data pre-processing and NMF analysis were carried out using web-based modules available via GenePattern (Broad Institute) [149]. Normalised probe intensity data was pre-processed to remove microarray platform noise and genes that have very little variation. The pre-processed dataset consisting of 26,959 probes was used as input for the NMF module in order to identify the number of likely clusters in the cell line dataset. NMF (Brunet approach) [150] was carried out for $k = 2$ to $k = 7$ clusters with 20 clusterings per value of k, 2000 NMF iterations per clustering, and the error function set to “divergence”. The most appropriate number of clusters (i.e. subgroups) was selected as $k = 5$ based on the maximal value of the cophenetic correlation coefficient which was 0.9875 for $k = 5$ (Figure 3-1).

The alignment of the 5 NMF-assigned cell line subgroups to previously reported subtypes of bladder cancer was first of all examined. Marker sets that define the MIBC subtypes described by the TCGA [32], LUND group [87], and the UNC group [74] were used to construct heatmaps using the cell line expression data (Figure 3-2). Mutation status for *FGFR3* and *TP53* was also available and was overlaid on the heatmaps.

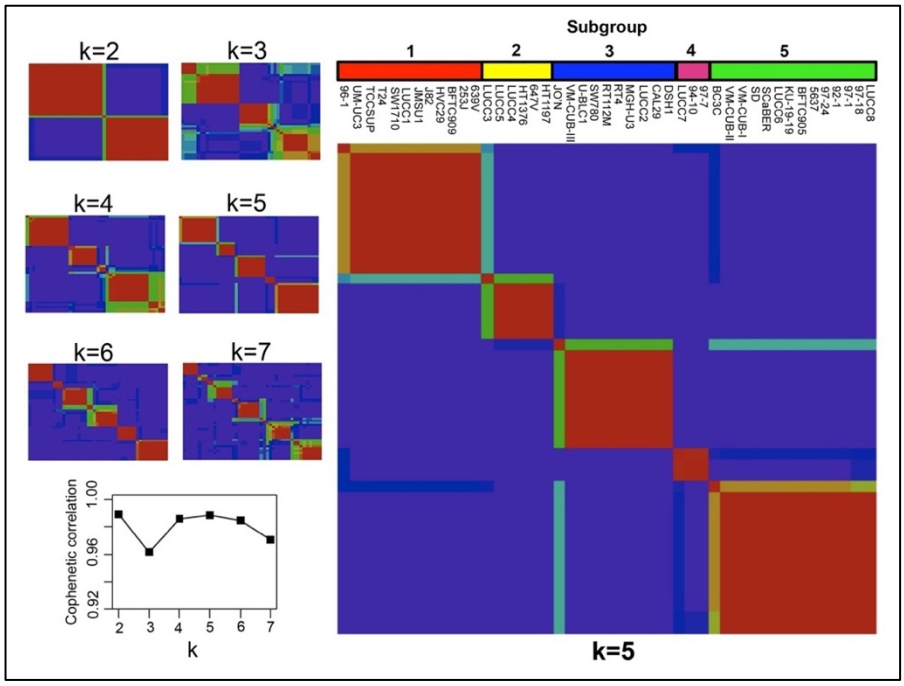

Figure 3-1: Unsupervised clustering using non-negative matrix factorisation (NMF) analysis.

NMF was performed on genome-wide gene expression microarray data for forty-five bladder tumour-derived cell lines. Cophenetic correlation coefficients were calculated for the data in a two to seven cluster solution. A recorded consensus matrix from a five-cluster solution of the cell line microarray data had the highest cophenetic correlation. Heatmaps for each consensus matrix were created. Red indicates agreement of the assigned clustering while blue indicates no agreement as samples were never assigned to the same cluster.

Subgroup 3 cell lines have features of luminal bladder tumours expressing high levels of markers associated with luminal differentiation (GATA3, FOXA1, PPARG, ELF3, KRT20 and uroplakins). Cell lines in this subgroup also have high expression of an FGFR3-associated gene expression signature and *FGFR3* mutations and fusions are more frequent than in any of the other subgroups. The other cell line subgroups exhibit features of basal-squamous tumours and have much lower levels of expression of the luminal markers that are characteristic of subgroup 3. *TP53* mutations are frequent in these four basal subgroups of cell lines and expression of the AXL tyrosine kinase receptor is elevated. Subgroups 2, 4 and 5 express higher levels of basal-squamous markers including KRT5, KRT14, KRT6A and KRT6B, and the tyrosine kinase receptors EGFR and mesenchymal-epithelial transition factor tyrosine kinase receptor (MET). Subgroup 1 cell lines exhibit features characteristic of the claudin-low subset of basal tumours described by the UNC group [74], expressing low levels of claudins (CLND3, CLND4, CLDN7) and markers of epithelial-to-mesenchymal (EMT) transition (high ZEB1, ZEB2, CDH2, SNAI, TWIST1, SPARC and VIM and low CDH1 and CDH3).

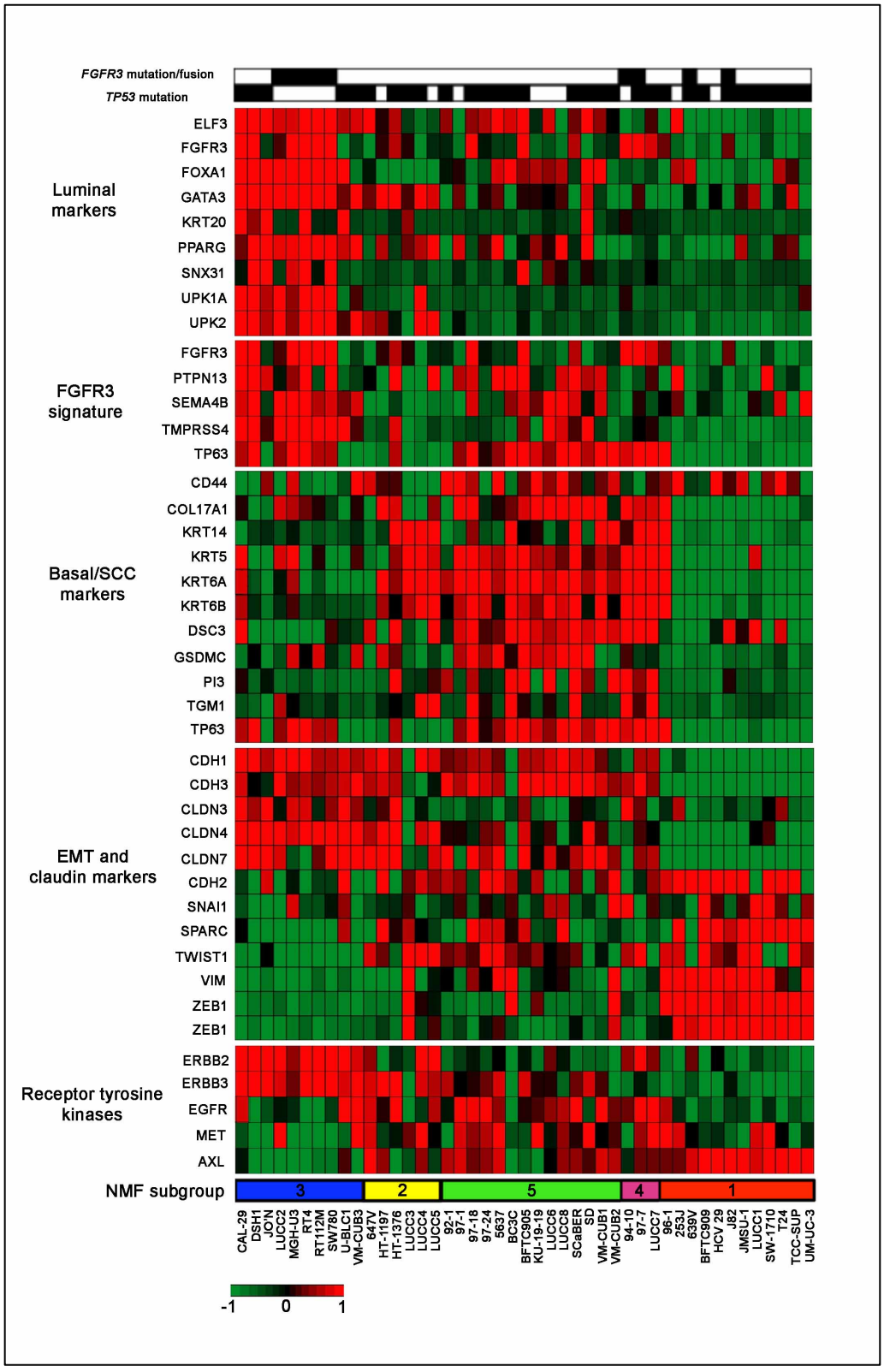

Figure 3-2: Heatmaps showing the level of expression of markers characteristic of luminal and basal subtypes of bladder tumours in cell line NMF subgroups.

In the heatmap, red represents high and green represents low gene expression. The mutation status of *FGFR3* and *TP53* is also shown at the top of the figure, where black represents mutant and white represents wildtype.

We further examined the differences between each of the subgroups using Significant Analysis of Microarrays (SAM) analysis, a supervised approach used to identify genes significantly differentially expressed between sets of samples. SAM was carried out within a stand-alone version of the Multiple Experiment Viewer (MeV) gene expression data analysis toolkit [151]. Data for each of the subgroups was compared to that from all other subgroups using SAM as follows: (subgroup 1 vs subgroups 2, 3, 4 and 5), (subgroup 2 vs subgroups 1, 3, 4 and 5), (subgroup 3 vs subgroups 1, 2, 4 and 5), (subgroup 4 vs subgroups 1, 2, 3 and 5), (subgroup 5 vs subgroups 1, 2, 3 and 4). Probes reporting significant differential gene expression were identified by setting the fold change to ≥ 2 and the median number of false significant genes to zero within the SAM analysis module. Lists of probes reporting differential gene expression from each comparison were then used to create a Venn diagram (Figure 3-3) and this was used to identify probes unique to each comparison. Intensity data for these probes was then extracted and used in hierarchical cluster analysis (Figure 3-4). This further analysis indicated that while subgroups 1, 3 and 5 bare strong resemblance to subsets of luminal and basal bladder tumours previously described by other groups, subgroups 2 and 4 may potentially represent novel subgroups of basal tumours.

Subgroup 4 contained 3 cell lines: LUCC7, 94-10 and 97-7. Only two probes reported significant differential gene expression in the comparison with all other cell lines. One of the probes is unannotated and the other detects keratinocyte differentiation associated differentiation protein (KRTDAP), which is upregulated in these 3 cell lines relative to all others. As there were only 3 cell lines supporting the existence of this basal subset and limited information in the literature regarding the role of KRTDAP, this subgroup was not investigated further in the current study.

Subgroup 2 exhibits strong basal-squamous features such as high expression of keratins 5 and 6 (Figure 3-2), but also exhibits significant differential upregulation of a number of genes. Eighty-seven probes corresponding to 50 genes were uniquely upregulated in cell lines from subgroup 2 as compared to all other subgroups (Appendix B). A heatmap of the expression of these genes is shown in Figure 3-5. One gene that was significantly upregulated in subgroup 2 was ECM1. Previous studies have demonstrated that ECM1 expression influences cancer development and progression, and it has been associated with poorer overall survival in hepatocellular, breast, and gastrointestinal carcinomas [118, 121, 152], however, the role

of ECM1 in bladder cancer has not been examined. MUC1 was also uniquely and significantly upregulated in subgroup 2. The complex described by Lee *et al*. was proposed to increase Ras/Raf/MEK/ERK signalling thus mediating resistance against the HER2 inhibitor trastuzumab [122]. Subtyping studies have shown that there are many similarities between molecular subgroups of basal and luminal breast cancers and bladder cancers, hence findings of interest in breast cancer are worthy of further investigation in bladder cancer. ECM1 and MUC1 were, therefore, selected as candidate genes for further investigation in this study.

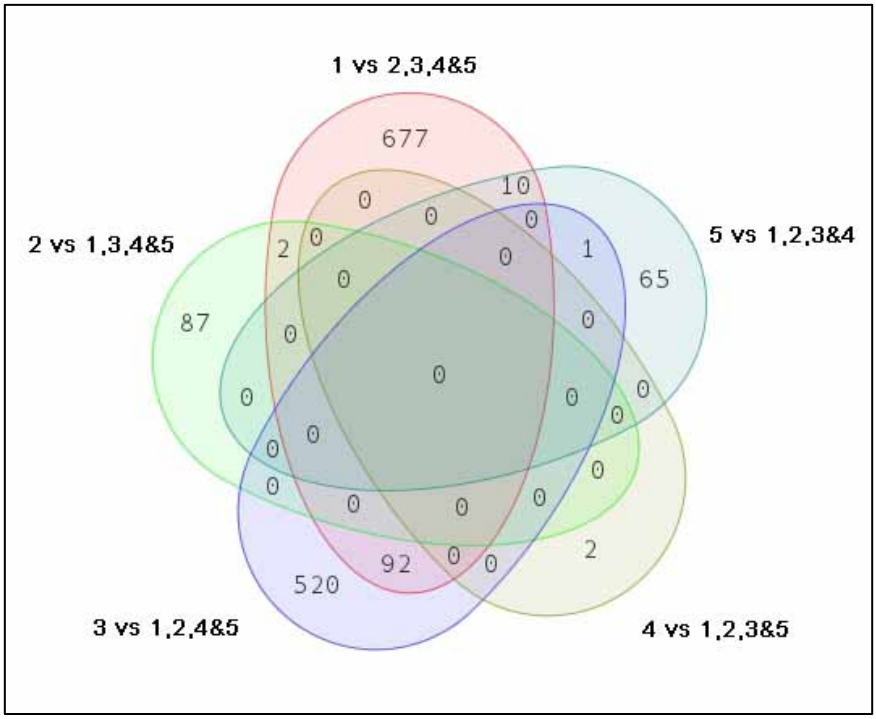

Figure 3-3: Venn diagram showing the overlap of the number of probes reporting differential gene expression in the cell line NMF subgroup comparisons.

Cell line subgroups were compared as indicated in the figure using SAM analysis. Probes reporting significant differential gene expression were identified by setting the fold change to ≥2 and the median number of false significant genes to 0 within the SAM analysis module. Lists of probes reporting differential gene expression from each comparison were then used to create the Venn diagram.

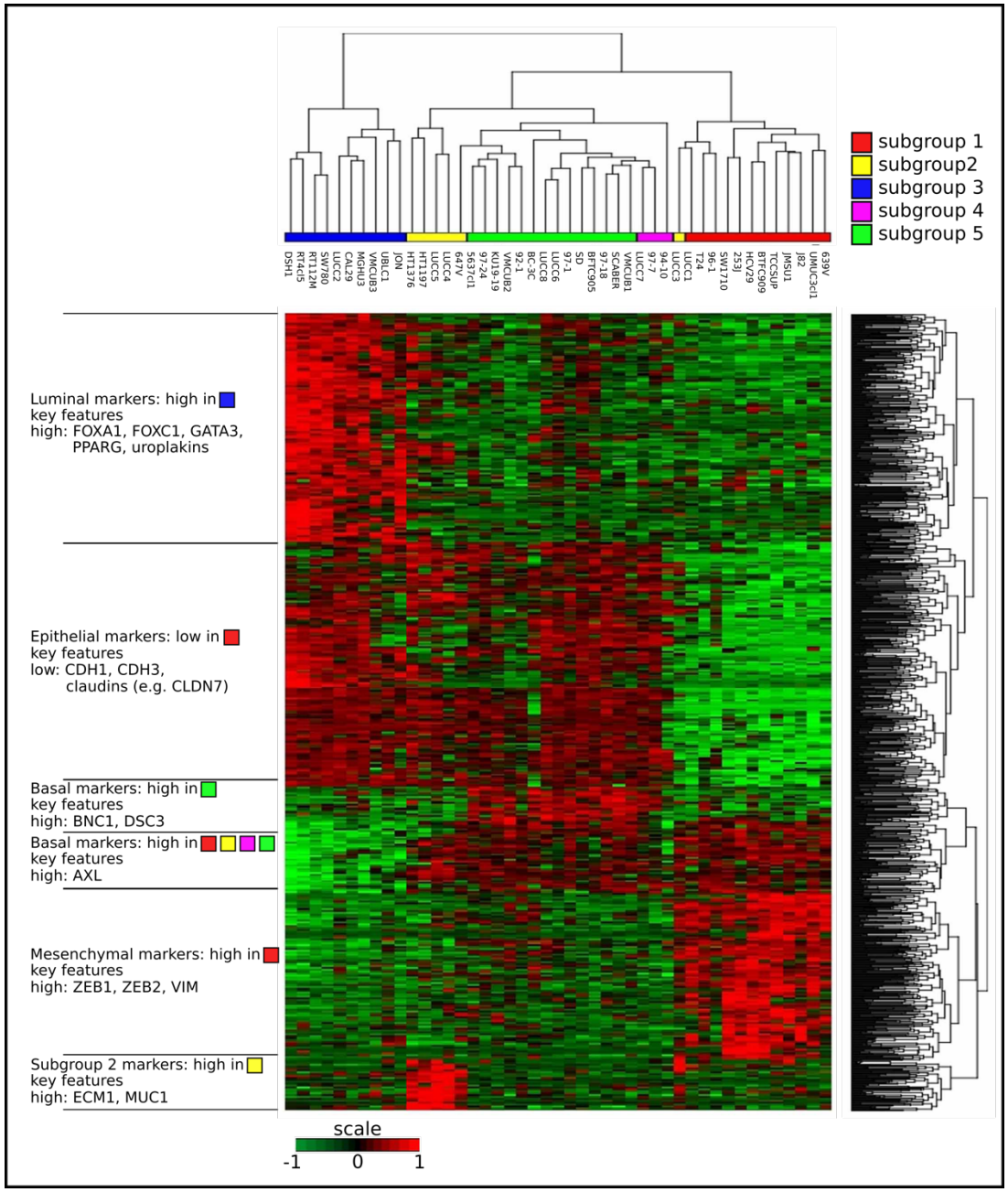

Figure 3-4: Hierarchical cluster analysis of gene expression data for probes identified by SAM analysis to be differentially expressed in cell line NMF subgroups.

Gene expression data for 1351 probes identified by Venn analysis to be uniquely differentially expressed in comparisons of NMF subgroups (Figure 3-3) were used in hierarchical cluster analysis. Two-way unsupervised hierarchical cluster analysis was conducted using Euclidean distance and average linkage. The features of the main clusters are highlighted on the left-hand side of the figure. On the heatmap, red represents high and green represents low mRNA expression.

Figure 3-5: Heatmap of genes significantly upregulated in subgroup 2.

On the heatmap, red represents high and green represents low mRNA expression

3.2.2 qRT-PCR analysis of ECM1 and MUC1 in cell lines

Microarray data showed elevated mRNA expression of ECM1 and MUC1 in the cell lines classified into subgroup 2 (Appendix C). To confirm mRNA expression levels across all 45 bladder tumour-derived cell lines qRT-PCR was employed. Expression levels of ECM1 were shown to be elevated relative to the NHU-Pool in 14 cell lines including all six of the cell lines classified into subgroup 2 (LUCC3, LUCC4, LUCC5, HT-1376, HT-1197, and 647V) (Figure 3-6). The highest expression level of ECM1 in subgroup 2 was seen in LUCC4 which was approximately 50x higher than that of the NHU-Pool sample, while 647V had the lowest ECM1 expression level which was approximately 0.5x higher compared to that of the NHU-Pool sample. MUC1 mRNA levels were elevated in 28 cell lines relative to the NHU-Pool sample including five of the six cell lines from subgroup 2, the exception being HT-1197 in which expression was reduced relative to the NHU-Pool sample (0.4x lower) (Figure 3-7). LUCC4 also had the highest expression level of MUC1 which was 800x higher than the NHU-Pool sample. A Pearson product-moment correlation was conducted to test concordance between the microarray and qRT-PCR data for MUC1 and ECM1 by measuring the linear correlation between the two datasets. qRT-PCR data correlated highly with the microarray expression data for both ECM1 ($r = 0.934$) and MUC1 ($r = 0.959$).

3.2.3 Western blot analysis of ECM1 and MUC1 in cell lines

The expression of ECM1 and MUC1 was also examined at the protein level in the cell line panel using western blot analysis (Figure 3-8). Of the 14 cell lines that showed elevated expression of ECM1 mRNA according to qRT-PCR data, 12 also stained positively for ECM1 protein expression on the western blot, including all six cell lines of subgroup 2. The most intensive staining for ECM1 was seen in LUCC4, LUCC5, HT-1376, HT-1197 and J82. Of the 28 cell lines that had elevated expression of MUC1 mRNA according to qRT-PCR, only 7 showed positive staining for the protein by western blot analysis (J82, TCC-SUP, 92-1, HT-1376, LUCC4, LUCC5, BC-3C). This included 3 of the 6 cell lines of subgroup 2 that had increased expression of MUC1 mRNA (HT-1376, LUCC4, LUCC5). Co-expression of both proteins was also examined. Five of the seven cell lines that had positive MUC1 protein expression also had positive ECM1 protein expression (LUCC5, LUCC4, HT-1376, TCC-SUP, J82) while of the 21 cell lines that had upregulated MUC1 mRNA but low protein expression, only LUCC1 had positive protein expression for ECM1 and one other (SCaBER) had increased ECM1 mRNA expression.

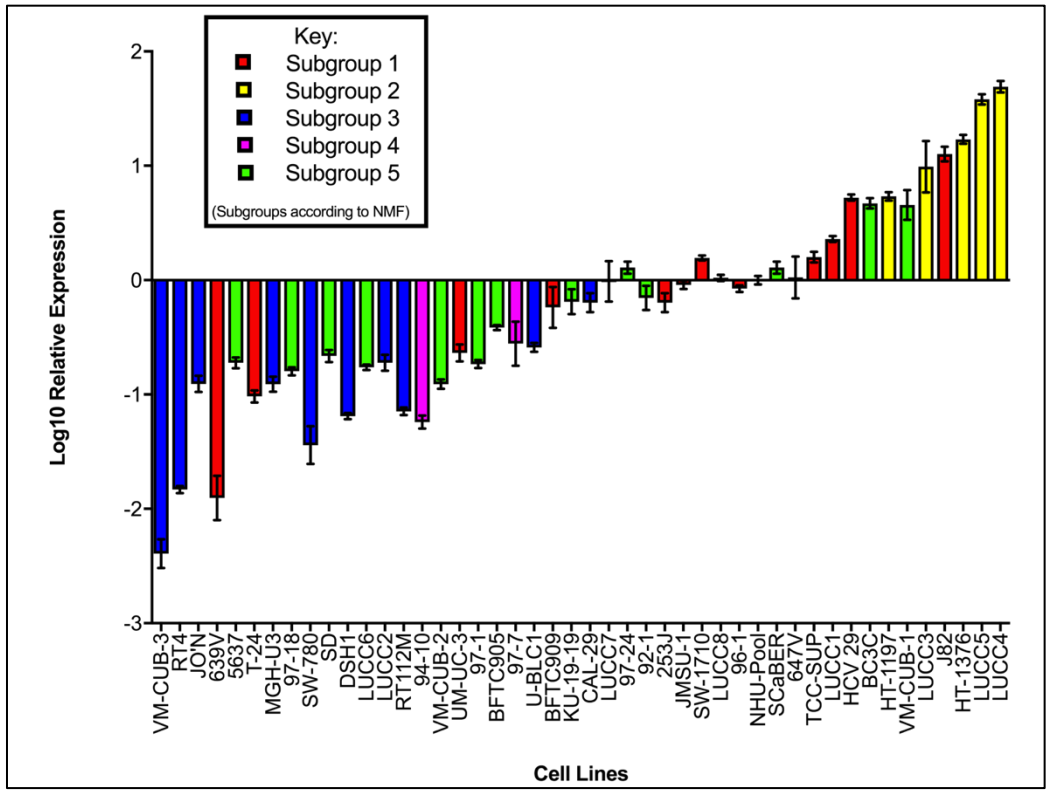

Figure 3-6: qRT-PCR analysis of ECM1 in 45 bladder tumour-derived cell lines.

The relative expression level of ECM1 mRNA was determined by qRT-PCR. Expression levels were normalised to the control gene SDHA and measured relative to a pooled normal urothelial cell sample (NHU-Pool). Data is ordered according to microarray results (Appendix C).

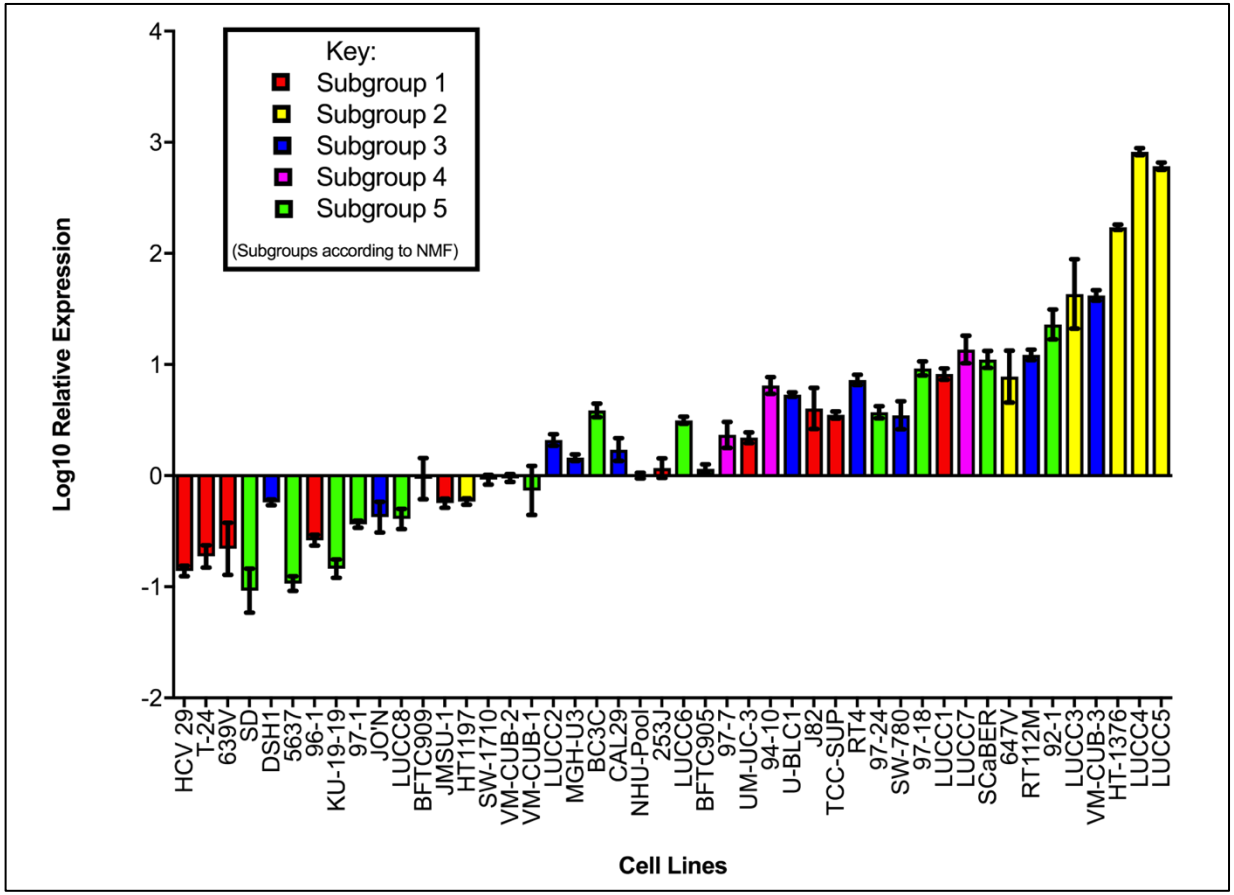

Figure 3-7: qRT-PCR analysis of MUC1 in 45 bladder tumour derived cell lines.

The relative expression level of MUC1 mRNA was determined by qRT-PCR. Expression levels were normalised to the control gene SDHA and measured relative to a pooled normal urothelial cell sample (NHU-Pool). Data is ordered according to microarray results (Appendix C).

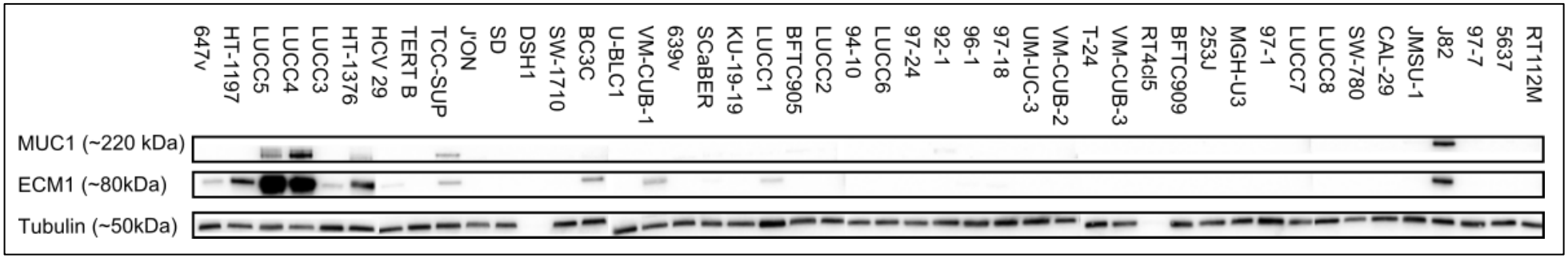

Figure 3-8: Western blot analysis of ECM1 and MUC1 protein levels in 45 bladder tumour-derived cell lines.

Total protein lysates were harvested from each cell line and 30 μg was analysed by western blot analysis with antibodies specific to ECM1, MUC1 and anti-tubulin alpha which was used as a loading control. For the cell lines DSH1 and RT4cl5 which do not express tubulin alpha, beta-actin expression was also assessed (Appendix D). Blots were analysed using the ChemiDoc MP System and Image Lab software.

3.2.4 Immunohistochemical staining analysis of ECM1 and MUC1 expression

3.2.4.1 Determination of the optimal antibody dilutions for immunohistochemical staining of ECM1 and MUC1

Optimisation of primary antibody dilutions for immunohistochemical analysis was carried out to obtain maximum sensitivity with minimum background staining. Sections cut from the FFPE blocks of the primary tumours from which the LUCC4, LUCC5 and LUCC6 cell lines were derived were stained with a range of ECM1 or MUC1 antibody dilutions (1:100, 1:200 or 1:500). Tumours were selected as positive or negative controls based on the mRNA and protein expression levels of ECM1 and MUC1 in the corresponding cell lines as determined by microarray, qRT-PCR, and western blot analysis. The tumour from which LUCC6 was derived was used as a negative control and this showed no staining for ECM1 at all antibody dilutions, except at the edges of tumour sections (Figure 3-9 A-D). The tumour from which LUCC4 was derived was chosen as the positive control and demonstrated heterogenous, mainly cytoplasmic staining for ECM1 with some areas staining very strongly, and others showing little staining. Some potential membranous staining could also be seen (Figure 3-9 E-H). The optimal antibody dilution for ECM1 immunohistochemistry was determined to be 1:200. The tumour from which LUCC6 was derived was also used as a negative control for MUC1 staining, and showed no positive staining (Figure 3-10 A-D). The tumour from which LUCC5 was derived was used as a positive control, and this tumour showed intense mainly cytoplasmic staining for MUC1 but there was also some observable membranous and nuclear staining. The optimal antibody dilution for MUC1 immunohistochemistry was established to be 1:200 (Figure 3-10 E-H).

ECM1 expression was also examined in sections from the FFPE blocks for the tumours from which LUCC3 and LUCC5 were derived and the tumours from which LUCC4 and LUCC6 were derived were again examined in this mini-panel as positive and negative controls, respectively. In the LUCC3 (Figure 3-11 A), LUCC4 (Figure 3-11 B) and LUCC5 (Figure 3-11 C) tumours staining was again heterogenous and largely cytoplasmic. No staining was noted in the LUCC6 tumour (Figure 3-11 D).

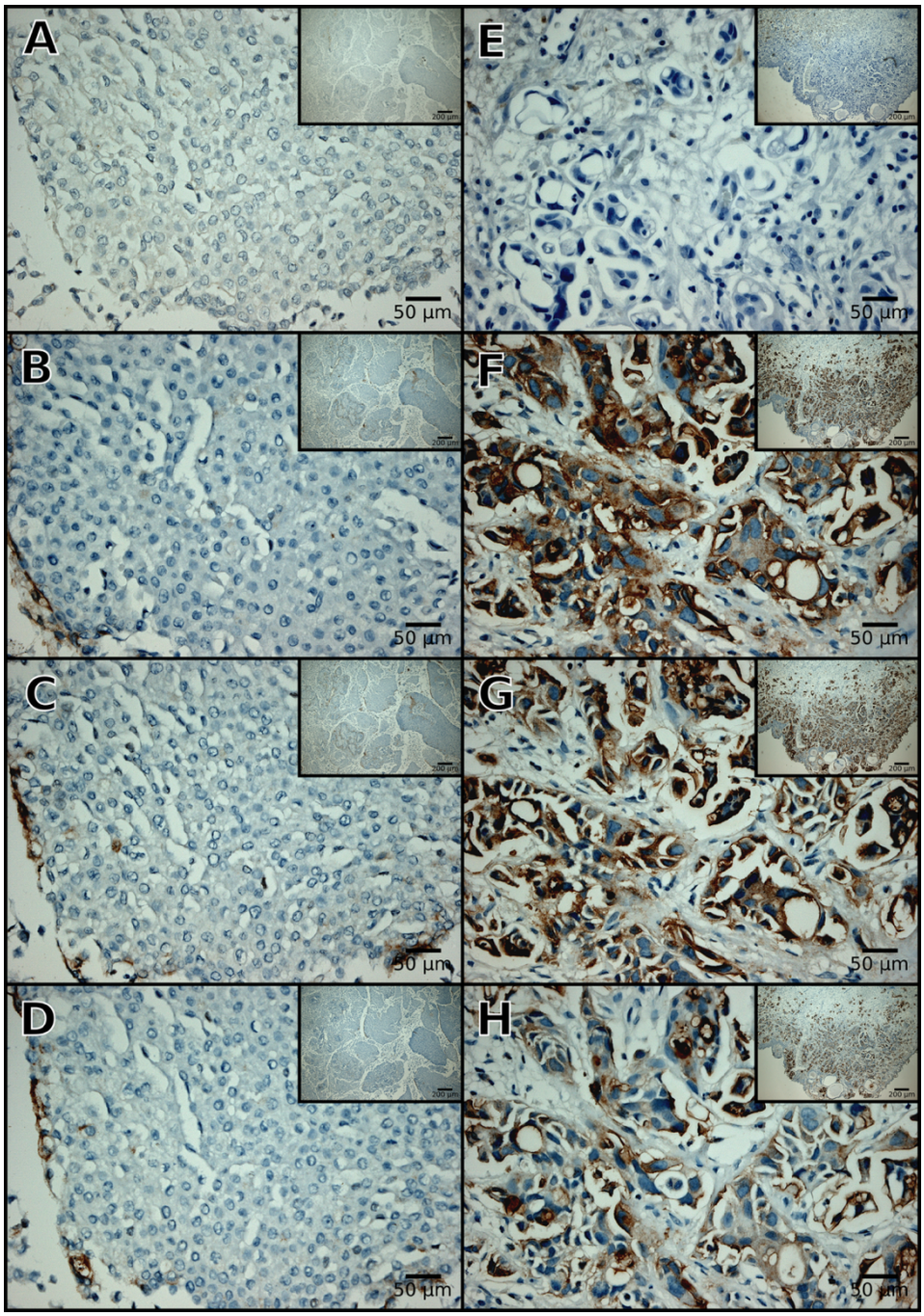

Figure 3-9: Photomicrographs of FFPE bladder tumour sections stained for ECM1 by immunohistochemistry.

FFPE sections of bladder tumours from which the cell lines LUCC6 and LUCC4 were derived were stained with an antibody specific to ECM1 using immunohistochemistry with a range of antibody dilutions in order to determine the optimal conditions for detection of ECM1 protein with minimal background staining. Sections of the LUCC6 tumour sample were used as a negative control and were stained at the following antibody dilutions: **A)** no antibody, **B)** 1:100, **C)** 1:200, and **D)** 1:500. Sections of the LUCC4 tumour sample were used as a positive control and were stained at the following antibody dilutions: **E)** no antibody, **F)** 1:100, **G)** 1:200, and **H)** 1:500. Images are at a magnification of 400X. Images were also taken at a magnification of 40X to assess larger section areas.

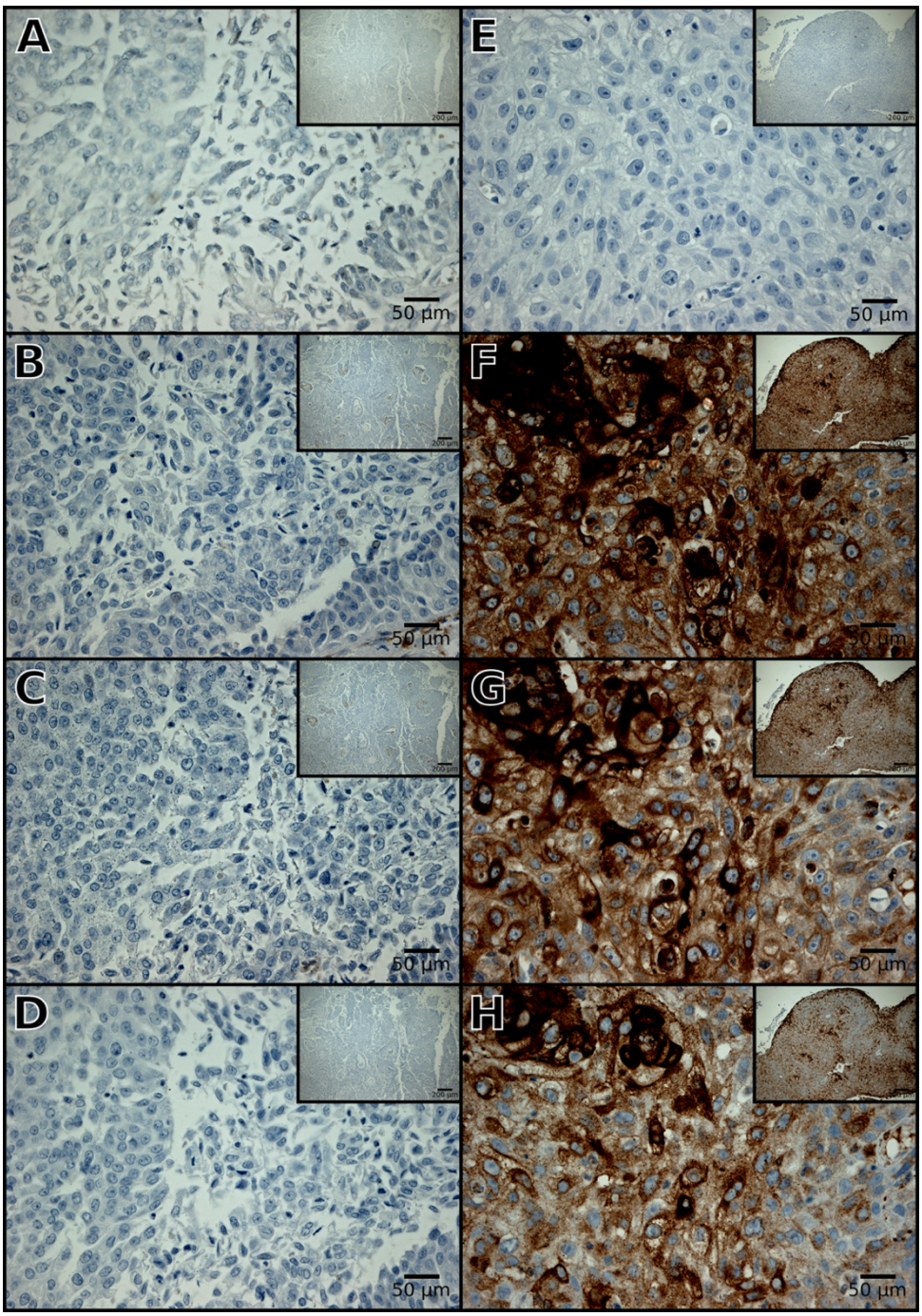

Figure 3-10: Photomicrographs of FFPE bladder tumour sections stained for MUC1 by immunohistochemistry.

FFPE sections of bladder tumours from which the cell lines LUCC6 and LUCC5 were derived were stained with an antibody specific to MUC1 using immunohistochemistry with a range of antibody dilutions in order to determine the optimal conditions for detection of MUC1 protein with minimal background staining. Sections of the LUCC6 tumour sample were used as a negative control and were stained at the following antibody dilutions: **A)** no antibody, **B)** 1:100, **C)** 1:200, and **D)** 1:500. Sections of the LUCC5 tumour sample were used as a positive control and were stained at the following antibody dilutions: **E)** no antibody, **F)** 1:100, **G)** 1:200, and **H)** 1:500. Images are at a magnification of 400X. Images were also taken at a magnification of 40X to assess larger section areas.

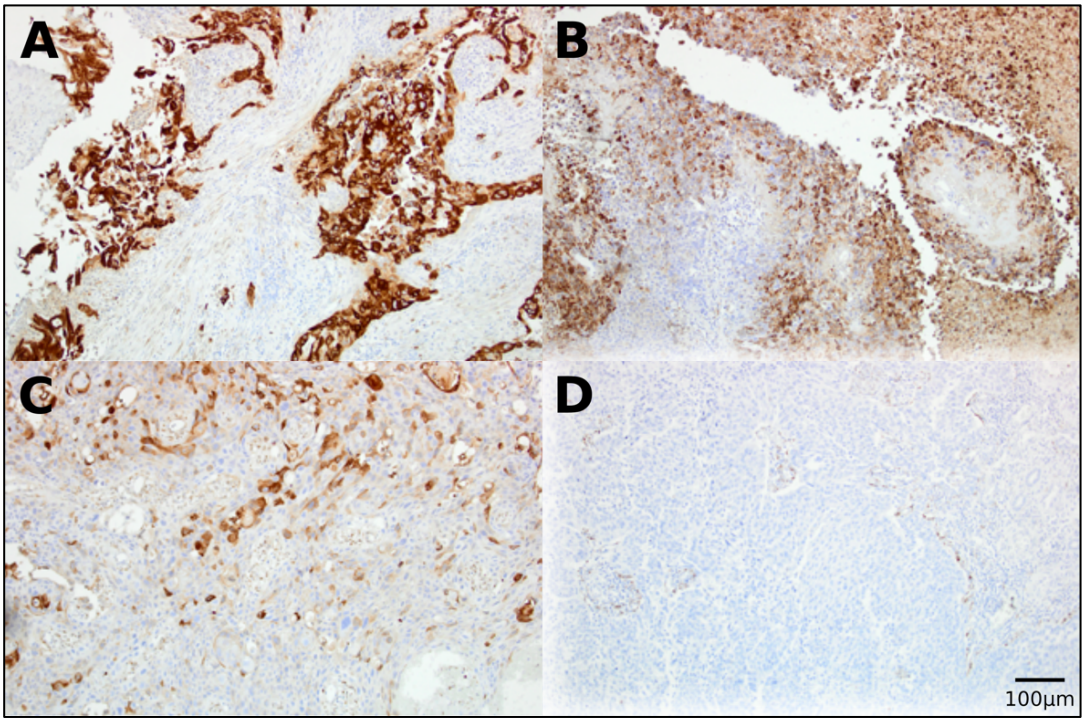

Figure 3-11: Photomicrographs of FFPE bladder tumour sections stained for ECM1 by immunohistochemistry.

FFPE sections of bladder tumours from which the cell lines **A)** LUCC3, **B)** LUCC4, **C)** LUCC5 and **D)** LUCC6 were derived were stained for ECM1 by immunohistochemistry. Slides were stained with an antibody specific to ECM1 at a dilution of 1:200. Images are at a magnification of 200X.

3.2.4.2 Immunohistochemical staining of ECM1 and MUC1 in fixed cell pellets

In order to investigate how the cellular localisation and staining intensity of ECM1 and MUC1 in the cell lines used in this study compared to that seen in the original tumours, immunohistochemistry was carried out on fixed cell pellets from a small panel of cell lines. This was also used as further validation of the ECM1 and MUC1 antibodies use in immunohistochemistry staining. Cell pellets were chosen based on qRT-PCR and western blot analysis to include samples that had high expression (LUCC3 and LUCC4), medium expression (LUCC8) and low expression (J'ON and KU-19-19) of both proteins (Figure 3-12 and Figure 3-13). TERT NHUC B, a normal human urothelial-derived cell line retrovirally transduced to express human telomerase reverse transcriptase for immortalisation was also assessed as a normal urothelial reference cell line. Protein expression of ECM1 and MUC1 protein was not detected in the TERT-B, J'ON and LUCC8 cell lines by immunohistochemistry (Figure 3-12 A B D and Figure 3-13 A B D), and MUC1 expression was not detected in the KU-19-19 cell line (Figure 3-13 C). A small degree of positive staining for ECM1 was observed in KU-19-19 (Figure 3-12 C), although ECM1 was not detected at the protein level by western blot analysis (Figure 3-8) and was down regulated at the mRNA level according to qRT-PCR analysis of this cell line (Figure 3-6). LUCC4 exhibited the most intense and uniform staining for both ECM1 and MUC1 with around 54% and 95% of cells staining positive for each protein respectively (Figure 3-12 F and Figure 3-13 F). LUCC3 also showed considerable staining for both proteins (Figure 3-12 E and Figure 3-13 E).

In the LUCC3 and LUCC4 cell lines which exhibited positive staining for ECM1 and MUC1, the pattern of staining for both proteins was similar with the most extensive staining seen in the cytoplasm, although some potential membranous staining could also be seen for ECM1. A small amount of nuclear staining could also be seen for MUC1 in the LUCC4 sample (Figure 3-13 F).

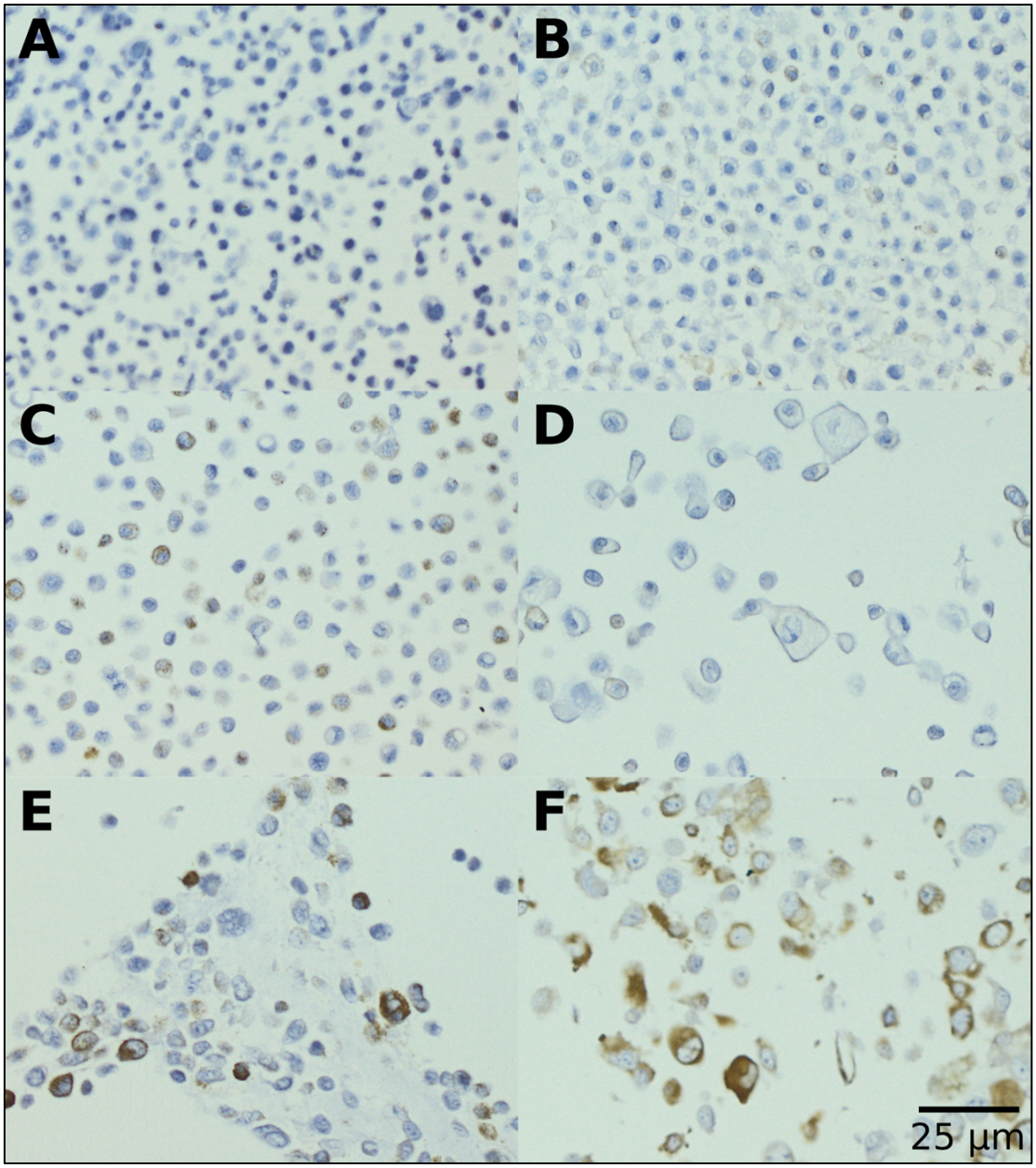

Figure 3-12: Photomicrographs of FFPE cell pellets stained for ECM1 by immunohistochemistry.

Sections of FFPE bladder tumour-derived cell pellets were stained for ECM1 by immunohistochemistry. Slides were stained with an antibody specific for ECM1 at a dilution of 1:200. Images show **A)** TERT NHUC B, **B)** JO'N, **C)** KU-19-19, **D)** LUCC8, **E)** LUCC3 and **F)** LUCC4 at a magnification of 400X.

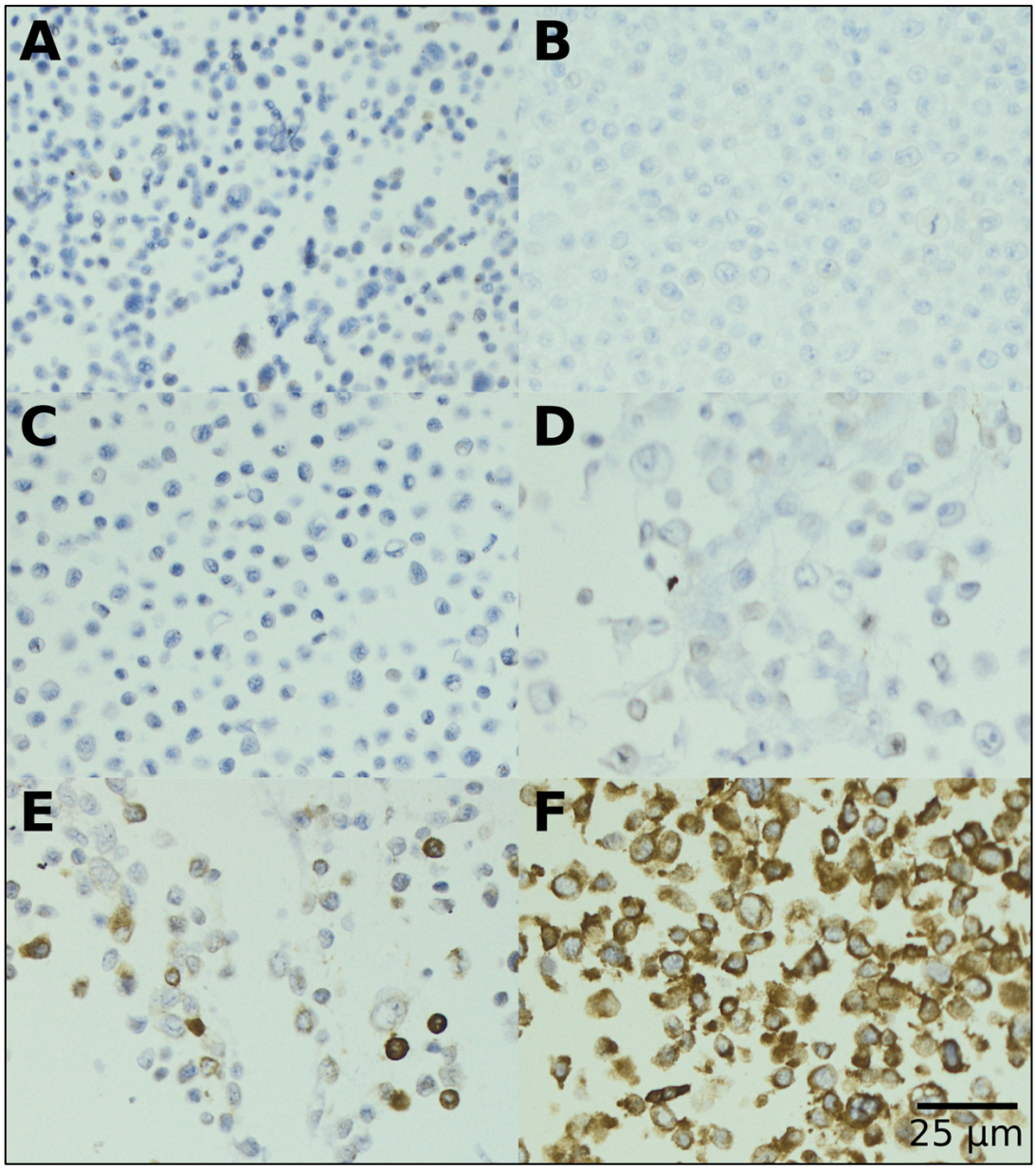

Figure 3-13: Photomicrographs of FFPE cell pellets stained for MUC1 by immunohistochemistry.

Sections of FFPE bladder tumour-derived cell pellets were stained for MUC1 by immunohistochemistry. Slides were stained with an antibody specific for MUC1 at a dilution of 1:200. Images show **A)** TERT NHUC B, **B)** JO'N, **C)** KU-19-19, **D)** LUCC8, **E)** LUCC3 and **F)** LUCC4 at a magnification of 400X.

3.2.5 Immunofluorescence staining of ECM1 and MUC1

3.2.5.1 Distribution of ECM1 and MUC1 in parental HT-1376

Immunofluorescence staining was conducted in HT-1376 in order to examine the expression and cellular localisation of ECM1 (Figure 3-14 and Figure 3-15) and MUC1 (Figure 3-16). Our results showed that ECM1 was mainly expressed in the cell cytoplasm where it exhibited a granular staining pattern (Figure 3-15). MUC1 was also noted to be mainly cytoplasmic, but some cells also demonstrated nuclear staining (Figure 3-16). The actin cytoskeleton and nucleus were also stained using Phalloidin and DAPI, respectively. This allows the total cell population to be viewed and thus the percentage of cells staining positively for ECM1 and MUC1 can be assessed. Staining for ECM1 was heterogeneous, with the majority of cells showing positive staining but around 10% of cells showing no ECM1 staining. MUC1 staining was largely homogeneous with >95% of cells showing positive staining. DAPI staining was confined to the nucleus and actin showed mainly cytoplasmic staining as expected.

3.2.5.2 Distribution of ECM1 in HT-1376 derived monoclonal cell lines

In order to determine if the heterogeneous staining for ECM1 seen in HT-1376 was the result of a mixed cell population or spaciotemporal regulation of ECM1 expression, monoclonal cell lines were generated by single cell cloning. ECM1 expression was examined by immunofluorescence in these lines (Figure 3-17). In total 9 individual monoclonal cell lines were established (data not shown). Three representative monoclonal cell lines (Clones 1-4) exhibiting different ECM1 staining profiles are shown in Figure 3-17. Three monoclonal cell lines including Clone 1 had high ECM1 expression with more than 80% of cells staining positively. In three monoclonal cell lines, including Clone 2 and Clone 3, approximately 15% of cells were positive for ECM1, and in a further three monoclonal cell lines, including Clone 4, no ECM1 staining was seen.

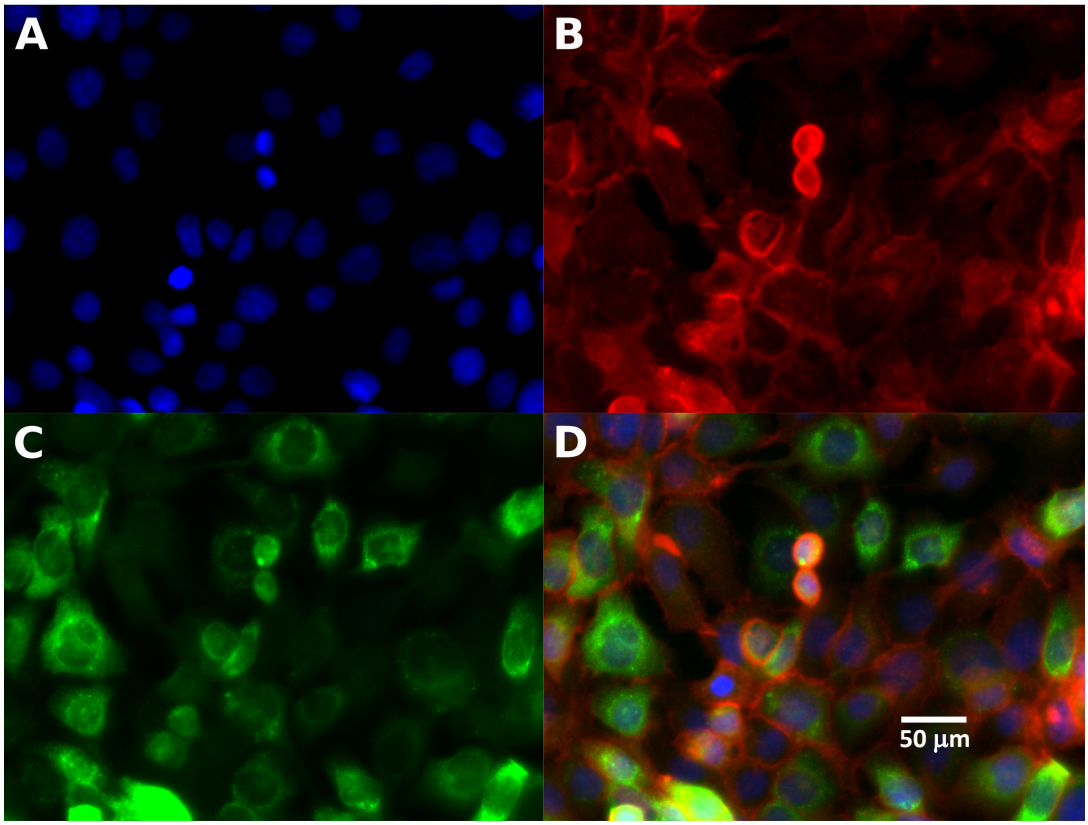

Figure 3-14: Photomicrographs of HT-1376 cells stained for ECM1 by immunofluorescence.

IF staining was carried out for ECM1 in HT-1376 cells cultured on glass cover slips and fixed with 4% paraformaldehyde. **A)** Nuclei were stained with DAPI (emitting at 461 nm – blue fluorescence); **B)** actin was stained with phalloidin (emitting at 568 nm – red fluorescence); **C)** ECM1 antibodies were conjugated with secondary Alexa Flour anti-mouse antibodies (Thermo Fisher Scientific) (emitting at 488 nm – green fluorescence); **D)** composite image. Images were taken with an EVOS FL Cell Imaging System (Thermo Fisher Scientific) and overlaid using Inkscape picture editing software. The scale bar on the merged image (50 μm) is representative of all images.

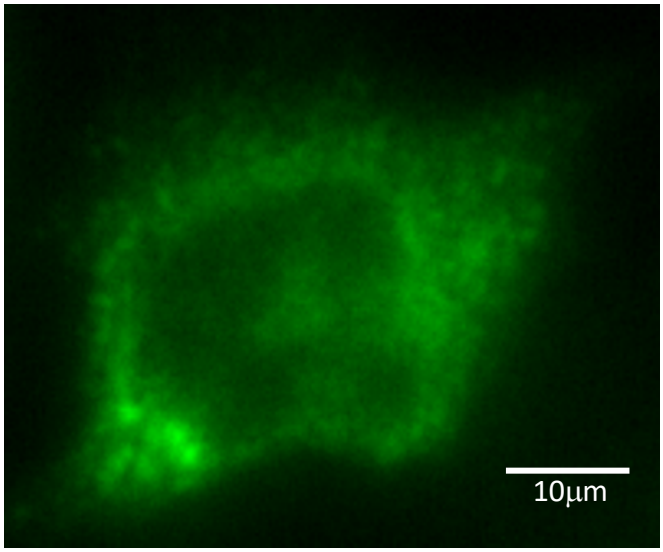

Figure 3-15: An enlarged photomicrograph of a representative HT-1376 cell stained for ECM1 by immunofluorescence.

IF staining was carried out for ECM1 in HT-1376 cells cultured on glass cover slips and fixed with 4% paraformaldehyde. An ECM1 antibody was conjugated with a secondary Alexa Flour anti-mouse antibody (Thermo Fisher Scientific) (emitting at 488 nm – green fluorescence). Images were taken with an EVOS FL Cell Imaging System (Thermo Fisher Scientific). ECM1 staining was cytoplasmic and demonstrated a granular appearance.

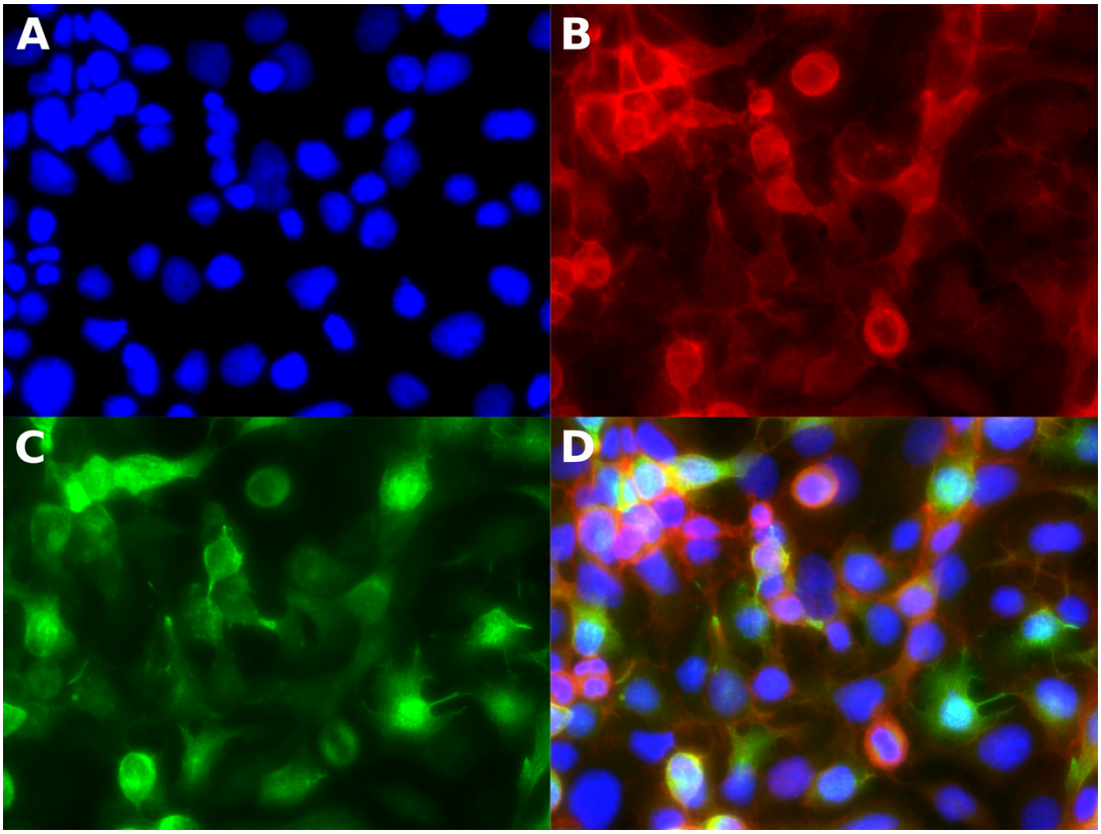

Figure 3-16: Photomicrographs of HT-1376 cells stained for MUC1 by immunofluorescence.

IF staining was carried out for MUC1 in HT-1376 cells cultured on glass cover slips and fixed with 4% paraformaldehyde. **A)** Nuclei were stained with DAPI (emitting at 461 nm – blue fluorescence); **B)** actin was stained with phalloidin (emitting at 568 nm – red fluorescence); **C)** MUC1 antibodies were conjugated with secondary Alexa Flour anti-mouse antibodies (Thermo Fisher Scientific) (emitting at 488 nm – green fluorescence); **D)** composite image. Images were taken with an EVOS FL Cell Imaging System (Thermo Fisher Scientific) and overlaid using Inkscape picture editing software. The scale bar on the merged image (50 μm) is representative of all images.

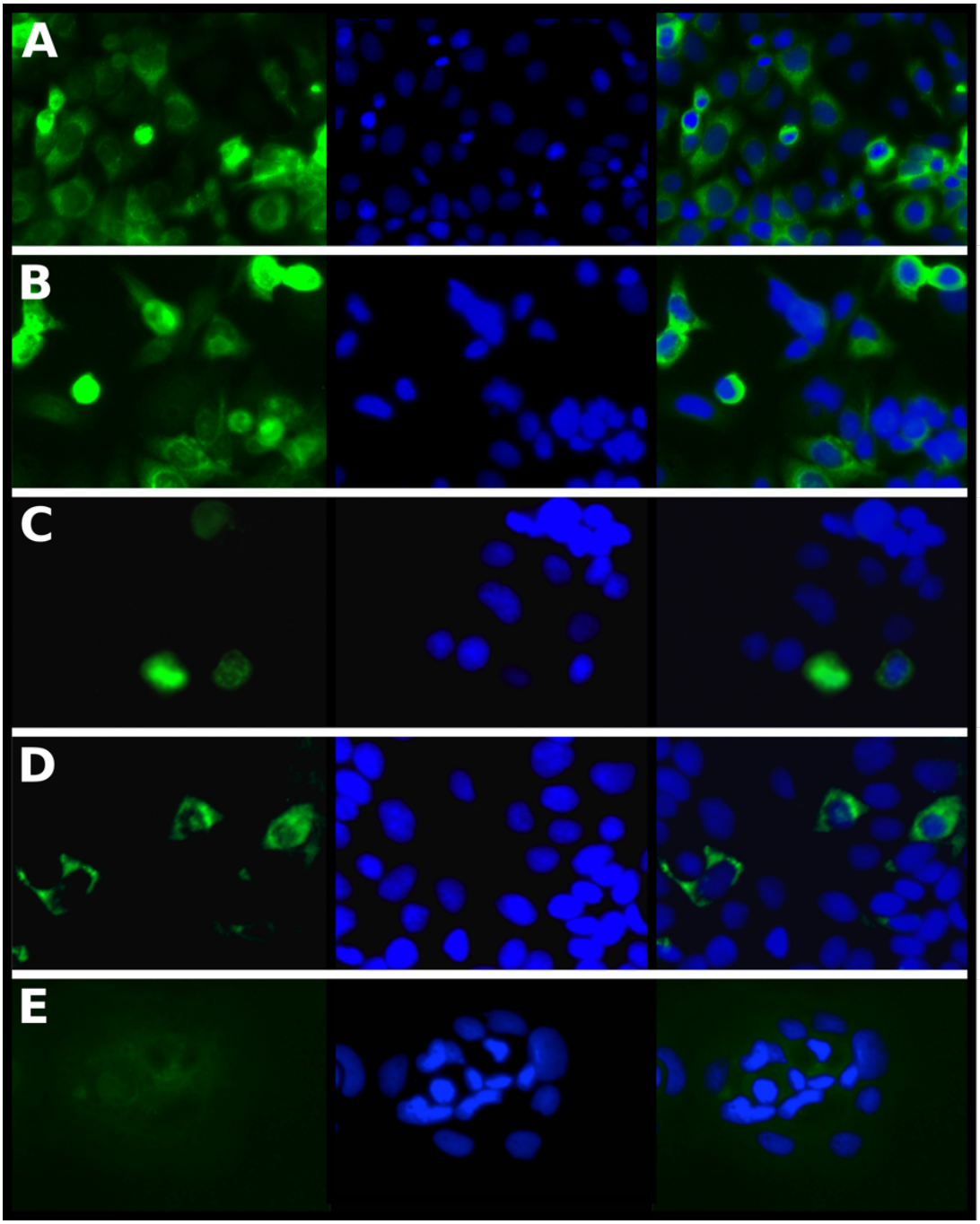

Figure 3-17: Photomicrographs of HT-1376 monoclonal cell lines stained for ECM1 by immunofluorescence.

IF staining was carried out for ECM1 in single cell clones of the HT-1376 cell line. Cells were cultured on glass cover slips and fixed with 4% paraformaldehyde. Nuclei were directly stained with DAPI (emitting at 461 nm – blue fluorescence), and ECM1 antibodies which were conjugated with secondary Alexa Flour anti-mouse antibodies (emitting at 488 nm – green fluorescence). Images were taken with an EVOS FL Cell Imaging System (Thermo Fisher Scientific) and overlaid using Inkscape picture editing software. Images show **A)** the parental HT-1376 cell line; **B)** Clone 1, a high ECM1 expressing clone; **C)** Clone 2 and **D)** Clone 3, intermediate ECM1 expressing clones; and **E)** Clone 4 which does not express detectable ECM1.

3.2.6 Analysis of secreted and glycosylated ECM1

The granular appearance of ECM1 detected by immunofluorescent staining of parental HT-1376 led to the hypothesis that ECM1 was being packaged for secretion. In order to address the question of whether ECM1 is secreted by ECM1-high bladder tumour derived cell lines, conditioned medium was collected from the parental HT-1376 cell line and the protein was precipitated out of the medium using TCA-precipitation. The protein isolated from the conditioned medium was subsequently analysed by western blot analysis and revealed the presence of ECM1 (Figure 3-18 A). In order to ensure that the detected ECM1 was not a contaminant from detached or non-viable cells in the conditioned medium, samples were cleared by centrifugation and passed through a 0.45uM syringe filter prior to TCA-precipitation.

A positive control of total protein isolated from the cultured adherent HT-1376 cells was also analysed by western blot analysis alongside the protein isolated from the conditioned medium (Figure 3-18 A). A comparison of ECM1 detected from the two sources revealed that ECM1 isolated from conditioned medium had a higher molecular weight than the ECM1 detected in the adherent cell lysate. Previous studies have reported that ECM1 N-glycosylation of Asn residues is important for the regulation of secretion [153]. It was therefore hypothesised that the higher molecular weight ECM1 seen in the secreted fraction may represent a glycosylated form of the protein. In order to assess whether this was the case, protein precipitated from conditioned medium was subjected to deglycosylation using a Glycoprofile™ II Enzymatic In-solution N-Deglycosylation kit. This showed a reduction in the size of ECM1 post glycosylation (Figure 3-18 B).

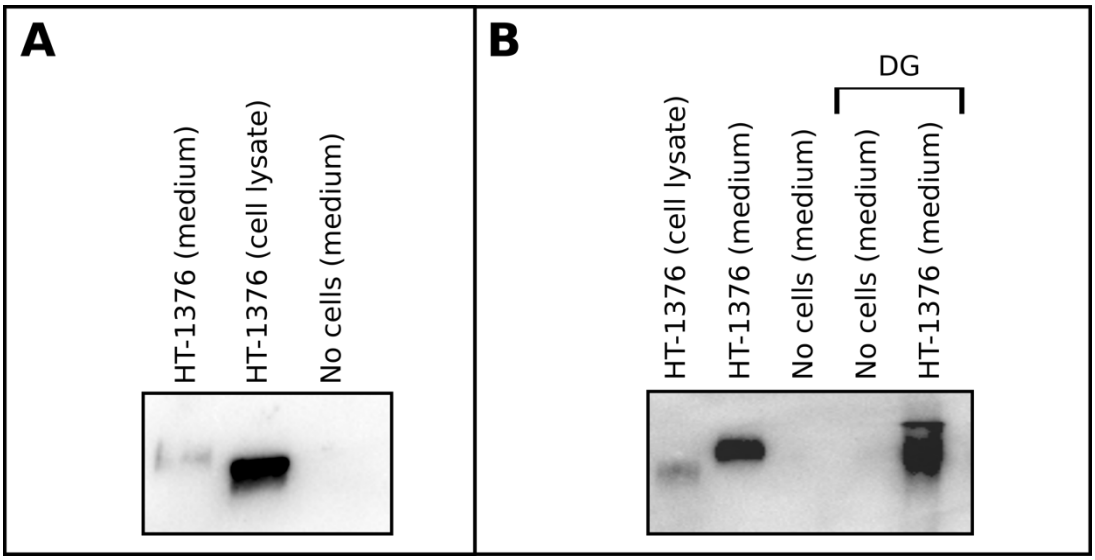

Figure 3-18: Western blot analysis of secreted and glycosylated ECM1.

A) HT-1376 cells were cultured in serum free media for 24 h. Conditioned medium and cell lysates were harvested. Conditioned medium and medium naive to cells (no cells) were spun at 13,000 rpm for 10 min then passed through a 0.45 μm syringe filter to remove cell debris. Protein was precipitated out of the medium using trichloroacetic acid (TCA), quantified and resuspended in western blotting loading dye. 20 μl of secreted protein and 30 μg of total protein lysate was analysed by western blotting with an antibody specific to ECM1. **B)** Medium was harvested and protein isolated as previously described. A Glycoprofile™ II, Enzymatic In-solution N-Deglycosylation Kit was used to carry out deglycosylation (DG). 20 μl of DG product or 30 μg of total protein lysate was analysed by western blotting with an antibody specific to ECM1. n=1.

3.2.7 Investigation of potential molecular mechanisms associated with ECM1 over-expression

3.2.7.1 DNA copy number analysis of the *ECM1* gene region

In order to assess potential reasons for increased ECM1 expression in the ECM1-high cell lines of subgroup 2, SNP 6.0 microarray data for all cell lines was interrogated for changes in copy number across the region of chromosome 1 containing the *ECM1* gene (1q21.2; hg19 chr1:150,508,011Mb-150,513,789Mb). Matched blood or the corresponding Epstein-Barr virus-transformed lymphoblastoid (EBV) cell line samples were used as normal reference samples where available. Copy number plots for chromosome 1 were viewed using Partek Genomics Suite software. All of the cell lines in subgroup 2 except HT-1197 had increased copy

number across the region of chromosome 1 encoding ECM1. The corresponding normal reference samples for these cell lines (where available) showed no increase in this region (data not shown). LUCC5 exhibited high-level amplification of the genomic region containing *ECM1* (Figure 3-19). Of the remaining thirty-nine cell lines that were not part of Subgroup 2, twelve also exhibited increased copy number in the *ECM1* gene region (data not shown).

3.2.7.2 Mutational analysis of the *ECM1* gene

Mutation was also considered as a potential mechanism of ECM1 upregulation. COSMIC (Catalogue of Somatic Mutations in Cancer) is an online database (http://cancer.sanger.ac.uk/cosmic) that holds information on somatic mutations in human cancers assembled from large-scale experiments such as The Cancer Genome Atlas (TCGA) and scientific literature. Somatic missense mutations in the *ECM1* gene were examined in COSMIC. A number of somatic mutations were identified that were present in individual samples only and were distributed across the whole *ECM1* gene. However, two mutations were identified in COSMIC that were present in two or more different tumour samples in exons 7 and 10 (hg19 coordinates: chr1:150483939 G>A, and chr1:150485894 C>T, respectively). A further two mutations were identified in two tumour samples in exon 8 that were a single base pair apart (hg19 coordinates: chr1:150484937 G>A, and chr1:150484939 C>T). PCR and Sanger sequencing were employed to screen the 6 cell lines from subgroup 2 for mutations in these regions (Figure 3-20). Matched normal reference samples were available for three of the cell lines (LUCC3 blood; LUCC4 EBV; LUCC5 EBV) and these were also screened to confirm germline or somatic status of any variants detected. No mutations were detected in these regions, although 2 common single nucleotide polymorphisms (SNPs) were identified (rs11801190 and rs13294) (Figure 3-20). LUCC3, LUCC3 blood, HT-1197 and HT-1376 cell lines were wildtype, LUCC5, and LUCC5 EBV were heterozygous, and LUCC4, LUCC4 EBV and 647V were homozygous for the rs11801190 SNP. LUCC4 and LUCC4 EBV cell lines were wildtype, 647V, HT-1197, HT-1376, LUCC5 and LUCC5 EBV were heterozygous, and LUCC3 and LUCC3 blood were homozygous for the rs13294 SNP. Where matched normal reference samples were available the SNP genotype matched that of the tumour-derived cell line confirming that the polymorphisms were germline.

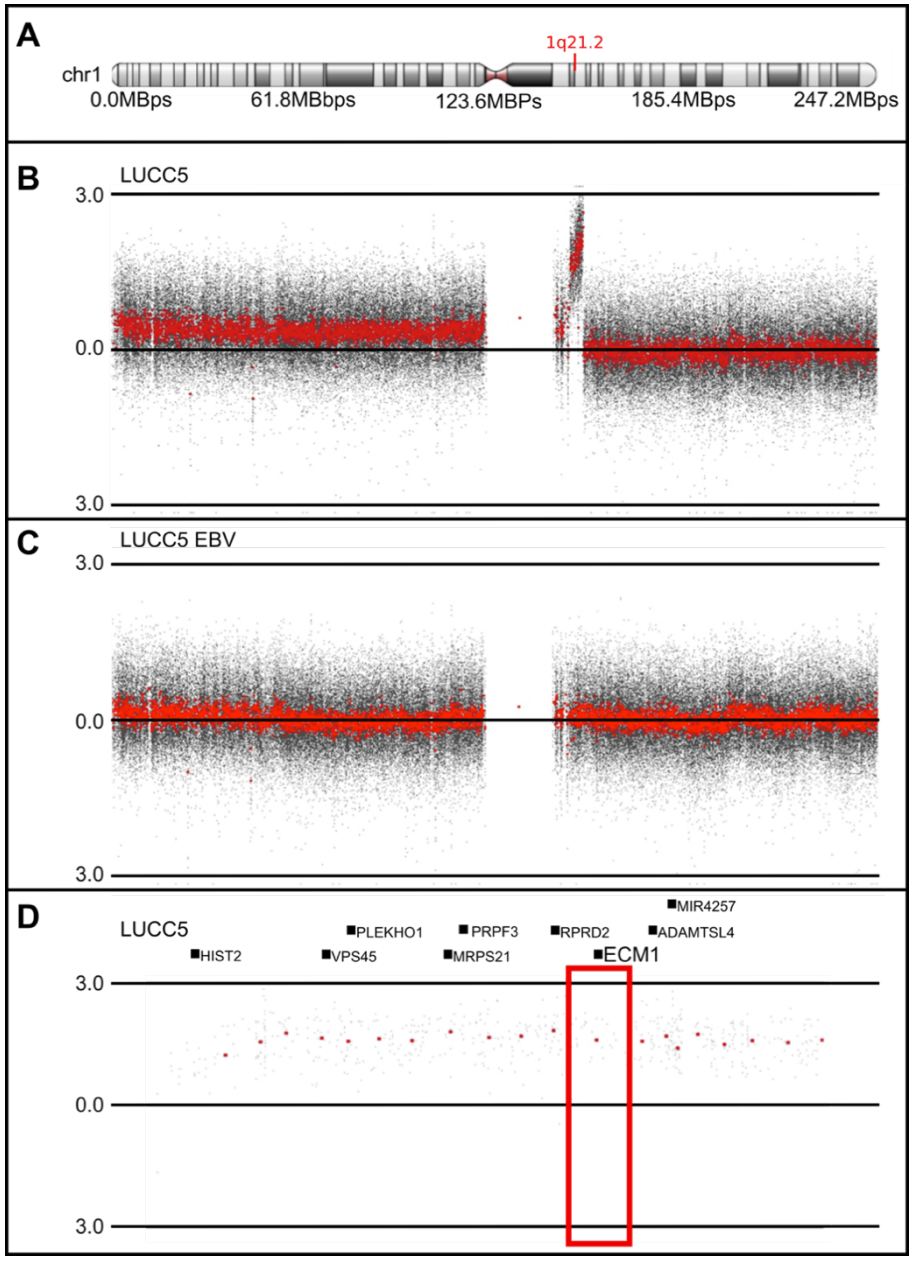

Figure 3-19: Copy number plots of chromosome 1 for LUCC5 and LUCC5 EBV showing amplification of the genomic region containing ECM1.

Copy number in LUCC5 was determined using SNP 6.0 microarrays and copy number plots for chromosome 1 were viewed using Partek Genomics Suite software. **A)** a reference map of chromosome 1 (hg18), **B)** chromosome 1 copy number plot for LUCC5 showing high level DNA amplification at chromosome region 1q21.1 which includes the ECM1 gene, **C)** chromosome 1 copy number plot for LUCC5 EBV showing a normal profile with no amplification at 1q21.1, **D)** magnified view of copy number data for LUCC5 across the region containing the ECM1 gene (highlighted by the red box).

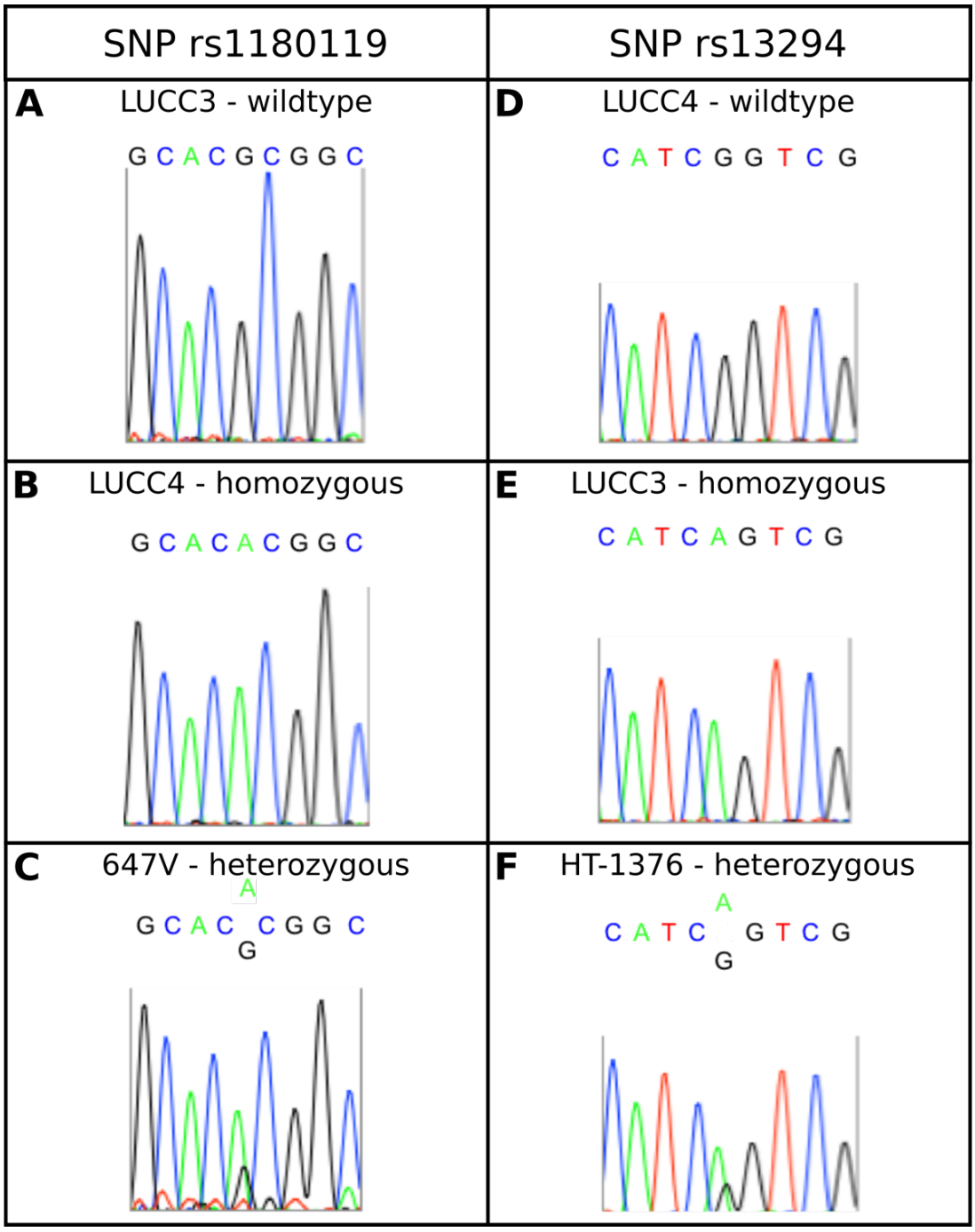

Figure 3-20: Common SNPs identified in bladder tumour-derived cell lines by Sanger sequencing of exons 7 and 8 of the *ECM1* gene.

PCR and Sanger sequencing were employed to screen the 6 cell lines from subgroup 2 for mutations in exons 7 and 8 of the ECM1 gene. Two common SNPs were identified: rs11801190 (exon 7) and rs13294 (exon 8) in 3 and 6 of the cell lines respectively. Examples of cell lines that were wildtype, heterozygous, and homozygous for these SNPs are shown above. **A)** LUCC3 was wildtype, **B)** LUCC4 homozygous, and **C)** 647V heterozygous for rs11801190. **D)** LUCC4 was wildtype, **E)** LUCC3 homozygous, and **F)** HT-1197 heterozygous for rs13294.

3.3 Discussion

Molecular subtyping based on genome-wide information offers the potential to guide more refined and personalised treatment approaches and better predict response than the traditional MIBC and NMIBC classification of bladder cancer. Moreover, it may enable the identification of new targets for treatment. Several subtypes of bladder cancer have now been described in primary tumour samples. Cell lines derived from primary tumours also represent a potential sample source for preliminary identification of subtypes as their molecular features often reflect those of the primary tumours from which they were derived. NMF analysis has been widely applied for the identification of molecular subtypes [32, 154, 155]. It is useful in a biological context as data is modeled on two non-negative matrices producing additive data by combining positive vectors. This lack of negative constraints supports the physical realities of gene expression, where negative copies of mRNA or negative transcription is not possible [156]. Furthermore, NMF compares individual pairs of genes thus detecting local behaviour of genes prior to correction for multiple comparisons. This allows the detection of sets of genes with correlated expression that would remain undetected by global gene behaviour analysis [157]. By using this quantitative method of cophenetic coefficient evaluation of subgroups, the analysis is not subjective and therefore the subtypes identified through NMF are reproducible and robust [150]. Prior to the start of this project, analysis of genome-wide expression array data from 45 bladder tumour-derived cell lines was analysed using NMF analysis and five potential subgroups were identified.

One of the subgroups identified had Basal/Squamous features (subgroup 2) (Hurst *et al,* unpublished data). This subgroup was characterised by 50 genes that were significantly upregulated according to significance analysis of microarrays (SAM). Within this gene list was extracellular matrix protein 1 (ECM1). ECM1 is of particular clinical relevance as increased expression has been associated with increased metastatic potential in laryngeal [119] and breast carcinomas [120], reduced overall and disease-free survival in patients with hepatocellular carcinoma [118] and poorer prognosis in malignant thyroid carcinoma [158]. MUC1 was also highlighted as uniquely and significantly upregulated in subgroup 2, and is of particular relevance as nearly three quarters of bladder carcinomas demonstrate MUC1 immunohistochemical staining in the basal and intermediate layers of the urothelium [135, 141]. High levels of MUC1 expression is also associated with multifocality [142] and higher-grade bladder tumours [143]. Both proteins have also been associated with

the formation of a complex in breast cancer cells in which ECM1 interacts with and stabilises EGFR, HER3 and MUC1 in the cell membrane of a breast cancer cell line. This complex is thought to result in increased EGFR and HER3 signalling through Ras/Raf/MEK/ERK, which enables the cells to overcome the inhibitive action of trastuzumab a monoclonal antibody used to inhibit the signalling activity of HER2 [122]. A number of similarities exist between the basal and luminal subgroups of breast cancer and bladder cancer, hence findings of interest in one carcinoma are worthy of investigation in the other. ECM1 and MUC1 were, therefore, selected as candidate genes for further investigation in this study.

Gene expression profiling using microarrays enables the expression of thousands of genes to be interrogated simultaneously, but error due to non-specific binding of targets to probes and cross hybridisation of probes to targets may affect the quality of gene expression data [159]. As a consequence of this it is good practice to validate differentially expressed genes identified by microarray analysis using a second independent technique. Here we used qRT-PCR to confirm the expression levels of ECM1 and MUC1 in the cell line panel as it represents an inexpensive option with high sensitivity and specificity, and rapid generation of results [160]. We found qRT-PCR and microarray data to be highly correlated, suggesting that the gene expression data obtained is representative of the true pattern of expression for ECM1 and MUC1.

As mRNA expression does not always relate directly to protein expression, we used western blot analysis to establish if ECM1 and MUC1 were also upregulated at the protein level. Seventy-five percent of the cell lines that had increased ECM1 mRNA also showed positive staining for the protein by western blot analysis, strongly implying that translational increases are directly related to increases in the transcription of ECM1. Our results suggest that an increase in transcription does not always equate to an increase in protein expression for MUC1 as only seven cell lines showed positive protein staining for MUC1 despite twenty-eight cell lines having upregulated mRNA (25%). Although MUC1 protein expression did not correlate absolutely with mRNA expression, an interesting trend was highlighted. Six out of the seven cell lines positive for MUC1 protein were also positive for ECM1 at the protein and mRNA levels, while only three of the twenty-one cell lines that had an increase in MUC1 mRNA but no MUC1 protein expression were positive for ECM1. This trend was also reported by Lee *et al*. [122] and while no

biological explanation has been proposed it implies that ECM1 may have post-translational effects on the expression of MUC1.

In addition to confirming western blot results of protein expression levels, immunohistochemistry provides information on the cellular localisation. In order to effectively analyse staining patterns antibodies must be validated for use in immunohistochemistry. Optimal antibody dilutions must also be established as using a concentration that is too high may result in non-specific low-affinity interactions generating false positive or high background staining [161] while using antibodies at concentration that is too low can result in false negative staining. We therefore performed an immunohistochemistry titration experiment for both the ECM1 and MUC1 antibodies using sections from tumours selected as positive or negative controls based on the mRNA and protein expression levels of the cell lines derived from these tumours. The results from this experiment determined the optimal antibody dilution to be 1:200 for both the ECM1 and MUC1 antibodies. No staining was detected in the negative controls suggesting that false-positivity due to non-specific binding of the secondary antibodies used in this study was not problematic, and that neither antibodies bind to alternative epitopes when used in immunohistochemistry.

Subsequent to antibody validation and dilution factor optimisation, cell pellets were also stained using the ECM1 and MUC1 antibodies. In accordance with published literature [115, 121, 162] our immunohistochemistry results from both tumour sections and cell pellets showed ECM1 staining to be largely cytoplasmic. This may reflect a high level of ECM1 synthesis and subsequent packaging of the protein into vesicles for secretion. Similar to reports in breast cancer-derived cell lines [122], a small amount of membranous staining could also be seen, and this may provide some support for the existence of the membrane bound complex involving ECM1 proposed by Lee *et al.* [122]. However, ECM1 is also thought to anchor many extracellular matrix proteins to keratinocyte membranes in order to maintain the skin's functional integrity [163] hence other membranous interactions may also explain the observed staining pattern.

Previous studies have reported MUC1 staining to be membranous [164, 165]. However, we observed MUC1 staining to be largely cytoplasmic and where staining for MUC1 was very intense, as was seen in LUCC4 cell line and the tumour from which LUCC5 was derived, the protein was also detected in the nucleus. In bladder

cancer, alterations in the cellular localisation of MUC1 have been observed during tumour progression [141-143]. In prostate cancer, a more diffused pattern of expression throughout the cytoplasm has been noted to be associated with more advanced disease [166], and in breast cancer a switch in MUC1 expression from membranous to cytoplasmic and nuclear expression is associated with increased metastatic potential [167]. Our results have shown MUC1 staining to be cytoplasmic and nuclear, and may therefore suggest it is characteristic of more aggressive and metastatic bladder tumours, reminiscent of the high-stage, high grade tumours from which these cell lines were derived (Appendix A).

Many of the same technical problems that affect immunohistochemistry are also encountered when using immunofluorescence, but this technique has the main advantage that due to the narrow wavelength ranges of the fluorescent dyes, filters that eliminate signals from other wavelengths can be applied to make detection highly selective for the specific signal of interest [161]. Furthermore, data generated from different wavelengths can be overlaid to assess co-localisation of two proteins [161]. Unfortunately, in this study investigation of co-localisation of MUC1 and ECM1 was not possible as primary antibodies for the two proteins were derived from the same species and as a consequence staining with differentially fluorescently labelled secondary antibodies could not be used to distinguish between the two. Conjugation of primary antibodies to fluorophores that emit light at different wavelengths could be an option to overcome this issue in future work.

Despite being unable to assess co-localisation of MUC1 and ECM1, immunofluorescent staining in the HT-1376 cell line showed that ECM1 is mainly cytoplasmic in localisation, confirming the results seen by immunohistochemistry in the LUCC3 and LUCC4 cell lines. This is similar to the pattern of staining for ECM1 seen by immunofluorescence in laryngeal carcinoma, in which ECM1 was also expressed mainly in the cytoplasm [119]. Furthermore, immunofluorescent analysis of HT-1376 also revealed that the pattern of cytoplasmic staining was granular in nature. Post-translational processing of proteins destined for secretion often occurs within the Golgi apparatus where macromolecules are ultimately packaged in transport vesicles for secretion and this can result in a granular appearance of the cytoplasm when occurring at high levels [168]. The granular appearance of the cytoplasm in our bladder-tumour derived cell lines may be indicative of such vesicles and imply that ECM1 is being secreted by these cells.

ECM1 was originally identified as a secreted protein following TCA protein precipitation from the conditioned medium of a murine osteogenic cell line [91] and assumptions of similar cellular processing of the human form of ECM1 were made due to the highly conserved nature of the murine and human forms of ECM1 [92]. Furthermore, *in vitro* experiments that have demonstrated the ability of human ECM1a to interact with extracellular components of the skin such as laminin 332, collagen type IV, and fibronectin, suggesting that ECM1 is secreted in order for these interactions to occur *in vivo* [169, 170]. To date there have been no attempts to establish if the human form of ECM1 is secreted by bladder tumour cells. In the current study, ECM1 could be detected following western blot analysis of the protein fraction that was TCA precipitated from conditioned medium of the human bladder tumour-derived cell line HT-1376, suggesting human ECM1 is secreted by this cell line.

Interestingly, the molecular weight of secreted ECM1 detected in conditioned media was larger than ECM1 detected in the cell lysate. Previous work investigating Urbacht-Weite disease identified N-glycosylation at asparagine (Asn) residues Asn444 and Asn354 encoded on exons 6 and 7 to be important in the regulation of the secretion of ECM1 [153]. We therefore hypothesised that the observed difference in size noted could be a result of ECM1 glycosylation. This was confirmed by enzymatic deglycosylation of ECM1 isolated from conditioned medium which resulted in a reduction in the molecular weight of ECM1 as detected by western blot analysis. Glycosylation of ECM1 may also explain the granular appearance of ECM1 staining seen by immunofluorescence. N-glycosylation occurs when preassembled glycans are transferred to Asn residues by glycosidases and glycosyltransferases in the endothelial reticulum (ER) and Golgi apparatus, and requires the transfer of proteins in membrane bound vesicles between the ER and Golgi, and from the Golgi to the membrane for secretion. This can result in a granular staining pattern when assessed by immunohistochemistry and immunofluorescence [153]. Our observations of granular ECM1 staining may, therefore, be indicative of post-translational glycosylation of ECM1 prior to secretion.

Immunofluorescent staining of ECM1 in the HT-1376 cell line also revealed that roughly 10% of cells were negative for ECM1. Results from immunohistochemical staining of ECM1 in FFPE LUCC3 and LUCC4 cell pellets also demonstrated heterogenous expression of ECM1 in these cell lines. A number of previous studies

have reported ECM1 staining in tumour sections, but there are very few reports of immunohistochemistry or immunofluorescent staining of ECM1 in cell pellets. In one of the few studies in which such samples have been examined, the hepatocellular carcinoma-derived cell line BEL-7407 showed homogenous staining for ECM1 by immunohistochemistry [162]. At present the reasons underlying the heterogeneous staining we observed in our bladder tumour-derived cell lines is unclear.

In order to investigate the possible cause of heterogeneous ECM1 expression in the cell lines, we generated a number of monoclonal cell lines by single cell cloning of the HT-1376 parental cell line. These cloned populations were then stained for ECM1 by immunofluorescence. It was hypothesised that if the cloned cell lines demonstrated homogeneous positive or negative staining for ECM1, this would indicate that the heterogeneous staining noted in the parental cell line was due to a heterogeneous cell population in the parental line. Conversly, if heterogenous expression of ECM1 in the cloned cell lines was observered then this could be indicative of regulated expression of ECM1 in response to another spaciotemporal factor. Our results showed varied ECM1 expression within the cloned cell lines which may suggest spaciotemporal regulation of ECM1 expression. A future study analysing cell-cycle-dependent regulation of ECM1 expression, for example by synchronising the cell population through inducible knockdown of divers of cell progression, or though drug treatments that activate checkpoints or block major metabolic pathways may be useful [171].

The expression patterns could also be indicative of diversity in the presumed monoclonal populations. The generation of monoclonal cell lines relies on single cell plating through limiting dilutions, but due to dividing doublets and intercellular interactions achieving single cell suspensions can be difficult and this can result in the plating of multiple cells [172]. Furthermore, even with clear documentation of single cell origins from light microscopy, variation can arise in a seemingly monoclonal population through asymmetric cell division [173]. This in turn can lead to differences in gene and protein expression [173, 174]. Our results may imply that the single cell clones derived from the HT-1376 parental cell line established were not truly monoclonal. In the current study it has not been possible to definitively ascertain why ECM1 is differentially expressed in the HT-1376, LUCC3 and LUCC4 cell line populations, but based on our results the remainder of the study was carried out using the parental rather than monoclonal cell lines as the majority of cells in the parental lines express high levels of ECM1.

As well as investigating expression levels of ECM1, we also aimed to assess potential molecular mechanisms associated with increased ECM1 expression in the ECM1-high cell lines. Copy number increases or decreases often have functional consequences which most commonly result in increased or decreased gene expression, respectively [175]. SNP 6.0 microarray data for all cell lines was interrogated for changes in copy number across the region of chromosome 1 containing the *ECM1* gene (1q21.2; hg19 coordinates chr1: 150,480,487-150,486,265). This analysis revealed increased copy number in five of the six ECM1-high cell lines (HT-1376, 647V, LUCC3, LUCC4, and LUCC5). Chromosome arm 1q commonly exhibits complex genomic rearrangements and amplifications in this region are common but heterogenous in bladder tumours, hence, identifying candidate genes in regions of amplification is difficult [176]. In a previous study, copy number analysis of 261 bladder tumours identified 37 samples with an amplification across the 1q21–24 region, and five candidate genes within this region were suggested including two that are also encoded on 1q21.2: B-cell lymphoma 9 (*BCL9*) - a nuclear component of the Wnt pathway [177], and the myeloid cell leukaemia protein 1 gene (*MCL1*) - a member of the anti-apoptotic B-cell lymphoma 2 (*BCL2)* family of genes [176, 178]. ECM1 expression may well be influenced by copy number alterations in ECM1-high cell lines, however 1q21.2 is a gene dense region and may also contain other oncogenes that may be targets for amplification. Moreover, as well as five ECM1-high cell lines, a further seventeen cell lines (JO'N, 5637, DSH1, LUCC6, LUCC2, 94-10, BFTC905, KU-19-19, CAL29, 97-24, 92-1, JMSU-1, 253J, SCaBER, TCC-SUP, LUCC1, and VM-CUB-1) also had increased copy number across the same region and of these cell lines, only five had upregulated ECM1 at the mRNA level. No definitive conclusion could therefore be made regarding copy number increase as the mechanism for increased expression of ECM1 in subgroup 2.

Mutation was also considered as a potential mechanism which might lead to increased ECM1 expression. Sanger sequencing was employed to screen the 6 cell lines from Subgroup 2 for mutations in exons 7, 8 and 10 that were identified by interrogation of the COSMIC database. Although mutations were not detected in these exons, two common SNPs (rs11801190 and rs13294) were detected. rs11801190 was identified in LUCC5 and LUCC5 EBV, LUCC4 and LUCC4 EBV and 647V. rs13294 was identified in 647V, HT-1197, HT-1376, LUCC5, and LUCC5 EBV, LUCC3 and LUCC3 blood. rs11801190 is a SNP in exon 7 of ECM1 that

occurs in around 10% of the population, does not result in a change to the amino acid sequence and has no apparent clinical significance [179]. The other SNP, rs13294, changes the encoded amino acid change (glycine to serine) in the ECM1 protein sequence however this SNP is not known to have any clinical significance and is present in around 30% of the population [179]. As the available normal samples exhibited the same SNPs as detected in their respective paired tumour-derived cell lines, this confirms that the SNPs are germline. Overall the data suggests that somatic mutations are not responsible for increased ECM1 expression, though mutations in other parts of the gene cannot be discounted. Recently, our laboratory has exome sequenced all paired cell lines in the ECM1-high panel. Further insight into the potential contribution of somatic mutation as a factor leading to increased expression of ECM1 will become available once this data is fully analysed.

Chapter 4
Identification of a subset of primary bladder tumours overexpressing ECM1 and phenotypic effects of ECM1 knockdown.

4.1 Introduction

In Chapter 3, ECM1 was shown to be upregulated in a subset of basal-squamous bladder tumour-derived cell lines. Cell lines represent an important tool for research but resemblance to the original tumours can be lost. An important aim of the project was to validate the existence of an ECM1-high subgroup in actual tumour samples. Publicly available microarray data generated from primary bladder tumours was examined for mRNA expression levels of ECM1. Patient metadata was also extracted and examined in order to relate increased expression of ECM1 to overall survival. Furthermore, differential gene expression between tumours expressing high and low levels of ECM1 was examined and pathway analysis was conducted based on these comparisons in order to gain a better insight into the functional role of ECM1 in primary bladder tumours. In order to further validate the existence of an ECM1-high subgroup in primary bladder tumours, ECM1 expression was assessed in four tissue microarrays constructed of over 900 formalin fixed paraffin embedded muscle-invasive bladder tumour cores using immunohistochemistry.

In Chapter 3, MUC1 was considered another potentially important candidate gene due to its reported association with aggressive, high-grade bladder tumours [180] and was confirmed to be upregulated in the cell lines of subgroup 2. MUC1 is also of interest as an interaction with ECM1 has been reported in a complex proposed to influence resistance to ERBB targeting treatments in breast cancer [122]. Our findings in Chapter 3 demonstrated a strong correlation between protein expression of MUC1 and ECM1 in the panel of cell lines. In this Chapter we aimed to assess the correlation between MUC1 and ECM1 protein expression in primary tumours by also assessing MUC1 expression in the tissue microarrays described above.

Previous studies in cell lines derived from normal tissues and other carcinomas have reported that ECM1 plays a role in wound healing, angiogenesis and cell migration. For example, a cholangiocarcinoma cell line exhibited reduced migration

and invasiveness *in vitro* in response to downregulation of ECM1 [120, 181] and downregulation of ECM1 in the breast cancer cell lines Hs578T and MD-AMB-231 led to a reduction in cell migration and wound healing ability, coupled with impaired attachment and invasiveness as determined by cell attachment assay and matrigel invasion assay [114]. The phenotypic effects of altering ECM1 in bladder cancer cell lines have not previously been described, hence, the expression of ECM1 was modulated in a subset of ECM1-high bladder tumour-derived cell lines using shRNA lentiviral transduction and the phenotypic impact of ECM1 knockdown was examined.

4.2 Results

4.2.1 Data mining, metadata and pathway analysis of publicly available bladder tumour transcriptome data

R2 provides an interactive interface for the computational language “R” and holds publicly available transcriptome data with corresponding patient metadata where available (http://r2.amc.nl). Expression array data for 308 fresh-frozen bladder tumours of all stages and grades [72], 116 FFPE muscle-invasive bladder tumours [75], 142 fresh-frozen muscle-invasive bladder tumours [75], and 412 fresh-frozen muscle-invasive bladder tumours [32] was interrogated and visualised in R2. Hierarchical clustering based on the mRNA expression levels of ECM1 was used to generate dendrograms (Figure 4-1 and Figure 4-2). These dendrograms showed that in all datasets, tumours overexpressing ECM1 formed a separate and distinct cluster from the low expressing tumours as opposed to a graduation of expression from high to low.

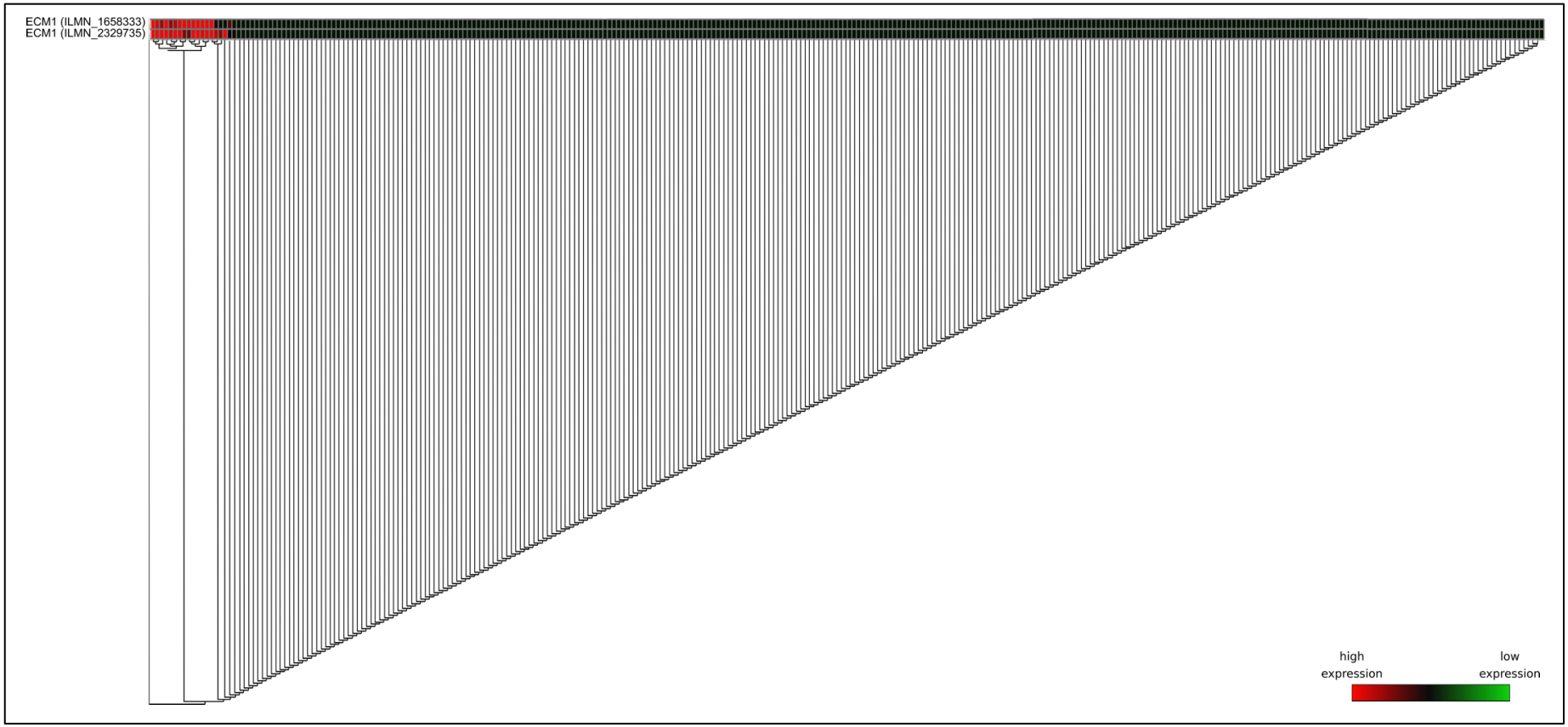

Figure 4-1: A dendrogram illustrating the results of hierarchical clustering based on mRNA expression levels of ECM1 in bladder tumour samples from the study of Sjodahl *et al*. (2012).

The microarray analysis and visualisation platform R2 was used to generate dendrograms based on hierarchical clustering of expression data for all probes that detected ECM1. The expression dataset for 308 fresh-frozen bladder tumours of all stages and grades [72] was interrogated. On the heatmap, red symbolises high expression of ECM1, while green symbolises low expression.

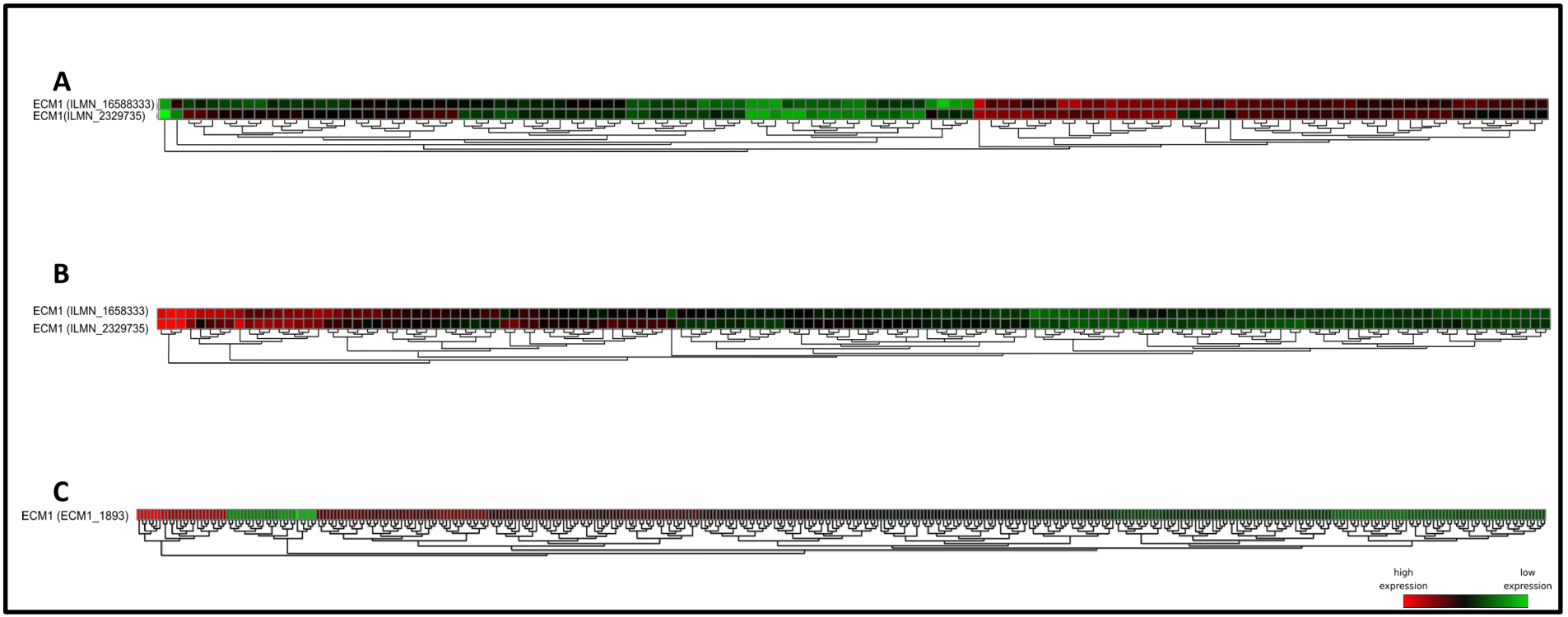

Figure 4-2: Dendrograms illustrating the results of hierarchical clustering based on mRNA expression levels of ECM1 in bladder tumour samples from the studies of Choi *et al*. (2014) and Robertson *et al*. (2017).

The microarray analysis and visualisation platform R2 was used to generate dendrograms based on hierarchical clustering of expression data for all probes that detected ECM1. The expression datasets for **A)** 116 formalin-fixed paraffin-embedded muscle-invasive bladder tumours [75], **B)** 142 fresh-frozen muscle-invasive bladder tumours [75], and **C)** 412 fresh-frozen muscle-invasive bladder tumours [32] were interrogated. On the heatmaps, red symbolises high expression of ECM1, while green symbolises low expression.

Subtyping information was available for the Sjödahl and TCGA datasets. We examined the subtypes to which the ECM1-high tumours were assigned in the original studies (Table 4-1 and Table 4-2). This revealed that the majority of ECM1-high tumours align with the Basal/Squamous subtypes defined in these studies. Analysis of the Sjödahl dataset showed that 9 out of 17 ECM1-high tumours, 9 werecategorised as SCC-like, a poor prognosis basal group with high expression of keratins 4, 6A/B/C, 14, and 16 and EGFR expression. A further 6 ECM1-high tumours were classified as “highly-infiltrated”, a subtype which is characterised by a high level of immune cell infiltration and the expression of an EMT signature. The remaining 2 ECM1-high samples were categorised as genomically unstable, a high-risk group consisting mainly of muscle-invasive tumours with increased HER2 expression and *TP53* mutations. Of the 26 ECM1-high tumours identified in the TCGA dataset, 18 were classified as basal-squamous, a basal group with stem cell like features. A further 3 tumours were categorised as neuronal which are characterised by a high level of *TP53* and *RB1* mutations. The remaining 5 ECM1-high tumours were distributed across the three TCGA luminal subtypes. The TCGA dataset also had subtyping information available which categorised selected samples into subtypes identified by other research groups. This information was available for 16 of the ECM1-high tumours and indicated that the majority of ECM1-high tumours were categorised into basal subgroups, with relatively few tumours assigned to luminal subtypes (Table 4-3).

Patient survival data was available for the TCGA dataset. A Kaplan-Meier plot relating ECM1 expression to overall survival was generated (Figure 4-3). Patients whose tumours expressed high levels of ECM1 had significantly poorer overall survival than patients with tumours expressing low levels of ECM1. Median overall survival for patients with ECM1-high tumours was 14.2 months compared to 38.2 months for patients with ECM1-low tumours (Figure 4-3; Mantel-Cox test, $p=0.0043$). Further analysis of the metadata for the TCGA study revealed a higher percentage of patients with ECM1-low tumours remained disease free compared to patients with ECM1-high tumours, who demonstrated a higher incidence of recurrence and tumour progression to a higher stage after initial resection of the tumour (Table 4-4). This is reflective of the poorer overall survival seen in Figure 4-3. No correlation was noted between ECM1 expression and other metadata such as metastasis, age, smoking or previous diagnosis of NMIBC (data not shown).

Table 4-1: ECM1-high samples in the Sjodahl dataset and their corresponding Lund University subtypes.

The microarray analysis and visualisation platform R2 was used to generate dendrograms based on hierarchical clustering of expression data for all probes that detected ECM1. Samples IDs were identified for those samples present in the ECM1-high cluster. Subtyping classification data from the Sjödahl study [72] was interrogated and the assigned subtype of each ECM1-high sample is displayed in the table.

Sample ID	Lund Group Subtype
GSM814116	genomically unstable (MS2a2)
GSM814222	genomically unstable (MS2a2)
GSM814062	highly infiltrated (MS2b1)
GSM814068	highly infiltrated (MS2b1)
GSM814146	highly infiltrated (MS2b1)
GSM814204	highly infiltrated (MS2b1)
GSM814214	highly infiltrated (MS2b1)
GSM814238	highly infiltrated (MS2b1)
GSM814101	SCC-like (MS2b2.2)
GSM814126	SCC-like (MS2b2.2)
GSM814127	SCC-like (MS2b2.2)
GSM814144	SCC-like (MS2b2.2)
GSM814173	SCC-like (MS2b2.2)
GSM814225	SCC-like (MS2b2.2)
GSM814268	SCC-like (MS2b2.2)
GSM814344	SCC-like (MS2b2.2)
GSM814354	SCC-like (MS2b2.2)

Table 4-2: ECM1-high samples in the TCGA 2017 dataset and their corresponding TCGA 2017 subtypes.

The microarray analysis and visualisation platform R2 was used to generate dendrograms based on hierarchical clustering of expression data for all probes that detected ECM1. Samples IDs were identified for those samples present in the ECM1-high cluster. Subtyping classification data was interrogated from the TCGA study [32] and the assigned subtype of each ECM1-high sample is shown in the table.

Sample ID	TCGA Subtype
TCGA-BL-A13I	Basal-squamous
TCGA-BT-A0YX	Basal-squamous
TCGA-CU-A0YN	Basal-squamous
TCGA-DK-AA6R	Basal-squamous
TCGA-E7-A7DV	Basal-squamous
TCGA-FD-A3B4	Basal-squamous
TCGA-FD-A3N5	Basal-squamous
TCGA-FD-A3SS	Basal-squamous
TCGA-FD-A5BX	Basal-squamous
TCGA-G2-A2ES	Basal-squamous
TCGA-G2-A3IB	Basal-squamous
TCGA-GU-A764	Basal-squamous
TCGA-HQ-A5NE	Basal-squamous
TCGA-UY-A8OB	Basal-squamous
TCGA-XF-AAN8	Basal-squamous
TCGA-ZF-A9RF	Basal-squamous
TCGA-ZF-AA5H	Basal-squamous
TCGA-ZF-AA5N	Basal-squamous
TCGA-BT-A3PH	Luminal
TCGA-K4-A6MB	Luminal
TCGA-DK-A3IQ	Luminal-infiltrated
TCGA-KQ-A41S	Luminal-infiltrated
TCGA-E5-A4TZ	Luminal-papillary
TCGA-FJ-A871	Neuronal
TCGA-XF-AAMH	Neuronal
TCGA-ZF-AA4R	Neuronal

Table 4-3: ECM1-high samples in the TCGA 2017 dataset and their corresponding subtypes according to criteria from five previous studies.

The microarray analysis and visualisation platform R2 was used to generate dendrograms based on hierarchical clustering of expression data for all probes that detected ECM1. Samples IDs were identified for those samples in the ECM1-high cluster. 16 ECM1-high samples were also assigned to subtypes previously described in five other studies [32, 47, 72, 74, 75].

Sample ID	2017 TCGA Subtype	2014 TCGA Subtype	UNC Subtype	MDA Subtype	Lund Subtype
TCGA.BL.A13I	Basal-squamous	Cluster-IV	Basal	Basal	Highly infiltrated (MS2b1)
TCGA.E7.A7DV	Basal-squamous	Unassigned	Basal	Basal	Highly infiltrated (MS2b1)
TCGA.FD.A3SS	Basal-squamous	Cluster-II	Basal	Basal	Highly infiltrated (MS2a1)
TCGA.FD.A5BX	Basal-squamous	Unassigned	Basal	TP53-like	Highly infiltrated (MS2b1)
TCGA.CU.A0YN	Basal-squamous	Cluster-III	Basal	Basal	SCC-like (MS2b2.2)
TCGA.FD.A3B4	Basal-squamous	Unassigned	Basal	Basal	SCC-like (MS2b2.2)
TCGA.FD.A3N5	Basal-squamous	Cluster-III	Basal	Basal	SCC-like (MS2b2.2)
TCGA.G2.A2ES	Basal-squamous	Cluster-III	Basal	Basal	SCC-like (MS2b2.2)
TCGA.G2.A3IB	Basal-squamous	Cluster-III	Basal	Basal	SCC-like (MS2b2.2)
TCGA.BT.A0YX	Basal-squamous	Cluster-III	Basal	Basal	Urobasal B (MS2b2.1)
TCGA.HQ.A5NE	Basal-squamous	Unassigned	Basal	Basal	Urobasal B (MS2b2.1)
TCGA.K4.A6MB	Luminal	Unassigned	Luminal	Luminal	Genomically unstable (MS2a1)
TCGA.BT.A3PH	Luminal	Cluster-I	Luminal	Luminal	Urobasal A (MS1b)
TCGA.DK.A3IQ	Luminal-infiltrated	Unassigned	Basal	TP53-like	Highly infiltrated (MS2b1)
TCGA.KQ.A41S	Luminal-infiltrated	Unassigned	Luminal	TP53-like	Highly infiltrated (MS2b1)
TCGA.E5.A4TZ	Luminal-papillary	Unassigned	Luminal	Basal	Urobasal B (MS2b2.1)

In order to investigate the impact of co-expression of ECM1 and MUC1 on patient survival a Kaplan-Meier plot was generated for TCGA data comparing tumours expressing high levels of ECM1, high levels of MUC1 and high levels of both ECM1 and MUC1 (Figure 4-4). There was no statistically significant difference between survival for patients whose tumours expressed high levels of ECM1 alone compared to tumours expressing high levels of both ECM1 and MUC1. For patients whose tumours expressed both ECM1 and MUC1 there was a statistically significant reduction in overall survival (p= 0.035) compared to patients whose tumours expressed MUC1 alone.

To identify other genes of potential interest in ECM1-high tumours, the IDs of the fresh-frozen samples that had upregulated ECM1 expression in the Sjödahl and Choi datasets were obtained from R2 [75, 182]. LIMMA analysis, conducted using the online platform GEO2R, was used to compare ECM1-high and ECM1-low tumours. Venn analysis was conducted using Partek Genomics software to identify overlapping probes in both datasets (section 2.2). Gene lists were compiled for those genes with a fold change greater than 2 or less than -2, and a p value less than 0.05 (Appendix E). This analysis identified 307 significantly altered probes. After the removal of unannotated probes, and a single representative probe being selected per gene, there were found to be 282 significantly altered genes. Eighty of these genes were significantly downregulated in the ECM1-high tumours compared to the ECM1-low tumours, and 202 genes that were significantly upregulated in the ECM1-high tumours compared to the ECM1-low tumours including ECM1. A number of extracellular and structural related proteins were also upregulated including 9 collagens and 6 keratins. The keratins 6a, 6b, 6c, 14, 16, and 16P2 which are typically basal [86] were upregulated in the ECM1-high tumours. Other upregulated basal markers were PLAU, S100A7, S100A8, and SPRR1B. Four luminal markers (TBX3, TOX3, UPK2, and UPK1A) were downregulated in the ECM1-high tumours. The EGFR ligand HB-EGF, and the EMT markers vimentin (VIM) and snail family transcriptional repressor 2 (SNAI2), were also upregulated in the ECM1-high tumours. Pathway analysis was conducted using MetaCore (Clarivate Analytics) to gain insight into the features of tumours overexpressing ECM1. The top 10 most upregulated and downregulated pathways in tumours expressing high levels of ECM1 were identified (Figure 4-5). Upregulated pathways were enriched for cell adhesion, TGF-beta signalling and extracellular matrix remodelling. Downregulated pathways were mainly related to stem cell differentiation and lipid metabolism.

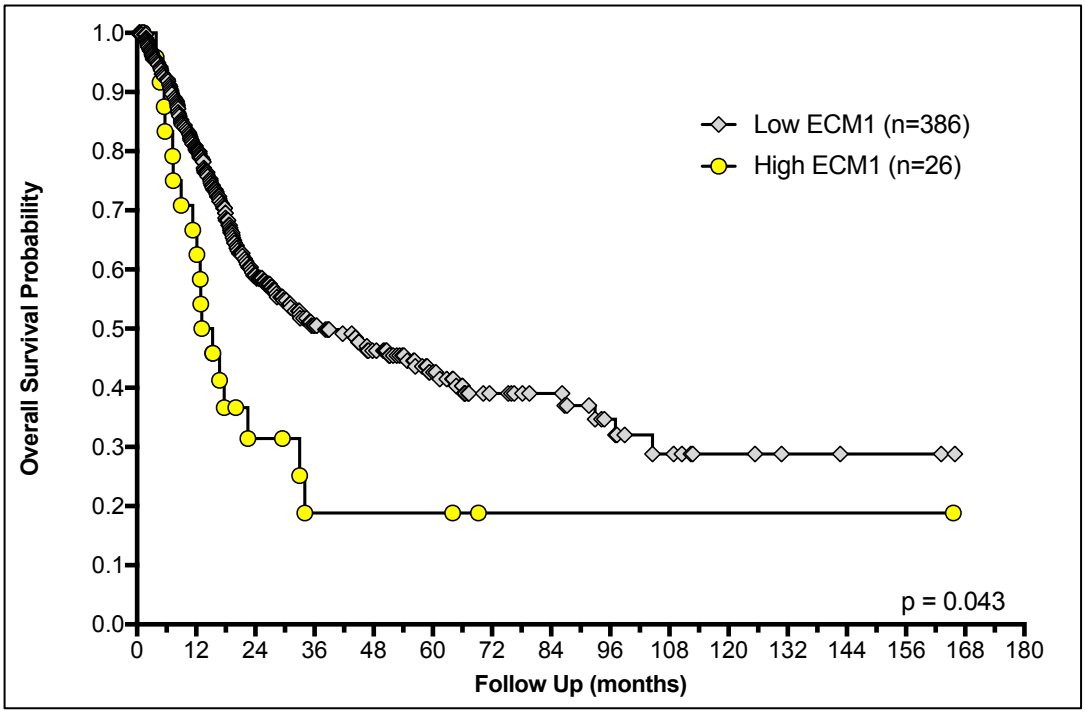

Figure 4-3: Kaplan-Meier plot for the TCGA data comparing patient survival based on high and low ECM1 expressing tumours.

The microarray analysis and visualisation platform R2 was used to interrogate expression array data from 412 fresh-frozen muscle-invasive bladder tumours (stage T2-T4) generated by TCGA [32]. A Kaplan-Meier plot was generated showing overall survival probability of patients with tumours expressing high or low levels of ECM1. The Mantel-Cox test was used to test whether there was a statistically significant difference in survival between the two groups. Patients whose tumours expressed high levels of ECM1 had statistically significant reduced overall survival ($p = 0.043$).

Table 4-4: Comparison of metadata from patients with tumours expressing high or low levels of ECM1 who remained disease free.

The microarray analysis and visualisation platform R2 was used to interrogate transcriptome data from 412 fresh-frozen muscle-invasive (stage T2-T4) bladder tumours generated by TCGA. Metadata was obtained from cBioPortal, the open access database for exploration of cancer genomic datasets. A comparison was conducted between patients with tumours that expressed high or low levels of ECM1 to determine the percentage of patients remaining disease free, and those whose tumours locally recurred or progressed to a higher stage.

	High (no.)	Low (no.)	High (%)	Low (%)
Disease Free	5	173	19.2	44.8
Recurred or Progressed	16	127	61.5	32.9
No data	5	86	19.23	22.3
TOTAL	26	386	100	100

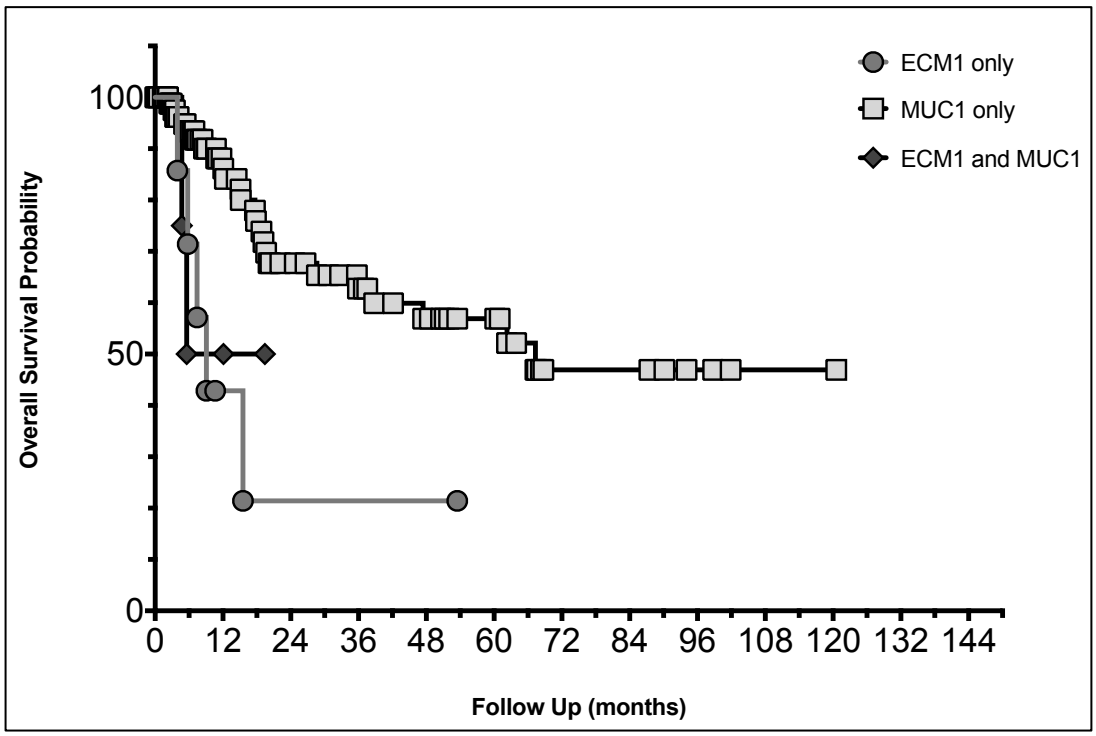

Figure 4-4: Kaplan-Meier plot comparing overall survival of patients with tumours expressing high levels of ECM1, MUC1, or ECM1 and MUC1 (TCGA dataset).

The microarray analysis and visualisation platform R2 was used to interrogate expression array data from 412 fresh-frozen muscle-invasive bladder tumours (stage T2-T4) from TCGA study [32]. A Kaplan-Meier plot was generated showing overall survival probability of patients with tumours expressing high levels of MUC1, ECM1, or both MUC1 and ECM1. The Mantel-Cox test was used to test whether there was a statistically significant difference in survival between the groups. Patients whose tumours expressed both ECM1 and MUC1 had statistically significant reduced overall survival compared to patients whose tumours expressed MUC1 alone ($p = 0.035$). Patients whose tumours expressed high levels of ECM1 also had statistically significant reduced overall survival compared to patients whose tumours expressed MUC1 alone ($p = 0.003$). No statistical significance was seen between the survival of patients whose tumours expressed ECM1 or ECM1 and MUC1 ($p = 0.809$).

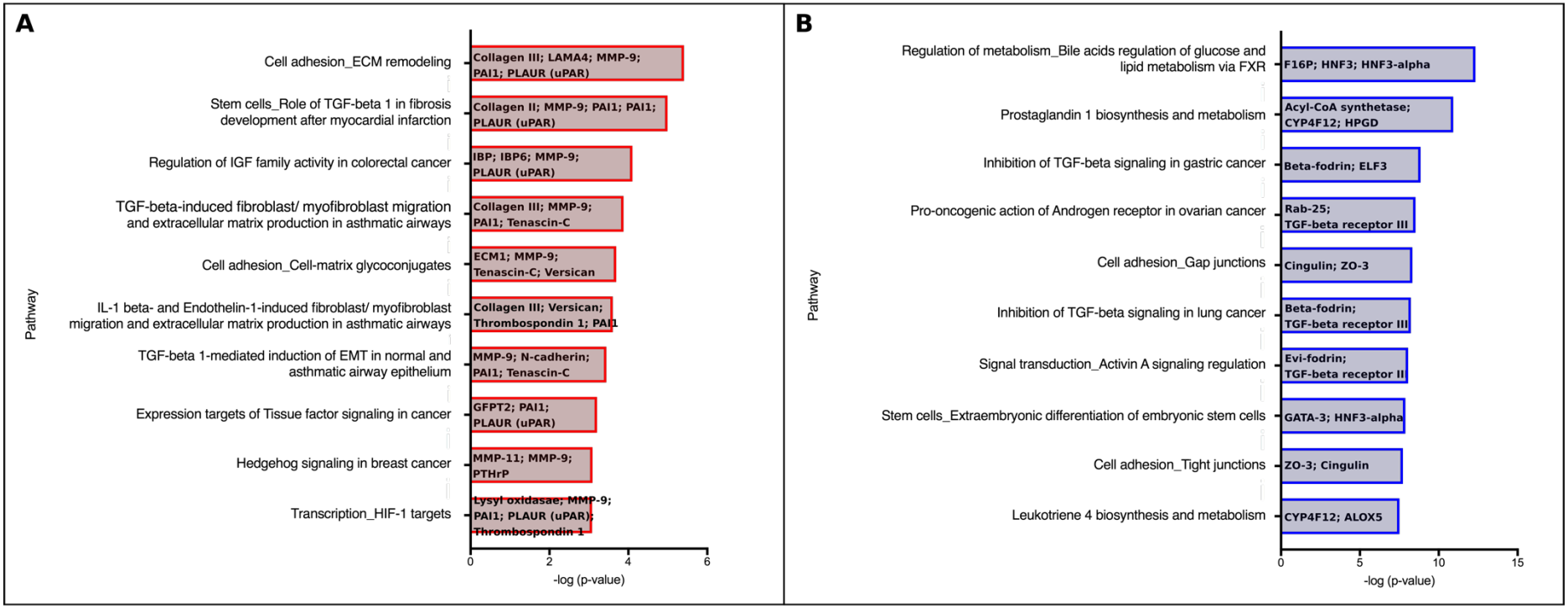

Figure 4-5: Pathway analysis of genes differentially expressed between ECM1 high and ECM1 low tumours.

R2 was used to interrogate expression data from the studies of Sjödahl *et al.* (2012) and Choi *et al.* (2014) [72, 75]. LIMMA analysis was conducted using GEO2R to determine genes that were significantly differentially expressed between tumours expressing high levels of ECM1 and low levels of ECM1 in each dataset. Venn analysis was conducted on these lists of probes using Partek Genomics software. Probes consistently upregulated and downregulated in both datasets were identified. Stringency settings were applied to include only probes that had a fold change greater than 2 or less than -2, and a p value less than 0.05. Pathway analysis was conducted in MetaCore in order to determine the top 10 most **A)** upregulated pathways and **B)** downregulated pathways based on these gene lists.

4.2.2 Immunohistochemistry analysis of ECM1 and MUC1 expression in a tissue microarray

Tissue microarrays (TMAs) comprising of 943 MIBC viable cores obtained from a collaborator were stained for ECM1 and MUC1 by immunohistochemistry. 108 cores (11.5%) stained positively for ECM1 of which 32 (3.4%) stained very strongly (+++) and 76 (8.1%) stained weakly (+). The remaining 835 (88.5%) were negative (-). ECM1 was mainly located in the cytoplasm of the cells, with some staining noted on the cell membrane. Nuclear staining was observed rarely. MUC1 staining was observed in a greater proportion of cores (n=386; 40.9%) with 111 (11.8%) staining moderately (++), and 275 (29.2%) staining weakly (+). The remaining 557 (59.1%) cores were negative (-). MUC1 staining was mainly located in the membrane and cytoplasm. Of the 108 ECM1-positive cores, 101 were also positive for MUC1. Staining of ECM1 and MUC1 was seen in similar locations on tumours positive for both. Representative examples of the ECM1 and MUC1 staining patterns are shown in Figure 4-6. The decode that will provide full metadata, including survival data, is awaited.

4.2.3 ECM1 knockdown in ECM1-high bladder tumour-derived cell lines

4.2.3.1 ECM1 isoform expression and selection of shRNAs for knockdown

The human ECM1 gene encodes three main splice variants: ECM1a, ECM1b and ECM1c. Reverse transcriptase PCR was performed using primers spanning alternatively spliced exons in order to identify the ECM1 isoforms expressed in each of the ECM1-high cell lines (Figure 4-7). Four bladder tumour-derived cell lines that do not fall into subgroup 2 (LUCC1, 97-7, J82, and VMCUB1) and a pooled sample of normal human urothelial cells (NHU-Pool) were also examined in order to determine if ECM1 isoform expression differed between the ECM1-high cell lines of subgroup 2 and cell lines assigned to the other subgroups (Figure 4-8) (Table 4-5). LUCC4 and LUCC5 were the only two cell lines to express all three isoforms of ECM1 with no other cell line of subgroup 2 expressing ECM1c. 647V expressed the ECM1a and ECM1b isoforms. HT-1376 and HT-1197 may also express ECM1b. For HT-1376 a band was seen at 166 bp for primer pair 6 indicative of ECM1b,

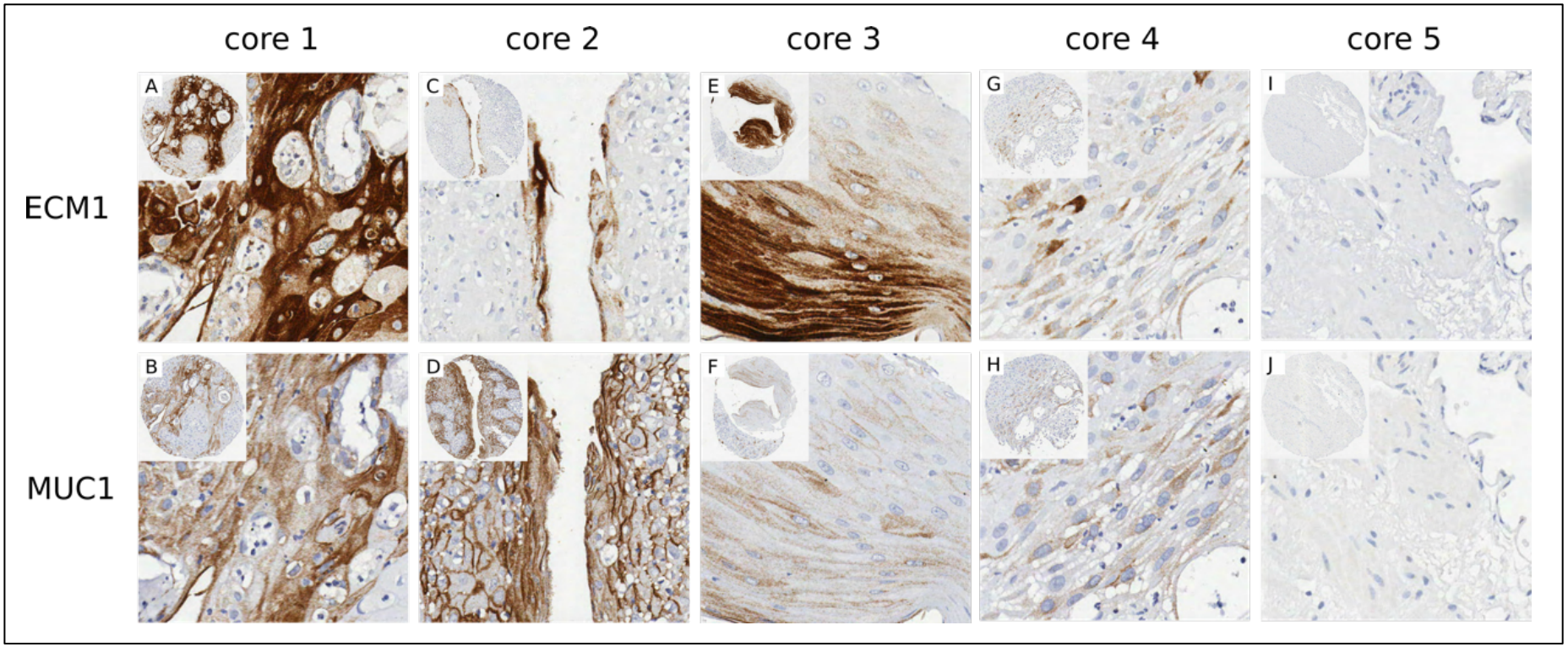

Figure 4-6: Photomicrographs of representative cores from the tumour microarray stained for ECM1 and MUC1 by immunohistochemistry.

TMAs consisting of FFPE cores from muscle-invasive bladder tumours were stained for ECM1 and MUC1 by IHC. Slides were stained using an antibody dilution of 1:200. Core 1 represents **A)** strong ECM1 staining (+++) and **B)** moderate MUC1 staining (++); core 2 represents **C)** weak ECM1 staining (+) and **D)** moderate MUC1 staining (++); core 3 represents **E)** strong ECM1 staining (+++) and **F)** weak MUC1 staining (+); core 4 represents **G)** weak ECM1(+) and **H)** weak MUC1 (+) staining; and core 5 represents negative staining for both **I)** ECM1 and **J)** MUC1 (-).

however a smear was seen below 100 bp for primer pair 4 making conclusive assessment of the expression of this isoform difficult. For HT-1197, a clear banding pattern indicating ECM1a expression was obtained using primers 1 to 5. Primer pair 6 failed and smearing below 100 bp for primer pair 4 made assessment of the expression of the ECM1b isoform difficult in this cell line. LUCC3 was the only cell line of the ECM1-high subgroup that definitively expressed only one isoform, ECM1a. J82 was not classified into subgroup 2 according to NMF analysis. However this cell line had elevated levels of ECM1 at both the mRNA and protein levels and was the only cell line outside of subgroup 2 that expressed isoforms other than ECM1a. The NHU-Pool sample also only expressed ECM1a (Table 4-5).

Short hairpin RNAs (shRNAs) delivered using a lentiviral vector system were chosen for ECM1 knockdown in four cell lines from subgroup 2 (HT-1376, LUCC4, HT-1197 and 647V). Plasmids containing shRNAs targeting the all three main splice variants of *ECM1* were selected in response to the observed expression pattern of the three isoforms in the cell lines.

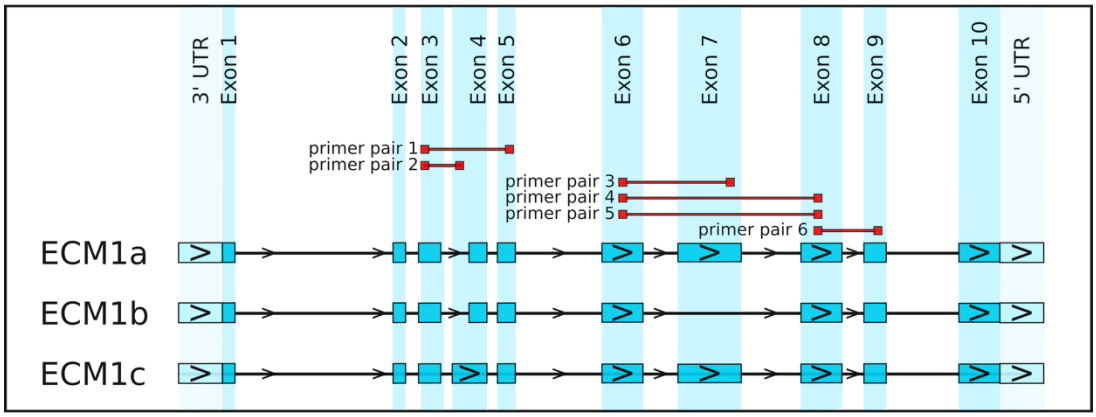

Figure 4-7 Primer pairs used to determine ECM1 isoform expression.

A diagram representing the linearised structures of the ECM1 isoforms a, b, c, illustrating the distribution of exons and the 3' and 5' untranslated regions (UTRs). The figure also depicts primers flanking alternatively spliced exons that were used in PCR analysis to differentiate between isoforms based on presence, absence or size of product. The represetntation of the ECM1 isoforms has been created from information obtained from the NCBI nucleotide database [183].

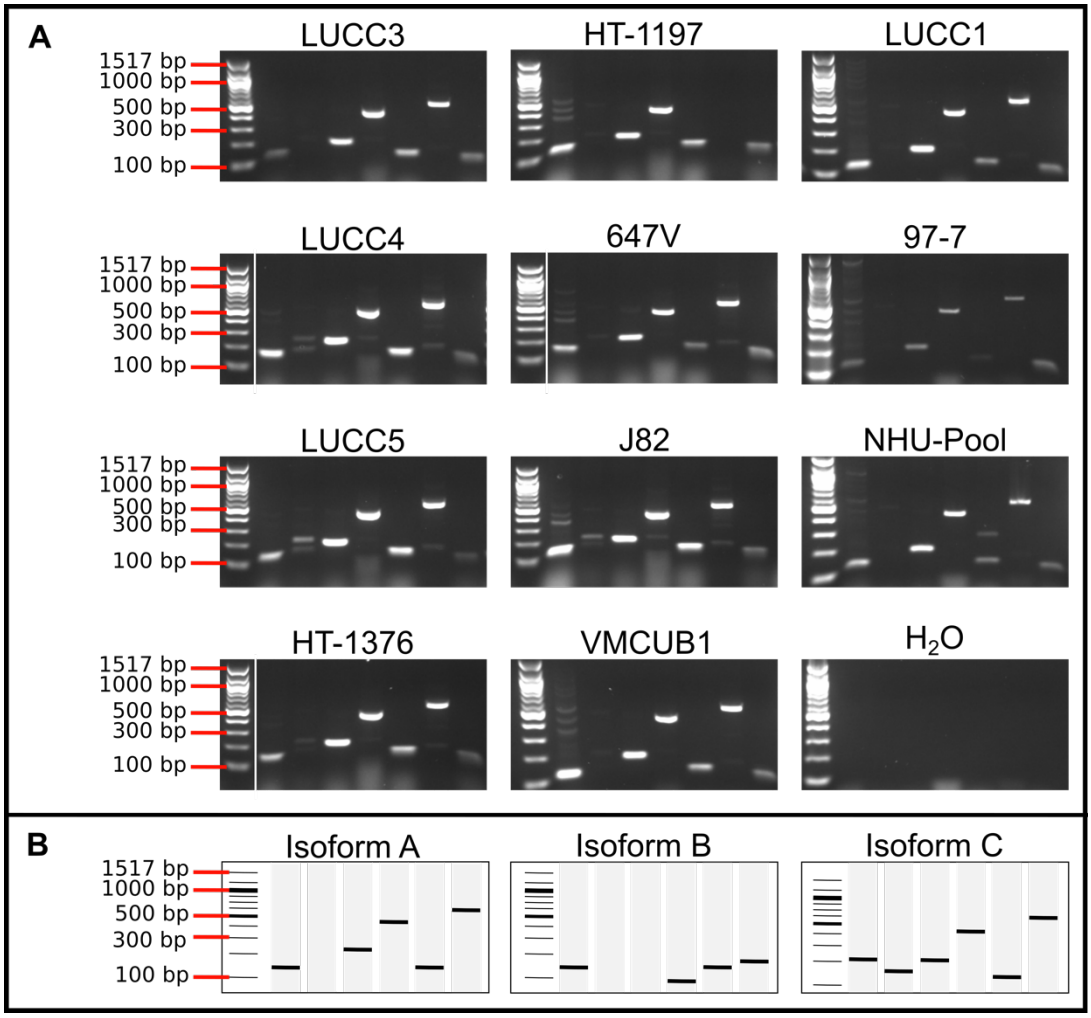

Figure 4-8: PCR analysis of ECM1 isoform expression in 11 cell lines.

PCR was used to identify which of the three isoforms of ECM1 (ECM1a, ECM1b and ECM1c) each cell line of subgroup 2 was expressing. Isoform expression was also assessed in an additional 4 bladder tumour-derived cell lines not classified into subgroup 2 and a pooled normal human urothelial sample (NHU-Pool). Water was used in place of cDNA as a negative control. Primers flanking alternatively spliced exons were used in order to differentiate between isoforms based on presence, absence or size of product. **A)** Images for each of the cell lines from left to right show: Lane 1: 100bp ladder (NEB), Lanes 2-7: PCR products generated using primer pairs 1, 2, 3, 4, 5, and 6, respectively, for the determination of ECM1 isoform expression (Chapter 2), Lane 8: PCR products generated using PICK3A primers as a positive control. **B)** An outline of the expected product sizes for each of the three isoforms. Representative of 1 experimental repeat.

Table 4-5: A summary of ECM1 isoform expression in 11 cell lines.

PCR was used to identify which of the three isoforms of ECM1 (ECM1a, ECM1b, and ECM1c) each cell line of subgroup 2 was expressing. An additional 4 bladder tumour-derived cell lines not classified into subgroup 2 and a pooled normal human urothelial sample (NHU-Pool) were also analysed. This table summarises which of the isoforms each cell line is expressing.

Cell Line	ECM1a	ECM1b	ECM1c
LUCC3	+	-	-
LUCC4	+	+	+
LUCC5	+	+	+
HT-1376	+	?	-
HT-1197	+	?	-
647V	+	+	-
J82	+	+	?
VM-CUB-1	+	-	-
LUCC1	+	-	-
97-7	+	-	-
NHU-Pool	+	-	-

4.2.3.2 Puromycin dose assay.

shRNA plasmids used for the ECM1 knockdown experiments contain a puromycin resistance cassette for the selection of successfully transduced cells. A puromycin dose assay was carried out to determine the lowest concentration of puromycin needed to efficiently kill untransduced cells. The minimum concentration of puromycin that killed all cells after 7 days was used as the selection dose. 647V was determined to require the lowest dose of puromycin at 0.3 μg/ml to kill all cells, whilst HT-1197 required the highest dose at 2.0 μg/ml (Figure 4-9). The selection dose for both HT-1376 and LUCC4 was determined to be 1 μg/ml (Figure 4-9). Cells were maintained in half the concentration of selection dose.

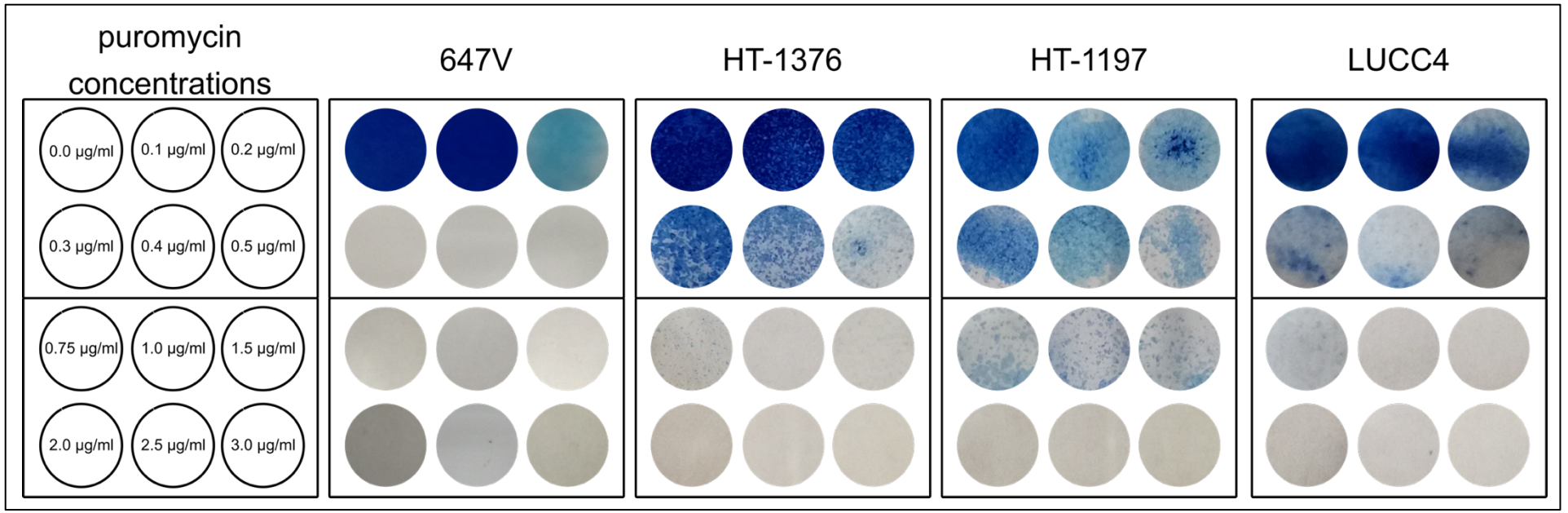

Figure 4-9: Puromycin dose response assay.

Cells were seeded at 250,000 cells per well in a 6-well dish, cultured for 48 h then treated with a range of puromycin doses (0-3.0 µg/ml) for 7 days. Cells were stained with bromophenol blue. The minimum concentration of puromycin required to kill all cells was determined for each cell line and was subsequently used as the selection dose in shRNA knockdown experiments. Representative of 1 experimental repeat.

4.2.3.3 Confirmation of ECM1 knockdown by qRT-RCR and western blot analysis

Four cell lines (HT-1376, LUCC4, HT-1197 and 647V) were stably transduced with shRNAs targeting ECM1 (KD1 and KD2) or control constructs (scramble and non-hairpin shRNAs). To assess the efficiency of knockdown, cDNA was generated from total RNA isolated from the transduced cells and real-time quantitative PCR (qRT-RCR) analysis conducted (Figure 4-10). For all cell lines transduced with KD1 or KD2, ECM1 expression was reduced to a level that was at least 80% lower than that seen in the parental cell line. The greatest knockdown efficiency (93.2%) was achieved for LUCC4 with KD1. The lowest knockdown efficiency was 80.6% for 647V with KD2. All scramble and non-hairpin (NHP) controls demonstrated levels of ECM1 similar to that of the parental cell lines apart from the NHP control for LUCC4 which expressed ECM1 at a level that was 40% less than that detected in the parental cell line.

Knockdown at the mRNA level does not always correlate with decreased protein expression, particularly in the case of stable proteins with long half-lives, and previous reports suggest that some genes require >95% knockdown at the mRNA level in order to induce changes in protein expression[207]. For this reason, and as proteins are widely considered to be the functional effectors of a cell, knockdown should also be validated at the protein level by western blot analysis[208]. Protein lysates were also harvested from knockdown and control cell lines and ECM1 protein levels were evaluated by western blot analysis. For HT-1376, LUCC4 and HT-1197 ECM1 could no longer be detected at the protein level (Figure 4-11). 647V ECM1 protein levels also appeared to be reduced in the scramble and NHP control cell lines despite these cells exhibiting only a 20-30% reduction in ECM1 at the mRNA level as compared to parental cells (Figure 4-11). This may be reflective of the much lower ECM1 transcript and protein levels in the 647V parental cell line compared to the other ECM1-high cell lines. As protein levels in the 647V parental cell line appeared low in western blot analysis, the slight reduction in ECM1 expression at the mRNA level in the scramble and NHP control of the 647V cell line compared to the parental may result in a reduction in protein below detectable levels using western blot analysis.

Western blot analysis of ECM1 levels was conducted over several subsequent passages (Appendix G) and prior to any further experiments to ensure continued knockdown of ECM1.

4.2.4 Cell-based phenotypic assays on ECM1 knockdown cells

4.2.4.1 Cell Morphology

Lentiviral transductions with either the ECM1 knockdown or control shRNAs were not associated with any observable differences in the cells' morphology as compared to their corresponding parental cell lines (Figure 4-12).

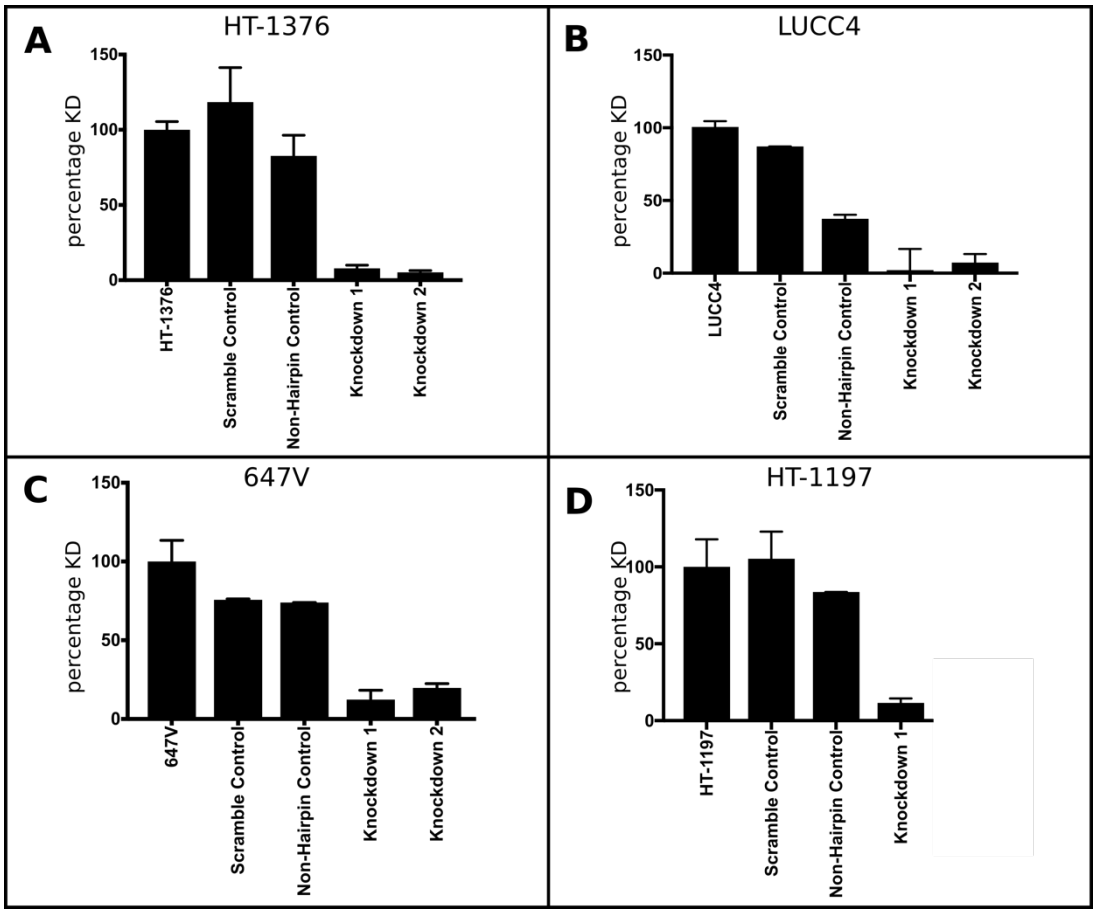

Figure 4-10: qRT-RCR confirmation of mRNA knockdown of ECM1.

Two shRNAs targeting ECM1 and two control shRNAs (scramble and non-hairpin control) were transduced into **A)** HT-1376 **B)** LUCC4 and **C)** 647V using lentiviral vectors. Only one shRNA was successfully transduced into **D)** HT-1197. Knockdown efficiency was examined by qRT-PCR analysis of ECM1. The expression of ECM1 was normalised against that of SDHA and relative to each parental cell line. Error bars indicate the range across triplicate wells.

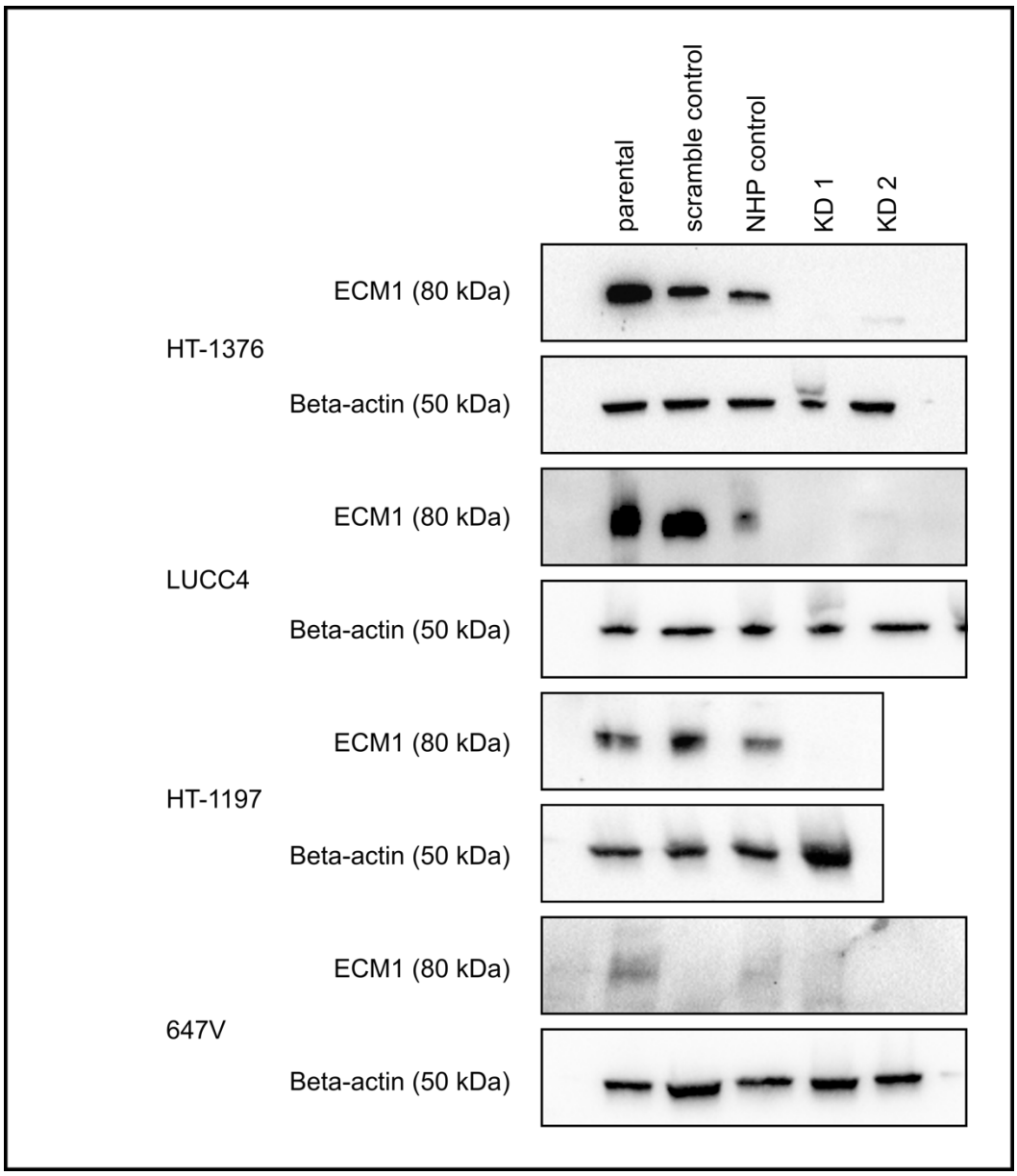

Figure 4-11: Western blot confirmation of knockdown of ECM1 at the protein level.

Two shRNAs targeting ECM1 and two control shRNAs (scramble control and NHP control) were transduced into HT-1376, LUCC4 and 647V using lentiviral vectors. Only one shRNA was successfully transduced into HT-1197. Knockdown efficiency was examined by western blot analysis using an antibody specific to ECM1.

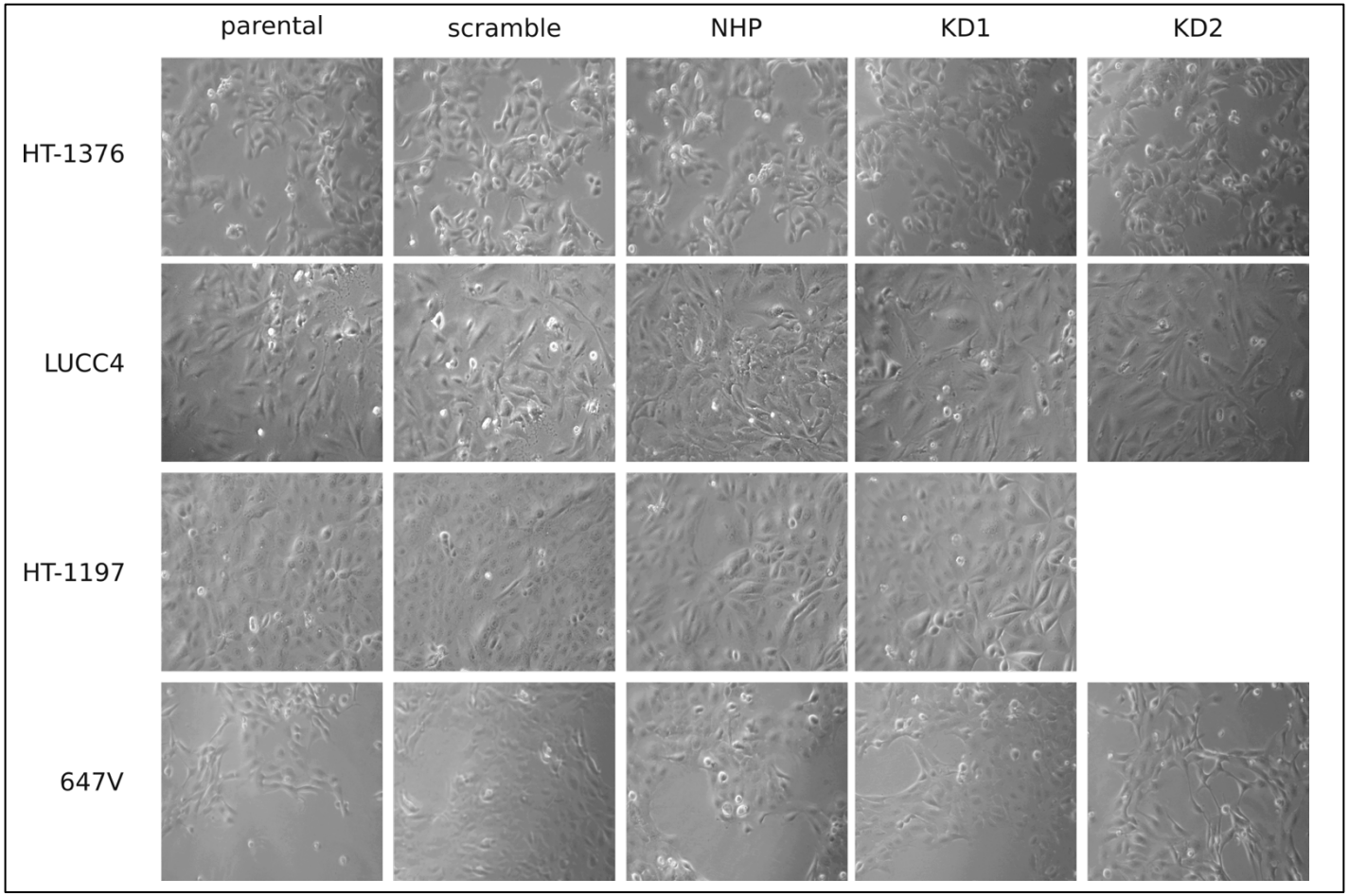

Figure 4-12: Photomicrographs of ECM1 knockdown, shRNA control and parental cell lines.

Phase contrast images were captured at 200X magnification for the four parental cell lines (HT-1376, LUCC4, HT-1197 and 647V) and the corresponding scramble control, NHP control and ECM1 knockdown cell lines at 50-100% confluence.

4.2.4.2 Growth curves

A growth curve for HT-1376 parental, both ECM1 shRNA knockdowns, and both controls was conducted (Figure 4-13 A). Five-thousand cells were seeded into 6 cm^2 dishes and cells were counted at 3, 6, 9, 12, 15, 18 and 21 days. One-way ANOVA and Tukey's multiple comparisons tests were applied. No significant difference was seen in cell counts between parental cell lines, or the corresponding ECM1 knockdown, scramble and NHP controls .

Growth curves for the parental, ECM1 knockdowns and shRNA controls were also generated for cell lines LUCC4, HT-1197, and 647V in a similar manner, but cell counts were made at a reduced number of time points (1, 7, 14, and 21 days) (Figure 4-13 B C D). No significant difference was seen between any of the parental cells lines, ECM1 knockdowns or scramble and NHP controls.

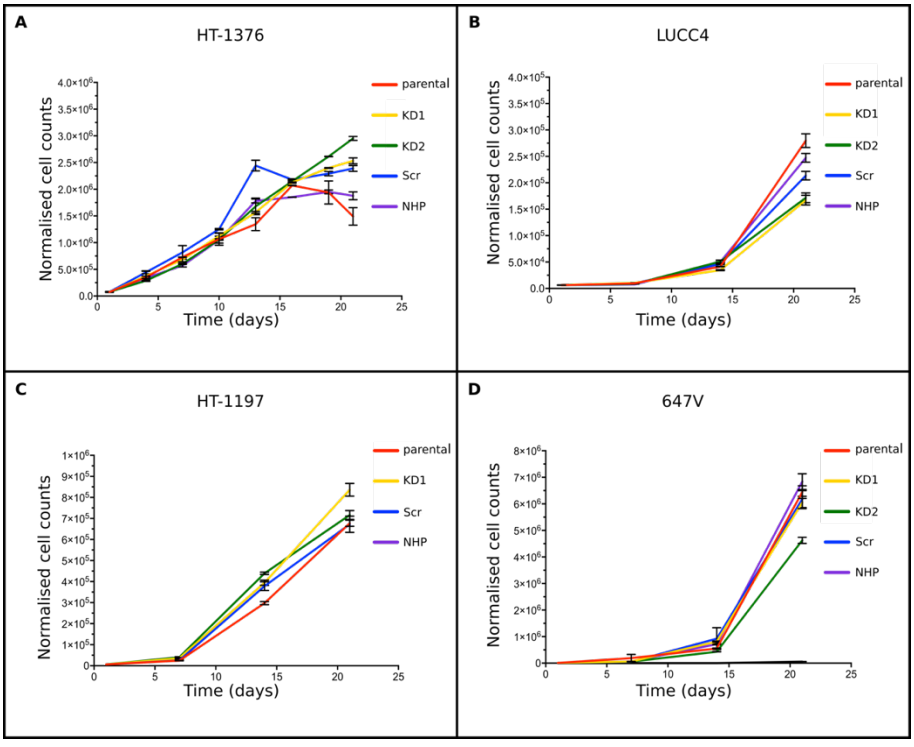

Figure 4-13: Growth curves for HT-1376, LUCC4, HT-1197 and 647V parental cell lines, ECM1 shRNA knockdowns and shRNA controls.

Growth curves were generated for **A)** HT-1376, **B)** LUCC4, **C)** HT-1197, and **D)** 647V parental, ECM1 knockdowns (KD1; KD2) and their non-hairpin (NHP) and scramble (Scr) control lines. Cell counts were made at 8 time points over 21 days (1, 4, 7, 10, 13, 15, 18, and 21 days) for HT-1376 and at four time points over 21 days (1, 7, 14 and 21 days) for LUCC4, HT-1197, and 647V. Three wells were counted for each time point. One-way ANOVA and Tukey's multiple comparison tests were used and showed that there were no statistically significant differences in the growth rates of the parental cell lines, the ECM1 knockdowns, scramble controls and NHP controls ($P>0.999$ in each comparison). Error bars show standard error of the mean. Representative of 1 experimental repeat.

4.2.4.3 Wound healing assays

The migration of HT-1376 parental, ECM1 knockdown, and scramble control cells was analysed using a wound healing assay (Figure 4-14). The shRNA controls and parental cell lines moved into the scratched area and the wound was completely closed within 48 h. Knockdown of ECM1 was seen to inhibit wound healing ability and movement into the scratched area was much slower for the knockdown cell lines with incomplete healing after 48 h. Semi-quantitative analysis was performed by measuring wound area using ImageJ software and percentage area closed was calculated. Ordinary one-way ANOVA and Tukey's multiple comparisons revealed a significant difference in wound healing after 24 h between KD1 and all control cell lines ($p < 0.005$ in all cases) and between both knockdowns and controls at 48 h ($p < 0.0001$ in all cases).

The effect of ECM1 on the migration of LUCC4, HT-1197 and 647V was also analysed using wound healing assays. For LUCC4, the scramble control closed the scratched area much more rapidly than the ECM1 knockdown (Figure 4-15). Semi-quantitative analysis was performed by measuring wound area using ImageJ software and percentage wound closure calculated. Ordinary one-way ANOVA and Tukey's multiple comparisons revealed a significant difference in wound healing between KD1 and the scramble control for the LUCC4 cell lines after 24 h ($p = 0.0079$) and 48 h ($p < 0.0001$). For HT-1197 knockdown of ECM1 was seen to slightly inhibit wound healing ability and movement into the scratched area was fractionally slower for the knockdown cell line compared to the scramble control (Figure 4-16). No statistically significant difference was noted between wound healing ability of the ECM1 knockdown and scramble control for HT-1197. Both the ECM1 knockdown and scramble control for 647V showed rapid closure of the scratch area with complete closure of the wound area for both cell lines after 24 h (Figure 4-17).

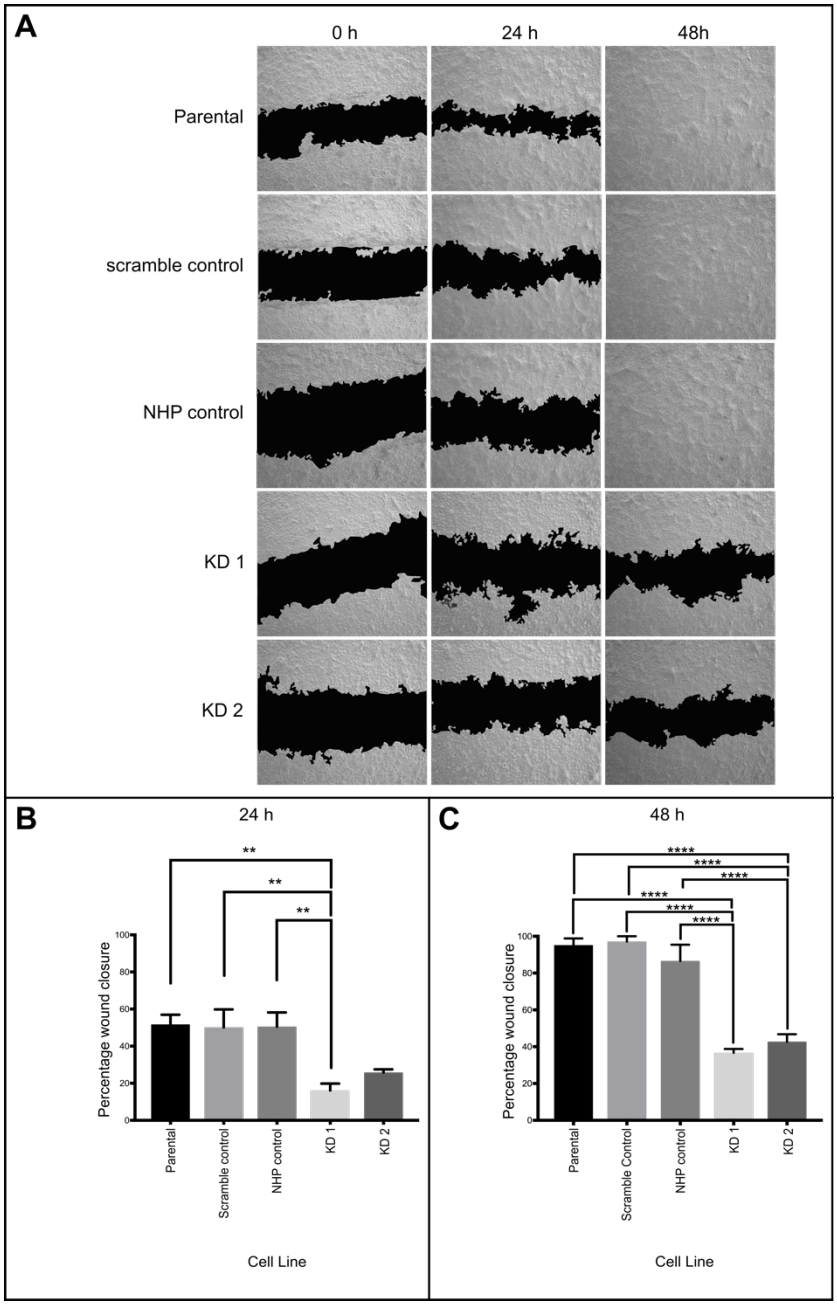

Figure 4-14: Wound healing assay carried out using HT-1376 parental, ECM1 knockdown and control cells.

The effect of ECM1 knockdown on the wound healing ability of the HT-1376 cell line was determined by the use of a wound healing assay. **A)** Images were captured at 50X magnification at 0, 24 and 48 h for the HT-1376 parental cell line, the two ECM1 knockdowns (KD1 and KD2) and two shRNA controls (HT-1376 scramble and NHP control). **B)** Statistical analysis of the percentage wound closure after 24 h was conducted using ordinary one-way ANOVA and Tukey's multiple comparisons. This showed KD1 to have a statistically significant slower wound healing rate after 24 h than the HT-1376 parental, scramble control, or NHP control lines ($p = 0.005$, 0.008, 0.007, respectively). **C)** Similar analysis of the percentage migration after 48 h showed that both KD1 and KD2 had a statistically significant slower wound healing rate than the HT-1376 parental, scramble control or NHP control lines ($p < 0.0001$ for all comparisons). Representative of three experimental repeats, each with three replicate wounds.

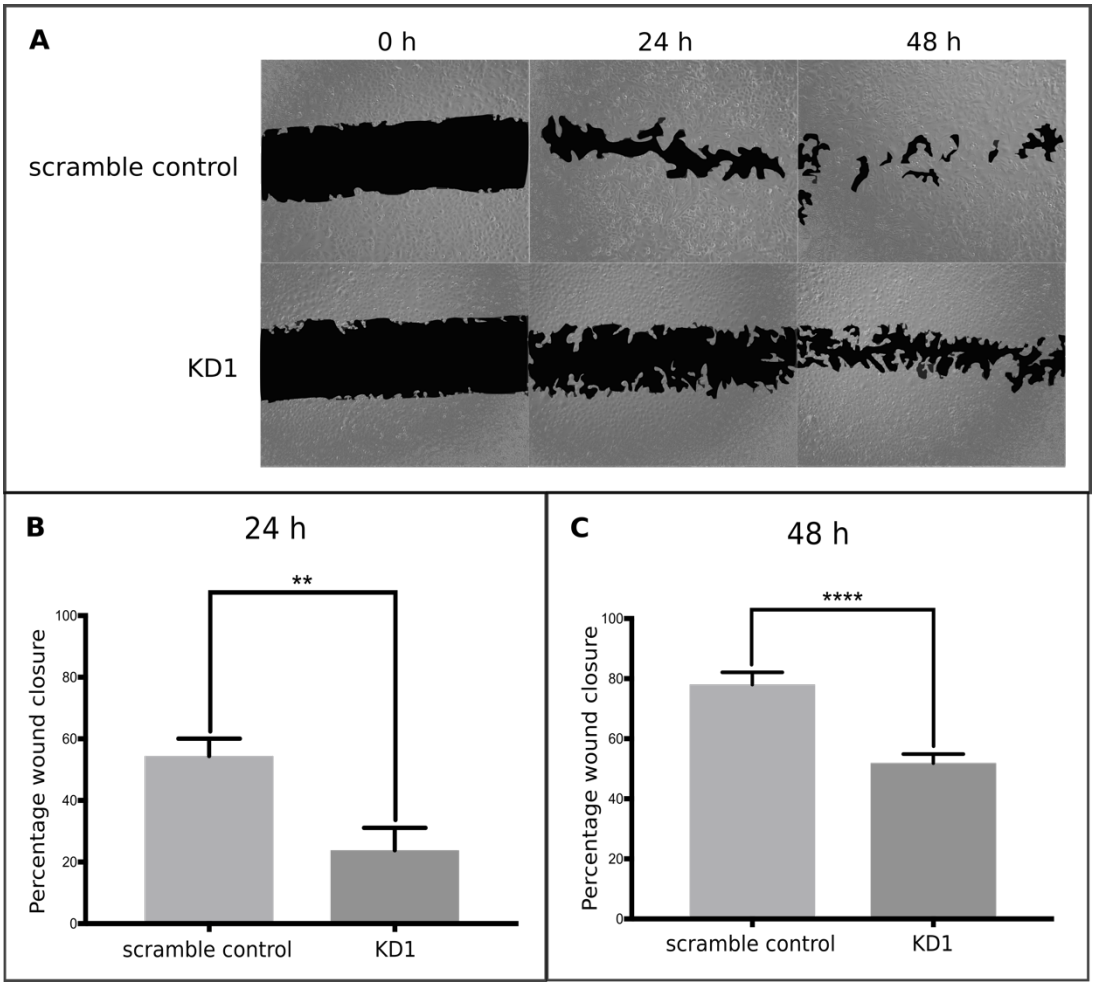

Figure 4-15: Wound healing assay carried out using LUCC4 ECM1 KD1 and scramble control cells.

The effect of ECM1 knockdown on the wound healing ability of the LUCC4 cell line was determined by the use of a wound healing assay. **A)** Images were captured at 50X magnification at 0, 24 and 48 h for an ECM1 knockdown (KD1) and scramble control line. **B)** Statistical analysis of the percentage wound closure after 24 h was conducted using ordinary one-way ANOVA and Tukey's multiple comparisons. This showed KD1 to have statistically significant slower wound healing rate after 24 h than the scramble control line ($p = 0.0079$). **C)** Similar analysis of the percentage wound closure after 48 h showed the ECM1 KD1 to have a statistically significant slower wound healing rate than the scramble control line ($p < 0.0001$). Representative of two experimental repeats, each with three replicate wounds.

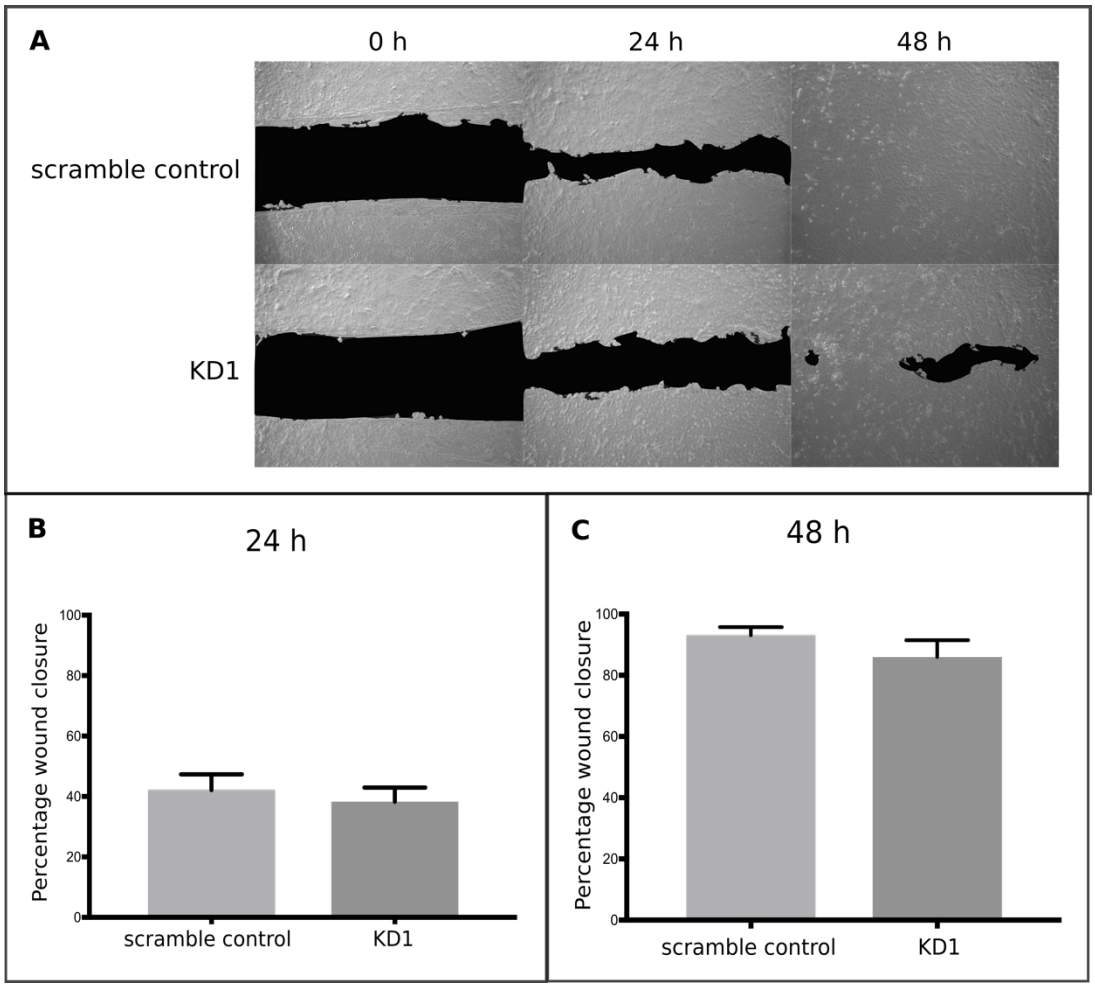

Figure 4-16: Wound healing assay carried out using HT-1197 ECM1 KD1 and scramble control cells.

The effect of ECM1 knockdown on the wound healing ability of the HT-1197 cell line was determined by the use of a wound healing assay. **A)** Images were captured at 50X magnification at 0, 24 and 48 h for ECM1 knockdown (KD1) and scramble control lines. **B)** Statistical analysis of the percentage migration after 24 h was conducted using ordinary one-way ANOVA and Tukey's multiple comparisons. This showed no significance between the wound healing ability of the ECM1 KD and scramble control lines ($p = 0.955$). **C)** Similar analysis of the percentage wound closure after 48 h was conducted and this showed no significant difference in the wound healing ability of the KD1 and the scramble control line ($p = 0.396$). Representative of two experimental repeats, each with three replicate wounds.

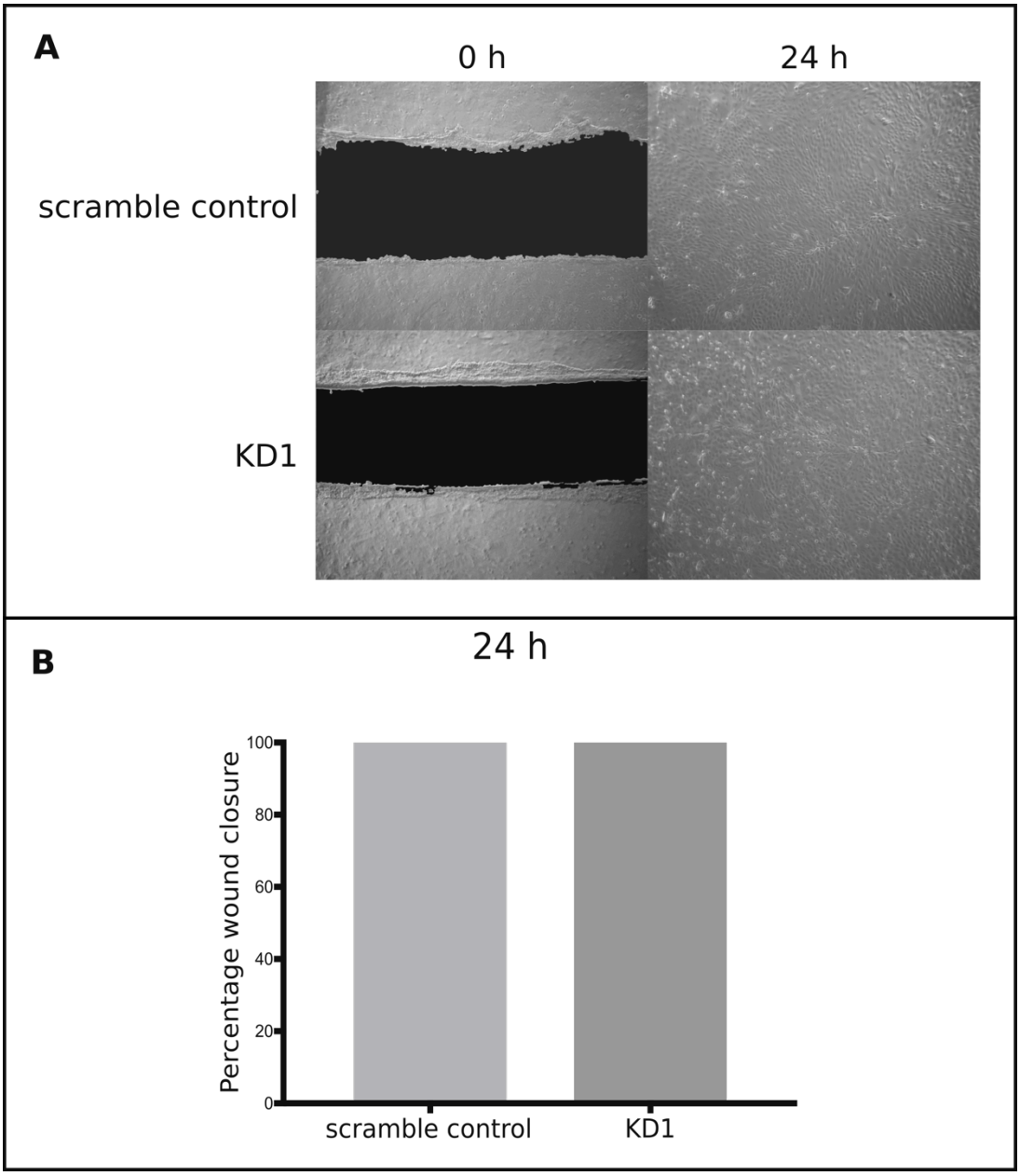

Figure 4-17: Wound healing assay carried out using 647V ECM1 KD1 and scramble control cells.

The effect of ECM1 knockdown on the wound healing ability of the 647V cell line was determined by the use of a wound healing assay. **A)** Images were captured at 50X and 100X magnification at 0 h and 24 h respectively for ECM1 knockdown (KD1) and scramble control lines. **B)** Statistical analysis of percentage migration after 24 h was conducted using ordinary one-way ANOVA. This showed no significant difference in the wound healing ability of the ECM1 KD and scramble control lines ($p > 0.999$). Representative of two experimental repeats, each with three replicate wounds.

In order to assess whether the ECM1-high cells lines were dependent upon ECM1 expression for the wound healing ability, treatment of the HT-1376 ECM1 KD1 cell line with recombinant ECM1 was carried out (Figure 4-18). Wound healing assays were conducted using the HT-1376 KD1 cell line in combination with recombinant ECM1 at concentrations ranging from 100 ng/ml to 1 μg/ml. As previously observed (section 4.2.4.3), KD1 had significantly reduced wound healing ability compared to the scramble control at 24 h ($p = 0.04$) and 48 h ($p = 0.0015$). A statistically significant reduction in wound healing as compared to the scramble control was also seen at 24 h for KD1 treated with 200 ng/ml ($p = 0.031$), 500 ng/ml ($p = 0.003$) and 750 ng/ml ($p = 0.021$) recombinant ECM1. However no significant difference was observed at concentrations of 100 ng/ml ($p = 0.069$) or 1 μg/ml ($p = 0.490$). At 48 h statistically significant reduced wound healing compared to the scramble control was noted for KD1 treated with 100 ng/ml ($p = 0.0004$), 200 ng/ml ($p = 0.0027$), 500 ng/ml ($p < 0.0001$) and 750 ng/ml ($p < 0.0001$). No statistical significance was noted between KD1 treated with 1 μg/ml recombinant ECM1 and the scramble control ($p= 0.276$) at 48 h, indicating that treatment with recombinant ECM1 at this concentration partially recovers the wound healing ability of the ECM1 knockdown cells.

4.2.4.4 Transwell Assays

Further examination of the effect of ECM1 knockdown on migratory ability was conducted using transwell assays. No differences in migratory ability of ECM1 knockdown cells (KD1 and KD2) and the control cell lines (parental, scramble and NHP) for HT-1376, HT-1197 or 647V were seen. LUCC4 ECM1 knockdown cell lines showed a decrease in migratory capacity of more than 90% as compared to the parental cell line and scramble control lines (Figure 4-19). The non-hairpin (NHP) control for LUCC4 had a 70% reduction in the number of migrated cells compared to the parental and scramble control lines.

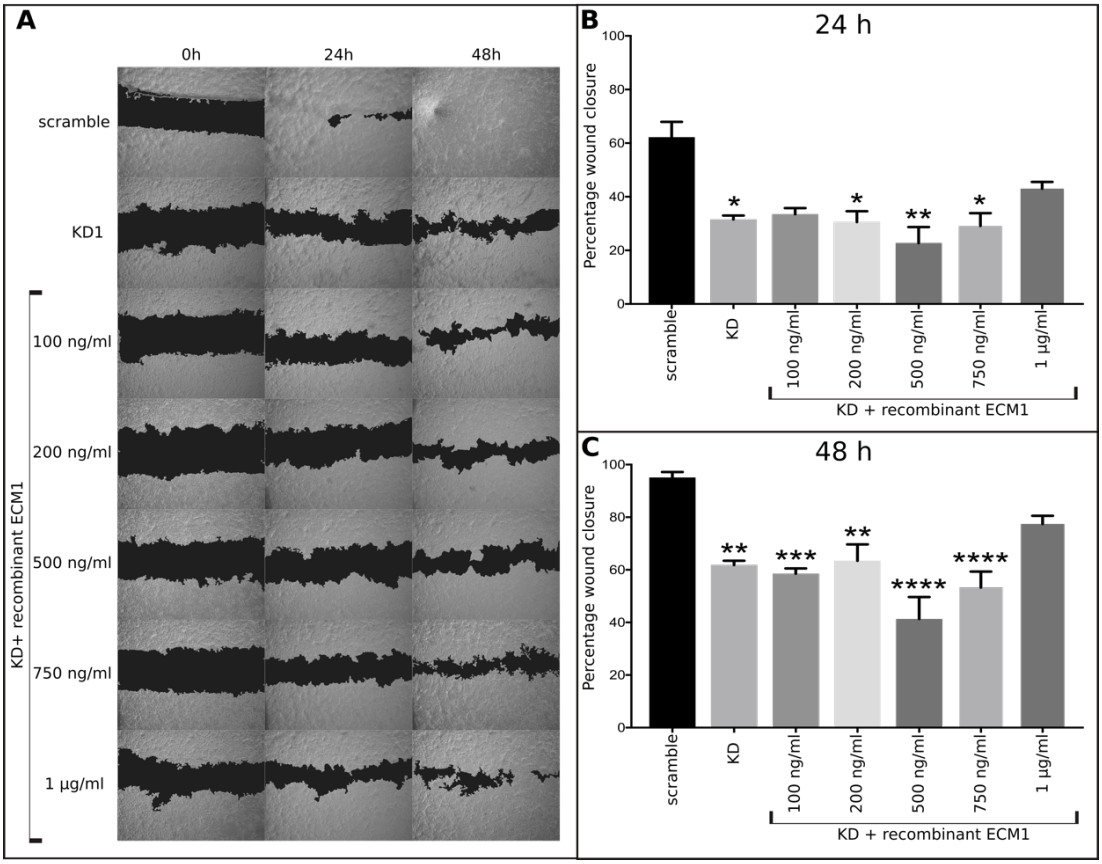

Figure 4-18: Wound healing assay carried out using HT-1376 scramble control and ECM1 knockdown cells treated with recombinant ECM1.

A wound healing assay was carried out using HT-1376 scramble control and KD1 lines treated with a range of recombinant ECM1 concentrations (0, 100, 200, 500, 750 ng/ml, and 1 µg/ml) in order to assess the effect of recombinant ECM1 treatment on wound healing ability. **A)** Images were captured at 50X magnification at 0, 24 and 48 h. Three replicate wells were treated at each concentration and three images were taken per well for analysis. **B)** Statistical analysis of the percentage migration after 24 h was conducted using ordinary one-way ANOVA and Tukey's multiple comparisons test. This showed KD1 to have a statistically significant slower wound healing rate after 24 h than the scramble control, as did KD1 treated with 200, 500 and 750 ng/ml recombinant ECM1 ($p = 0.04$, 0.031, 0.003 and 0.021 respectively). No statistical significance was noted between KD1 treated with 100 ng/ml or 1 µg/ml recombinant ECM1 and the scramble control ($p = 0.069$ and 0.490 respectively). **C)** Similar statistical analysis was conducted at 48 h and showed KD1 to have statistically significant slower wound healing rate after 48 h than the scramble control, as did KD1 treated with 100, 200, 500 and 750 ng/ml recombinant ECM1 ($p = 0.0015$, 0.0004, 0.0027, <0.0001 and <0.0001 respectively). No statistical significance was noted between KD1 treated with 1 µg/ml recombinant ECM1 and the scramble control ($p= 0.276$). (Key: * p = 0.05-0.01; ** p = 0.009-0.001; *** p = 0.0009-0.0001; **** p = <0.0001). Representative of 2 repeats.

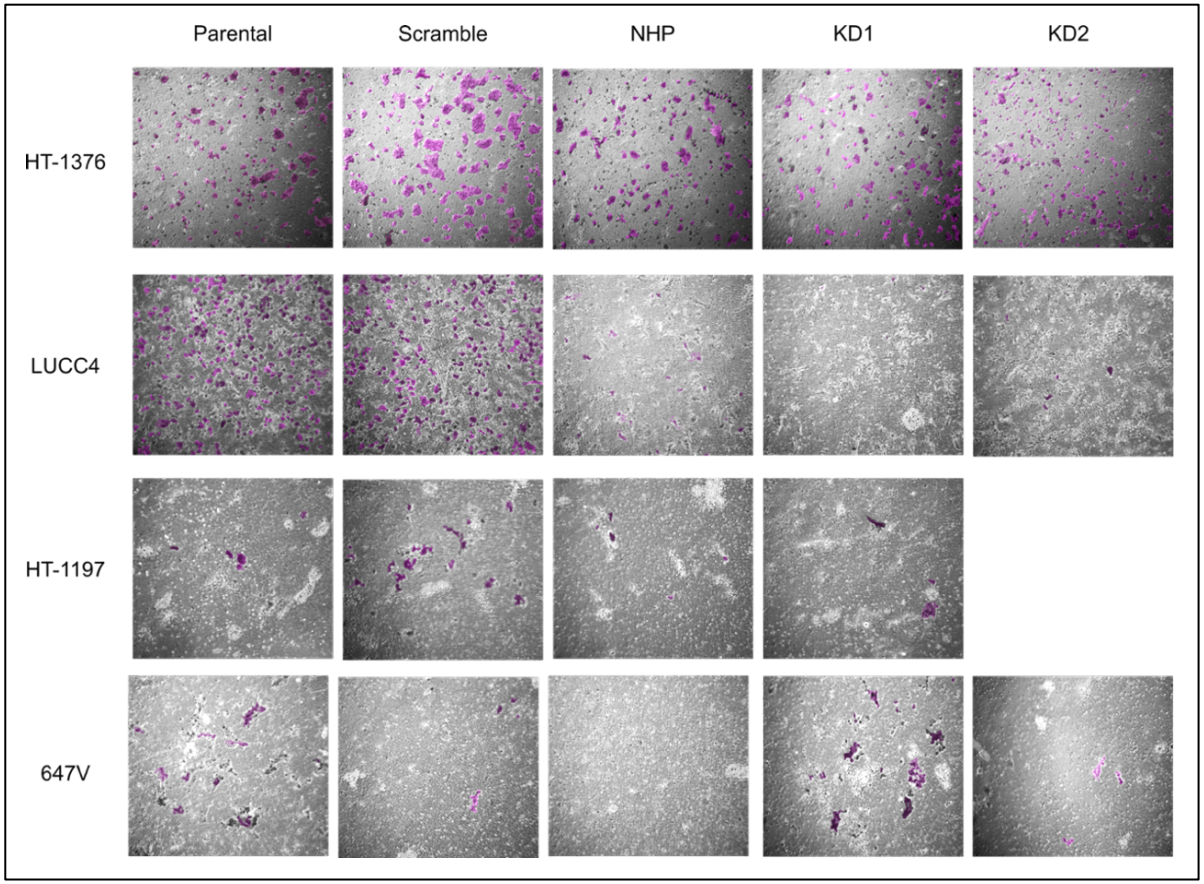

Figure 4-19: Transwell assays in HT-1376, LUCC4, HT-1197 and 647V cell lines with shRNA-mediated knockdown of ECM1.

The effect of ECM1 on the migration capacity of **A)** HT-1376, **B)** LUCC4, **C)** HT-1197 and **D)** 647V cell lines was determined by the use of transwell assays for each parental cell line, two ECM1 shRNA knockdown lines (except in the case of HT-1197), and two shRNA control lines (scramble and NHP). No difference was seen between ECM1 knockdown and control cell lines for HT-1376, HT-1197 or 647V. In LUCC4, ECM1 knockdown cells showed a >90% reduction in migrated cells compared to the parental and scramble controls. Representative of 1 experimental repeat.

4.3 Discussion

The ease of availability and longevity of cell lines makes multiple experiments and repeats with the same cell lines possible. However, some resemblance to the original tumour can be lost as the conditions under which cells are cultured may not truly reflect the original conditions in which the primary tumour developed, for example, nutrients are more readily available to cultured cells, there is no immune competition and no extracellular matrix components. This can result in different characteristics being acquired by cell lines compared to the tumour of origin[75]. In order to validate whether the subset of ECM1-high cell lines classified into subgroup 2 exhibited characteristics that truly reflected those of primary tumours hierarchical clustering based on mRNA expression levels of ECM1 was performed using publicly available gene expression data generated from primary bladder tumours. We found that ECM1 overexpressing tumours partitioned into distinct clusters in four different datasets which suggests a ECM1-high subgroup is also present in primary bladder tumours.

Previous studies have shown an association between ECM1 expression and decreased survival rates in other carcinomas including laryngeal [119, 184], breast [116] and hepatocellular carcinomas [118]. In this study, a Kaplan–Meier plot was using transcriptome data obtained from the latest TCGA study [185, 186], revealed that high ECM1 expression was significantly associated with reduced overall survival and a higher likelihood of progression to a higher stage as compared to tumours expressing low levels of ECM1. The association of high ECM1 expression with lower survival rates and a higher likelihood of progression may highlight ECM1 as a potential prognostic marker in bladder cancer patients.

To gain further insights into the functional role of ECM1 in primary bladder tumours, differential pathway analysis was carried out using MetaCore with gene lists generated by LIMMA comparisons of ECM1-high and ECM1-low expressing bladder tumours in publicly available transcriptome datasets. This determined the top 10 most upregulated and downregulated pathways in ECM1-high tumours. An interesting feature of the genes identified by LIMMA analysis was the high expression of six keratins in the ECM1-high tumours. Keratins are broadly categorised into type 1 and type 2 keratins, and form obligate heteropolymers in set pairs between these two types [187]. Their normal physiological function is to protect

the structural integrity of the epithelium from mechanical and non-mechanical stress factors [187], and they are also involved in the regulation of a diverse range of cellular functions, including apico-basal polarisation, control of protein translation and organisation of the positioning of organelles within the cell [187]. Keratins are also used as diagnostic tools and as prognostic markers for a variety of cancer types including colorectal, lung and breast cancer, and may play a regulatory role in tumorigenesis of cancers of an epithelial origin [187, 188].

Our analysis showed upregulation of each of the three distinct isoforms of keratin 6 (KRT6a, KRT6b, and KRT6c) [189] and its type two partner keratin 16 (KRT16) were upregulated in the ECM1-high tumours. KRT6 and KRT16 are predominantly expressed in squamous epithelia [189], and in bladder cancer keratin 6 is highly expressed in basal-squamous muscle-invasive tumours, and is associated with poor survival outcomes and increased recurrence in patients [190]. In addition to keratin 6, 10 markers typical of the basal subtype of bladder cancer were also upregulated in the ECM1-high tumours, and four luminal markers were downregulated [86]. Furthermore, the majority of ECM1-high tumours fell into basal-squamous subtypes according to the original studies in which they were classified. This suggests that ECM1-high tumours are a Basal/Squamous subgroup.

The EGFR ligand heparin-binding EGF-like growth factor (HB-EGF) was also upregulated in the ECM1-high tumours. Increased expression of HB-EGF is seen in a number of cancers including ovarian, breast and oesophageal tumours, and is associated with tumour progression, cell proliferation and increased metastatic potential [191-194]. In bladder cancer, HB-EGF overexpression has been demonstrated to enhance tumorigenesis in mice [195], and has been correlated with decreased survival rates in patients [196]. It may be proposed that high expression of HB-EGF in the ECM1-high tumours contributes to the decreased survival rates noted for these patients.

An association between HB-EGF, and EGFR mediated EMT has been reported as increased expression of the mesenchymal marker vimentin (VIM) and decreased expression of the epithelial marker e-cadherin was observed at the protein level by immunofluorescence staining in stably transduced keratinocytes with constitutively expressing HB-EGF [197]. Moreover, in the same model, increased expression of EMT markers including SNAI2 and ZEB1 was observed at the mRNA level, suggesting that HB-EGF is a mediator of the molecular mechanisms

that control EMT and may promote an invasive cell phenotype [197]. In our analysis, the EMT markers VIM and SNAI2 were also upregulated in the ECM1-high tumours. The transformation of tumour cells from an epithelial to a mesenchymal phenotype has long been associated with tumour invasion and metastasis [198], and thus our results may suggest that ECM1-high tumours have an increased metastatic potential. However, unlike previous findings in breast cancer which showed increased likelihood of lymph node metastasis in ECM1 positive tumours compared to ECM1 negative tumours [96], our interrogation of the TCGA dataset revealed no association between ECM1 expression and metastatic potential in MIBC. MIBC has a high risk of metastasis with half of all patients developing metastatic disease within 2 years [199]. It is therefore possible that while ECM1-high tumours may have a metastatic phenotype, a similar proportion of ECM1-low tumours may have similar metastatic potential via ECM1-independent mechanisms.

An interesting feature of the pathway analysis was the upregulation of transforming growth factor-beta (TGF-beta) signalling in ECM1-high tumours coupled with a downregulation of stem cell differentiation pathways. TGF-beta signalling has previously been demonstrated to promote self-renewal of bladder cancer stem cells [200], and similarly TGF-beta signalling in glioma cells maintains stemness by upregulation of SOX2 [201]. The increase in TGF-beta signalling and downregulation of differentiation pathways, may suggest that ECM1-high tumours have a stem cell-like phenotype. Moreover, initial identification of bladder cancer stem cells demonstrated an enrichment of basal-like markers including increased keratin 5 and decreased keratin 20 [202]. The assignment of ECM1-high tumours to mainly Basal/Squamous subtypes high in these markers may further indicate increased stemness of these tumours.

To further validate the existence of an ECM1-high subgroup of bladder cancers we examined ECM1 and MUC1 protein expression by immunohistochemistry in a set of four tissue microarrays (TMAs) consisting of 943 interpretable MIBC specimens. TMAs are made up of small cores of FFPE tumour blocks, arranged in a matrix embedded in a wax block. These can be sliced and fixed to slides so a large number of tumours can be analysed simultaneously thereby saving on time and laboratory reagents. Furthermore, the close proximity of multiple tumour cores fixed to the same slide reduces the variability of staining between tumours and allows for much faster scoring. This makes TMAs a valuable tool for the assessment of biomarker expression by immunohistochemistry.

Analysis of ECM1 expression in the MIBC TMAs showed mainly cytoplasmic staining confirming our observations in Chapter 3 and those of previous studies in hepatocellular carcinoma, breast cancer and thyroid carcinoma [96, 115, 118]. Although the cellular localisation of ECM1 was similar to reports in hepatocellular and breast carcinoma, percentage positivity was much lower. Our findings showed that 11.5% of cores stained positively for ECM1 to some extent and with 3.4% staining strongly, In contrast, ECM1 positivity has been reported to be 75% in breast cancer and 73% in hepatocellular carcinoma [121, 162]. This may reflect the restricted amount of tumour tissue available on TMAs, which can pose a problem as heterogeneity within tumours may result in false negative staining [203]. Indeed, ECM1 expression was seen to be heterogeneous across the tumours from which the LUCC4 and LUCC5 cell lines were derived. Often several cores from the same tumour are incorporated into the TMA to account for this, and while this is most likely the case for our TMAs, the TMA maps are currently unavailable and would need to be consulted to confirm this. Nevertheless, the low percentage of positive tumours correlates well with the percentage of tumours expressing high levels of ECM1 at the transcript level, with around 5% of samples in the TCGA dataset expressing high levels of ECM1. The low level of ECM1 staining in the TMAs is therefore likely a true reflection of a lower percentage of ECM1 positive bladder tumours compared to other carcinomas.

Immunohistochemistry analysis of MUC1 was also conducted on the TMAs, as this protein was considered to represent another potentially important candidate that was upregulated at the mRNA level in the ECM1-high subgroup of bladder tumour-derived cell lines. Although ECM1's role in bladder cancer has not been previously investigated, MUC1 is one of the most explored tumour associated antigens in urothelial carcinomas [204]. High levels of MUC1 staining in bladder tumours have been correlated with increased invasiveness [205]. Previous reports estimate that around 60% of bladder tumours across all stages and grades are positive for MUC1 with significant correlation to higher grade and squamous differentiated tumours [205, 206]. In the current study a slightly lower percentage of tumours were positive for MUC1 (40.9%). This may be affected by the presence of multiple cores from the same tumour present on the microarray. This cannot currently be discerned as the TMA maps containing information for each core is not available at present.

Previous reports have correlated increased expression of MUC1 in bladder tumours

with poor overall survival [137], and our results from mining publicly available data, demonstrate that high ECM1 expression in tumours is associated with poorer survival in patients. It would be interesting to interrogate survival data for the cohort of patients whose tumours were assessed for ECM1 and MUC1 expression on the TMA, but this will not be possible until the TMA maps and patient metadata are made available. Furthermore, it would be interesting to assess the effects of co-expression of ECM1 and MUC1 on survival as 101 of the 108 tumours that stained positively for ECM1 were also positive for MUC1. While the decode and metadata is not available for the TMAs at present, the metadata for the most recent TCGA study is publicly available and this was examined. A Kaplan-Meier plot comparing overall survival of patients whose tumours expressed high levels of MUC1, high levels of ECM1 or ECM1 and MUC1 was generated. Although there was a significant decrease in survival of patients expressing both MUC1 and ECM1 compared to MUC1 alone, there was no difference in survival between patients expressing ECM1 alone and both ECM1 and MUC1. This suggests that ECM1 expression could be the major influencing factor associated with reduced survival rates.

Very little is known about the biological mechanisms by which ECM1 acts. However, a number of studies have examined the role of ECM1 by modulating expression in various carcinoma cell lines [114, 122, 181]. The two most common methods used for knockdown studies are small interfering RNA (siRNA), and the vector-based approach of short hairpin RNA (shRNA). shRNAs are introduced into cells in a plasmid form using bacterial or viral vectors generating a relatively stable knockdown of target genes compared to the transient knockdown induced by siRNA [207]. For this reason, shRNA knockdown was chosen for the current study. For the purpose of this project, a lentiviral-based system was employed as it can also be used to infect non-dividing cells [208].

In order to select shRNAs for our knockdown study we conducted PCR analysis of ECM1 isoform expression in the ECM1 high cell lines to ensure that the shRNAs selected targeted the most relevant isoforms. The human *ECM1* gene encodes for three main splice variants: ECM1a, ECM1b, and ECM1c. To our knowledge, previous investigations into the role of ECM1 in cancer have not specified isoform or have focused on the major ECM1a isoform. While all cell lines examined expressed the ECM1a isoform, with the exception of LUCC3, the ECM1-high cell lines also expressed at least one other isoform. Alternative splicing is a crucial mechanism in the regulation of cell differentiation, embryo development, and cell

specific functions, while dysregulation of isotype expression is known to be important in the pathology of cancer [209]. It is possible that differential ECM1 isoform expression in conjunction with increased expression levels play an important role in influencing tumour progression. The observed expression of multiple ECM1 isoforms in the bladder cancer cell lines led to the selection of shRNAs that targeted all known isoforms of ECM1 for use in this study.

It has previously been reported that ECM1 siRNA knockdown in the breast cancer cell lines Hs578T and MDAMB231 resulted in cytoskeletal rearrangement and decreased membrane ruffling [114]. However, similar observations were not made in hepatocellular and thyroid carcinomas [115, 162]. In our bladder cancer cell lines, ECM1 knockdown did not result in any observable differences in cell morphology.

Treatment with recombinant ECM1 has been reported to promote endothelial cell proliferation [122], and in breast cancer-derived cell lines treatment with recombinant ECM1 resulted in increased cell proliferation [122]. Furthermore, in cervical cancer transfection of HeLa cells with ECM1 resulted in increased cell proliferation [210]. The effects of ECM1 expression on cell proliferation are not universal to all carcinomas. In thyroid and cholangiocarcinoma cancer cell lines, no changes to cell proliferation were observed in response to ECM1 knockdown [115, 181]. Similarly, in the current study no differences in cell proliferation were observed in ECM1 knockdown cell lines. The lack of an observable impact of ECM1 knockdown on cell proliferation or cell morphology could possibly be attributed to the fact that the role of ECM1 in bladder cancer cannot be fully elucidated from cell line studies. ECM1 is a secreted protein and has been seen to interact with a number of other extracellular components [102]. The absence of an extracellular matrix or tumour microenvironment under cell culture conditions might mean that the role of ECM1 in bladder cancer is not completely reflected *in vitro*.

We also investigated the impact of ECM1 knockdown on wound healing ability of ECM1-high cell lines. In previous studies, silencing of ECM1 using antibody treatments or siRNA knockdown has been shown to induce a significant reduction in wound healing in breast cancer-derived cell lines [114, 120] and hepatocellular carcinoma-derived cell lines [162]. Furthermore, Urbach–Wiethe disease, is characterised by disruption to wound healing ability resulting from loss of function mutations in *ECM1*. In the current study we demonstrated that knockdown of ECM1

results in reduced wound healing ability, implying that ECM1 plays a regulatory role in promoting wound healing in ECM1-high cells.

In order to further confirm the potential role of ECM1 in wound healing, HT-1376 ECM1 knockdown cells were treated with a range of concentrations of recombinant ECM1 and a wound-healing assay was conducted. In cultured healthy endothelial cells 20 ng/ml recombinant ECM1 was sufficient to stimulate cell proliferation [93] and 200 ng/ml of recombinant human ECM1 induced cell proliferation in breast cancer-derived cell lines [122]. Unlike these previous reports, concentrations below 200 ng/ml had no effect on the wound healing ability of the HT-1376 derived ECM1 knockdown cells. Furthermore, treatment with concentrations up to 750 ng/ml also had no effect on the wound healing ability of this line. There was a slight increase in the wound healing ability of cell lines treated with 1 μg/ml recombinant ECM1. It is unclear why treatment with recombinant ECM1 at concentrations below 1 μg/ml had no effect on the wound healing ability of the HT-1376 knockdown cells, however, one possible explanation may relate to isotype. The recombinant ECM1 used was the ECM1a isoform according to the protein sequence specified by the manufacturer. We have identified that while ECM1a was commonly expressed across our panel of cell lines, most ECM1-high cell lines also express at least one other isoform. It could therefore be proposed that in this setting it is not ECM1a that contributes to the wound healing ability of these cell lines but one of the other isoforms, and so treatment with recombinant ECM1a would not have an effect.

The wound healing assay is a relatively cheap and simplistic method for monitoring cell migration and requires no specialist equipment [211-213]. However, since images are captured at several specific timepoints, wound healing assays can be time consuming and variability in initial scratch area means reproducibility is an issue [212]. Another method of measuring cell migratory ability is the three-dimensional system of transwell assays. Cells are seeded onto a porous insert containing serum free media, while media containing serum is placed in the well below. This creates a gradient that attracts cells to move through the membrane towards the higher concentration of serum and the number of cells that have migrated through the membrane can then be stained and counted [213].

Previous reports in breast cancer have demonstrated that cell lines overexpressing ECM1 have increased migration ability as determined by a transwell assay [120]. This

was echoed in the LUCC4 cell line in which reduced migration by transwell assay was observed in the ECM1 knockdown cell line compared to the scramble control and parental cell lines. This implies that ECM1 regulates migration ability in this cell line. However, HT-1376, HT-1197 and 647V did not exhibit any differences in migration ability in relation to the level of ECM1 expression when examined using the same assay. A key difficulty with transwell assays is the determination of an appropriate endpoint as cells exhibit large variability in response. Alterations to the time frame of the transwell assay might have revealed differences in migration for knockdown cells derived from the other cell lines, but there was not enough time available to repeat the assays. In order to better determine migration over time and to obtain kinetic data for the cell lines it is also possible to fluorescently label and track cells, however labelling of cells has the potential to alter cell behaviour and thus complicates experimental design [212]. This approach is also expensive and requires specialist equipment and was beyond the scope of the current project. Our current data suggest that there is not a generalisable effect of ECM1 expression on migration ability in our panel of ECM1-high cell lines.

Chapter 5
Mediators of ECM1 dependent effects and activation of downstream signalling pathways

5.1 Introduction

Although the normal physiological function of ECM1 has not been fully elucidated, the protein has been linked to angiogenesis [93], [94], cell differentiation (including keratinocyte differentiation and endochondral ossification) [95] and cell proliferation [96], and it is therefore thought to be important in embryo development and wound healing. ECM1 has also been reported to bind to several extracellular matrix proteins including collagen type IV, fibronectin, laminin 332, fibulin-1C/1D and MMP-9 [90] implicating a role in maintaining the structural integrity of the skin.

In Chapter 4 we showed that patients with ECM1-high tumours have reduced overall survival, and that ECM1 plays a role in wound healing in ECM1-high bladder tumour derived cell lines *in vitro*. A role for ECM1 in wound healing has also been implicated in other cancers including hepatocellular, breast, and gastrointestinal carcinomas [118, 121, 152]. Despite the potential importance of ECM1 in cancer very little is understood about the mechanisms and signalling pathways through which ECM1 exerts its biological functions.

A potential mechanism by which ECM1 acts could be through the activation of EGFR signalling. EGFR has been reported to interact with ECM1 in breast cancer-derived cell lines, and this was proposed to result in resistance to the ERBB2 targeting monoclonal antibody trastuzumab through increased Ras/Raf/MEK/ERK signalling [122]. In this study we investigated whether a similar physical interaction between the two proteins exists in our ECM1-high bladder cancer cell lines using co-immunoprecipitation. We also sought to assess the effects of ECM1 on the Ras/Raf/MEK/ERK and PI3K/PTEN/AKT signalling cascades downstream of EGFR using the ECM1 knockdown and control cell lines described in Chapter 4 and treatment with recombinant ECM1 protein prior to assessment of the phosphorylation levels of EGFR and the downstream effector proteins ERK and AKT.

Molecular subtyping in bladder cancer has led to the identification of tumours exhibiting basal features that may be more sensitive to EGFR inhibitors, supporting the idea that patient stratification to identify cohorts of patients who are likely to respond well prior to treatment can improve success rates [86]. In the complex proposed by Lee *et al.* the interaction of ECM1 and EGFR resulted in resistance to ERBB targeting drugs [122], hence, we propose that our ECM-high subgroup represents an different subset of basal-like tumours with high EGFR that may not respond well to EGFR inhibitiors. In this Chapter we sought to investigate the potential impact of ECM1 expression on the response to EGFR inhibition *in vitro*.

Despite evidence for an interaction between ECM1 and EGFR in breast cancer [122], the understanding of ECM1-dependent mediators in carcinogenesis is limited. In order to assess a potential role for ECM1 in the activation of EGFR and other receptor tyrosine kinases (RTKs), we carried out a screen of the tyrosine phosphorylation status of 49 human RTKs using a phospho-RTK array with ECM1 shRNA knockdown and control cell lines. To relate the findings from the phospho-RTK array to potential treatment options for patients with ECM1-high bladder tumours, we also treated ECM1-high cell lines with agents targeting the RTKs identified as being of interest by the phospho-RTK array analysis.

5.2 Results

5.2.1 Interaction between ECM1 and EGFR

In order to investigate a potential physical interaction between ECM1 and EGFR co-immunoprecipitation (co-IP) was conducted using protein lysates from the HT-1376 and 647V cell lines. Immunoprecipitation using an ECM1 antibody did not show any co-immunoprecipitation of EGFR in either cell line as determined by western blot analysis (Figure 5-1). Immunoprecipitation with an EGFR antibody and western blot analysis using an ECM1 antibody also yielded no evidence of a physical interaction (Figure 5-1). Co-IP was carried out under a range of conditions including omitting vortexing and centrifugation steps from the protocol. The protocol was also carried out using a buffer containing minimal detergent, but a physical interaction could still not be detected between ECM1 and EGFR (data not shown).

Unstable and transient interactions can be difficult to detect by co-immunoprecipitation. Therefore we employed crosslinking prior to immunoprecipitation to enable the use of the detergent based RIPA lysis buffer without potential disruption to the interaction. Crosslinking was conducted using 3,3'-Dithiobis(sulfosuccinimidylpropionate) (DTSSP) as it is unable to cross membranes, thus reducing the formation of large cross-linked protein complexes which may impair formation of specific interactions of interest and create difficulties in the detection of co-immunoprecipitated proteins. Moreover, the spacer arm can be broken by the beta-mercaptoethanol present in the laemmli buffer used to elute proteins from the capture beads [214], so no extra steps are required before analysing the samples by western blot. Despite employment of DTSSP, EGFR was still not detected in samples immunoprecipitated using an ECM1 antibody (Figure 5-1).

Successful immunoprecipitation of both EGFR and ECM1 using their respective antibodies was confirmed by the positive detection of each protein on western blots with and without the use of a crosslinker (Figure 5-2). Neither EGFR or ECM1 were detected in the negative control samples that were immunoprecipitated using water instead of antibody or an antibody against the viral protein Sv-40 T Ag which does not interact with ECM1 or EGFR.

5.2.2 Effects of recombinant ECM1 treatment on EGFR phosphorylation and signalling in ECM1 knockdown cells

5.2.2.1 Time course assay of ECM1 induced EGFR, ERK, and AKT phosphorylation

Although a physical interaction could not be detected between ECM1 and EGFR, the potential influence of ECM1 on the activation of EGFR and the downstream Ras/Raf/MEK/ERK and PI3K/PTEN/AKT signalling pathways was investigated. The levels of phosphorylation of EGFR and the downstream effector proteins ERK and AKT were measured using western blot analysis of ECM1 knockdown and scramble control cell lines derived from HT-1376 (Figure 5-3), 647V (Figure 5-4), HT-1197 (Figure 5-5) and LUCC4 (Figure 5-6). ECM1 knockdown cell lines were also treated with 1 μg/ml recombinant ECM1 and lysates harvested after 5 min, 10 min, 20 min, 1 h and 24 h prior to analysis of total EGFR, p-EGFR, total ERK, p-ERK, total AKT, and p-AKT by western blot analysis.

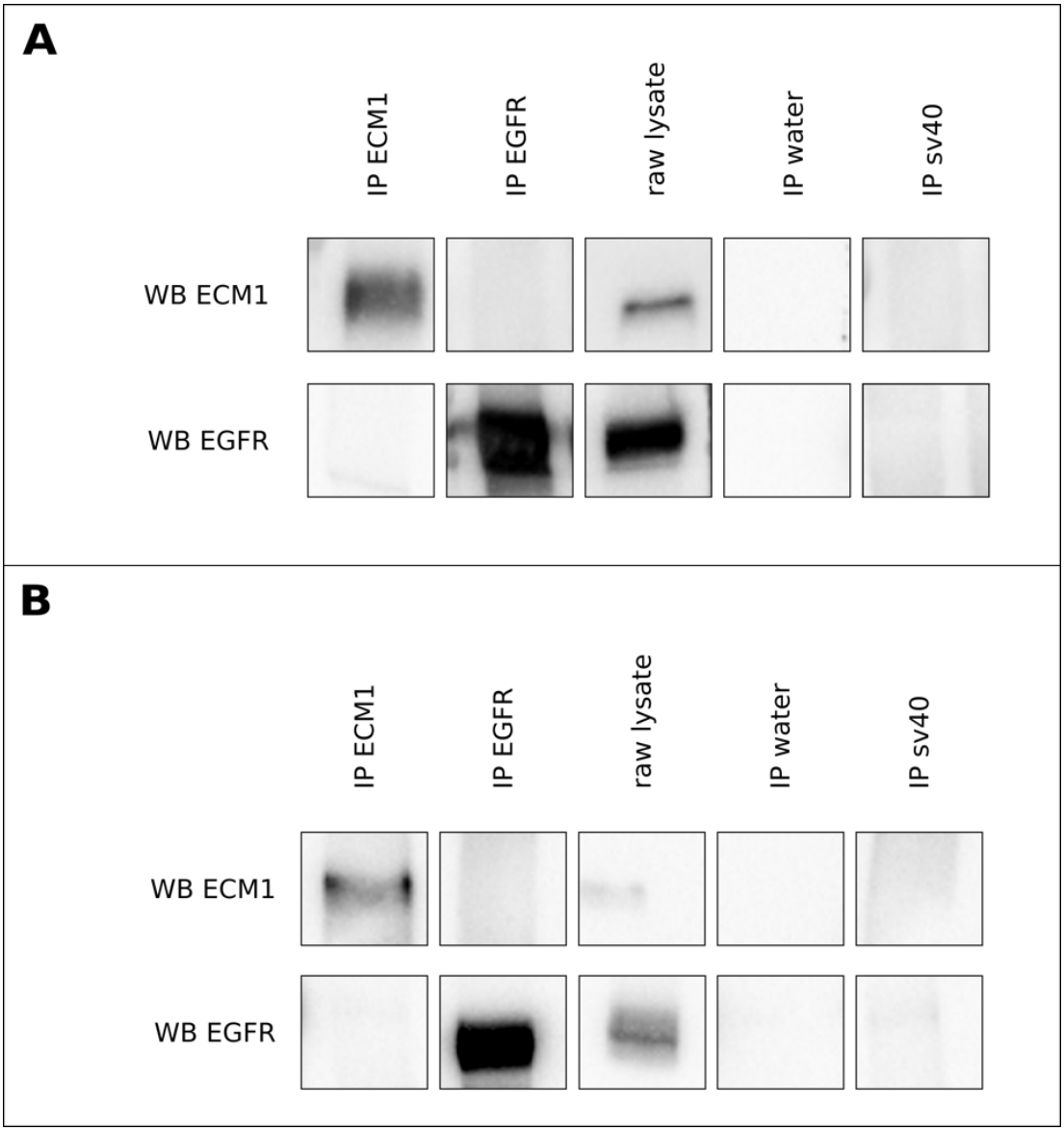

Figure 5-1: Co-immunoprecipitation of ECM1 and EGFR from HT-1376 and 647V cell lysates.

Total protein lysates harvested from the cell lines **A)** HT-1376 and **B)** 647V were used in co-IP with either anti-ECM1 or anti-EGFR antibodies and IP products were analysed by western blotting. Negative controls of water in place of antibody, or an Sv-40 T Ag antibody against a protein that does not interact with either ECM1 or EGFR were used. Blots were analysed using the ChemiDoc MP system. Representative of multiple experimental repeats.

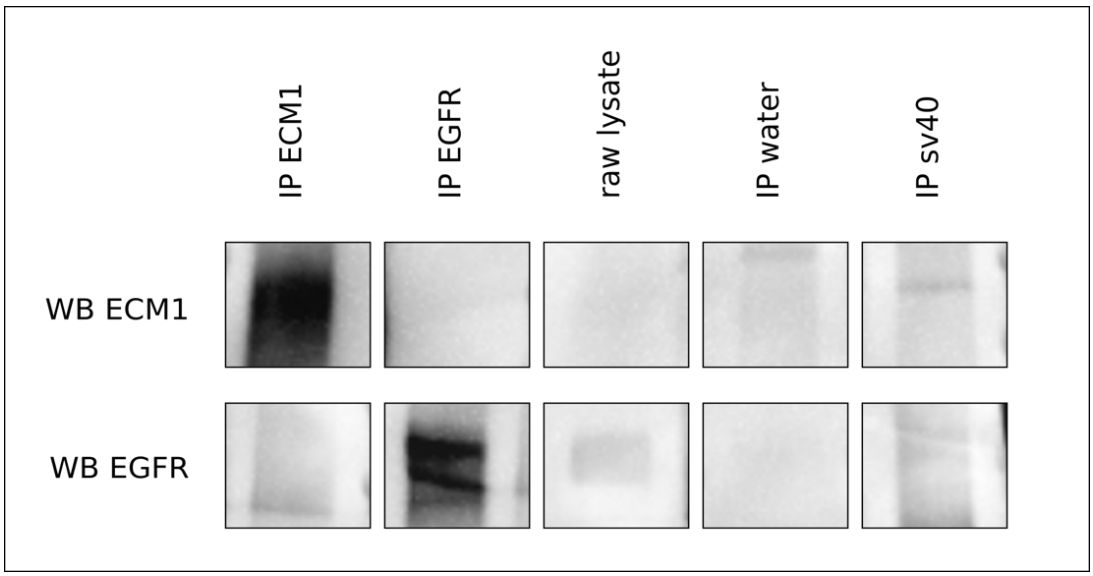

Figure 5-2: Co-immunoprecipitation of ECM1 and EGFR from HT-1376 cell lysates following pre-treatment with a crosslinker.

HT-1376 cells were incubated with the crosslinker DTSSP before lysis. Total protein lysates were used in co-IP with either anti-ECM1 or anti-EGFR antibodies and IP products were analysed by western blotting. Negative controls of water in place of antibody, or an Sv-40 T Ag antibody against a protein that does not interact with either ECM1 or EGFR were used. Blots were analysed using the ChemiDoc MP System. Representative of 4 experimental repeat.

There was slightly less p-EGFR in the untreated ECM1 knockdown compared to the scramble control for HT-1376. Treatment of the ECM1 knockdown with recombinant ECM1 led to an increase in the level of p-EGFR, with phosphorylation peaking after 20 min, when a higher level of phosphorylation was seen in comparison to the scramble control sample (Figure 5-3). The level of p-ERK in the untreated ECM1 knockdown was significantly lower than the level seen in the scramble control, with p-ERK being undetectable by western blot analysis. Treatment with recombinant ECM1 resulted in phosphorylation of ERK to a level comparable to that seen in the scramble control within 5 minutes of treatment, and p-ERK remained elevated for the full 24 h period (Figure 5-3). The untreated ECM1 knockdown also had a much lower level of p-AKT compared to the scramble control. Treatment with recombinant ECM1 led to an increase in p-AKT after 5 min to a level that was 40% lower than the level seen in the scramble control. The phosphorylation level of AKT decreased after 10 min, 20 min and 1 h of treatment to a level more closely resembling that seen in the untreated knockdown, and after 24 h the level was comparable to that seen in the scramble control after 24 h (Figure 5-3).

Similar results were obtained for 647V. There was 25% less p-EGFR in the untreated ECM1 knockdown compared to the scramble control. Treatment with recombinant ECM1 resulted in an initial decrease in the level of p-EGFR after 5 min. The levels of p-EGFR increased after 5 min, and after 20 min the level was comparable to that seen in the scramble control (Figure 5-4). The level of ERK phosphorylation was similar in the 647V ECM1 knockdown and scramble control lines. A 30% increase in p-ERK levels was observed after 5 min of recombinant ECM1 treatment after which levels of p-ERK fluctuated but remained elevated in the ECM1-treated samples compared to the untreated ECM1 knockdown for 1 h post-treatment (Figure 5-4). The level of AKT phosphorylation was 60% lower in the 647V ECM1 knockdown compared to the scramble control. A reduction in p-AKT to a level that was half the level in the untreated knockdown line was observed after 5 min of treatment with recombinant ECM1, and p-AKT remained low for the full 24 h treatment period.

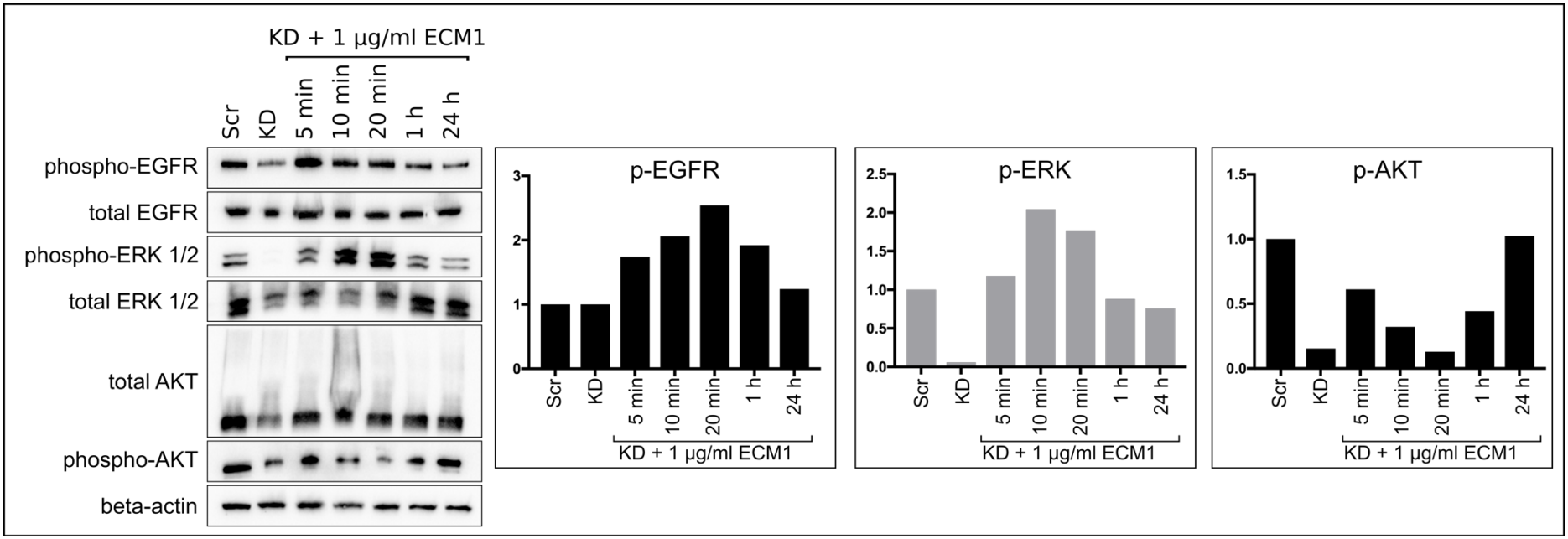

Figure 5-3: Western blot analysis of total and phosphorylated EGFR, ERK and AKT in HT-1376.

Phosphorylation of EGFR, ERK and AKT was examined in the HT-1376-derived scramble controls and ECM1 knockdown (KD) cells pre- and post-treatment with recombinant ECM1. After serum starvation for 24 h, ECM1 KD cells were incubated with 1 µg/ml recombinant ECM1 at 37 °C for 5 min, 10 min, 20 min, 1 h, or 24 h. Total and phosphorylated levels of EGFR, ERK and AKT were analysed by western blotting. Phosphorylation was quantified relative to total expression for the proteins of interest using Image Lab software. Western blots are representative of 3 experimental repeats, histograms represent quantified phosphorylated protein expression from the presented blot.

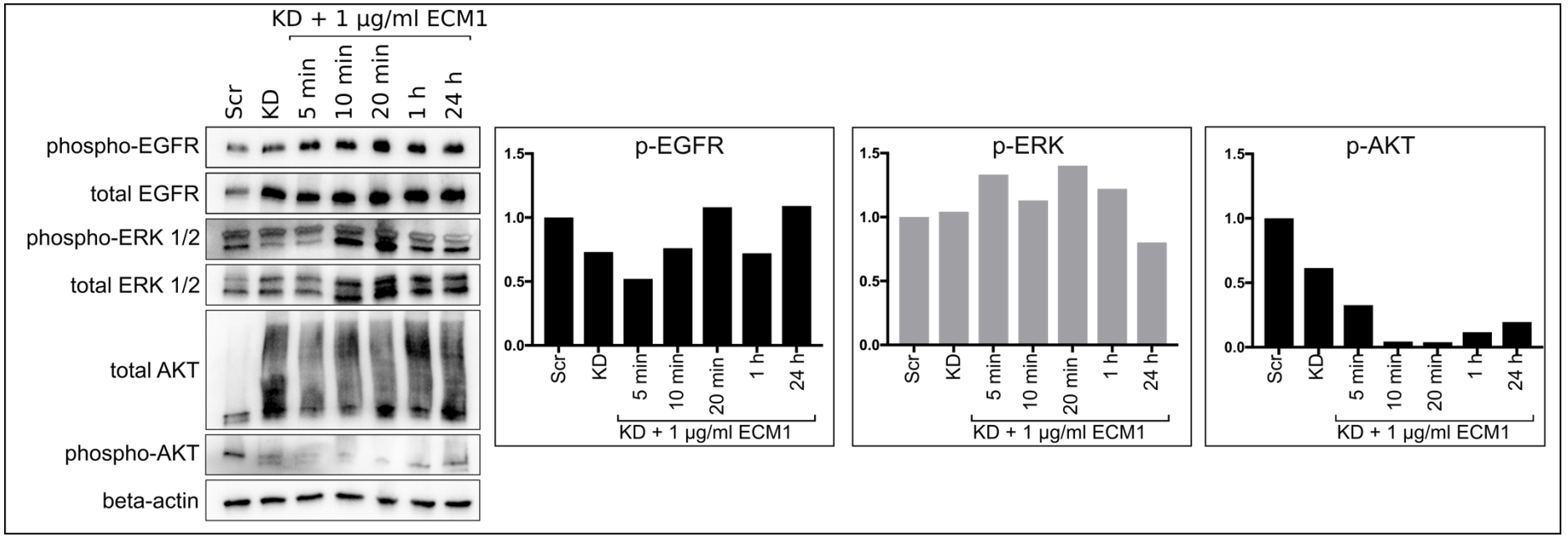

Figure 5-4: Western blot analysis of total and phosphorylated EGFR, ERK and AKT in 647V.

Phosphorylation of EGFR, ERK and AKT was examined in the 647V-derived scramble controls and ECM1 knockdown (KD) cells pre- and post-treatment with recombinant ECM1. After serum starvation for 24 h, ECM1 KD cells were incubated with 1 µg/ml recombinant ECM1 at 37 °C for 5 min, 10 min, 20 min, 1 h, or 24 h. Total and phosphorylated levels of EGFR, ERK and AKT were analysed by western blotting. Phosphorylation was quantified relative to total expression for the protein of interest using Image Lab software. Western blots are representative of 2 experimental repeats, histograms represent quantified phosphorylated protein expression from the presented blot.

The level of p-EGFR in HT-1197 was slightly higher in the untreated ECM1 knockdown cell line compared to the scramble control. A 40% increase in the level of p-EGFR was observed after 5 min of treatment with recombinant ECM1. The level of p-EGFR then fluctuated across the 24 h period with a 50% decrease in p-EGFR being detected after 10 min and equivalent level of p-EGFR being detected at 1 h as compared to the untreated ECM1 knockdown (Figure 5-5). ERK phosphorylation was 60% lower in the untreated ECM1 knockdown compared to the control sample for HT-1197. Treatment with recombinant ECM1 did not lead to an increase in the phosphorylation of ERK above the level observed in the scramble control. AKT phosphorylation was 80% lower in the untreated knockdown compared to the scramble control. Treatment with recombinant ECM1 did not lead to an increase in the phosphorylation of AKT (Figure 5-5).

The LUCC4 scramble and ECM1 knockdown cell lines had no detectable p-EGFR in any of the samples, however, p-ERK was present in all samples (Figure 5-6). p-ERK levels were slightly lower in the ECM1 knockdown cells than in the scramble control cells. Following treatment of the ECM1 knockdown cell line with recombinant ECM1, p-ERK levels increased by 20% after 5 min, decreased by 30% at 10 and 20 min, and increased again by 70% at 24 h compared to the untreated ECM1 knockdown. AKT phosphorylation was also lower in the ECM1 knockdown compared to scramble control. Following recombinant ECM1 treatment of the ECM1 knockdown cell line, p-AKT levels decreased by 50% after 5 min and 10 min, then increased to a level which was 150% higher than the scramble control after 1 h and 24 h (Figure 5-6).

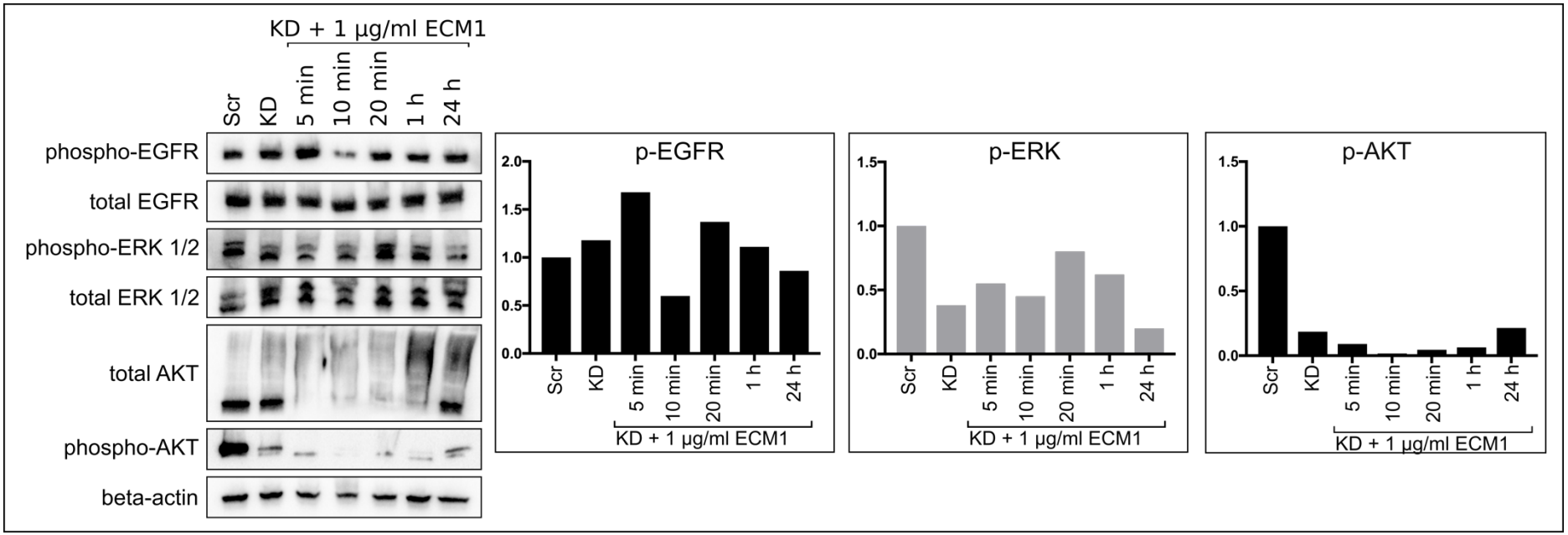

Figure 5-5: Western blot analysis of total and phosphorylated EGFR, ERK and AKT in HT-1197.

Phosphorylation of EGFR, ERK and AKT was examined in the HT-1197-derived scramble controls and ECM1 knockdown (KD) cells pre- and post-treatment with recombinant ECM1. After serum starvation for 24 h, ECM1 KD cells were incubated with 1 µg/ml recombinant ECM1 at 37 °C for 5 min, 10 min, 20 min, 1 h, or 24 h. Total and phosphorylated levels of EGFR, ERK and AKT were analysed by western blotting. Phosphorylation was quantified relative to total expression for the protein of interest using Image Lab software. Western blots are representative of 1 experimental repeat, histograms represent quantified phosphorylated protein expression from the presented blot.

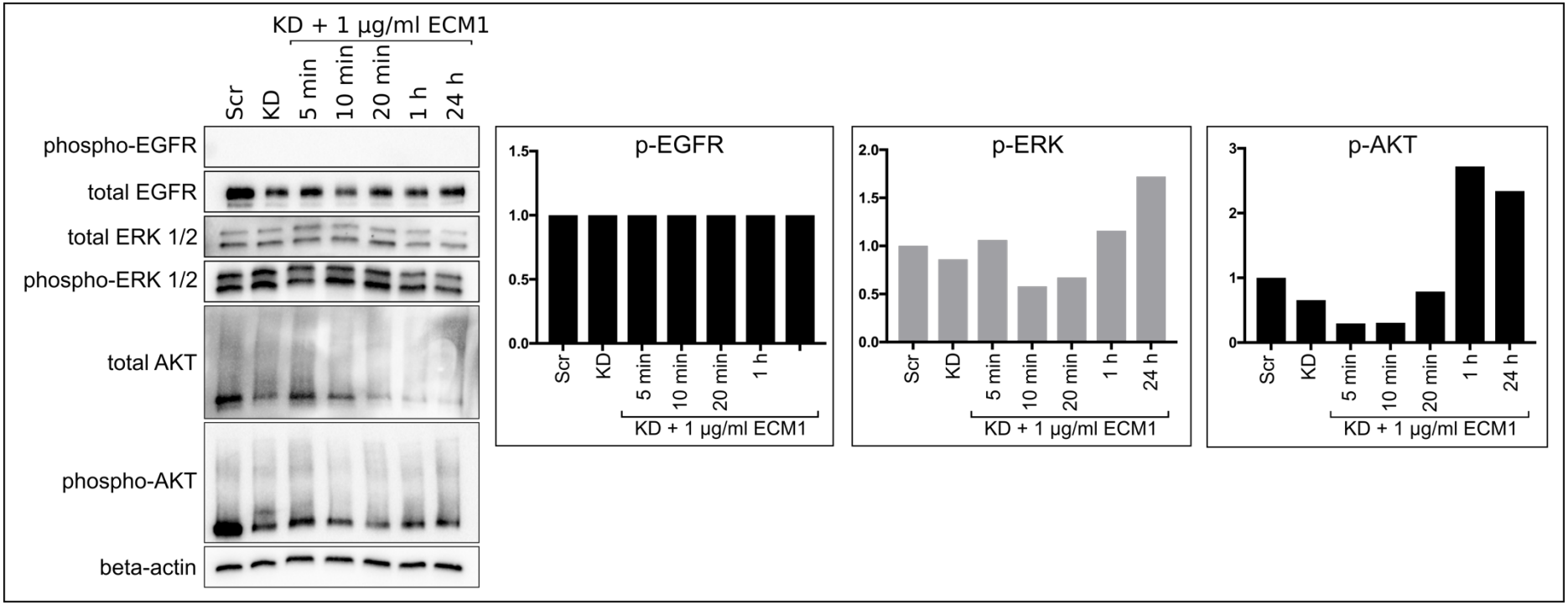

Figure 5-6: Western blot analysis of total and phosphorylated EGFR, ERK and AKT in LUCC4.

Phosphorylation of EGFR, ERK and AKT was examined in the LUCC4-derived scramble controls and ECM1 knockdown (KD) cells pre- and post-treatment with recombinant ECM1. After serum starvation for 24 h, ECM1 KD cells were incubated with 1 µg/ml recombinant ECM1 at 37 °C for 5 min, 10 min, 20 min, 1 h, or 24 h. Total and phosphorylated levels of EGFR, ERK and AKT were analysed by western blotting. Phosphorylation was quantified relative to total expression for the protein of interest using Image Lab software. Western blots are representative of 2 experimental repeats, histograms represent quantified phosphorylated protein expression from the presented blot.

5.2.3 Phospho-RTK array analysis

To identify if there were other receptor tyrosine kinases (RTKs) involved in ECM1 dependent signalling we employed the use of a phospho-RTK array. The use of this array permits assessment of the relative level of tyrosine phosphorylation of 49 different human RTKs (Figure 5-7 A). Analysis of the phospho-RTK array data suggested that ECM1 knockdown leads to a decrease in phosphorylation of EGFR (Figure 5-7 B, coordinates B1/B2), and hepatocellular growth factor receptor (HGFR), which is also known as MET (Figure 5-7 B, coordinates C3/C4), in the HT-1376 ECM1 knockdown cell line relative to the scramble control. There was also a decrease in phosphorylation of EGFR in HT-1376 knockdown cells treated with 1 μg/ml recombinant ECM1 relative to the scramble control, however no difference was observed between the ECM1 treated and untreated knockdown lines (Figure 5-7 B and Figure 5-7 C).

As foetal bovine serum used to supplement cell line growth media contains high levels of growth factors which may stimulate phosphorylation of receptor tyrosine kinases (RTKs), we also assessed the HT-1376 ECM1 knockdown cell line grown in the absence of serum for 24 h. A decrease in phosphorylation of both EGFR and MET in HT-1376 ECM1 knockdown cells out of serum relative to the scramble control was observed. There was a 0.2-fold increase in phosphorylation of EGFR in HT-1376 ECM1 knockdown cell line grown out of serum relative to the HT-1376 ECM1 knockdown cell line grown in serum after an exposure time of 2 min, but no difference was noted after a 10 min exposure time (Figure 5-7 B and Figure 5-7 C). A 5-fold increase in phosphorylation of MET in HT-1376 knockdown cells out of serum relative to the HT-1376 knockdown cell line grown in serum was observed at an exposure time of 2 min, and a 3-fold increase after a 10 min exposure time (Figure 5-7 B and Figure 5-7 D).

Analysis of two further cell lines, LUCC4 and 647V, also revealed a decrease in phosphorylation of EGFR in the ECM1 knockdown cell lines compared to the scramble controls (Figure 5-8 B, coordinates B1/B2; and Figure 5-8 C). Phosphorylation of MET was also decreased in the LUCC4 ECM1 knockdown cell line compared to the scramble control, however, no phosphorylation of MET was detected in either the 647V ECM1 knockdown or scramble control lines (Figure 5-8 B and Figure 5-8 D). In both the LUCC4 ECM1 knockdown and scramble control cell lines, phosphorylation of insulin receptor (INS-R) (Figure 5-8B, coordinates

B17/B18) and type-1 insulin like growth factor receptor (IGF-IR) (Figure 5-8B, coordinates B19/B20) was observed. Phosphorylation was higher for these receptors in the LUCC4 ECM1 knockdown cell line compared to the scramble control line (Figure 5-8 E and Figure 5-8 F).

5.2.4 Western blot analysis of p-MET levels in ECM1 knockdown and scramble control cell lines

The phosphorylation level of MET in HT-1376, LUCC4, HT-1197 and 647V scramble control and ECM1 knockdown cell lines was further assessed using western blot analysis (Figure 5-9). In contrast to findings in HT-1376 and LUCC4 by phospho-RTK array analysis, these results indicated a slightly higher level of MET phosphorylation in the ECM1 knockdown cell lines than in the scramble control cell lines for LUCC4, 647V and HT-1197. Western blot analysis showed a lower level of MET phosphorylation in the ECM1 knockdown cell line than in the scramble control cell lines for HT-1376, confirming the results obtained using the phospho-RTK array. We also observed that treatment of the ECM1 knockdown cells with recombinant ECM1 resulted in an increase in MET phosphorylation after 5-10 min for LUCC4, 647V and HT-1197 but not for HT-1376. For ease of comparison, a summary Table of EGFR and MET phosphorylation status according to western blot analysis and phospho-RTK array was generated (Table 5-1).

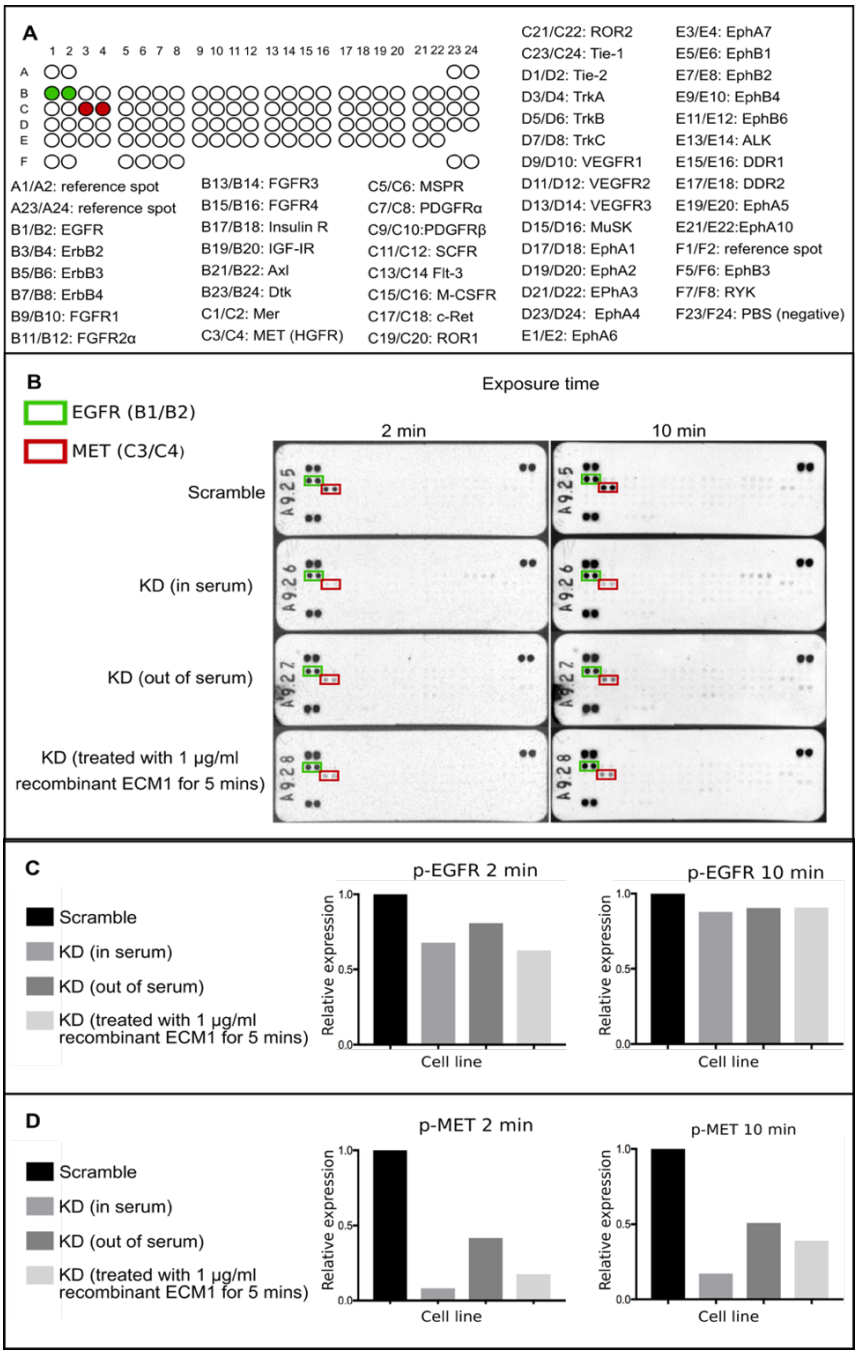

Figure 5-7: Analysis of RTK phosphorylation in HT-1376 scramble control, ECM1 knockdown (+/- serum), and ECM1 knockdown cells treated with recombinant ECM1.

A) A map outlining coordinates of receptors on the Human Phospho-RTK array (R&D). **B)** A comparative analysis of HT-1376 scramble control and HT-1376 ECM1 knockdown cell grown in media supplemented with serum and without serum and treated with 1 µg/ml recombinant ECM1 for 5 minutes. Cell lysates were analysed using the phospho-RTK array shown in **A.** Each pair of horizontal spots represents one receptor. Three pairs of spots in the top right, top left and bottom left corners are positive p-tyrosine controls. Images were captured using a ChemiDoc MP System and Image J software was used to quantify phosphorylation at 2 min and 10 min exposure times for **C)** EGFR and **D)** MET. Representative of 1 experimental repeat.

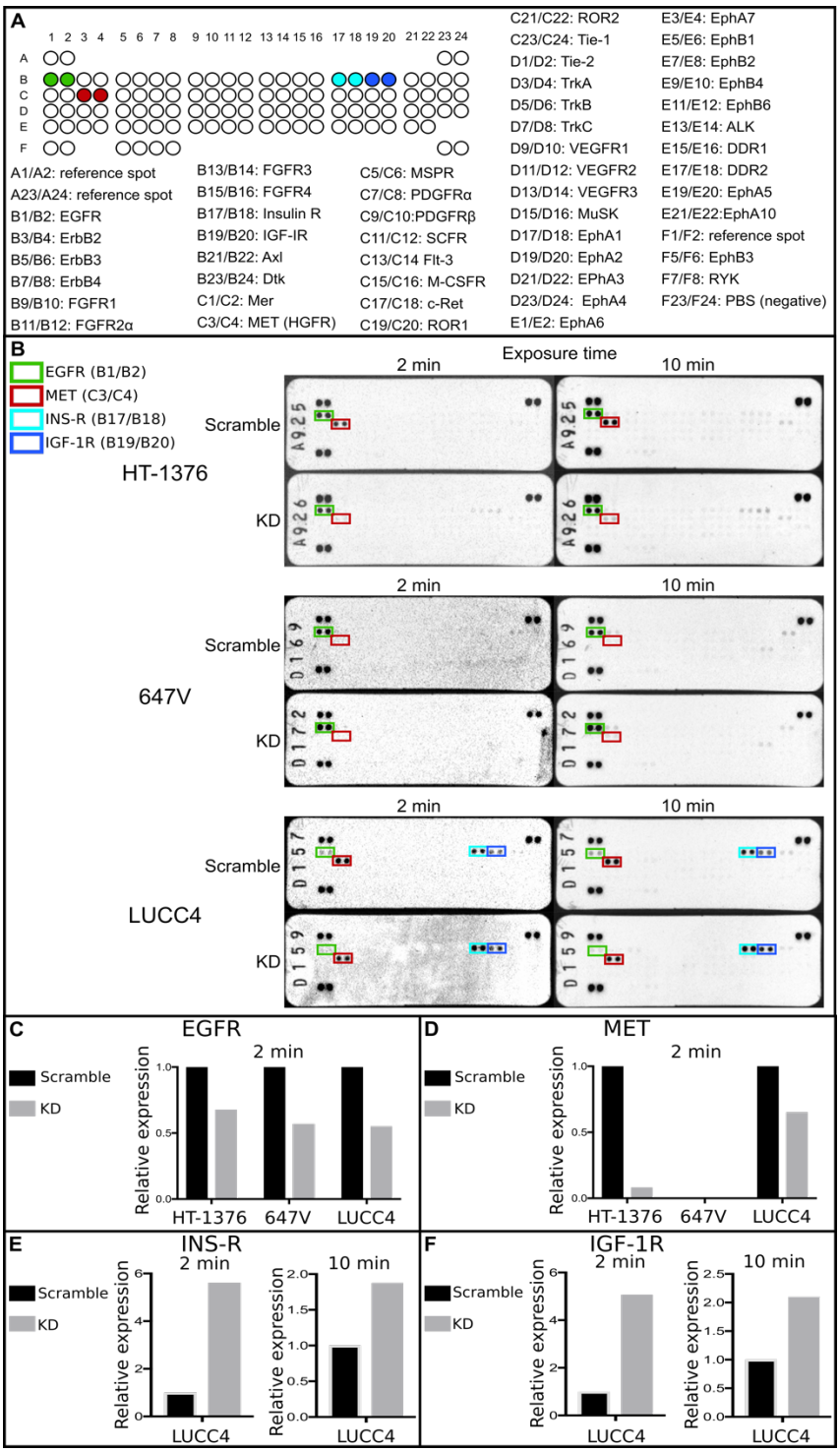

Figure 5-8: Analysis of RTK phosphorylation in LUCC4, 647V and HT-1376 ECM1 knockdown and scramble control cell lines.

A) A map outlining coordinates of receptors on the Human Phospho-RTK array (R&D). **B)** A comparative analysis of HT-1376, LUCC4 and 647V ECM1 knockdown and scramble control cell lines. Cell lysates were analysed using the phospho-RTK array shown in **A.** Each pair of horizontal spots represents one receptor. Three pairs of spots in the top right, top left and bottom left corners are positive p-tyrosine controls. Images were captured using a ChemiDoc MP System and Image J software was used to quantify phosphorylation at 2 min and 10 min exposure times for **C)** EGFR, **D)** MET, **E)** INS-R and **F)** IGF-1R. Representative of 1 experimental repeat.

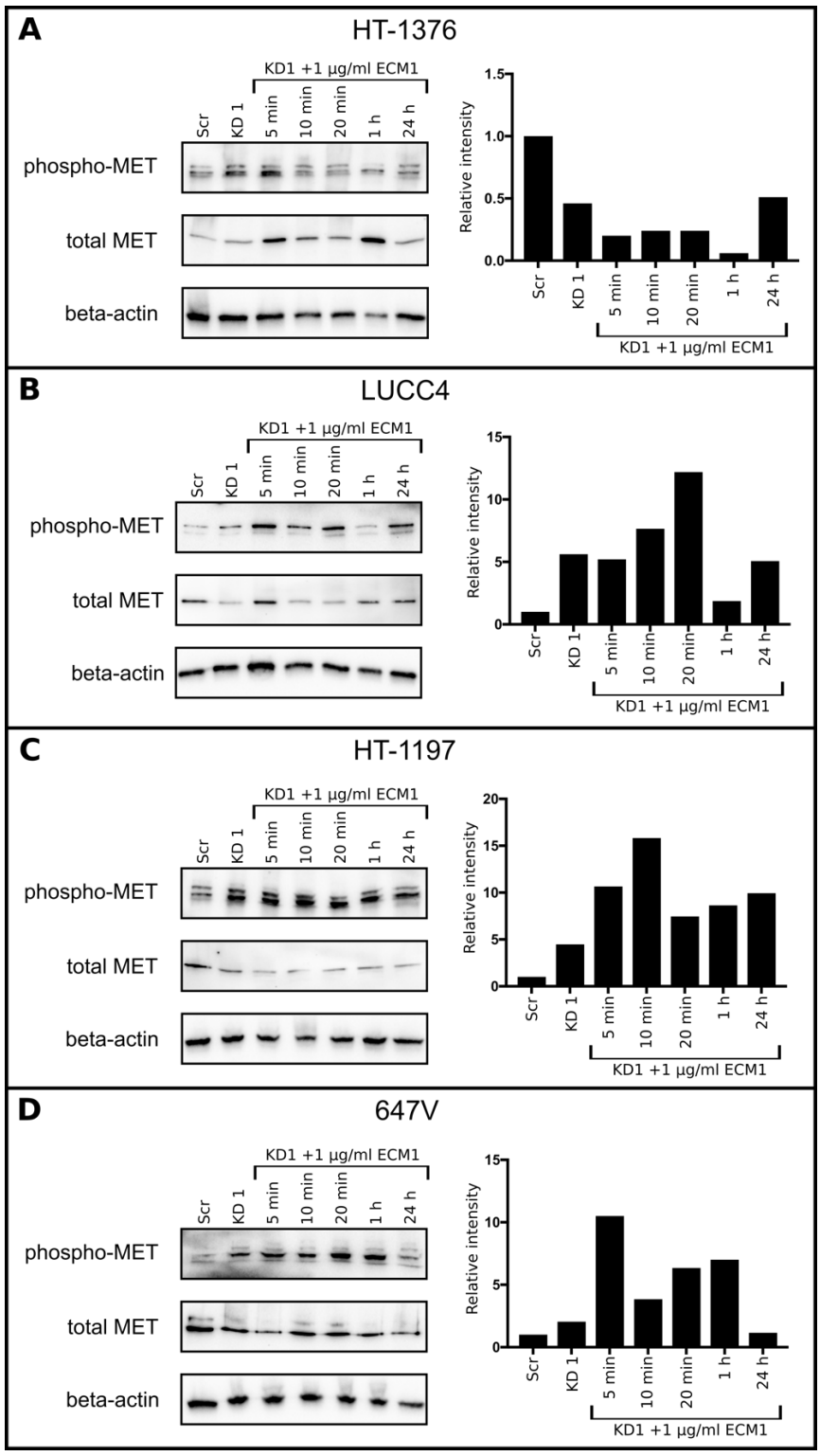

Figure 5-9: Western blot analysis of p-MET levels in ECM1 knockdown cells.

Phosphorylation of MET was examined in scramble control and ECM1 knockdown cells pre- and post-treatment with recombinant ECM1 in **A)** HT-1376, **B)** LUCC4, **C)** HT-1197 and **D)** 647V cell lines. After serum starvation for 24 h, ECM1 KD cells were incubated with 1 µg/ml recombinant ECM1 at 37 °C for 5 min, 10 min, 20 min, 1 h or 24 h. Total and phosphorylated levels of MET were analysed by western blot analysis. Phosphorylation was quantified relative to total MET expression for both proteins using Image Lab software. Representative of 1 experimental repeat.

Table 5-1: A summary of the phosphorylation levels of EGFR and MET in ECM1 knockdown and scramble control cell lines.

Phosphorylation of EGFR and MET was examined in scramble control and ECM1 knockdown (KD) cells for HT-1376, LUCC4, HT-1197, and 647V by western blot analysis and phospho-RTK array. For western blot analysis, phosphorylation was quantified relative to total expression of each protein using Image Lab software. For phospho-RTK array analysis, image J software was used to quantify phosphorylation after an exposure time of 2 min. Differences in phosphorylation between the scramble control and ECM1 KD cell lines were presented relative to the scramble control which was given a unit value of 1. Relative phosphorylation is presented as +/- where values of 0 = -, ≤1 = +, >1 to ≤2 = ++, >2 to ≤4 = +++, and >4 = ++++.

Cell Line	Western Blot				Phospho-RTK array			
	p-EGFR		p-MET		p-EGFR		p-MET	
	Scramble Control	ECM1 KD	Scramble Control	ECM1 KD	Scramble Control	ECM1 KD	Scramble Control	ECM1 KD
HT-1376	++	++	++	+	++	+	++	+
LUCC4	-	-	++	++++	++	+	++	+
HT-1197	++	++	++	++++	N/A	N/A	N/A	N/A
647V	++	+	++	+++	++	+	-	-

5.2.5 Microarray analysis of HT-1376 ECM1 knockdown and scramble control cell lines

Microarray analysis using a whole genome transcript array was carried out to identify changes in gene expression induced by ECM1 knockdown in the HT-1376 cell line. Differential gene expression in the HT-1376 ECM knockdown KD1 and scramble control cell lines was assessed using LIMMA analysis conducted in R2. A list of the differentially expressed genes that exhibited at least a 2-fold difference and a p-value less than 0.05 was generated (Appendix J). This analysis identified 307 significantly altered probes. After the removal of unannotated probes, and a single representative probe being selected per gene, 169 genes were found to be significantly differentially expressed between the ECM1 knockdown and scramble control cell lines. There were a total of 101 genes significantly downregulated in the ECM1 knockdown compared to the scramble control, including ECM1. Amongst the other significantly downregulated genes in the ECM1 knockdown were 16 genes encoding 5S ribosomal RNA (rRNA), 8 keratins (keratins 1, 4, 5, 6A, 6B, 6C, 10 and 24), the EGFR ligand AREG, and the transcription factor ELF5. Sixty-eight genes were significantly upregulated in the ECM1 knockdown compared to the scramble control cells. To gain further insights into the consequences of ECM1 knockdown, pathway analysis was conducted on the list of significantly differentially expressed genes using Metacore. This determined the top ten most highly upregulated and downregulated pathways in the ECM1 knockdown compared to the scramble control (Figure 5-10). Cell adhesion, keratinocyte differentiation and cytoskeleton remodelling were amongst the most highly downregulated pathways. The most common features in the top ten upregulated pathways involved developmental pathways, in particular pathways mediated by TGF-beta and which involve extracellular matrix remodelling. Gene Ontology (GO) localisation analysis was also conducted using Metacore (Table 5-2). This examines the most common cellular localisations that products of the significantly upregulated and downregulated genes are transported to, tethered in, or maintained in some respect. This analysis revealed extracellular regions as the main location of interest.

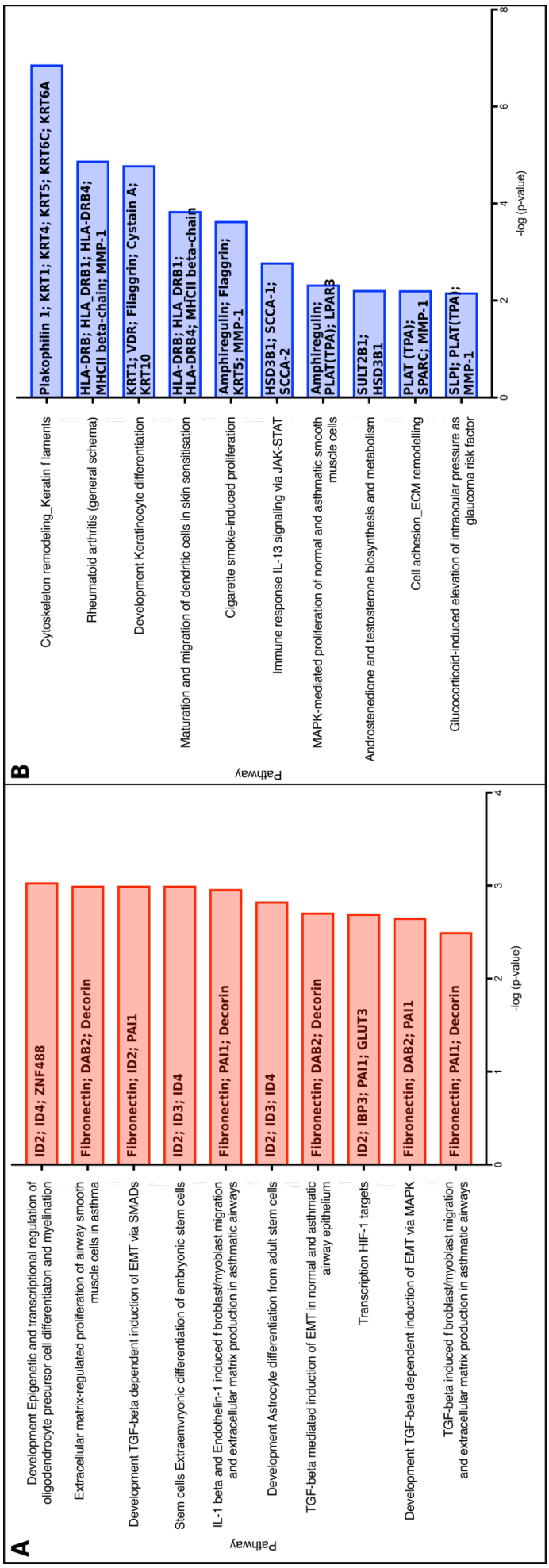

Figure 5-10: Pathway analysis of genes differentially expressed between HT-1376 ECM1 knockdown and scramble control cells.

Microarray analysis was conducted on total RNA isolated from lysates from three consecutive passages of HT-1376 ECM1 knockdown (KD1) cells and the scramble control cells. LIMMA analysis was conducted using R to determine genes that were significantly differentially expressed between the ECM1 KD compared to the control. Stringency settings were applied to include only probes that had a fold change greater than 2 or less than -2, and a LIMMA p value less than 0.05. This gene list was used to conduct pathway analysis in Metacore in order to determine the top 10 most **A)** upregulated pathways and **B)** downregulated pathways in ECM1 knockdown cells compared to the scramble control cells.

Table 5-2: Top 10 Gene Ontology (GO) localisations of genes differentially expressed in HT-1376 ECM1 knockdown cells compared to scramble control cells.

Microarray analysis was conducted on total RNA isolated from lysates for three sequential passages of HT-1376 knockdown (KD1) and the scramble control cells. LIMMA analysis was conducted to determine genes that were significantly differentially expressed between the ECM1 KD compared to the scramble control. Stringency settings were applied to include only probes that had a fold change greater than 2 or less than -2, and a LIMMA p value less than 0.05. This gene list was used to conduct GO analysis in Metacore in order to determine the top 10 most common cellular localisations of the products of significantly altered genes.

GO Term	P value	Gene Names
MHC Class II Protein Complex	1.413E-20	DRB4, DRB1-1, DRB1-11, DRB1-8, 2B1C, DRB1-15, DRB1-4, 2B1E, DRB1-10, 2B1D, DRB1-3, DRB1-9, 2B1G
Cornified Envelope	1.369E-19	LCE3E, PRR9, PKP1, SPRR1A, KRT1, DSG3, LCE3D, FLG, CSTA, SPRR4, CNFN, SPRR2E, CDSN, KRT10, PI3, SPRR1B
Extracellular Region	3.420E-16	Factor H, SULT2B1, ACE2, SERPINB10, FN1, KLKs, PAM, DESC1, ENPP1, LEKTI, PLAC8, MALS-1, CASP14, SCCA-1, Kallikrein 7, PKP1, MUC16, AKR1C1, KRT1, DRB1-1, CTH, DRB1-11, DSG3, DRB1-8, SH3BGRL2, AREG, Siglec-6, CSTA, SCCA-2, 2B1C, KRTDAP, PAI1, DRB1-15, GLUT3, SPARC, KRT6C, DRB1-4, 2B1E, KRT6B, MMP-1, FBN2, DAB2, FGF12, AL1A1, DRB1-10, 2B1D, BChE, CNFN, PAI2, ASSY, Kallikrein 5, SLPI, DRB1-3, FBN, DMKN, SLCO4C1, PDGF-D, IBP3, SBSN, CASP1, PSG1, 5'-NTD, DCN proteoglycan, PLAT (TPA), HPGD, CDSN, KRT5, MXRA7, KRT10, TFPI, MME, ECM1, FBN1, PI3, NPX1, SCIN, NPNT, CLCA2, SPP1, KLK6, SPRR1B, DRB1-9, KRT6A, MA1A1, STEAP4, 2B1G, SPOCK, DCN
Extracellular Space	1.050E-15	Factor H, SULT2B1, ACE2, SERPINB10, FN1, PAM, ENPP1, LEKTI, MALS-1, CASP14, SCCA-1, Kallikrein 7, PKP1, MUC16, AKR1C1, KRT1, DRB1-1, CTH, DRB1-11, DSG3, DRB1-8, SH3BGRL2, AREG, CSTA, SCCA-2, 2B1C, KRTDAP, PAI1, DRB1-15, GLUT3, SPARC, KRT6C, DRB1-4, 2B1E, KRT6B, MMP-1, DAB2, FGF12, AL1A1, DRB1-10, 2B1D, BChE, CNFN, PAI2, ASSY, Kallikrein 5, SLPI, DRB1-3, DMKN, SLCO4C1, PDGF-D, IBP3, SBSN, 5'-NTD, PLAT (TPA), HPGD, CDSN, KRT5, KRT10, TFPI, MME, ECM1, FBN1, PI3, SCIN, NPNT, SPP1, Kallikrein 6, SPRR1B, DRB1-9, KRT6A, MA1A1, STEAP4, 2B1G, SPOCK, DCN
Extracellular Region Part	1.536E-15	Factor H, SULT2B1, ACE2, SERPINB10, FN1, PAM, ENPP1, LEKTI, MALS-1, CASP14, SCCA-1, Kallikrein 7, PKP1, MUC16, AKR1C1, KRT1, DRB1-1, CTH, DRB1-11, DSG3, DRB1-8, SH3BGRL2, AREG, CSTA, SCCA-2, 2B1C, KRTDAP, PAI1, DRB1-15, GLUT3, SPARC, KRT6C, DRB1-4, 2B1E, KRT6B, MMP-1, FBN2, DAB2, FGF12, AL1A1, DRB1-10, 2B1D, BChE, CNFN, PAI2, ASSY, Kallikrein 5, SLPI, DRB1-3, DMKN, SLCO4C1, PDGF-D, IBP3, SBSN, 5'-NTD, PLAT (TPA), HPGD, CDSN, KRT5, MXRA7, KRT10, TFPI, MME, ECM1, FBN1, PI3, SCIN, NPNT, SPP1, Kallikrein 6, SPRR1B, DRB1-9, KRT6A, MA1A1, STEAP4, 2B1G, SPOCK, DCN
Clathrin-Coated Endocytic Vesicle Membrane	1.095E-14	DRB4, DRB1-1, DRB1-11, DRB1-8, 2B1C, DRB1-15, DRB1-4, 2B1E, DRB1-10, 2B1D, DRB1-3, DRB1-9, 2B1G
Extracellular Exosome	2.575E-14	Factor H, SULT2B1, ACE2, FN1, PAM, LEKTI, MALS-1, CASP14, SCCA-1, PKP1, MUC16, AKR1C1, KRT1, DRB1-1, CTH, DRB1-11, DSG3, DRB1-8, SH3BGRL2, CSTA, SCCA-2, 2B1C, PAI1, DRB1-15, GLUT3, KRT6C, DRB1-4, 2B1E, KRT6B, DAB2, AL1A1, DRB1-10, 2B1D, CNFN, ASSY, SLPI, DRB1-3, DMKN, SLCO4C1, PDGF-D, IBP3, SBSN, 5'-NTD, PLAT (TPA), HPGD, CDSN, KRT5, KRT10, MME, ECM1, FBN1, PI3, SCIN, NPNT, SPP1, SPRR1B, DRB1-9, KRT6A, MA1A1, STEAP4, 2B1G
Extracellular Vesicle	3.533E-14	Factor H, SULT2B1, ACE2, FN1, PAM, LEKTI, MALS-1, CASP14, SCCA-1, PKP1, MUC16, AKR1C1, KRT1, DRB1-1, CTH, DRB1-11, DSG3, DRB1-8, SH3BGRL2, CSTA, SCCA-2, 2B1C, PAI1, DRB1-15, GLUT3, KRT6C, DRB1-4, 2B1E, KRT6B, DAB2, AL1A1, DRB1-10, 2B1D, CNFN, ASSY, SLPI, DRB1-3, DMKN, SLCO4C1, PDGF-D, IBP3, SBSN, 5'-NTD, PLAT (TPA), HPGD, CDSN, KRT5, KRT10, MME, ECM1, FBN1, PI3, SCIN, NPNT, SPP1, SPRR1B, DRB1-9, KRT6A, MA1A1, STEAP4, 2B1G
Extracellular Organelle	3.902E-14	Factor H, SULT2B1, ACE2, FN1, PAM, LEKTI, MALS-1, CASP14, SCCA-1, PKP1, MUC16, AKR1C1, KRT1, DRB1-1, CTH, DRB1-11, DSG3, DRB1-8, SH3BGRL2, CSTA, SCCA-2, 2B1C, PAI1, DRB1-15, GLUT3, KRT6C, DRB1-4, 2B1E, KRT6B, DAB2, AL1A1, DRB1-10, 2B1D, CNFN, ASSY, SLPI, DRB1-3, DMKN, SLCO4C1, PDGF-D, IBP3, SBSN, 5'-NTD, PLAT (TPA), HPGD, CDSN, KRT5, KRT10, MME, ECM1, FBN1, PI3, SCIN, NPNT, SPP1, SPRR1B, DRB1-9, KRT6A, MA1A1, STEAP4, 2B1G
Clathrin-Coated Endocytic Vesicle	4.020E-13	DRB4, DRB1-1, DRB1-11, DRB1-8, 2B1C, DRB1-15, DRB1-4, 2B1E, DRB1-10, 2B1D, DRB1-3, DRB1-9, 2B1G

5.2.6 Drug sensitivity experiments using agents that target EGFR and MET

Differences in the phosphorylation levels of EGFR and MET were detected by phospho-RTK array analysis of ECM1 knockdown and scramble control cell lines. The pharmacological agents erlotinib and tivantinib (ARQ197) were used to determine the sensitivity of ECM1-high cell lines to EGFR and MET inhibition, respectively.

5.2.6.1 Erlotinib

To determine whether an EGFR inhibitor reduces cell viability of ECM1-high cell lines, we treated the parental cell lines HT-1376, HT-1197, LUCC4 and 647V with the EGFR inhibitor erlotinib (Figure 5-11). Cells were treated with either 0.1% DMSO or with erlotinib at a final concentration of 1 nM, 5 nM, 10 nM, 25 nM, 50 nM, 125 nM, 250 nM, 500 nM or 1 μM over a period of 6 days. For the HT-1376 (Figure 5-11 A) and 647V (Figure 5-11 D) cell lines a maximal effect of 35-40% growth inhibition was achieved at 1 μM. As less than 50% growth inhibition was achieved, half the maximal effective concentration (EC_{50}) could not be determined. Half the maximal inhibitory concentration (IC_{50}) values for the cell lines 647V and HT-1376 were 139.0 nM and 252.6 nM, respectively. Compared to the control treatment (0.1% DMSO) no dose-dependent changes in cell viability were seen for either HT-1197 (Figure 5-11 G) or LUCC4 (Figure 5-11 J) which were both highly resistant to treatment. Neither EC_{50} or IC_{50} could not be calculated using non-linear regression analysis due to the limited cell death in these cell lines.

In order to determine if ECM1 influenced resistance against erlotinib, for each of the cell lines examined (HT-1376, LUCC4, HT-1197, 647V) an ECM1 knockdown (KD1) and scramble control were also treated with either 0.1% DMSO or erlotinib at a final concentration of 1 nM, 5 nM, 10 nM, 25 nM, 50 nM, 125 nM, 250 nM, 500 nM, or 1 μM over a period of 6 days (Figure 5-11). In the HT-1376 cell line a maximal effect of 24% growth inhibition for the scramble control (Figure 5-11 B), and 21% for the ECM1 knockdown (Figure 5-11 C) was achieved at 1 μM erlotinib. As less than 50% growth inhibition was achieved for HT-1376, absolute EC_{50} could not be determined. However relative IC_{50} was calculated as 126.7 nM and 249.3 nM for the ECM1 KD and scramble control lines, respectively. For 647V, cell viability was reduced to 41% and 47% at 1 μM erlotinib for the scramble control (Figure 5-11 E)

and ECM1 knockdown (Figure 5-11 F), respectively. IC_{50} for the 647V ECM1 knockdown was determined to be 10.99 μM, and IC_{50} for the scramble control was determined to be 44.32 μM. In the HT-1197 cell line cell viability remained at 100% across all treatment concentrations (Figure 5-11 G, H, I). Cell viability in the LUCC4 ECM1 knockdown and scramble control cell lines remained at between 85-100% across all treatment concentrations of erlotinib (Figure 5-11 J, K, L). One-way ANOVA was also performed to compare both IC_{50} and maximal response achieved in the parental, scramble control and ECM1 knockdown cell lines. No significant difference was noted in IC_{50} or maximal response in terms of percentage cell viability post-treatment for any of the cell lines.

5.2.6.2 Tivantinib

To explore the effect of the MET inhibitor tivantinib (ARQ197) on the growth of ECM1-high bladder tumour-derived cell lines, we treated the parental cell lines HT-1376, LUCC4, 647V and HT-1197 with either 0.1 % DMSO or tivantinib at a final concentration of 10 nM, 100 nM, 500 nM, 1 μM, 2 μM, 4 μM, 6 μM, 8 μM or 10 μM over a period of 6 days (Figure 5-12). For the HT-1376 (Figure 5-12 A) and LUCC4 (Figure 5-12 D) cell lines, complete killing was not achieved. Tivantinib achieved maximum effect at 0.1 μM for LUCC4 and 10 μM for HT-1376, representing a reduction in cell viability of 50% and 40% respectively. Compared to the control treatment of 0.1% DMSO, maximal dose-dependent growth inhibition of 80% was achieved at 0.5 μM tivantinib for HT-1197 (Figure 5-12 G). Complete cell death of 647V cell line was achieved at 1 μM (Figure 5-12 H). As less than 50% growth inhibition was achieved in the LUCC4 and HT-1376 cell lines, absolute EC_{50} could not be determined, however IC_{50} values were calculated to be 0.01 μM for LUCC4, 2.79 μM for HT-1376, 0.35 μM for 647V and 0.25 μM for HT-1197.

In order to determine if ECM1 influenced resistance of cell lines to the MET inhibitor, where less than 80% cell death was noted in the parental cell line (LUCC4 and HT-1376) an ECM1 knockdown (KD1) and scramble control were also treated with tivantinib (Figure 5-12). One-way ANOVA was carried out to compare both IC_{50} and maximal response achieved in the parental, scramble control and ECM1 knockdown for HT-1376 and LUCC4 cell lines treated with tivantinib. For the HT-1376 scramble control cell lines (Figure 5-12 B) and ECM1 knockdown cell line (Figure 5-12 C) treatment with tivantinib resulted in the maximal effect of 50-55% reduction in cell viability at concentrations greater than 1 μM, and IC_{50} was

determined to be 0.89 μM and 0.77 μM, respectively. No significant difference was observed in IC_{50} or maximal response for HT-1376 between the ECM1 KD, scramble control or parental cell lines. The LUCC4 scramble control (Figure 5-12 E) and ECM1 knockdown (Figure 5-12 F) cell lines were also treated with tivantinib. Treatment with tivantinib led to a maximal reduction in cell viability of 65% for the scramble control and 53% for the ECM1 knockdown, and IC_{50} was determined to be 130 nM and 1.21 μM respectively. No significant difference was noted in IC_{50}. However, a significant difference was noted for the maximal response to tivantinib, with the scramble control demonstrating significantly reduced cell viability compared to the parental or ECM1 knockdown cell lines ($p = 0.00013$).

5.2.6.3 Dual treatment with erlotinib and tivantinib

Since there are a number of overlapping effector proteins in the MET and EGFR pathways, it was proposed that resistance may be due to of crosstalk between the two receptors. The effect of simultaneous MET and EGFR dual inhibition in HT-1376 was examined to identify if dual treatment led to enhanced reduction in cell viability compared to individual treatments alone (Figure 5-13). HT-1376 cells were treated with either 0.1% DMSO or doses corresponding to 0.1x, 0.125x, 0.25x, 0.5x, 1x, 2x or 4x the IC_{50} for each drug. For example, for the HT-1376 parental 0.1x the IC_{50} equates to 25.3 nM erlotinib and 279 nM tivantinib. An isobologram was created to determine if dual treatment provides an agonistic or synergistic effect, and this suggested dual tivantinib and erlotinib treatment had an additive effect. IC_{50} for dual treatment was determined to be 0.01x each drug's IC_{50} (2.53 nM erlotinib and 27.9 nM tivantinib). The creation of an isobologram requires the calculation of each drug's individual IC_{50}, therefore similar experiments could not be conducted for the LUCC4, 647V and HT-1197 cell lines.

Dual tivantinib and erlotinib treatment was also carried out for both the HT-1376 ECM1 knockdown and scramble control cell lines in order to determine if ECM1 influenced sensitivity (Figure 5-13). The HT-1376 ECM1 knockdown cell line exhibited a maximal reduction in cell viability of 73% and an IC_{50} of 0.13x each drug's individual IC_{50} (16.5 nM erlotinib and 116.3 nM tivantinib). For the scramble control, a maximal reduction in cell viability of 56% was achieved and the IC_{50} was determined to be 0.21x each drugs IC_{50} (52.4 nM erlotinib and 160.7 nM tivantinib). One-way ANOVA comparing IC_{50} and maximal response achieved in the parental, scramble control and ECM1 knockdown cell lines with dual treatment was

conducted and showed no significant differences in terms of percentage cell viability post-treatment.

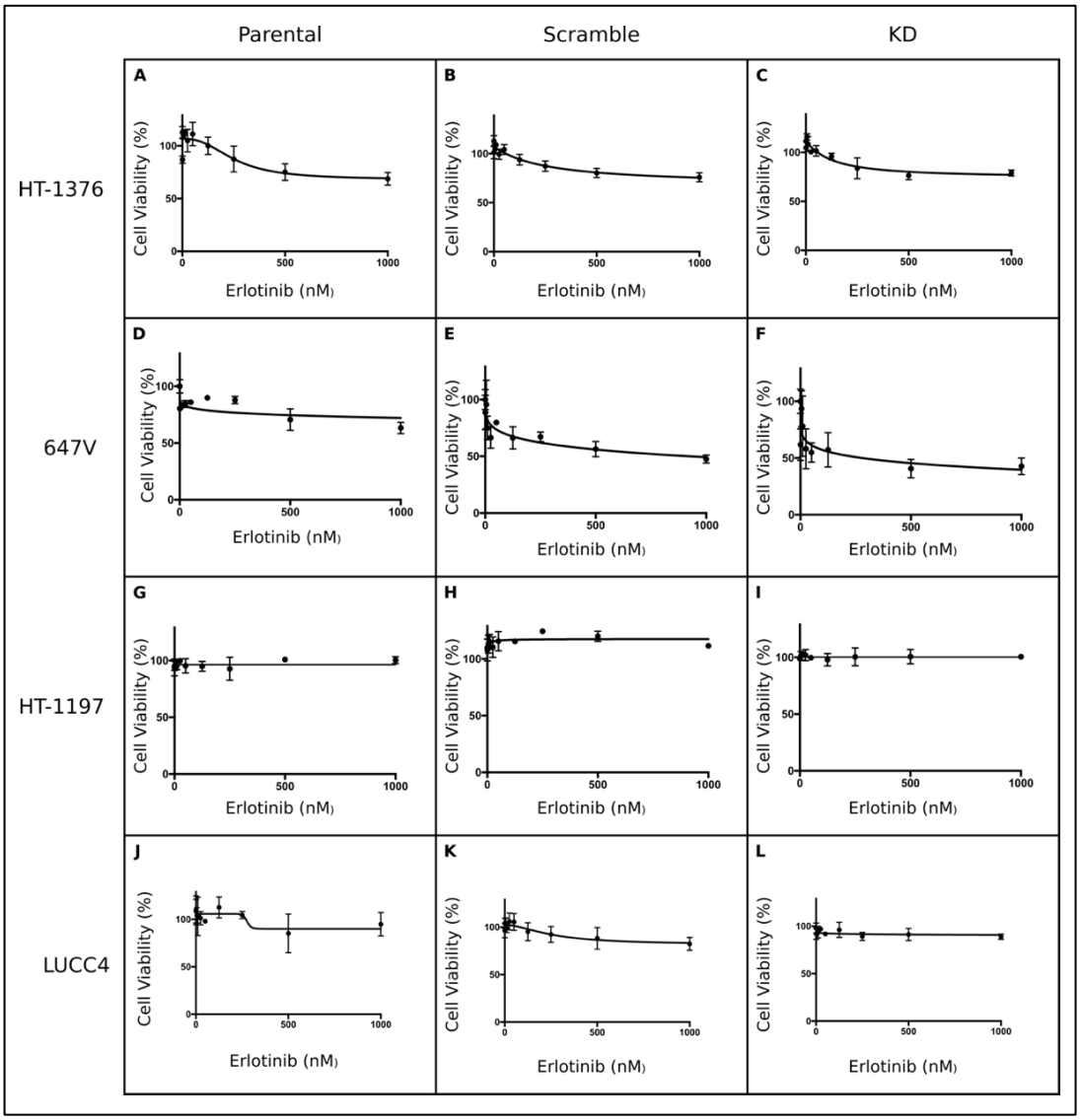

Figure 5-11: Treatment of HT-1376, LUCC4, HT-1197 and 647V cell lines with the EGFR inhibitor erlotinib.

3000-7000 cells were plated in each well of a 96 well plate in order to achieve 80% confluency in the untreated control at the end of the assay for each of the following cell lines: **A)** HT-1376 parental, **B)** HT-1376 scramble control, **C)** HT-1376 KD, **D)** LUCC4 parental, **E)** LUCC4 scramble control, **F)** LUCC4 KD, **G)** HT-1197 parental, **H)** HT-1197 scramble control, **I)** HT-1197 KD, **J)** 647V parental, **K)** 647V scramble control and **L)** 647V KD. Cells were incubated with 0.1% DMSO or 1 nM, 5 nM, 10 nM, 25 nM, 50 nM, 125 nM, 250 nM, 500 nM, or 1 μM erlotinib for 6 days. Five replicate wells were used for each concentration of drug. Conversion of the redox dye resazurin to fluorescent resorufin was measured and was taken as proportional to the number of viable cells. Data are displayed as percentage cell viability relative to the DMSO control. Representative of 1 experimental repeat.

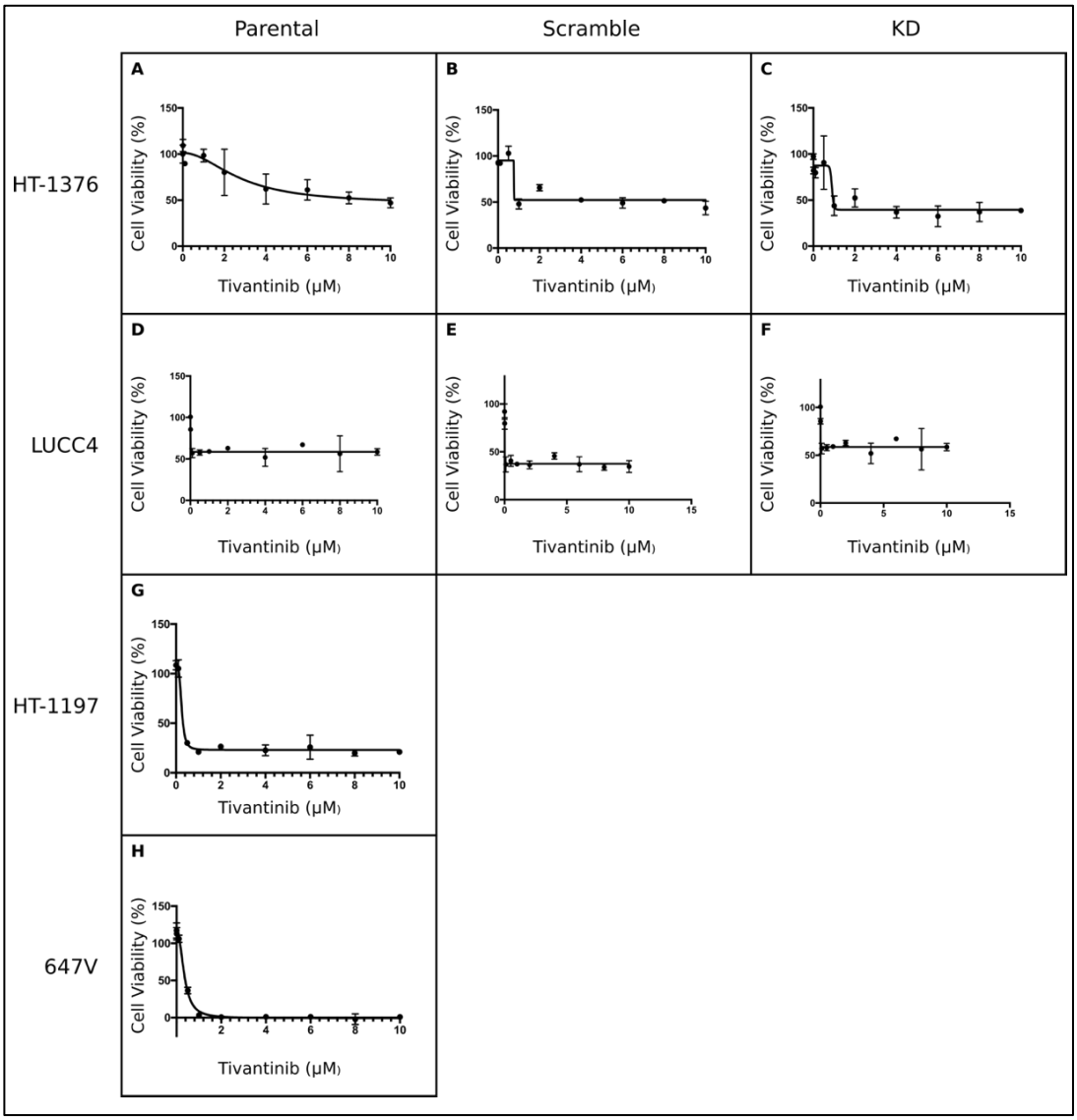

Figure 5-12: Treatment of HT-1376, LUCC4, HT-1197 and 647V cell lines with the MET inhibitor tivantinib.

3000-7000 cells were plated in each well of a 96 well plate in order to achieve 80% confluency in the untreated control at the end of the assay for each of the following cell lines: **A)** HT-1376 parental, **B)** HT-1376 scramble control, **C)** HT-1376 KD, **D)** LUCC4 parental, **E)** LUCC4 scramble control, **F)** LUCC4 KD, **G)** HT-1197 parental and **H)** 647V parental. Cells were incubated with 0.1% DMSO or 10 nM, 100 nM, 500 nM, 1 μM, 2 μM, 4 μM, 6 μM, 8 μM or 10 μM tivantinib for 6 days. Five replicate wells were used for each concentration of drug. Conversion of the redox dye resazurin to fluorescent resorufin was measured and was taken as proportional to the number of viable cells. Data are displayed as percentage cell viability relative to the DMSO control. Representative of 1 experimental repeat.

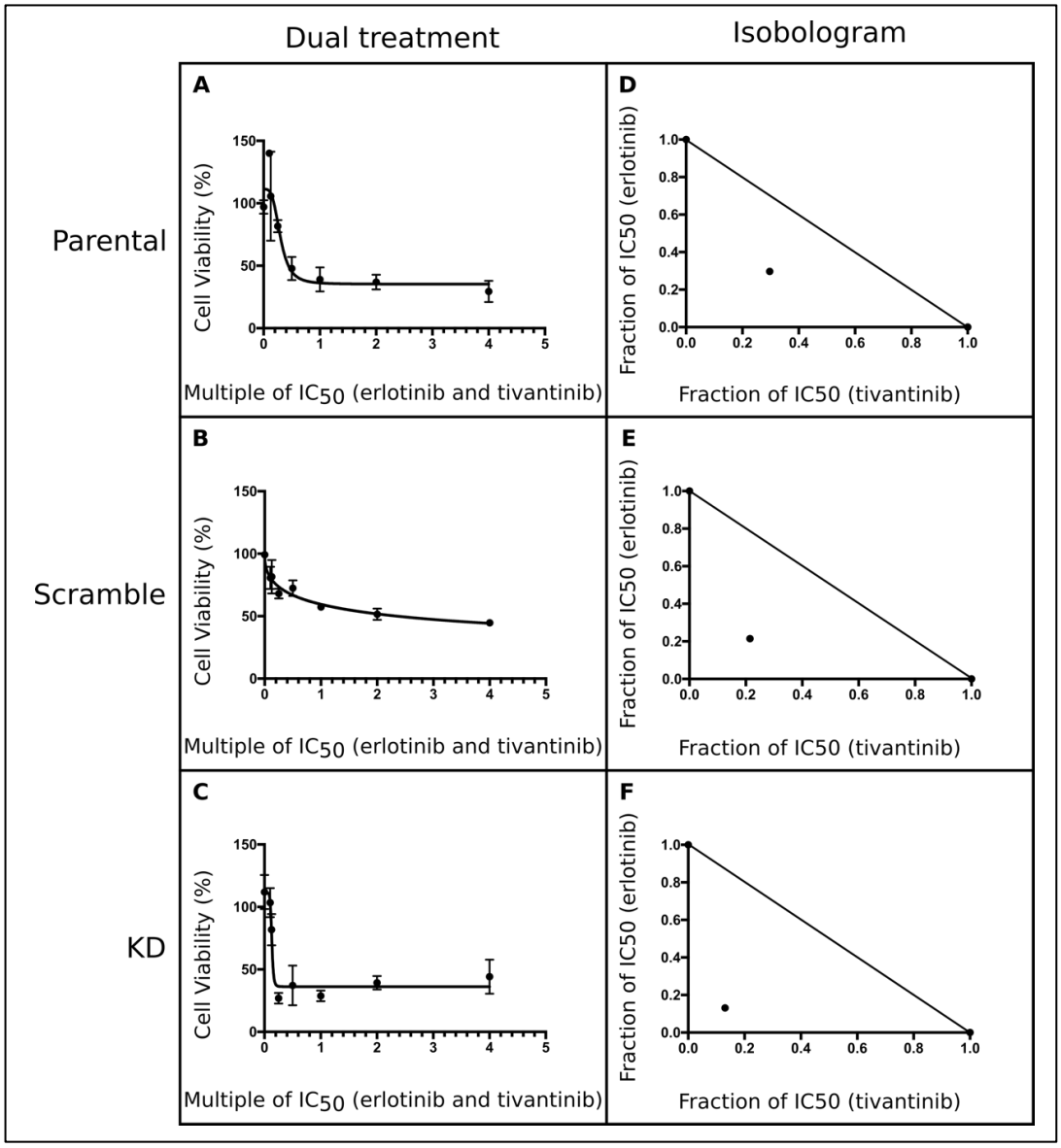

Figure 5-13: Dual treatment of HT-1376 parental, scramble control and ECM1 KD cell lines with the EGFR inhibitor erlotinib and the MET inhibitor tivantinib.

3000 cells were plated in each well of a 96 well plate. Cells were incubated with 0.1% DMSO or ratios of 0.1x, 0.125x, 0.25x, 0.5x, 1x, 2x or 4x the previously determined IC_{50} of each individual drug for dual treatment over 6 days. Five replicate wells were used for each drug concentration. Conversion of the redox dye resazurin to fluorescent resorufin was measured and was taken as being proportional to the number of viable cells. Data are displayed as percentage cell viability relative to the DMSO control for **A)** HT-1376 parental, **B)** HT-1376 scramble control and **C)** HT-1376 ECM1 KD cell lines. Isobolograms were created for **D)** HT-1376 parental, **E)** HT-1376 scramble control and **F)** HT-1376 ECM1 KD cell lines, determining the IC_{50} of dual erlotinib and tivantinib treatment in relation to each drug's individual action. This showed that combination treatment had a synergistic effect as the experimental IC_{50} falls below the additive line. Representative of 1 experimental repeat.

5.3 Discussion

Despite evidence for the involvement of ECM1 in cancer, very little is understood about the mechanisms and signalling pathways through which ECM1 mediates its effects. It has been suggested that ECM1 may be involved in EGFR signalling, as EGFR and ECM1 have been co-immunoprecipitated in breast cancer-derived cell lines [122]. This interaction was proposed to increase signalling through the Ras/Raf/MEK/ERK pathway, thereby mediating resistance to the ERBB2 targeting monoclonal antibody, trastuzumab.

Overexpression of epidermal growth factor receptor (EGFR) has been associated with high stage and grade muscle-invasive bladder tumours, poor clinical outcome, disease progression and disease recurrence following adjuvant chemotherapy [59, 215]. Due to its role in MIBC progression and treatment resistance, EGFR represents a potential therapeutic target in MIBC. Although several trials have been conducted into the use of EGFR inhibitors for the treatment of MIBC, so far these have shown limited success. For example, a phase II study with the small molecule inhibitor gefitinib showed no improvement in survival or progression when the inhibitor was used as a first or second line treatment [216, 217].

Molecular subtyping of MIBC led to the proposal that stratification of patients based on the molecular features of the tumours could be beneficial and may increase the effectiveness of EGFR inhibitors by enabling pre-selection of patients most likely to respond [86]. Rebouissou *et al.* described an aggressive basal subtype thought to be dependent on EGFR for growth that represents around a quarter of all MIBC cases [86]. Classification of 22 bladder tumour-derived cell lines using a set of 40 genes differentially expressed between basal and non-basal tumours identified eleven of the cell lines as basal. Of these 11 cell lines, 9 showed 50% growth inhibition following treatment with the EGFR small molecule inhibitor erlotinib at a concentration of less than 1 μM. In contrast, only one of the non-basal cell lines exhibited sensitivity to the drug [86]. This suggests that the described molecular subtypes of MIBC may independently predict response to EGFR inhibitors, and highlights the potential for the stratification of MIBC based on molecular subtypes as an effective strategy for the allocation of therapeutic options.

Although our ECM1-high subtype also exhibits basal-like features for example increased of keratins 5 and 6 and EGFR, none of these cell lines were used in the study of Rebouissou *et al*. We proposed that our ECM1-high subgroup may represent a subset of basal tumours expressing EGFR that are not sensitive to EGFR inhibition as a result of an interaction between ECM1 and EGFR in the complex proposed in breast cancer [122]. We investigated the potential for this complex to exist in the ECM1-high cell lines using co-immunoprecipitation, but a physical interaction between ECM1 and EGFR in our ECM1-high cell lines could not be detected.

Although a physical interaction between ECM1 and EGFR not detected we also considered the potential for ECM1 to influence EGFR signalling indirectly, for example via another mediator. In breast cancer-derived cell lines, recombinant ECM1 treatment has been demonstrated to initiate ERK phosphorylation [122], and similarly a recent study demonstrated that recombinant ECM1 treatment stimulated ERK and AKT phosphorylation in cardiac fibroblast cells grown in culture [218]. We examined the effects of ECM1 expression on the phosphorylation of EGFR and two effectors of downstream signalling, ERK and AKT. Increased levels of p-EGFR were noted in the HT-1376, HT-1197, and 647V cell lines in response to treatment with recombinant ECM1. Moreover, ERK phosphorylation was lower in ECM1 knockdown cell lines compared to the scramble controls for HT-1376 and HT-1197, and an increase in the level of ERK phosphorylation was noted for HT-1376, HT-1197 and 647V in response to recombinant ECM1 treatment. Our results imply that ECM1 plays a role in initiating activation of the EGFR pathway, and that ERK is a downstream target of EGFR activation. It is interesting that despite changes to ERK and AKT signalling, no changes to cell-proliferation were noted in the ECM1 knockdowns compared to the control cell lines. This suggests the activation of another unidentified feedback mechanism by which the ECM1 knockdown cells can maintain cell proliferation.

Phosphorylation of EGFR could not be detected in the LUCC4 scramble control cell line or ECM1 knockdown (with or without treatment with recombinant ECM1) implying that the receptor is not active in these cell lines, and activation is not initiated by ECM1. A previous study in breast cancer derived cell lines reported that while there was no change in EGFR or ERK phosphorylation in response to treatment with recombinant ECM1 alone, treatment with both ECM1 and EGF resulted in a significant increase in p-EGFR and p-ERK compared to EGF treatment

alone [122]. The HT-1376, HT-1197 and 647V cell lines are grown in media supplemented with 10% foetal bovine serum which contains high levels of growth factors such as EGF, whereas the LUCC4 cell line is cultured in media supplemented with just 1% serum and contains lower levels of growth factors. This may explain the absence of EGFR phosphorylation in the LUCC4 cell line, and the dual role of ECM1 and EGF in the activation of EGFR in LUCC4 may be an interesting line for future investigation.

Despite a lack of EGFR phosphorylation, ERK phosphorylation was observed to be slightly reduced in the LUCC4 ECM1 knockdown compared to the scramble control cell line, and an increase in the level of p-ERK was seen in response to treatment with recombinant ECM1. In this cell line it seems that although the downstream Ras/Raf/MEK/ERK pathway is activated by ECM1 it is not initiated through EGFR. ERK signalling is initiated by the activation of RAS which can be induced by a number of receptor tyrosine kinases such as EGFR, FGFR, and VGFR [219], hence, there is the potential that ERK signalling in LUCC4 is initiated through another receptor. ERK phosphorylation was lower in the LUCC4 ECM1 knockdown cell lines compared to the scramble control suggesting that the Ras/Raf/MEK/ERK pathway is a downstream target in all ECM1-high cell lines irrespective of the upstream receptor.

A smear instead of one defined band was noted for total AKT in both the ECM1 knockdown and the scramble controls cell lines for HT-1197, HT-1376 and LUCC4, and in the ECM1 knockdown cell line for 647V. Previous studies have demonstrated that this may be a consequence of AKT ubiquitination [220-222]. Ubiquitination most commonly targets proteins for degradation, however, ubiquitination of AKT mediated by K63 has recently been shown to alter cellular localisation and increase AKT signalling which in turn can promote cancer progression [222]. The smeared appearance of total AKT we noted for the ECM1-high cell lines may suggest that AKT-ubiquitination is also occuring in our cell lines, although the consequences of this ubiquitination are unclear. In the 647V cell line, the smearing patter observed for total AKT was accompanied by a reduction in the level of p-AKT in the ECM1 knockdowns cells compared to scramble control cells, perhaps implying that in this cell line ECM1 reduces ubiquitination of AKT. This in turn may result in decreased AKT degradation and increased availability of the protein for phosphorylation. A similar trend was not noted in the other cell lines (HT-1376, HT-1197, and LUCC4) suggesting ubiquitination is independent of ECM1

expression status in these cell lines, and it is unclear whether the potential ubiquitination we have observed would target AKT for degradation or alter the localisation of the protein. Regardless of potential ubiquitination, p-AKT was reduced in the untreated ECM1 knockdown samples compared to scramble controls for all cell lines, suggesting that like ERK, AKT is a downstream target in our ECM1-high cell lines.

Our results suggest that ECM1 influences the Ras/Raf/MEK/ERK and PI3K/PTEN/AKT signalling pathways potentially through EGFR activation. Activation of other receptor tyrosine kinases may also result in similar downstream signalling effects and there is very little information in the literature regarding ECM1 dependent mediators in carcinogenesis. Phospho-receptor tyrosine kinase (Phospho-RTK) array analysis demonstrated reduced levels of p-EGFR in all ECM1 knockdown cells compared to the scramble control lines providing further evidence of a role for ECM1 in EGFR pathway activation.

Phospho-RTK array analysis also identified MET as another potential receptor involved in ECM1-mediated signalling. A 10-fold decrease in MET phosphorylation was noted in the ECM1 knockdown compared to the scramble control for the HT-1376 cell line. MET is a transmembrane tyrosine kinase receptor which is activated via interaction with its only known endogenous ligand, hepatocyte growth factor (HGF). MET initiates signalling through pathways such as Ras/Raf/MEK/ERK and PI3K/PTEN/AKT, that promote cell proliferation, migration and regulate apoptosis. This receptor plays an important role in embryogenesis and wound-healing [60]. These steps are also crucial for the dissemination of tumour cells, and increased MET expression and activation has been repeatedly implicated in tumorigenesis, progression and metastasis of a number of carcinomas including breast cancer, non-small cell lung cancer and hepatocellular carcinoma [223-225]. Increased MET signalling in muscle-invasive bladder cancer shows a strong correlation with increased metastatic potential and poor outcome [226]. The difference in the level of p-MET detected in the HT-1376 ECM1 knockdown and scramble control cells was also mirrored in the LUCC4 samples implying that ECM1 influences MET activation. MET phosphorylation was not a feature identified by phospho-RTK array analysis of 647V. This cell line expresses much lower levels of ECM1 at both the mRNA and protein levels compared to either LUCC4 or HT-1376 and may respond differently.

Results obtained by western blot and phospho-RTK array analysis were not always concordant. There are a number of technical differences between the two approaches that may have influenced the observed results. One of the most notable differences between the techniques is the source of the antibodies used to assess tyrosine phosphorylation. Factors such as antibody-antigen affinity and cross reactivity can influence detection of a protein and could have contributed to the observed differences in the levels of phosphorylation measured [227]. Furthermore, differences in the lysis buffers and the phosphatase inhibitors these buffers contain could also influence the detected levels of receptor phosphorylation. For example, degraded phosphatase inhibitors can result in reduced signal and multiple bands on western blots, while transfer and running buffers contaminated with sodium azide can inactivate the horseradish peroxidase used in the detection step and therefore mask signals which might result in differences being observed between the two methods [228, 229]. Regardless of the reason for the discrepancy, it is difficult to determine without further analysis which method is a truer representation.

Quantification of western blot and phosphoarray results are hard to standardised due to a number of differences including image acquisition techniques, analysis software and background normalisation methods [230]. These differences become accentuated when attempting to quantify phosphorylation status, as differences in the affinities of the antibodies used to detect the phosphorylated and total proteins by western blotting can lead to ratio calculations being unreliable [231]. It has been argued that western blots should not be used in a quantitative respect, but only to demonstrate large differences in protein levels that are immediately obvious to the naked eye [230].

In the LUCC4 cell line, type 1 insulin-like growth factor receptor (IGF-1R) and insulin receptor (INSR) were also highlighted as activated by phospho-RTK array analysis. Both receptors are important for the regulation of energy metabolism and cell growth [232], and signalling through these receptors has also been reported to be widely involved in carcinogenesis and tumour progression [233]. Overexpression of INSR is seen in a number of different carcinomas including breast, colon, lung, ovary and thyroid, and is reported to provide these cancers with a selective advantage over non-malignant tissue as they are more sensitive to the mitogenic effects of insulin [234]. IGF-1R is reported to be important in the acquisition of a neoplastic phenotype, anchorage independent growth and inhibition of apoptosis

[233]. High levels of the IGF-1R ligands IGF-1 and IGF-2, have been reported in MIBC and are associated with poorer survival in patients [234]. As higher levels of phosphorylation were observed in the LUCC4 ECM1 knockdown cell line compared to the scramble control cell line, it may suggest that IGF-1R and INSR activation is a feedback mechanism by which LUCC4 ECM1 knockdown cells can maintain cell proliferation. As phosphorylation of IGF-1R and INSR was not detected by the analysis of HT-1376 and 647V it is unlikely to be a common feature of ECM1 high cell lines. Nevertheless, it does highlight that multiple receptors in tumour cells can activate pathways that influence factors such as growth, metastasis and drug resistance, and could pose difficulties when considering targeted approaches to therapy.

In order to investigate the effects of ECM1 knockdown on gene expression, microarray analysis was conducted to compare genome-wide expression in the HT-1376 ECM1 knockdown and scramble control cell lines. A striking feature of this analysis was the more than three-fold downregulation of 16 genes encoding 5S ribosomal RNA (rRNA) in the ECM1 knockdown compared to the scramble control. The ribosome is a complex involved in the synthesis of proteins from mRNA and 5S rRNA forms a key structural and functional component of this complex [235, 236]. Increased transcription of ribosomal genes is a common feature across many human cancers [237]. In a study which examined 721 tumour samples from six cancer types (bladder cancer, lung adenocarcinoma, lung squamous cell carcinoma, kidney renal clear cell carcinoma, head and neck squamous cell carcinoma and stomach adenocarcinoma) a 2 to 10-fold amplification of 5S rDNA was detected in almost every cancer genome relative to paired adjacent normal tissue [237]. A potential reason for the increase in rRNA is the need for cancer cells to increase production of macromolecules such as proteins in order to facilitate cell replication [238]. Decreased expression of 5S rRNA in response to ECM1 knockdown suggests that ECM1 either directly or indirectly regulates 5S rRNA expression which in turn may increase protein synthesis in ECM1-high cells.

The expression of the transcription factor E74-like transcription factor 5 (ELF5) was also downregulated in the HT-1376 knockdown cell line compared to the scramble control cell line. ELF5 is a member of a large family of transcription factors known as the epithelium twenty-six (ETS) family [239]. ELF5 is only expressed in a selected set of normal human epithelial tissues, including the salivary glands, skin, breast and bladder [240], and plays a regulatory role in cell differentiation of specific cell

types, for example, it is upregulated during keratinocyte differentiation *in vitro* [241]. In bladder cancer most evidence indicates that ELF5 plays a tumour suppressor role. In a study that compared high and low stage bladder tumours, ELF5 was found to be significantly lower in MIBC [239]. Our results appear to contradict this observation as knockdown of ECM1 in HT-1376, a cell line derived from a muscle-invasive bladder tumour, led to downregulation of ELF5. In breast cancer-derived cell lines sustained ELF5 expression leads to a basal-like aggressive subtype, and ELF5 knockdown results in suppression of a basal pattern of gene expression [242]. Moreover, ELF5 expression is significantly higher in basal compared to luminal breast cancer subtypes at the mRNA level [242]. Our microarray analysis suggests ECM1 may regulate ELF5 expression which in turn could be regulating a more basal phenotype. Indeed, a number of genes found to be downregulated in the ECM1 knockdown including kallikrein-related peptidases (KLK) 5, 6 and 7, keratinocyte differentiation associated protein (KRTDAP), amphiregulin (AREG), and five keratins (keratins 1, 10, 4, 5, and 6) have been shown to have higher expression at the mRNA level in basal MIBC compared to non-basal MIBC [86]. Joint expression of keratin 6 and keratin 5 is also commonly associated with a basal subtype of MIBC [74, 190]. As basal markers are downregulated in the HT-1376 ECM1 knockdown cell line, this implies that ECM1 promotes the expression of genes related to a basal phenotype which could potentially be mediated through activation of ELF5.

AREG is an EGFR ligand which is expressed at higher levels in basal MIBC and was downregulated in the HT-1376 ECM1 knockdown cells. EGFR has multiple ligands, and although each ligand binds to EGFR causing dimerization of the receptor, it is widely believed that they each have distinct downstream biological actions [243-245]. AREG has been reported to influence the EGFR recycling pathway [246-248]. Stimulation of the laryngeal carcinoma-derived cell line HEp2 with recombinant AREG leads to the ubiquitination and internalisation of EGFR into endosomes. However, unlike EGF or TGF-α stimulated degradation, AREG stimulated ubiquitination is transient and is quickly lost resulting in EGFR being recycled to the cell surface where it can continue to signal [246]. AREG-mediated EGFR recycling is thought to lead to a more sustained level of ERK phosphorylation as opposed to transient activation [249]. ERK phosphorylation was reduced in the HT-1376 ECM1 knockdown cell line according to western blot analysis and a decrease in AREG expression was detected in the same cells by microarray

analysis. It might be that ECM1-mediated expression of AREG leads to an increase in Ras/Raf/MEK/ERK signalling.

Activation of the EGFR pathway by ECM1 was highlighted by phospho-RTK array analysis which showed a reduction in the level of p-EGFR in all ECM1 knockdown cells compared to the scramble controls. Altered MET phosphorylation was also observed in the HT-1376 and LUCC4 ECM1 knockdown cells compared to the scramble controls according to phospho-RTK array analysis. Due to the potential involvement of ECM1 in the activation of the MET and EGFR pathways we chose to assess the response of ECM1 high cell lines to EGFR and MET inhibitors.

There are a wide range of inhibitors that can be used to target EGFR. The two main classes of these drugs are monoclonal antibodies such as cetuximab and panitumumab, which are currently used in the treatment of advanced metastatic colorectal cancer and head and neck cancer [250, 251], and small molecule inhibitors such as erlotinib, gefitinib, vandetanib and lapatinib which are currently used to treat pancreatic cancer, NSCLC, advanced medullary thyroid cancer and advanced breast cancer [252]. This wide range of accessible inhibitors makes a logical selection for use in cell viability assays difficult. Inhibitors may not be selective for EGFR and may inhibit other members of the ERBB family due to the closeness in structural similarity of the receptors [253], and standardised quantitative descriptions of the selectivity of inhibitors is very often inadequate or completely absent [252]. Selective entropy, a quantification of the binding distribution of inhibitors in a selectivity panel, can be used to overcome this issue. The higher the entropy value, the more kinases the drug binds to while low entropy denotes selectivity [252]. The approach of selective entropy allows for the assignment of a defined value of a drug's selectivity and can be used to rank inhibitors for use and guide selection.

The small molecule inhibitor erlotinib is highly selective for EGFR. It has one of the lowest selective entropy values (0.9) for any EGFR inhibitor [254], and does not cross-react with other ERBB receptors. In MIBC, erlotinib has undergone a phase II open-label trial in 20 patients with clinical stage T2 disease [255]. Patients in this trial were treated with adjuvant erlotinib for four weeks. Upon surgical pathology, 12 patients were clinically down-staged to T0 or T1, and 15 had organ-confined disease suggesting erlotinib may be beneficial prior to surgical resection for MIBC [255]. As it may be of clinical benefit to MIBC patients and has high selectivity, erlotinib was selected for use in our drug viability assays.

The present study found the ECM1-high bladder tumour-derived cell lines to be resistant to erlotinib treatment, with LUCC4 and HT-1197 showing complete resistance to the drug and only partial growth inhibition being observed for HT-1376 and 647V. ECM1 has previously been linked to resistance to ERRB targeting drugs [122]. In order to investigate the impact of ECM1 expression on resistance to EGFR targeting drugs, ECM1 knockdown and scramble control cell lines were treated with erlotinib. ECM1 knockdown cell lines showed no difference in cell viability post-treatment compared to the scramble control cell lines, suggesting that ECM1 expression alone does not influence resistance to the drug. A previous investigation of erlotinib resistance in non-small-cell lung cancer reported a correlation between increased expression of EGFR, MET and *IGF-1R* and erlotinib resistance. It was proposed that increased expression of the other two receptors results in sustained Ras/Raf/MEK/ERK and PI3K/PTEN/AKT signalling when EGFR is inhibited [256]. As the MET and IGF-1R receptors were also highlighted by phospho-RTK array analysis, it is possible that the ECM1-high cell lines are not exclusively dependent on EGFR signalling and can continue to signal via pathways essential for growth and survival despite EGFR inhibition with erlotinib.

MET inhibitors are not yet common place in the clinic, however, there are a number of commercially available inhibitors and some are currently undergoing clinical trials. The most commonly cited MET inhibitors are SU11274, PHA665752 and MGCD265 (glesatinib). There is very little published data on the kinetics of these drugs and they are not thought to be highly selective for MET [257]. More recently developed inhibitors such as tivantinib (ARQ197) are much more selective. Tivantinib is a non-ATP competitive inhibitor which has a high affinity for MET and showed no alternative inhibitory effects when tested against a panel of 230 human kinases [258]. It was established as safe for human use in a phase 1 open-label trial in patients with incurable advanced solid tumours, demonstrating manageable side effects such as vomiting and nausea, fatigue and diarrhoea [259]. Tivantinib was selected for cell viability assays in the current study due to its relatively high specificity and safety as demonstrated in trials.

Tivantinib treatment of ECM1-high cell lines mediated cell growth inhibition to a greater extent than erlotinib treatment. Results were comparable to reports of tivantinib treatment in myeloma derived cell lines, where complete killing or notable levels of cell death (>50%) were achieved with 1 μM tivantinib [260]. In the current

study <1μM tivantinib treatment resulted in maximal growth inhibition of approximately 50% in HT-1376 and LUCC4, and 80-100% in HT-1197 and 647V. Although the action of tivantinib in 647V was promising, MET phosphorylation was not detected by phospho-RTK array analysis of this cell line. Total MET was detected in 647V by western blot analysis. This implies that phosphorylation of the receptor may not be a wholly suitable marker for sensitivity to MET inhibition. Indeed, suggestions have been made that tivantinib may not inhibit MET kinase activity in the traditional sense but may act to delay activation of MET in the dephosphorylated form [261], thus our results may imply that tivantinib is targeting dephosphorylated MET in this cell line. Recent reports suggest that tivantinib inhibits tubulin synthesis and leading to G2/M phase cell cycle arrest in lung carcinoma-derived cell lines [262], and this could pose another mechanism by which tivantinib treatment resulted in complete cell death of 647V cell lines.

The impact of ECM1 expression on resistance to tivantinib was also assessed through treatment of ECM1 knockdown and scramble control cell lines derived from HT-1376 and LUCC4. While HT-1376 ECM1 knockdown and scramble control cell lines showed no difference in cell viability post-treatment, a significant difference was noted between the maximal response achieved in the LUCC4 ECM1 knockdown, scramble and parental control, however, it was the scramble control that showed the greatest reduction in cell viability in response to treatment, suggesting that resistance was not ECM1 mediated. As with erlotinib, these results suggest that patients who may benefit from MET inhibition cannot be stratified based on the level of ECM1 expression.

Cross-talk between the MET and EGFR pathways may also contribute to a lack of sensitivity to erlotinib and tivantinib in the ECM1-high cells. Focal amplification of MET in lung cancer has been reported to result in resistance to the EGFR inhibitor gefitinib, potentially through MET heterodimerisation with ERBB3 resulting in the activation of the PI3K/PTEN/AKT pathway [263]. MET inhibition alone had no effect on gefitinib resistant lung cancer cell lines, but these lines were sensitive to combination treatment with MET and EGFR inhibitors *in vitro* [263], suggesting co-dependence on EGFR and MET signalling. Similarly, in gastric cancer-derived cell lines, resistance to MET inhibition correlated with high levels of EGFR activation and sustained downstream signalling of the RAS/RAF/MEK/ERK pathway [264, 265]. As both resistance to individual treatments targeting EGFR and MET, and high levels of ERK phosphorylation were seen in our the ECM1-high cell lines, it was

proposed that dual treatment may have greater efficacy. Dual treatment in HT-1376 resulted in an additive effect of these drugs in combination and may suggest that simultaneous inhibition of EGFR and MET could be an effective approach to targeted treatment in patients that exhibit resistance to individual EGFR and MET treatments. Furthermore, the lower IC_{50} attained may enable a reduction in the dose required for patients and limit side effects. However, as no difference was noted between dual inhibition of the HT-1376 ECM1 knockdown compared to the parental or scramble control cell lines, ECM1 does not appear to influence the effectiveness of dual treatment.

Chapter 6
Final Discussion

Preliminary work carried out by the Knowles group prior to the start of this study identified a subset of bladder-tumour derived cell lines (subgroup 2) that had basal-squamous features but also exhibited unique and significant upregulation of 50 genes including ECM1 and MUC1 (Hurst *et al*. unpublished data). The first aim of this project was to confirm the expression levels of ECM1 and MUC1 in the bladder tumour-derived cell line panel. qRT-PCR and western blot analysis confirmed high levels of ECM1 and MUC1 in subgroup 2 at both the protein and mRNA levels. Furthermore, immunohistochemistry analysis confirmed high protein expression in formalin-fixed paraffin embedded (FFPE) cell pellets and in the corresponding primary tumours for a subset of the cell lines. Conditions under which cells are cultured differ from the original conditions in which the primary tumour developed, for example, cell lines face no immune competition or contact with extracellular matrix components. This may select for differing characteristics in the cell lines compared to tumours. However, the results from the immunohistochemistry staining suggest that the high ECM1 and MUC1 protein expression detected in the cell lines from subgroup 2 is a real feature and truly reflects expression in the original tumours.

In both cell lines and tumours, immunohistochemistry analysis revealed that ECM1 expression was largely cytoplasmic in location, confirming previous observations in breast, thyroid and hepatocellular carcinomas [115, 121, 162]. This may suggest an interaction between ECM1 and cytoplasmic proteins, or it may reflect a high level of protein synthesis and subsequent packaging of the protein into vesicles for secretion. Immunofluorescence staining of ECM1 in the HT-1376 cell line revealed a granular pattern of cytoplasmic staining which can be indicative of post-translational processing and packaging into transport vesicles destined for secretion by the Golgi apparatus [168]. Secretory vesicles may release proteins directly into the extracellular space and whole nanovesicles may also be actively shed by tumour cells in the form of exosomes [266].

Tumour-derived exosomes are small membrane-bound vesicles of around 40–150 nm in diameter that transport signalling molecules in the form of proteins, mRNAs,

miRNAs, and lipids from tumour cells into the microenvironment [267, 268]. These vesicles may have a number of pro-carcinogenic signalling functions and have been proposed to regulate tumour development and progression, mediate cancer immunity and immune invasion, and promote inflammation, angiogenesis and metastasis [267, 269-271]. Bladder tumour-derived exosomes have been shown to promote the malignant transformation of immortalised non-malignant urothelial cells *in vitro*, and exosomes isolated from the urine of patients with high-grade MIBC, induced migration and invasion of a low-grade bladder cancer-derived cell line (5637) [267]. Our observation of cytoplasmic vesicles containing ECM1, and the detection of ECM1 in conditioned medium, may suggest a role for ECM1 as an exosomal protein. Furthermore, EGFR and MUC1 have previously been detected in bladder tumour-derived exosomes [268, 272, 273]. Future work isolating of exosomes from ECM1-high bladder tumour-derived cell lines to assess whether ECM1 is present within such vesicles, and to and assess if a correlation exists between ECM1, EGFR, and MUC1 being present within the same exosomes would be of interest.

Previous studies have not yet assessed whether ECM1 is secreted in exosomes, however, ECM1 was originally identified as a secreted protein following TCA protein precipitation from the conditioned media of a murine osteogenic cell line [91]. Furthermore, the human form of ECM1 has been demonstrated to interact with extracellular components of the skin such as laminin 332, collagen type IV, and fibronectin, suggesting ECM1 is secreted in order for these interactions to occur [169, 170]. In the current study, ECM1 could be detected following western blot analysis of the protein fraction of conditioned media from the human bladder tumour-derived cell line HT-1376, suggesting human ECM1 is secreted by this cell line.

Secreted ECM1 may not only influence those cells expressing high levels of the protein but also other neighbouring cells and components of the microenvironment. Traditionally, cancer has been viewed as a disease of transformed, hyperproliferative cells [274, 275]. The influence of the dynamic network of immune cells, fibroblasts, vascular tissue, and extracellular matrix that make up the tumour microenvironment is increasingly seen as an important influencing factor in tumour progression and development [274, 276, 277]. In non-cancer studies, ECM1 has been shown to interact with components of the extracellular matrix in the skin [169, 170], and has also been noted to modulate immune cell responses. For example, in ECM1 knockout mice, early mortality within 6 weeks occurs due to high levels of undefined

autoinflammatory disease. Furthermore, chimeric mice with ECM1 deficient bone marrow also show high inflammatory disease attributed to the lack of migration of T helper 2 cells and regulator T cells from the peripheral tissues into areas of inflammation [170]. As this study showed that loss of ECM1 led to increased autoimmunity, this may suggest that increased expression of ECM1 in tumours could be important in tumour cell immune evasion. Therefore, investigating the role that ECM1 plays in relation to the tumour microenvironment may warrant further investigation, perhaps by assessing potential interactions between ECM1 and components of the tumour extracellular matrix, or through comparative assessment of immune markers in ECM1-high and ECM1-low tumours.

Immunohistochemistry analysis of primary tumours and cell pellets also showed MUC1 staining to be largely cytoplasmic. MUC1 has been reported at the apical surface of secretory epithelia [164, 165, 167]. Reports of alterations in the cellular localisation of MUC1 are common in malignant disease. In the urothelium MUC1 expression is normally confined to the apical membranes of superficial umbrella cells [136, 137]. However, in three quarters of bladder carcinomas, staining of MUC1 can be observed and is primarily located in the basal and intermediate layers of the urothelium [135, 141]. In prostate cancer a more diffused pattern of expression throughout the cytoplasm has been noted to be associated with more advanced disease [166], and in breast cancer a switch from membranous MUC1 expression to cytoplasmic and nuclear localisation is associated with increased metastatic potential [167]. These observations suggest that the cytoplasmic MUC1 staining we observed might be associated with more aggressive disease.

The membranous and cytoplasmic staining of MUC1 most likely relates to its roles in cell-cell adhesion, lubrication of mucus membranes, and interactions with membrane bound and cytoplasmic signalling molecules including EGFR, Wnt–β-catenin, p53, and NF-κB [180, 278, 279]. The cytoplasmic and extracellular domains of MUC1 have also been detected in the nuclei of a number of tumour-derived cell lines including human breast epithelial adenocarcinoma, human trophoblast-derived choriocarcinoma and pancreatic cancer-derived cell lines [280]. In the current study, MUC1 was also detected in the nucleus when staining was very intense as was the case in the LUCC4 cell line. Previous studies have suggested that MUC1 can translocate to the nucleus following autoproteolysis [281, 282] where it may act as transcriptional regulator [278, 280, 283]. In pancreatic ductal adenocarcinoma, MUC1 has been demonstrated to directly associate with EGFR, leading to the cleavage of

the MUC1 cytoplasmic domain and its translocation into the nucleus where it is thought to associate with the transcription factor hypoxia-inducible factor-1α (HIF-1α), which in turn promotes platelet-derived growth factor A (PDGFA) expression leading to cell proliferation [284]. The nuclear staining observed in the bladder tumour-derived cell lines may, therefore, be suggestive of MUC1 acting as a transcriptional co-factor.

Subsets of ECM1-high bladder tumours were also identified by interrogation of publicly available transcriptome datasets [32, 72, 75] and by immunohistochemistry analysis of ECM1 and MUC1 protein expression in four tissue microarrays (TMAs) consisting of 943 muscle-invasive bladder tumour cores. Previous studies have shown an association between ECM1 expression and increased metastasis and decreased survival rates in laryngeal [119, 184], breast [116], and hepatocellular carcinomas [118]. Clinical data is not yet available for the samples on the TMAs used in the current study, but patient metadata was available for the publicly available microarray data from the latest TCGA study [32]. Survival analysis showed that patients with ECM1-high tumours had statistically significant poorer overall survival than those with low ECM1 expressing tumours. Furthermore, patients with tumours expressing high ECM1 and MUC1 also had statistically significant poorer overall survival compared to patients whose tumours expressed high MUC1 alone. There was no difference in survival between patients with tumours expressing high ECM1 alone and those expressing both ECM1 and MUC1, suggesting that ECM1 expression could be the major influencing factor associated with reduced survival rates. Despite a link between high ECM1 expression and increased metastasis in other carcinomas, ECM1-high bladder tumours did not exhibit a significant difference in metastasis compared to low ECM1 expressing tumours.

We examined somatic mutation and increased DNA copy number as potential molecular mechanisms by which ECM1 expression is increased. No somatic mutations were detected by PCR and direct sequencing of selected exonic regions of the *ECM1* gene. Assessment of DNA copy number across the 1q21.2 region where the *ECM1* gene is located revealed increased copy number in five of the six ECM1-high cell lines (HT-1376, 647V, LUCC3, LUCC4 and LUCC5). This may explain the increased ECM1 expression noted in these cell lines as copy number increases can lead to increased gene expression [175]. However, there are also other candidate oncogenes in this region including *BCL9*, a nuclear component of the Wnt pathway, and *MCL1,* a member of the anti-apoptotic *BCL2* family of genes [176-

[178]. ECM1 expression may be influenced by copy number alteration but this highly gene dense region may also contain other oncogenes that could be targets for activation.

The functional role of ECM1 has been investigated to some extent in other carcinomas including breast, thryroid, cholangiocarcinoma and hepatocellular carcinomas [114, 115, 120, 181], but its role in bladder cancer had not been examined. The current study is the first to investigate the functional role of ECM1 in bladder cancer. We examined the phenotypic effects of ECM1 shRNA knockdown on cell growth, migration and wound healing capabilities of bladder tumour-derived cells. shRNA knockdown of ECM1 in four ECM1-high cell lines did not alter cell growth or morphology but reduced wound healing ability was observed. This mirrors previous reports in other carcinomas. For example, in multiple breast cancer and hepatocellular carcinoma-derived cell lines, silencing of ECM1 using antibody treatments or siRNA knockdown induced a significant reduction in wound healing ability [114, 120]. Furthermore, a similar effect is seen in the physiological symptoms of Urbach–Wiethe disease, in which patients with loss of function mutations to ECM1 present with disrupted wound healing ability [110]. Wound healing is a process that is highjacked during tumour cell migration and metastasis [285], hence, the observed effects of ECM1 knockdown on wound healing ability may hint at a role for ECM1 in metastasis.

The effect of ECM1 knockdown on the wound healing capability of the HT-1376 ECM1 knockdown cell line could not be recovered by treatment with recombinant ECM1 up to 750 ng/ml. In previous studies concentrations of recombinant ECM1a between 20 ng/ml and 200 ng/ml were sufficient to stimulate phenotypic effects, for example in cultured healthy endothelial cells 20 ng/ml recombinant ECM1a was sufficient to stimulate cell proliferation [93], while 200 ng/ml of recombinant human ECM1a also induced cell proliferation in breast cancer-derived cell lines [122]. It is unclear why treated with recombinant ECM1 had no effect on the wound healing ability of HT-1376 ECM1 knockdown cells at these concentrations, but there are a number of possible explanations. In the current study we determined that the ECM1 high cell lines used in the wound healing assays express ECM1a and at least one other isoform. Although the precise role of each isoform has not been fully elucidated, there is some suggestion that they have different functions. For example, ECM1b expression has previously been reported to be induced in differentiated keratinocytes [105], while ECM1a has been associated with

angiogenesis and is expressed in the endothelium of developing blood vessels [169]. It may be proposed that an isoform other than ECM1a contributes to the wound healing ability of our ECM-high bladder tumour-derived cell lines. Assessing the effect of conditioned media from the shRNA control or parental cell lines on the wound healing ability of ECM1 knockdown cells would have been beneficial in identifying if other isoforms secreted by the ECM1-high cell lines alter wound healing ability. Previous investigations into the role of ECM1 in cancer have either not specified isotype, or focused on the major ECM1a isoform [93, 120, 122]. Alternative splicing is a critical mechanism for the regulation of cell specific functions and dysregulation of isotype expression is known to be important in the pathology of cancer [209]. The expression of different ECM1 isoforms in the ECM1-high cell lines may hold information on the role of ECM1 in the pathogenesis of bladder cancer and future investigations modulating the expression of specific ECM1 isoforms in bladder-tumour derived cell lines may be of interest.

The ineffectiveness of recombinant ECM1 in rescuing the wound healing ability of ECM1 knockdown cells may also relate to post-translational modifications of ECM1. For example, glycosylation can dramatically change the physical structure and integrity of a protein, and this may influence cellular interactions and signaling cascades that can have a direct impact on cell growth, survival and metastasis [286]. In the current study, the molecular weight of secreted ECM1 detected in the protein fraction of conditioned media of HT-1376 was larger than ECM1 detected in the cell lysate. N-glycosylation at asparagine residues was reported to be important in the regulation of the secretion of ECM1 [153]. Deglycosylation of the secreted ECM1 isolated from the conditioned media of HT-1376 led to a reduction in molecular weight implying that secreted ECM1 is glycosylated.

We also investigated the direct effects of ECM1 knockdown on global gene expression by comparing microarray data for the HT-1376 ECM1 knockdown and scramble control cell lines. Genes that were downregulated in the ECM1 knockdown included eight keratins (keratins 1, 4, 5, 6A, 6B, 6C, 10 and 24) and the serine proteases known as human kallikrein-related peptidases (KLKs) 5 and 7. These genes may be of importance in relation to the reduced wound healing ability observed in ECM1 knockdown cell lines, as increased expression of keratins and serine proteases are characteristic of hyperproliferative wound healing of epithelial tissue [287-289]. The calcium receptor CALB2 and the EGFR ligand AREG were also significantly downregulated in the HT-1376 ECM1 knockdown cells compared to the

scramble control cells, and both proteins have been associated with wound healing. Mesothelial cells cultured from CALB2 knockout mice showed significantly decreased wound healing ability compared to CALB2 wildtype cells [290], and a previous study has also reported that treatment with recombinant AREG leads to increased wound healing ability in bladder tumour-derived cell lines [291]. Our results indicate that ECM1 regulates the expression of AREG, CALB2, keratins and kallikrein-related peptidases, and this may be suggestive of a role linked to increased wound healing in ECM1-high cell lines.

In breast cancer cells ECM1 has been seen to directly interact with EGFR, and this in turn stabilises interactions between EGFR and MUC1 as part of a membrane embedded protein complex that mediates Ras/RAf/MEK/ERK signalling [122]. Normal urothelium express relatively low levels of EGFR [132]. In contrast, approximately half of all bladder tumours overexpress EGFR [59], and there is a significant association between EGFR expression, tumour grade, invasiveness, and poorer survival for patients [55, 133]. Due to the importance of EGFR in bladder cancer and the previously discussed similarities that exist between the molecular subtypes of bladder and breast cancer, we investigated whether there was a physical interaction between the two proteins in our ECM1 high bladder tumour-derived cell lines. A physical interaction could not be detected between EGFR and ECM1 by coimmunoprecipitation, implying either no interaction or a weak and transient physical interaction between the two proteins. However, ECM1 may still influence EGFR signalling via an indirect mechanism such as interaction with one of the EGFR ligands. ECM1 has previously been reported to interact with EGF-like repeats in the vascular regulator perlecan [94]. This motif consists of six cystine residues that form three disulphide bonds, and it resembles a key interaction site found on the epidermal growth factor [292]. The ability for ECM1 to interact with this motif on perlecan suggests it may also be able to interact with ligands of EGFR which also harbour this motif such as EGF. In the current study, we evaluated the impact of ECM1 on the activation of the EGFR pathway by examining the effects of ECM1 knockdown and recombinant ECM1 treatment on the phosphorylation status of EGFR and the downstream effector proteins ERK and AKT. Three of the ECM1 knockdown cell lines treated with recombinant ECM1 exhibited increased phosphorylation of EGFR, implying that ECM1 plays a role in initiating activation of EGFR. Furthermore, ERK and AKT phosphorylation decreased in response to ECM1 shRNA knockdown, while ERK phosphorylation increased in response to ECM1 treatment of the ECM1 knockdown cell lines suggesting that both

Ras/Raf/MEK/ERK and PI3K/PTEN/AKT are important pathways downstream of ECM1. The ability of ECM1 to interact with EGF-like repeats, and the apparent ECM1-mediated activation of EGFR signalling warrants further investigation into possible interactions between ECM1 and EGFR ligands in the future.

Phospho-RTK array analysis also revealed decreased EGFR phosphorylation in the ECM1 knockdown cell lines compared to the scramble controls derived from the cell lines HT-1376, LUCC4 and 647V, further suggesting the EGFR pathway is activated by ECM1 and may represent a potential target in ECM1 high tumour cells. However, treatment of ECM1-high cell lines with the EGFR inhibitor erlotinib resulted in a maximal effect on cell viability of only 40%. Furthermore, no significant differences in cell viability were observed when ECM1 knockdown and scramble control cell lines were treated with erlotinib suggesting that ECM1 does not influence resistance to erlotinib. However, a key limitation of this study was that a control cell line with known sensitivity to erlotinib was not used. As such, the possibility of reduced activity of erlotinib in this batch resulting in lack of sensitivity observed cannot be ruled out. It may therefore be important to repeat this analysis in the future.

A decrease in MET phosphorylation in HT-1376 and LUCC4 ECM1 knockdown cell lines compared to the scramble control cell lines was demonstrated by phospho-RTK array and western blot analysis, suggesting that ECM1 plays a role in initiating activation of MET. We treated the four cell lines of subgroup 2 (HT-1376, HT1197, 647V and LUCC4) with the MET inhibitor tivantinib and this resulted in varied responses to the drug. Complete cell death was achieved for 647V and an 80% reduction in cell viability for HT-1197, but a <50% reduction in cell viability was noted for HT-1376 and LUCC4. MET inhibition did not result in a significantly different reduction in cell viability between the parental, scramble control and ECM1 knockdown cell lines for HT-1376 or LUCC4 implying ECM1 does not promote tivantinib resistance.

Although inhibition of EGFR and MET did not result in complete cell death, both the Ras/Raf/MEK/ERK and PI3K/PTEN/AKT pathways were highlighted as activated by ECM1 expression, thus downstream inhibition of ERK or AKT may be an attractive therapeutic avenue to pursue. Over the past 30 years, ERK has been consistently demonstrated to play an important role in cancer but there has been little focus on the development of selective ERK inhibitors [293]. This may be because ERK was

considered the sole downstream target of MEK and thus inhibiting ERK alone was not assumed to have any improved benefits over inhibitors targeting upstream targets [293, 294]. More recently ERK has been demonstrated to influence other pathways that may determine cell fate. For example, ERK was seen to positively regulate the expression of the oncogenic factor *O*-GlcNAc which maintains a malignant phenotype in cancer cells [295]. Hence, there may be more benefits to therapeutics targeting ERK than previously thought. Currently only two ERK inhibitors are in clinical trials: BVD-523 a competitive ATP kinase inhibitor, and GDC0994 a selective inhibitor that prevent phosphorylation of ERK. BVD-523 demonstrated anti proliferative activity in pancreatic and colorectal cancer-derived cell lines with activating BRAF mutations, and is in the recruitment stage of two phase I/II clinical trials for solid tumours, melanoma and hematologic malignancies [296]. GDC-0994 has demonstrated encouraging activity in RAS-mutated cancer cell lines and animal models in combination with the MEK inhibitor cobimetinib, and is currently in dose escalation trials in patients with locally advanced or metastatic solid tumours [297]. To our knowledge no trials have been conducted in bladder cancer patients.

AKT may also represent a potential target for cancer therapy but development of AKT inhibitors has proved difficult due to the existence of three isozymes that differ in tissue distribution, function and ligand affinity [298]. Very few compounds have been included in clinical trials and no AKT inhibitor has been approved for use in the clinic [299]. The use of ERK and AKT inhibitors in the treatment of bladder cancer is therefore not yet possible, but may be an interesting avenue for future investigation if suitable inhibitors were to be developed.

In conclusion our study has described a subgroup of ECM1-high bladder tumour-derived cell lines with basal-squamous features and high expression of ECM1. We have shown that a subset of primary tumours with similar features can be identified by analysis of publicly available datasets and immunohistochemical analysis of ECM1. It is unclear whether this subgroup represents a new MIBC subtype in its own right, or if it represents a subset of tumours that fit within the current basal-squamous subtype. High ECM1 expression in this subset of tumours is associated with poorer overall survival in patients and highlights ECM1 as a potential prognostic marker. Assessment of the phenotypic effects of shRNA knockdown of ECM1 in a panel of ECM1-high cell lines enabled us to established that ECM1 plays a role in promoting wound healing ability. Comparative analysis of microarray

data from ECM1 knockdown and scramble control cell lines for one ECM1-high cell line (HT-1376) suggested that this could be through ECM1-mediated modulation of genes involved in cell migration and wound contraction such as keratins, CALB2, and AREG. Confirmation of similar effects in other ECM1-high cell lines is required.

Phospho-array analysis of ECM1 knockdown cell lines treated with recombinant ECM1 demonstrated that ECM1 plays a role in the activation of EGFR and MET signaling and that ERK and AKT are downstream targets of this. A physical interaction between EGFR and ECM1 could not be established, hence, the mechanism by which this occurs may differ from that previously described in breast cancer cell lines [122]. Despite the apparent ECM1-modulated activation of EGFR and MET, inhibitors targeting EGFR and MET showed variable effects in our ECM1-high cell line panel and resistance to these inhibitors was not ECM1-dependent. Further studies assessing the potential efficacy of ERK and AKT inhibitors in ECM1 high bladder tumour cells is warranted.

Appendix A - Cell lines used in the study

Bladder tumour-derived cell lines used in this study, and their origins, stage, grade, and type of tumour from which they were derived.

A panel of forty-five bladder tumour-derived cell lines was collected for this study. Stages and grades of tumours are as described in referenced literature, and is based on the tumour-node-metastasis system. 'NR' denotes not recorded.

Cell Line	Type	Grade	Stage	Origin	Reference
253J	TCC	G4	T4	Lymph node metastasis, retroperitoneal	[300, 301]
5637	TCC	G2	NR	Bladder, primary	[302]
639V	TCC	G3	"small"	Ureter, primary	[300, 303]
647V	TCC	G2	"malignant" "stage B"	Bladder, primary	[300, 303]
92-1	TCC	G3	T4	Bladder	[304, 305]
96-1	TCC	G2/G3	T3	Bladder, recurrence	[304] [305]
97-1	TCC	G1/G2	T1/T2	Bladder, papillary	[304] [305]
97-18	TCC	G3	T2	Bladder	[305]
97-24	TCC	G3	T3	Bladder	[305]
97-7	TCC	G2/G3	T1	Bladder	[305]
BC3c	TCC	G4	"stage C" (UICC)	Bladder, "invasive solid TCC"	[306]
BFTC905	TCC	G3	"stage D1"(Jewett)	Bladder, primary, papillary	[307]
BFTC909	TCC	G3	T4N2M1	Renal pelvis, primary	[307]
CAL 29	TCC	G4	T2	Bladder, primary, invasive	[308]
DSH1	TCC	G2	T1a	Bladder, recurrence, papillary	[309]
HCV-29	TCC	NR	NR	Irradiated cancer-free bladder from patient with bladder cancer	Fogh, Unpublished
HT-1197	TCC	G4 "poorly differentiated"	"Invading the bladder muscularis" (T2 at least)	Bladder, recurrence	[310]
HT-1376	TCC	G3 "poorly differentiated"	"Invading the bladder muscularis" (T2 at least)	Bladder, primary	[310]
J82	TCC	G3 "poorly differentiated"	T3	Bladder, primary, papillary with solid areas	[311]

JMSU-1	TCC	G3	T4N2M1	Established from malignant ascitic fluid of a patient with bladder cancer	[312]
JO'N	TCC	NR	NR	Lymph node metastasis, retroperitoneal	Unpublished
KU-19-19	TCC	G3	pT3b	Bladder, primary	[313]
LUCC1	TCC	G3	T3bN1	Ureter, primary	Pitt, unpublished
LUCC2	TCC	G2	T2	Bladder, primary	Pitt, unpublished
LUCC3	TCC	G3	T2 at least	Bladder	Pitt, unpublished
LUCC4	TCC	G3	T2 at least	Bladder, recurrence	Pitt, unpublished
LUCC5	TCC	G3	T2 at least	Bladder, primary	Pitt, unpublished
LUCC6	TCC	G3	Ta	Renal pelvis, papillary	Pitt, unpublished
LUCC7	TCC	G3	T3	Renal pelvis,	Pitt, unpublished
LUCC8	TCC	G2	Ta	Bladder, primary	Pitt, unpublished
MGH-U3	TCC	G1	non-invasive	"non-Bladder,recurrence	[314]
RT112M	TCC	G2	NR	Bladder, primary	[315]
RT4	TCC	G1	T2	Bladder, recurrence	[316]
SCaBER	True squamous cell carcinoma	NR “Moderately differentiated”	T3	Bladder, primary	[317]
SD	TCC	NR	NR	Bladder, primary	[318]
SW-1710	TCC	NR	NR	Bladder, papillary	[319]
SW-780	TCC	G1	NR	Bladder, primary	[302, 319]
T24	TCC	G3	NR	Bladder	[320]
TCCSUP	TCC	G4	NR	confirmed Bladder, primary	[321]
U-BLC1	TCC	G3	T2	least Bladder, primary	[322]
UM-UC-3	TCC	NR	NR	Bladder	[323]
VM-CUB-1	TCC	NR	NR	Bladder, primary	[324]
VM-CUB-2	TCC	NR	NR	Lymph node metastasis	[324]
VM-CUB-3	TCC	NR	NR	Bladder primary	[324]

Appendix B - Genes uniquely and significantly upregulated in subgroup 2

Genes uniquely and significantly upregulated in an ECM1-high subgroup of bladder cancer derived cell lines.

Genome-wide microarray-based gene expression profiling was performed on a panel of 45 bladder tumour-derived cell lines. NMF analysis of the gene expression data defined five subgroups, and SAM analysis was used to identify genes enriched within NMF groups. The microarray probe IDs and gene names are shown for the genes that were uniquely and significantly upregulated in subgroup 2.

Gene probe IDs	Gene symbol	Gene name
225714_s_at; 230767_at; 235456_at; 235608_at; 236168_at; 237732_at; 238727_at; 240272_at; 241417_at; 242726_at	Unannotated	
226071_at	ADAMTSL4	A disintegrin and metalloproteinase with thrombospondin motifs ADAMTS-like 4
204664_at	ALPP	Alkaline phosphatase, placental
219714_s_at	CACNA2D3	Calcium channel, voltage-dependent, alpha 2/delta subunit 3
206193_s_at	CDSN	Corneodesmosin
213385_at	CHN2	Chimerin (chimaerin) 2
232127_at	CLCN5	Chloride channel, voltage-sensitive 5
213317_at; 217628_at; 219866_at	CLIC5	Chloride intracellular channel 5
203104_at	CSF1R	Colony stimulating factor 1 receptor
204720_s_at	DNAJC6	Dnaj (Hsp40) homolog, subfamily C, member 6
207324_s_at	DSC1	Desmocollin 1
206642_at	DSG1	Desmoglein 1
209365_s_at	ECM1	Extracellular matrix protein 1
204271_s_at; 204273_at; 206701_x_at	EDNRB	Endothelin receptor type B
209343_at	EFHD1	EF-hand domain family, member D1
1558579_at	FLJ37786	Uncharacterized LOC642691
207112_s_at; 214987_at; 225998_at; 226002_at; 229114_at	GAB1	GRB2-associated binding protein 1
208283_at; 207086_x_at; 207739_s_at; 208155_x_at	GAGE1	G antigen 1

206640_x_at	GAGE12C	G antigen 12C
208235_x_at	GAGE12F	G antigen 12F
207663_x_at	GAGE3	G antigen 3
214466_at; 226701_at	GJA5	Gap junction protein, alpha 5, 40kda
1560316_s_at; 225700_at; 225706_at; 227525_at	GLCCI1	Glucocorticoid induced transcript 1
209631_s_at; 214586_at	GPR37	G protein-coupled receptor 37 (endothelin receptor type B-like)
204515_at	HSD3B1	Hydroxy-delta-5-steroid dehydrogenase, 3 beta- and steroid delta-isomerase 1
222223_s_at	IL1F5	
205403_at; 211372_s_at	IL1R2	Interleukin 1 receptor, type II
229125_at	KANK4	KN motif and ankyrin repeat domains 4
220267_at	KRT24	Keratin 24
232300_at	LOC100128309	Uncharacterised LOC100128309
1560679_at	LOC151438	Uncharacterised LOC151438
226793_at	LOC283267	Uncharacterised LOC283267
207114_at	LY6G6C	Lymphocyte antigen 6 complex, locus G6C
204777_s_at	MAL	Mal, T-cell differentiation protein
1554652_s_at	MAST4	Microtubule associated serine/threonine kinase family member 4
207847_s_at; 211695_x_at; 213693_s_at	MUC1	Mucin 1, cell surface associated
1569020_at	NEDD9	Neural precursor cell expressed, developmentally down-regulated 9
1553534_at	NLRP10	NLR family, pyrin domain containing 10
1556029_s_at; 209755_at	NMNAT2	Nicotinamide nucleotide adenylyltransferase 2
204684_at	NPTX1	Neuronal pentraxin I
205259_at	NR3C2	Nuclear receptor subfamily 3, group C, member 2
204802_at; 204803_s_at; 231100_at	RRAD	Ras-related associated with diabetes
238909_at	S100A10	S100 calcium binding protein A10
219932_at	SLC27A6	Solute carrier family 27 (fatty acid transporter), member 6
216236_s_at; 222088_s_at	SLC2A14	Solute carrier family 2 (facilitated glucose transporter), member 14
202497_x_at; 202498_s_at; 202499_s_at	SLC2A3	Solute carrier family 2 (facilitated glucose transporter), member 3
201534_s_at; 201535_at	UBL3	Ubiquitin-like 3

Appendix C - Levels of ECM1 and MUC1 in 45 bladder tumour-derived cell lines according to microarray analysis

The relative expression level of ECM1 and MUC1 was determined at the mRNA level in a panel of 45 bladder tumour-derived cell lines by microarray analysis using GeneChip Human Genome U133 Plus 2.0 Arrays. Expression levels were measured relative to a pooled normal urothelial cell sample (NHU-Pool).

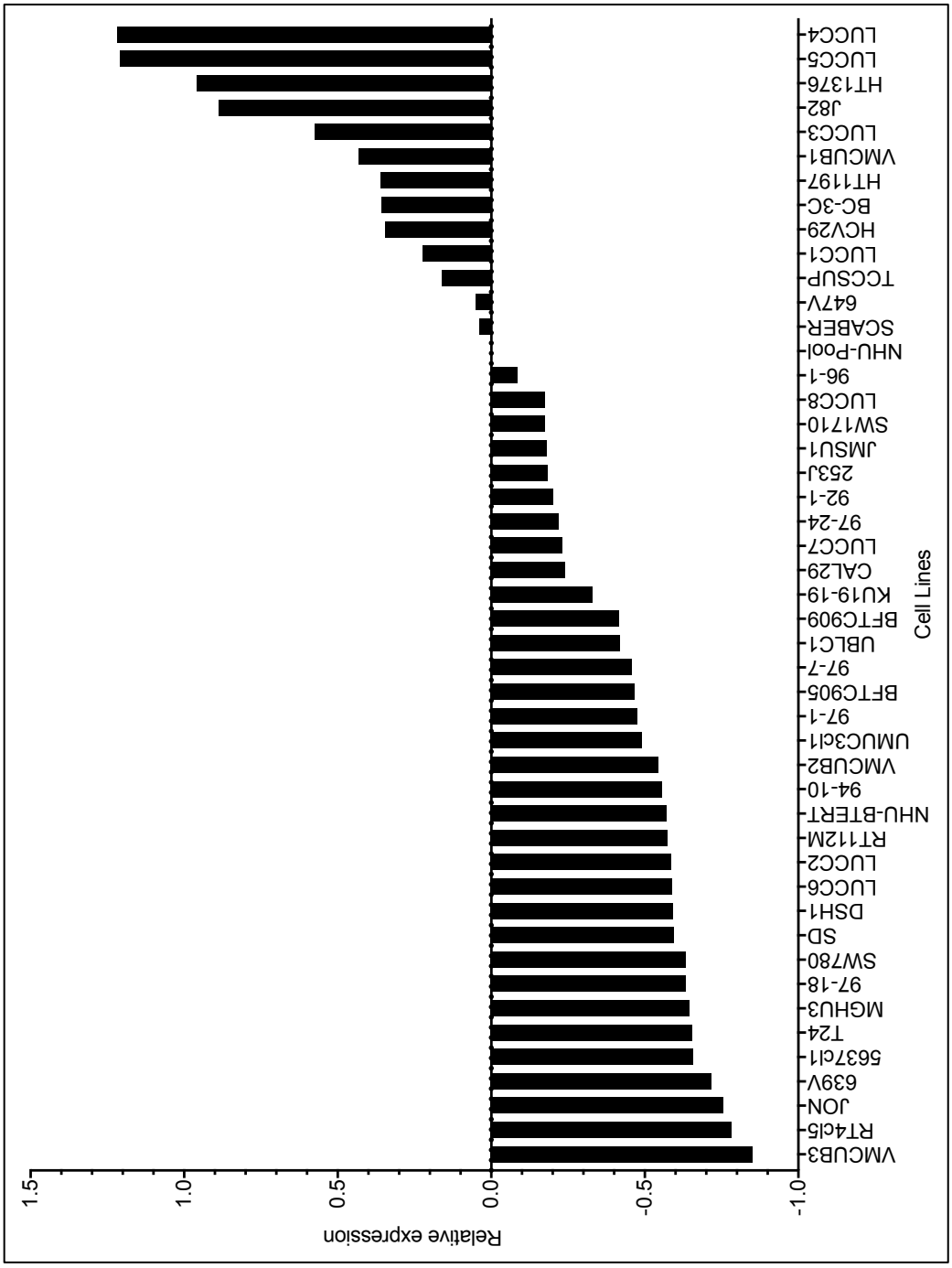

Expression of ECM1 (Probe ID: 209365_s_at) according to microarray analysis of 45 bladder tumour-derived cell lines.

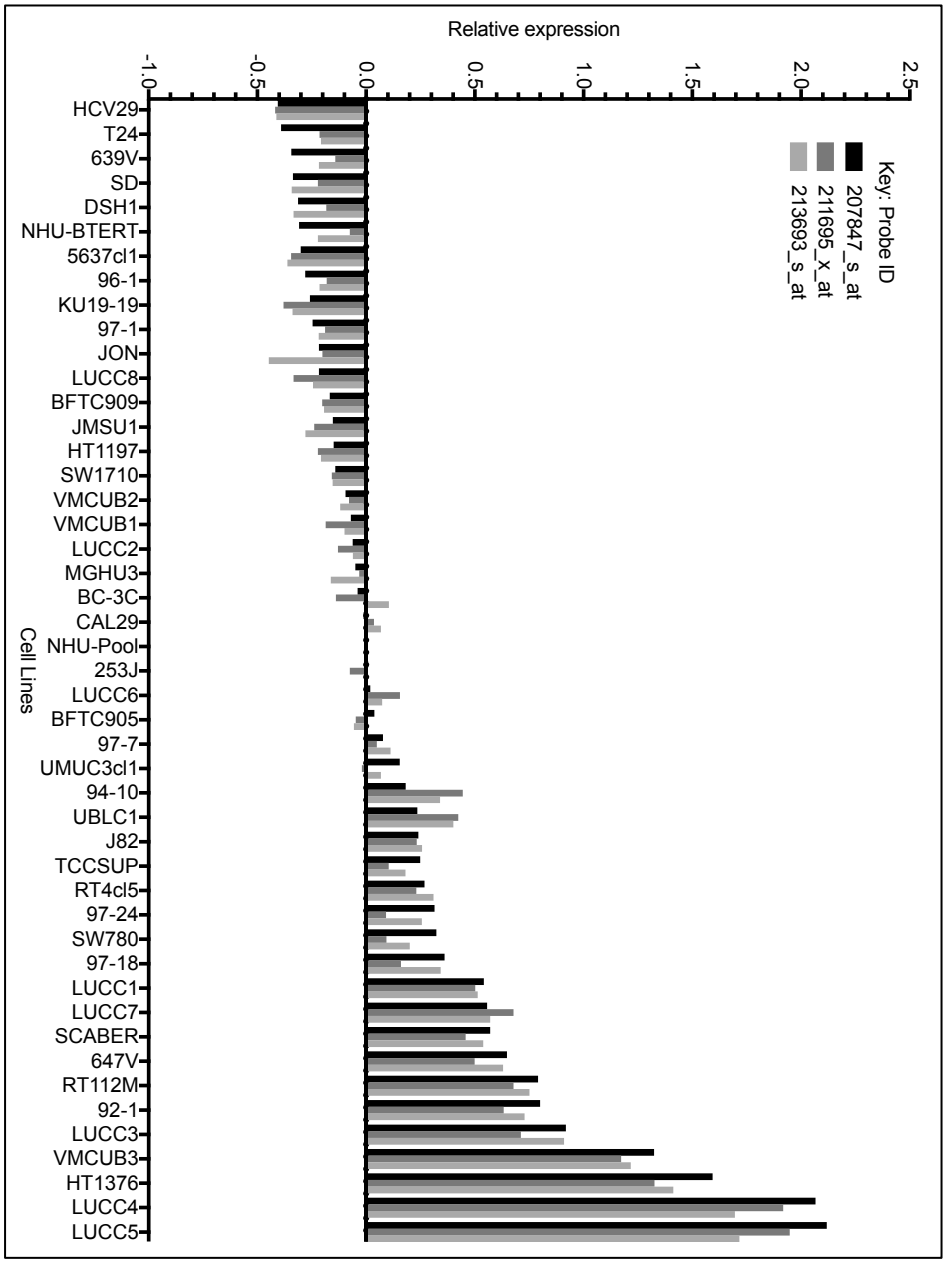

Expression of MUC1 (Probe IDs: 207847_s_at; 211695_x_at; 213693_s_at) according to microarray analysis of 45 bladder tumour-derived cell lines.

Appendix D - Western blot analysis of beta-actin

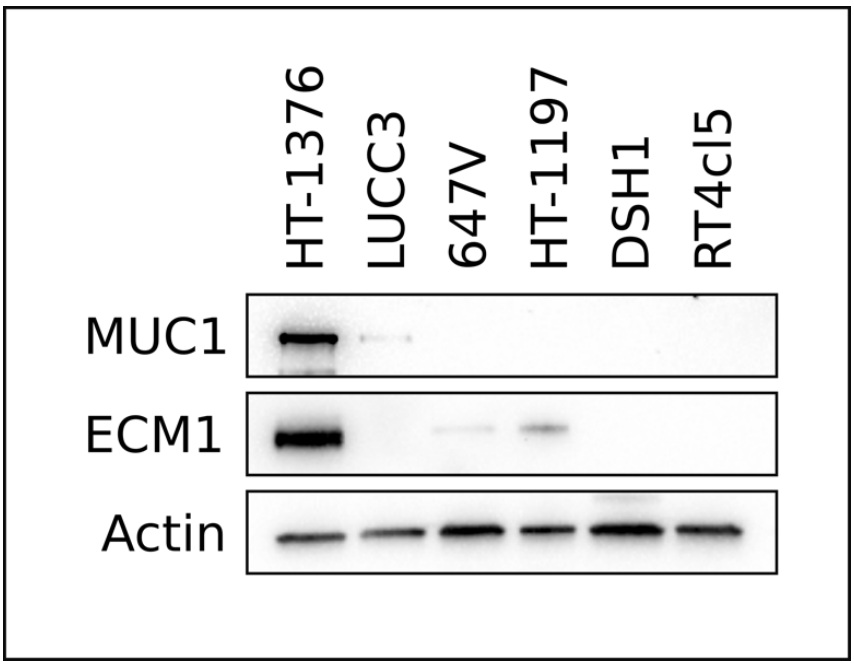

Western blot analysis of ECM1, MUC1 and beta-actin levels in 6 bladder tumour-derived cell lines.

The expression of ECM1 and MUC1 was examined at the protein level in the cell line panel of 45 bladder tumour-derived cell lines using western blot analysis (Figure 3.8). For this panel, tubulin-alpha expression was assessed as a loading control, however the cell lines DSH1 and RT4 do not express tubulin-alpha. For these cell lines beta-actin expression was also assessed. The expression of ECM1 and MUC1 was also reassessed in parallel for these cell lines, and four ECM1-high cell lines (HT-1376, LUCC3, HT-1197, and 647V) were used as positive controls. Total protein lysates were harvested for each cell line and 30 μg was analysed by western blot with antibodies specific to ECM1, MUC1 and anti-beta actin. Blots were analysed using the ChemiDoc MP System and Image Lab software.

Appendix E - Data mining and LIMMA analysis of publicly available bladder tumour datasets

Genes that were significantly altered in ECM1-high bladder tumours.

R2 was used to interrogate expression data from the studies of: Sjödhal *et al.* and Choi *et al.* that used fresh-frozen samples [72, 75]. LIMMA analysis, conducted using the online platform GEO2R, was used to compare ECM1-high and ECM1-low tumours. Stringency settings were applied to include only probes that had a fold change greater than 2 or less than -2 and a p value less than 0.05. Venn analysis was conducted on these lists of probes using Partek Genomics software to identify overlapping probes in both datasets. Unannotated probes were removed, and a single representative probe was selected being selected per gene, generating a list of genes significantly upregulated or downregulated in the ECM1-high tumours compared to the ECM1-low tumours.

A list of significantly upregulated genes in ECM1-high bladder tumours.

Illumina Probe ID	Gene Symbol	p-value	Fold Change		ILMN_1732151	COL6A1	2.19E-14	5.20		ILMN_1685433; ILMN_2402392	COL8A1	1.3E-12	3.93		ILMN_1663866	TGFBI	3.03E-11	4.15
ILMN_2329735	ECM1	2.45E-53	4.39		ILMN_1739496	PRRX1	3.82E-14	4.23		ILMN_1736178	AEBP1	2.07E-12	4.07		ILMN_1706498	DSE	3.94E-11	3.16
ILMN_2413644	TM4SF19	1.14E-25	4.82		ILMN_1729117	COL5A2	4.37E-14	5.31		ILMN_1780255	KLK6	2.6E-12	4.59		ILMN_1757552	PTRF	4.18E-11	3.02
ILMN_1718182	THRA	4.44E-22	3.76		ILMN_1667460; ILMN_2345142	SULF2	1.63E-13	3.55		ILMN_2324002	CALD1	3.38E-12	2.75		ILMN_1767665	GPX8	4.25E-11	3.29
ILMN_1719759	TNC	6.94E-20	5.97		ILMN_2232177	ACTN1	2.04E-13	3.10		ILMN_1701308	COL1A1	3.55E-12	5.30		ILMN_1660691	RAB31	6.41E-11	2.66
ILMN_2163873	FNDC1	1.37E-19	4.53		ILMN_1687652	TGFB3	2.15E-13	2.57		ILMN_1792455	TMEM158	4.3E-12	4.83		ILMN_1746928	TMPRSS11D	7.05E-11	2.61
ILMN_1707070	PCOLCE	1.65E-17	3.39		ILMN_2150851; ILMN_2150856	SERPINB2	2.25E-13	3.65		ILMN_1674367	SPRR2F	4.87E-12	4.65		ILMN_1698772; ILMN_1721354; ILMN_1669820	KRT6B	7.49E-11	2.51
ILMN_1785732	TNFAIP6	1.68E-16	4.75		ILMN_1758895	CTSK	3.04E-13	4.84		ILMN_1657111	AHNAK2	8.03E-12	5.33		ILMN_1732967	PPP1R18	8.15E-11	2.42
ILMN_2351466	NTM	6.37E-16	3.38		ILMN_1805192	ITPRIP	4.01E-13	2.36		ILMN_1801616	EMP1	1.04E-11	3.33		ILMN_1726589	CD248	9.13E-11	3.30
ILMN_1671142	GPR68	7.41E-16	3.20		ILMN_1709747	EXOG	4.26E-13	3.49		ILMN_1802654	GLT8D2	1.23E-11	2.76		ILMN_1670926	CHST15	1.09E-10	3.33
ILMN_1699489	TUBB6	1.26E-15	3.62		ILMN_1765446	EMP3	5.95E-13	2.52		ILMN_1678493	CHN1	1.31E-11	2.55		ILMN_1691156	MT1A	1.28E-10	4.80
ILMN_1792679	ITGA5	1.48E-15	3.41		ILMN_1795359	SPRR2A	8.03E-13	5.63		ILMN_2353054	KLK5	1.8E-11	3.02		ILMN_2363658	PXDN	1.72E-10	2.51
ILMN_1765557	OLFML2B	9.05E-15	2.99		ILMN_1713751	ADAM19	9.07E-13	3.73		ILMN_1784884	LILRB3	1.81E-11	3.45		ILMN_1686664	MT2A	2.18E-10	6.04
ILMN_1706505	COL5A1	1.26E-14	5.05		ILMN_1711439	EMILIN1	1.04E-12	2.39		ILMN_1666932	FCGR2A	2.09E-11	3.14		ILMN_1738578	FILIP1L	2.67E-10	2.45
ILMN_1793476	PRKCDBP	1.61E-14	3.52		ILMN_2191967	SPRR2D	1.14E-12	5.12		ILMN_1676413	VSNL1	2.86E-11	2.47		ILMN_2342579; ILMN_1691341	IL7R	2.74E-10	3.02

ILMN_1684554	COL16A1	2.87E-10	3.07	ILMN_2410523	DDR2	1.38E-09	2.05	ILMN_1689088	COLEC12	7.77E-09	2.59	ILMN_2123743	FCER1G	2.73E-08	3.19
ILMN_1779875	THY1	3.45E-10	3.08	ILMN_1810275		1.4E-09	2.86	ILMN_1687301	VCAN	8.22E-09	3.85	ILMN_2105573	CCL3L3	2.74E-08	4.03
ILMN_2344216	STX2	3.6E-10	2.55	ILMN_1785272; ILMN_2104356	COL1A2	1.55E-09	4.15	ILMN_1796712; ILMN_2046730	S100A10	8.35E-09	2.95	ILMN_2158713	IL36G	2.94E-08	2.24
ILMN_1659895	MSN	4.04E-10	2.96	ILMN_2307861; ILMN_1706643	COL6A3	1.84E-09	4.06	ILMN_1667295	VASN	9.05E-09	2.40	ILMN_1693826	HAVCR2	3.12E-08	2.86
ILMN_1655077	PRDM1	6.75E-10	2.35	ILMN_1741003	ANXA5	1.9E-09	2.51	ILMN_1806733	COL18A1	1.04E-08	2.42	ILMN_2211018	SPRR2E	3.13E-08	2.60
ILMN_1656057	PLAU	6.76E-10	3.72	ILMN_2184184	ANXA1	2.7E-09	3.47	ILMN_1740015; ILMN_2396444	CD14	1.11E-08	3.02	ILMN_2167805; ILMN_1790529	LUM	3.28E-08	3.42
ILMN_1721876	TIMP2	7.94E-10	3.49	ILMN_1758146	SIRPA	2.92E-09	3.17	ILMN_1727271	WARS	1.34E-08	2.32	ILMN_1655468	DSG3	3.49E-08	3.10
ILMN_1734276	PMEPA1	9.14E-10	3.47	ILMN_1723978	LGALS1	2.97E-09	3.18	ILMN_1706687	KLHL5	1.49E-08	2.20	ILMN_2197365	RGS2	3.55E-08	3.01
ILMN_1764709	MAFB	9.85E-10	2.68	ILMN_2109708	TYMP	3.3E-09	3.43	ILMN_1741632	RAB3IL1	1.5E-08	2.25	ILMN_1652631	GLIPR2	3.81E-08	2.91
ILMN_1670490	PDPN	9.91E-10	3.35	ILMN_1687978	PHLDA1	3.95E-09	3.22	ILMN_1722622; ILMN_2379599	CD163	1.7E-08	2.95	ILMN_1696360	CTSB	5.03E-08	2.09
ILMN_1683194; ILMN_1768227; ILMN_2347145	DCN	1.2E-09	3.23	ILMN_1815057	PDGFRB	4.06E-09	2.84	ILMN_1656837	RBP1	1.71E-08	3.25	ILMN_1686116	THBS1	5.8E-08	2.85
ILMN_1761281		1.2E-09	2.16	ILMN_1773079	COL3A1	4.97E-09	3.63	ILMN_1741356	PRICKLE1	1.81E-08	2.45	ILMN_1667430; ILMN_1780058	DEGS1	6.04E-08	2.30
ILMN_1787919	PARVB	1.25E-09	2.20	ILMN_1772612	ANGPTL2	5.04E-09	2.64	ILMN_2061435	MEG3	1.84E-08	2.52	ILMN_1715748	FLNC	7.05E-08	3.09
ILMN_2143795		1.28E-09	3.33	ILMN_2136089		5.14E-09	3.00	ILMN_1772964	CCL8	1.86E-08	3.74	ILMN_1721732	GSDMC	7.21E-08	2.32
ILMN_2410929	PAPSS2	1.35E-09	2.27	ILMN_1715068	AQP9	5.56E-09	3.24	ILMN_2380237	C1QTNF1	1.97E-08	2.63	ILMN_1651429	SELM	7.68E-08	2.62

ILMN_1663119	DSC2	8.13E-08	3.09	ILMN_1673352	IFITM2	2.33E-07	2.53	ILMN_1724533	LY96	6.33E-07	2.83	ILMN_1754576	KRT6C	2.97E-06	4.44
ILMN_2364521; ILMN_1701877	AXL	9.44E-08	2.14	ILMN_1768940	COL15A1	2.35E-07	2.56	ILMN_1654396; ILMN_2175912	ITGB2	7.46E-07	2.92	ILMN_1676563	HTRA1	3.11E-06	2.18
ILMN_1789196; ILMN_1757604	TPM2	9.98E-08	2.63	ILMN_1743199	EGR2	2.51E-07	2.49	ILMN_2206746	BGN	7.95E-07	2.45	ILMN_1720048	CCL2	3.23E-06	2.99
ILMN_2129161	LRRC32	1.23E-07	2.19	ILMN_1751161	COL7A1	2.83E-07	3.23	ILMN_1686623	CSF1R	8.28E-07	2.53	ILMN_1803686	ADA	3.34E-06	2.10
ILMN_1797009; ILMN_2129572	F3	1.28E-07	2.17	ILMN_2266595	LILRA5	3.1E-07	2.62	ILMN_2174127	DCBLD2	1.07E-06	2.85	ILMN_1667966	FAM129A	3.66E-06	2.29
ILMN_1775708	SLC2A3	1.37E-07	2.93	ILMN_1854469	BICC1	3.16E-07	2.36	ILMN_1699829; ILMN_2115125	CTGF	1.17E-06	2.73	ILMN_1784749; ILMN_1779558	GAS6	0.0000039	2.09
ILMN_1680738	NREP	1.75E-07	2.44	ILMN_1792473	AIF1	3.34E-07	2.57	ILMN_1781626	C1S	1.29E-06	3.00	ILMN_1797704		0.0000039	2.84
ILMN_1797875	ALOX5AP	1.79E-07	3.43	ILMN_1756071	MFGE8	3.56E-07	2.41	ILMN_1691476	MYLK	1.61E-06	2.23	ILMN_2082585	SNAI2	4.05E-06	2.42
ILMN_1735877		1.8E-07	2.81	ILMN_2350634	EFEMP1	3.58E-07	3.42	ILMN_1805750	IFITM3	1.64E-06	2.47	ILMN_1785902	C1QC	4.37E-06	2.58
ILMN_2082209	TOX2	1.82E-07	2.67	ILMN_2121408	HBEGF	3.97E-07	2.19	ILMN_1670305	SERPING1	1.64E-06	2.27	ILMN_1737988; ILMN_2360415	PRNP	4.97E-06	2.18
ILMN_2058251; ILMN_1782538	VIM	1.91E-07	2.60	ILMN_2404154	SERPINA1	4.47E-07	3.49	ILMN_1710544	PCDH7	1.71E-06	2.54	ILMN_1760347; ILMN_2169152	SRGN	0.0000054	3.12
ILMN_2063586	CLIC4	2.03E-07	2.65	ILMN_1729216	CRYAB	4.48E-07	2.15	ILMN_1796734	SPARC	1.71E-06	2.25	ILMN_2149226	CAV1	5.64E-06	2.39
ILMN_1672611	CDH11	2.09E-07	2.81	ILMN_1808590	GUCY1A3	5.02E-07	2.13	ILMN_1678842	THBS2	1.75E-06	4.01	ILMN_1789733	CLIP3	5.85E-06	2.05
ILMN_1698732	PALLD	2.17E-07	2.56	ILMN_2308849	MYADM	5.3E-07	2.59	ILMN_1795762	PLEK	2.43E-06	2.91	ILMN_1778668	TAGLN	6.63E-06	2.76
ILMN_2338323	CDC25B	2.24E-07	2.43	ILMN_1695290	FERMT2	6.02E-07	2.10	ILMN_1778977	TYROBP	2.71E-06	2.79	ILMN_1810844	RARRES2	0.000009	2.56

ILMN_1699931	HCST	0.0000095	2.44	ILMN_2173611	MT1E	0.0000194	2.97	ILMN_1757351	S100A7	0.000043	4.40
ILMN_1674160	BIN1	0.0000108	2.06	ILMN_2087656	SLCO2B1	0.0000198	2.10	ILMN_1665035	KRT14	0.0000464	3.18
ILMN_2094266	HES2	0.0000109	2.27	ILMN_1682717	IER3	0.00002	2.32	ILMN_1729801	S100A8	0.0000467	6.10
ILMN_1669362	IGFBP6	0.0000123	2.41	ILMN_1790689	CRISPLD2	0.0000259	2.15	ILMN_1769759	SERPINB13	0.0000484	2.29
ILMN_1803213	MXRA5	0.0000138	2.74	ILMN_1796409	C1QB	0.000027	2.61	ILMN_1711174	SPRR1B	0.0000539	2.27
ILMN_1801246	IFITM1	0.0000146	2.61	ILMN_2390919; ILMN_1774602	FBLN2	0.0000282	2.19	ILMN_1687501	MOXD1	0.0000604	2.14
ILMN_1677198	C1R	0.0000151	2.04	ILMN_1738546	KRT16P2	0.0000333	2.43	ILMN_2219002	KRT6A	0.0000783	5.93
ILMN_1736760	KRT16	0.0000164	3.00	ILMN_1655595	SERPINE2	0.0000396	3.16				

A list of significantly downregulated genes in ECM1-high bladder tumours.

Illumina Probe ID	Gene Symbol	p-value	Fold Change	ILMN_1775742; ILMN_1778338	RNF128	5.53E-11	-2.45	ILMN_1782015	FCRLB	1.14E-09	-3.20
ILMN_1653161	SNCG	3.91E-16	-4.97	ILMN_2355486	FAM3B	7.19E-11	-4.17	ILMN_1746801	CGN	1.29E-09	-2.76
ILMN_1777663	TOP2B	1.91E-14	-2.04	ILMN_1707088	DENND2D	7.93E-11	-2.14	ILMN_1685934	UPK2	1.52E-09	-4.30
ILMN_1764166	BCKDHB	2.55E-13	-2.03	ILMN_1693090	CROT	1.50E-10	-2.14	ILMN_1680110	ADIRF	1.71E-09	-3.14
ILMN_2137208	GOLT1A	2.96E-13	-3.20	ILMN_1708340	DAPK1	1.56E-10	-2.07	ILMN_1679051	PTPRR	1.78E-09	-2.79
ILMN_1658498	SLC44A3	3.51E-13	-2.51	ILMN_1759818; ILMN_2060115	SORL1	1.61E-10	-2.62	ILMN_1733042	BCAS1	2.49E-09	-3.24
ILMN_1713449	TBX3	1.14E-12	-2.80	ILMN_2091347; ILMN_1696432	IDH1	1.66E-10	-2.12	ILMN_1751346	ERBB3	6.08E-09	-2.27
ILMN_2286400; ILMN_1757660	CAPS	1.47E-12	-2.78	ILMN_1719753	VGLL1	2.01E-10	-3.15	ILMN_1786353	CNGA1	6.16E-09	-2.21
ILMN_1666536	VSIG2	2.15E-12	-6.18	ILMN_1796925	CXADR	2.33E-10	-2.44	ILMN_1713496; ILMN_2388701	ST3GAL5	6.18E-09	-2.45
ILMN_1761000	ACER2	3.60E-12	-2.79	ILMN_1795839	SCCPDH	2.62E-10	-2.17	ILMN_1787266	SPINK1	6.34E-09	-9.50
ILMN_1675656	PPFIBP2	4.23E-12	-2.69	ILMN_1714167; ILMN_2312194	CYB5A	4.42E-10	-2.30	ILMN_1766770	SNX31	6.39E-09	-3.58
ILMN_2413833	TOX3	5.15E-12	-2.76	ILMN_1755234	SSH3	6.16E-10	-2.29	ILMN_2163723	KRT7	1.08E-08	-3.96
ILMN_1800225; ILMN_2364384	PPARG	9.38E-12	-3.98	ILMN_1656111	MYLIP	7.59E-10	-2.12	ILMN_1769201	ELF3	1.13E-08	-2.48
ILMN_1782069; ILMN_2399174	TRAK1	1.48E-11	-2.56	ILMN_1758731	CYP2J2	8.88E-10	-3.24	ILMN_2325347	B3GALNT1	1.37E-08	-2.00
ILMN_1652797	FAM174B	2.95E-11	-3.22	ILMN_2173291; ILMN_1659215	CYP4B1	1.06E-09	-3.56	ILMN_1726809	BHLHE41	1.50E-08	-2.04

ILMN_1762262; ILMN_2337974	PKIA	1.61E-08	-2.06	ILMN_1796737	ZBTB7C	1.10E-07	-2.10	ILMN_1655637	UPK1A	1.33E-06	-4.84
ILMN_1751901	TMEM163	1.95E-08	-2.10	ILMN_1663640	MAOA	1.35E-07	-2.29	ILMN_2204545	ST3GAL4	1.39E-06	-2.03
ILMN_1730777	KRT19	2.83E-08	-2.85	ILMN_1801216	S100P	1.41E-07	-3.00	ILMN_1776519	RAP1GAP	1.60E-06	-2.21
ILMN_1745623	CRACR2B	3.37E-08	-2.09	ILMN_1771544	FMO9P	1.94E-07	-3.81	ILMN_1740917	SCNN1B	1.73E-06	-2.51
ILMN_1737089	CAPN5	3.49E-08	-2.42	ILMN_1730977;	SLC44A4	2.34E-07	-2.33	ILMN_1658384	CRTAC1	1.82E-06	-4.56
ILMN_1771538	PSCA	3.60E-08	-4.62	ILMN_1811272	HCAR1	3.11E-07	-2.26	ILMN_1673704	INA	1.93E-06	-2.67
ILMN_1656285	METTL7A	3.94E-08	-2.37	ILMN_1710962	TMEM97	3.13E-07	-2.56				
ILMN_1753584	KRT8	4.07E-08	-2.49	ILMN_1703279	CXorf57	3.62E-07	-2.27				
ILMN_1695110	BCAT2	5.08E-08	-2.03	ILMN_2392261;	FABP6	4.00E-07	-2.37				
ILMN_2384857; ILMN_1725726	DHRS2	5.19E-08	-4.97	ILMN_1791123	TMPRSS2	5.20E-07	-2.85				
ILMN_1694106	GPD1L	6.74E-08	-2.18	ILMN_2352090	GPRC5C	5.21E-07	-2.18				
ILMN_1775114; ILMN_2087941	ENTPD3	7.51E-08	-2.17	ILMN_1736670	PPP1R3C	5.41E-07	-2.58				
ILMN_2370882; ILMN_1705247	ACSL5	7.82E-08	-2.18	ILMN_1791826	RAB25	6.02E-07	-2.07				
ILMN_1777740	THEM6	9.21E-08	-2.04	ILMN_1805561	SLC14A1	7.62E-07	-2.93				
ILMN_1690040	TM7SF2	9.54E-08	-2.01	ILMN_2153837	SCNN1G	1.28E-06	-2.42				

Appendix F - ECM1 isoforms, mRNA and amino acid sequences

The human ECM1 gene encodes for four splice variants: ECM1a, ECM1b, ECM1c and ECM1d. PCR was performed using primers spanning alternatively spliced exons in order to identify which ECM1 isoforms were expressed in each of the ECM1-high cell lines, as well as in other bladder tumour-derived cell lines that do not fall into this subgroup and normal human urothelial cells (NHU-Pool) (section 4.2.3.1). In order to design primers to assess which isoforms of ECM1 were expressed intron and exon sequences for ECM1a, ECM1b, and ECM1c were obtained from the National Centre for Biotechnology Information nucleotide bank [183]. For the ECM1d isoform the mRNA sequence was obtained from [106]. The amino acid sequences of each isoform were obtained from the NCBI protein bank [325] in order to view differences between isoforms in at the protein level.

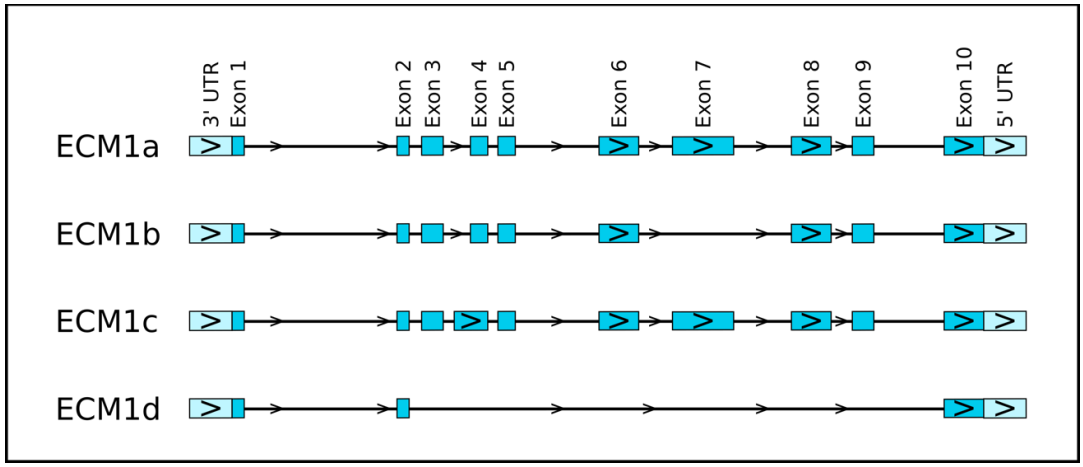

Schematic representation of the ECM1 mRNA isoforms.

A diagram representing the structures of the ECM1 isoforms a, b, c and d, illustrating the distribution of exons and the 3' and 5' untranslated regions (UTR). The figure has been created from information obtained from [183] and [106].

AGAGGAGGAGCAGCTGGGACTGAGTCATGGCAGGAAGCTGAGGAGGGCGGGAGATCA
CACCAGACAATTATAAAAGAAGAGCTGGTCCTGAAGCTCACAACCGTAACAGCCACCAGA
CAAGCTTCAGTGGCCGGCCCTTCACATCCAGACTTGCCTGAGAGGACCCACCTCTGAGTGT
CCAGTGGTCAGTTGCCCCAGGATGGGGACCACAGCCAGAGCAGCCTTGGTCTTGACCTAT
TTGGCTGTTGCTTCTGCTGCCTCTGAGGGAGGCTTCACGGCTACAGGACAGAGGCAGCTG
AGGCCAGAGCACTTTCAAGAAGTTGGCTACGCAGCTCCCCCCTCCCCACCCCTATCCCGAA
GCCTCCCCATGGATCACCCTGACTCCTCTCAGCATGGCCCTCCCTTTGAGGGACAGAGTCA
AGTGCAGCCCCCTCCCTCTCAGGAGGCCACCCCTCTCCAACAGGAAAAGCTGCTACCTGCC
CAACTCCCTGCTGAAAAGGAAGTGGGTCCCCCTCTCCCTCAGGAAGCTGTCCCCCTCCAAA
AAGAGCTGCCCTCTCTCCAGCACCCCAATGAACAGAAGGAAGGAACGCCAGCTCCATTTG
GGGACCAGAGCCATCCAGAACCTGAGTCCTGGAATGCAGCCCAGCACTGCCAACAGGAC
CGGTCCCAAGGGGGCTGGGGCCACCGGCTGGATGGCTTCCCCCCTGGGCGGCCTTCTCCA
GACAATCTGAACCAAATCTGCCTTCCTAACCGTCAGCATGTGGTATATGGTCCCTGGAACC
TACCACAGTCCAGCTACTCCCACCTCACTCGCCAGGGTGAGACCCTCAATTTCCTGGAGAT
TGGATATTCCCGCTGCTGCCACTGCCGCAGCCACACAAACCGCCTAGAGTGTGCCAAACTT
GTGTGGGAGGAAGCAATGAGCCGATTCTGTGAGGCCGAGTTCTCGGTCAAGACCCGACC
CCACTGGTGCTGCACGCGGCAGGGGGAGGCTCGGTTCTCCTGCTTCCAGGAGGAAGCTC
CCCAGCCACACTACCAGCTCCGGGCCTGCCCCAGCCATCAGCCTGATATTTCCTCGGGTCT
TGAGCTGCCTTTCCCTCCTGGGGTGCCCACATTGGACAATATCAAGAACATCTGCCACCTG
AGGCGCTTCCGCTCTGTGCCACGCAACCTGCCAGCTACTGACCCCCTACAAAGGGAGCTG
CTGGCACTGATCCAGCTGGAGAGGGAGTTCCAGCGCTGCTGCCGCCAGGGGAACAATCA
CACCTGTACATGGAAGGCCTGGGAGGATACCCTTGACAAATACTGTGACCGGGAGTATGC
TGTGAAGACCCACCACCACTTGTGTTGCCGCCACCCTCCCAGCCCTACTCGGGATGAGTGC
TTTGCCCGTCGGGCTCCTTACCCCAACTATGACCGGGACATCTTGACCATTGACATCGGTC
GAGTCACCCCCAACCTCATGGGCCACCTCTGTGGAAACCAAAGAGTTCTCACCAAGCATA
AACATATTCCTGGGCTGATCCACAACATGACTGCCCGCTGCTGTGACCTGCCATTTCCAGA
ACAGGCCTGCTGTGCAGAGGAGGAGAAATTAACCTTCATCAATGATCTGTGTGGTCCCCG
ACGTAACATCTGGCGAGACCCTGCCCTCTGCTGTTACCTGAGTCCTGGGGATGAACAGGT
CAACTGCTTCAACATCAATTATCTGAGGAACGTGGCTCTAGTGTCTGGAGACACTGAGAA
CGCCAAGGGCCAGGGGGAGCAGGGCTCAACTGGAGGAACAAATATCAGCTCCACCTCTG
AGCCCAAGGAAGAATGAGTCACCCCAGAGCCCTAGAGGGTCAGATGGGGGGAACCCCAC
CCTGCCCCACCCATCTGAACACTCATTACACTAAACACCTCTTGGATTTGGTGTCCTCATTG
TCTATCTAATGTCTCACCCGCAGTGTTTTAAGTGGATCTTGGTGCCCTGGCCCAGGAGGGC
ACTGGCGTTTTCAGACACACCACAGACAAACACACCCTCCTAAGCCTGCTTGTATTTCCTTC
AGTGCCTGGCCCCTGAGGCCCACGGCCCTGCCCCCTTCACTGAGCAGATGTTCACAGGCT
GTGGGATGCGACCATAACTAAACAGCTTGACGTCAAAAAAAAAAAAAAAAAA

The 5’ -> 3’ mRNA sequence (NM_004425.3) of the ECM1a isoform obtained from the NCBI nucleotide database [183].

AGAGGAGGAGCAGCTGGGACTGAGTCATGGCAGGAAGCTGAGGAGGGCGGGAGATCA
CACCAGACAATTATAAAAGAAGAGCTGGTCCTGAAGCTCACAACCGTAACAGCCACCAGA
CAAGCTTCAGTGGCCGGCCCTTCACATCCAGACTTGCCTGAGAGGACCCACCTCTGAGTGT
CCAGTGGTCAGTTGCCCCAGGATGGGGACCACAGCCAGAGCAGCCTTGGTCTTGACCTAT
TTGGCTGTTGCTTCTGCTGCCTCTGAGGGAGGCTTCACGGCTACAGGACAGAGGCAGCTG
AGGCCAGAGCACTTTCAAGAAGTTGGCTACGCAGCTCCCCCCTCCCCACCCCTATCCCGAA
GCCTCCCCATGGATCACCCTGACTCCTCTCAGCATGGCCCTCCCTTTGAGGGACAGAGTCA
AGTGCAGCCCCCTCCCTCTCAGGAGGCCACCCCTCTCCAACAGGAAAAGCTGCTACCTGCC
CAACTCCCTGCTGAAAAGGAAGTGGGTCCCCCTCTCCCTCAGGAAGCTGTCCCCCTCCAAA
AAGAGCTGCCCTCTCTCCAGCACCCCAATGAACAGAAGGAAGGAACGCCAGCTCCATTTG
GGGACCAGAGCCATCCAGAACCTGAGTCCTGGAATGCAGCCCAGCACTGCCAACAGGAC
CGGTCCCAAGGGGGCTGGGGCCACCGGCTGGATGGCTTCCCCCCTGGGCGGCCTTCTCCA
GACAATCTGAACCAAATCTGCCTTCCTAACCGTCAGCATGTGGTATATGGTCCCTGGAACC
TACCACAGTCCAGCTACTCCCACCTCACTCGCCAGGGTGAGACCCTCAATTTCCTGGAGAT
TGGATATTCCCGCTGCTGCCACTGCCGCAGCCACACAAACCGCCTAGAGTGTGCCAAACTT
GTGTGGGAGGATACCCTTGACAAATACTGTGACCGGGAGTATGCTGTGAAGACCCACCAC
CACTTGTGTTGCCGCCACCCTCCCAGCCCTACTCGGGATGAGTGCTTTGCCCGTCGGGCTC
CTTACCCCAACTATGACCGGGACATCTTGACCATTGACATCGGTCGAGTCACCCCCAACCT
CATGGGCCACCTCTGTGGAAACCAAAGAGTTCTCACCAAGCATAAACATATTCCTGGGCT
GATCCACAACATGACTGCCCGCTGCTGTGACCTGCCATTTCCAGAACAGGCCTGCTGTGCA
GAGGAGGAGAAATTAACCTTCATCAATGATCTGTGTGGTCCCCGACGTAACATCTGGCGA
GACCCTGCCCTCTGCTGTTACCTGAGTCCTGGGGATGAACAGGTCAACTGCTTCAACATCA
ATTATCTGAGGAACGTGGCTCTAGTGTCTGGAGACACTGAGAACGCCAAGGGCCAGGGG
GAGCAGGGCTCAACTGGAGGAACAAATATCAGCTCCACCTCTGAGCCCAAGGAAGAATG
AGTCACCCCAGAGCCCTAGAGGGTCAGATGGGGGGAACCCCACCCTGCCCCACCCATCTG
AACACTCATTACACTAAACACCTCTTGGATTTGGTGTCCTCATTGTCTATCTAATGTCTCAC
CCGCAGTGTTTTAAGTGGATCTTGGTGCCCTGGCCCAGGAGGGCACTGGCGTTTTCAGAC
ACACCACAGACAAACACACCCTCCTAAGCCTGCTTGTATTTCCTTCAGTGCCTGGCCCCTGA
GGCCCACGGCCCTGCCCCCTTCACTGAGCAGATGTTCACAGGCTGTGGGATGCGACCATA
ACTAAACAGCTTGACGTCAAAAAAAAAAAAAAAAA

The 5’ -> 3’ mRNA sequence (NM_022664.2) of the ECM1b isoform obtained from the NCBI nucleotide database [183].

AATTATAAAAGAAGAGCTGGTCCTGAAGCTCACAACCGTAACAGCCACCAGACAAGCTTC
AGTGGCCGGCCCTTCACATCCAGACTTGCCTGAGAGGACCCACCTCTGAGTGTCCAGTGG
TCAGTTGCCCCAGGATGGGGACCACAGCCAGAGCAGCCTTGGTCTTGACCTATTTGGCTG
TTGCTTCTGCTGCCTCTGAGGGAGGCTTCACGGCTACAGGACAGAGGCAGCTGAGGCCA
GAGCACTTTCAAGAGGTTGGCTACGCAGCTCCCCCCTCCCCACCCCTATCCCGAAGCCTCC
CCATGGATCACCCTGACTCCTCTCAGCATGGCCCTCCCTTTGAGGGACAGAGTGGAAAGG
AGGGAAGAGGCCCTCGCCCCCACTCCCAGCCCTGGCTAGGAGAAAGGGTGGGCTGCTCA
CACATTCCCCCTTCTATAGTGCAGCCCCCTCCCTCTCAGGAGGCCACCCCTCTCCAACAGGA
AAAGCTGCTACCTGCCCAACTCCCTGCTGAAAAGGAAGTGGGTCCCCCTCTCCCTCAGGAA
GCTGTCCCCCTCCAAAAAGAGCTGCCCTCTCTCCAGCACCCCAATGAACAGAAGGAAGGA
ACGCCAGCTCCATTTGGGGACCAGAGCCATCCAGAACCTGAGTCCTGGAATGCAGCCCAG
CACTGCCAACAGGACCGGTCCCAAGGGGGCTGGGGCCACCGGCTGGATGGCTTCCCCCC
TGGGCGGCCTTCTCCAGACAATCTGAACCAAATCTGCCTTCCTAACCGTCAGCATGTGGTA
TATGGTCCCTGGAACCTACCACAGTCCAGCTACTCCCACCTCACTCGCCAGGGTGAGACCC
TCAATTTCCTGGAGATTGGATATTCCCGCTGCTGCCACTGCCGCAGCCACACAAACCGCCT
AGAGTGTGCCAAACTTGTGTGGGAGGAAGCAATGAGCCGATTCTGTGAGGCCGAGTTCT
CGGTCAAGACCCGACCCCACTGGTGCTGCACGCGGCAGGGGGAGGCTCGGTTCTCCTGCT
TCCAGGAGGAAGCTCCCCAGCCACACTACCAGCTCCGGGCCTGCCCCAGCCATCAGCCTG
ATATTTCCTCGGGTCTTGAGCTGCCTTTCCCTCCTGGGGTGCCCACATTGGACAATATCAA
GAACATCTGCCACCTGAGGCGCTTCCGCTCTGTGCCACGCAACCTGCCAGCTACTGACCCC
CTACAAAGGGAGCTGCTGGCACTGATCCAGCTGGAGAGGGAGTTCCAGCGCTGCTGCCG
CCAGGGGAACAATCACACCTGTACATGGAAGGCCTGGGAGGATACCCTTGACAAATACTG
TGACCGGGAGTATGCTGTGAAGACCCACCACCACTTGTGTTGCCGCCACCCTCCCAGCCCT
ACTCGGGATGAGTGCTTTGCCCGTCGGGCTCCTTACCCCAACTATGACCGGGACATCTTGA
CCATTGACATCGGTCGAGTCACCCCCAACCTCATGGGCCACCTCTGTGGAAACCAAAGAG
TTCTCACCAAGCATAAACATATTCCTGGGCTGATCCACAACATGACTGCCCGCTGCTGTGA
CCTGCCATTTCCAGAACAGGCCTGCTGTGCAGAGGAGGAGAAATTAACCTTCATCAATGA
TCTGTGTGGTCCCCGACGTAACATCTGGCGAGACCCTGCCCTCTGCTGTTACCTGAGTCCT
GGGGATGAACAGGTCAACTGCTTCAACATCAATTATCTGAGGAACGTGGCTCTAGTGTCT
GGAGACACTGAGAACGCCAAGGGCCAGGGGGAGCAGGGCTCAACTGGAGGAACAAATA
TCAGCTCCACCTCTGAGCCCAAGGAAGAATGAGTCACCCCAGAGCCTTAGAGGGTCAGAT
GGGGGGAACCCCACCCTGCCCCACCCATCTGAACACTCATTACACTAAACACCTCTTGG

The 5’ -> 3’ mRNA sequence (NM_001202858.1) of the ECM1c isoform obtained from the NCBI nucleotide database [183].

ACAACCGTAACAGCCACCAGACAAGCTTCAGTGGCCGGCCCTTCACATCCAGACTTGCCTG
AGAGGACCCACCTCTGAGTGTCCAGTGGTCAGTTGCCCCAGGATGGGGACCACAGCCAG
AGCAGCCTTGGTCTTGACCTATTTGGCTGTTGCTTCTGCTGCCTCTGAGGGAGCCTCCCCA
TCCCTTGCTGAAGTCCAGGGAAGGCCCTCCCAGTGGCCCCTGACTTGCCCTTCTTCCCTCC
AGGCTTCACGGCTACAGGACAGAGGCAGCTGAGGCCAGAGCACTTTCAAGAAG

The 5'-3' mRNA sequence of the ECM1d isoform was obtained from [106].

ECM1a
MGTTARAALVLTYLAVASAASEGGFTATGQRQLRPEHFQEVGYAAPPS PPLSRSLPMDHPDSSQHGPPFEGQSQVQPPPSQEATPLQQEKLLPAQL PAEKEVGPPLPQEAVPLQKELPSLQHPNEQKEGTPAPFGDQSHPEPES WNAAQHCQQDRSQGGWGHRLDGFPPGRPSPDNLNQICLPNRQHVVY GPWNLPQSSYSHLTRQGETLNFLEIGYSRCCHCRSHTNRLECAKLVWE EAMSRFCEAEFSVKTRPHWCCTRQGEARFSCFQEEAPQPHYQLRACP SHQPDISSGLELPFPPGVPTLDNIKNICHLRRFRSVPRNLPATDPLQRELL ALIQLEREFQRCCRQGNNHTCTWKAWEDTLDKYCDREYAVKTHHHLCC RHPPSPTRDECFARRAPYPNYDRDILTIDIGRVTPNLMGHLCGNQRVLT KHKHIPGLIHNMTARCCDLPFPEQACCAEEEKLTFINDLCGPRRNIWRDP ALCCYLSPGDEQVNCFNINYLRNVALVSGDTENAKGQGEQGSTGGTNIS STSEPKEE
ECM1b
MGTTARAALVLTYLAVASAASEGGFTATGQRQLRPEHFQEVGYAAPPS PPLSRSLPMDHPDSSQHGPPFEGQSQVQPPPSQEATPLQQEKLLPAQL PAEKEVGPPLPQEAVPLQKELPSLQHPNEQKEGTPAPFGDQSHPEPES WNAAQHCQQDRSQGGWGHRLDGFPPGRPSPDNLNQICLPNRQHVVY GPWNLPQSSYSHLTRQGETLNFLEIGYSRCCHCRSHTNRLECAKLVWE DTLDKYCDREYAVKTHHHLCCRHPPSPTRDECFARRAPYPNYDRDILTI DIGRVTPNLMGHLCGNQRVLTKHKHIPGLIHNMTARCCDLPFPEQACCA EEEKLTFINDLCGPRRNIWRDPALCCYLSPGDEQVNCFNINYLRNVALVS GDTENAKGQGEQGSTGGTNISSTSEPKEE
ECM1c
MGTTARAALVLTYLAVASAASEGGFTATGQRQLRPEHFQEVGYAAPPS PPLSRSLPMDHPDSSQHGPPFEGQSGKEGRGPRPHSQPWLGERVGC SHIPPSIVQPPPSQEATPLQQEKLLPAQLPAEKEVGPPLPQEAVPLQKEL PSLQHPNEQKEGTPAPFGDQSHPEPESWNAAQHCQQDRSQGGWGHR LDGFPPGRPSPDNLNQICLPNRQHVVYGPWNLPQSSYSHLTRQGETLN FLEIGYSRCCHCRSHTNRLECAKLVWEEAMSRFCEAEFSVKTRPHWCC TRQGEARFSCFQEEAPQPHYQLRACPSHQPDISSGLELPFPPGVPTLDN IKNICHLRRFRSVPRNLPATDPLQRELLALIQLEREFQRCCRQGNNHTCT WKAWEDTLDKYCDREYAVKTHHHLCCRHPPSPTRDECFARRAPYPNY DRDILTIDIGRVTPNLMGHLCGNQRVLTKHKHIPGLIHNMTARCCDLPFPE QACCAEEEKLTFINDLCGPRRNIWRDPALCCYLSPGDEQVNCFNINYLR NVALVSGDTENAKGQGEQGSTGGTNISSTSEPKEE
ECM1d
MGTTARAALVLTYLAVASAASEGASPSLAEVQGRPSQWPLTCPSSLQA SRLQDRGS

The amino acid sequences of all four ECM1 isoforms obtained from NCBI protein bank and Horev *et al.* [106, 325].

Appendix G - Confirmation of ECM1 knockdown by western blot analysis

Four cell lines (HT-1376, LUCC4, HT-1197 and 647V) were stably transfected with shRNAs targeting ECM1 (KD1 and KD2) or scramble and non-hairpin (NHP) controls. To assess the efficiency of knockdown protein lysates were harvested from knockdown and control cell lines and ECM1 protein levels were evaluated by western blot analysis (section 4.2.3.3). Western blot analysis of ECM1 levels was conducted over several subsequent passages and prior to any further experiments to ensure continued knockdown of ECM1. For HT-1376, HT-1197, and LUCC4 ECM1 could no longer be detected at the protein level between 1 and 10 passages. For 647V also demonstrated reduced levels of ECM1 in knockdown compared to parental cells for all 10 passages, however reduced ECM1 was also seen in the control samples.

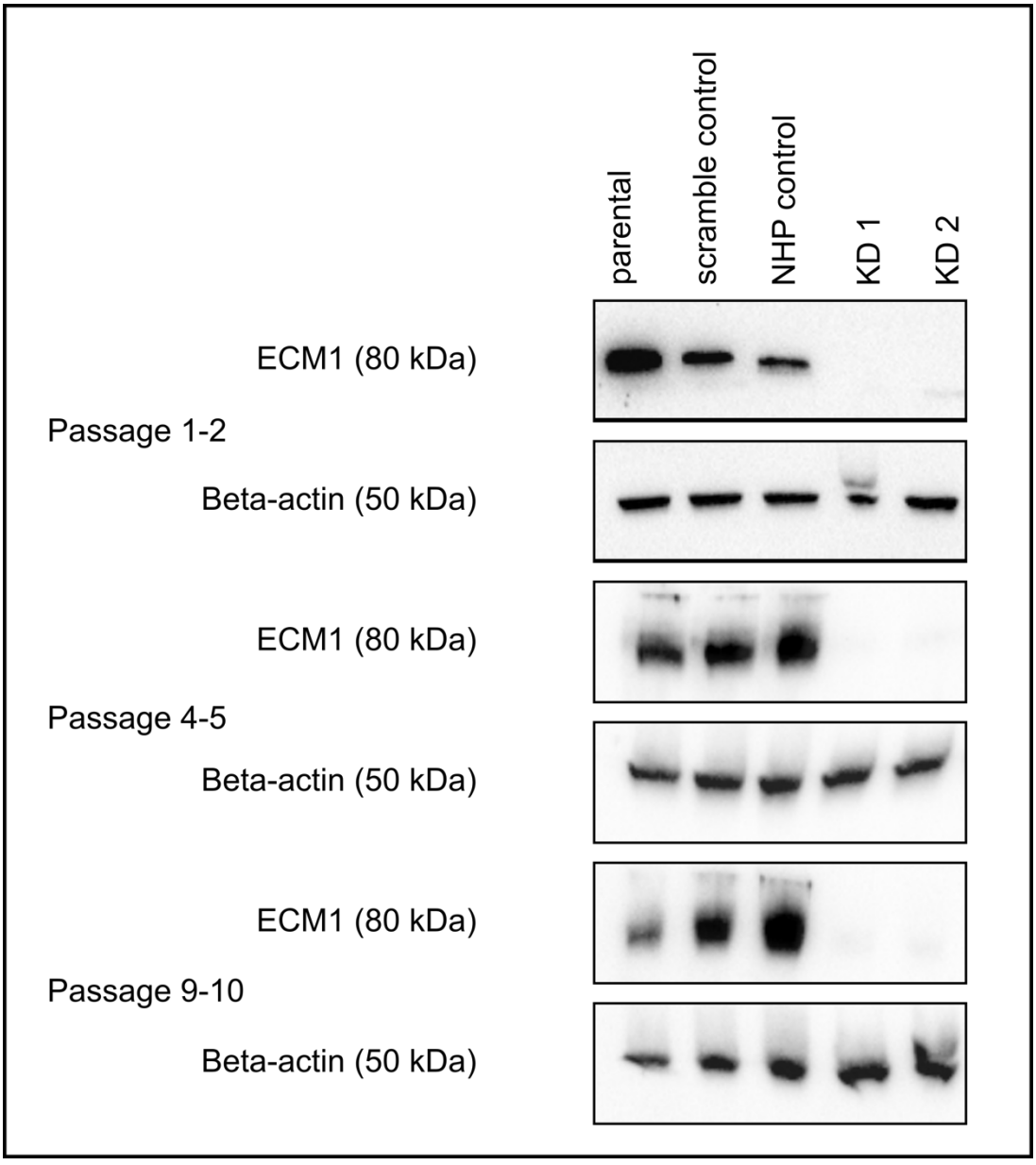

Western blot confirmation of knockdown of ECM1 at the protein level in HT-1376 over 10 passages.

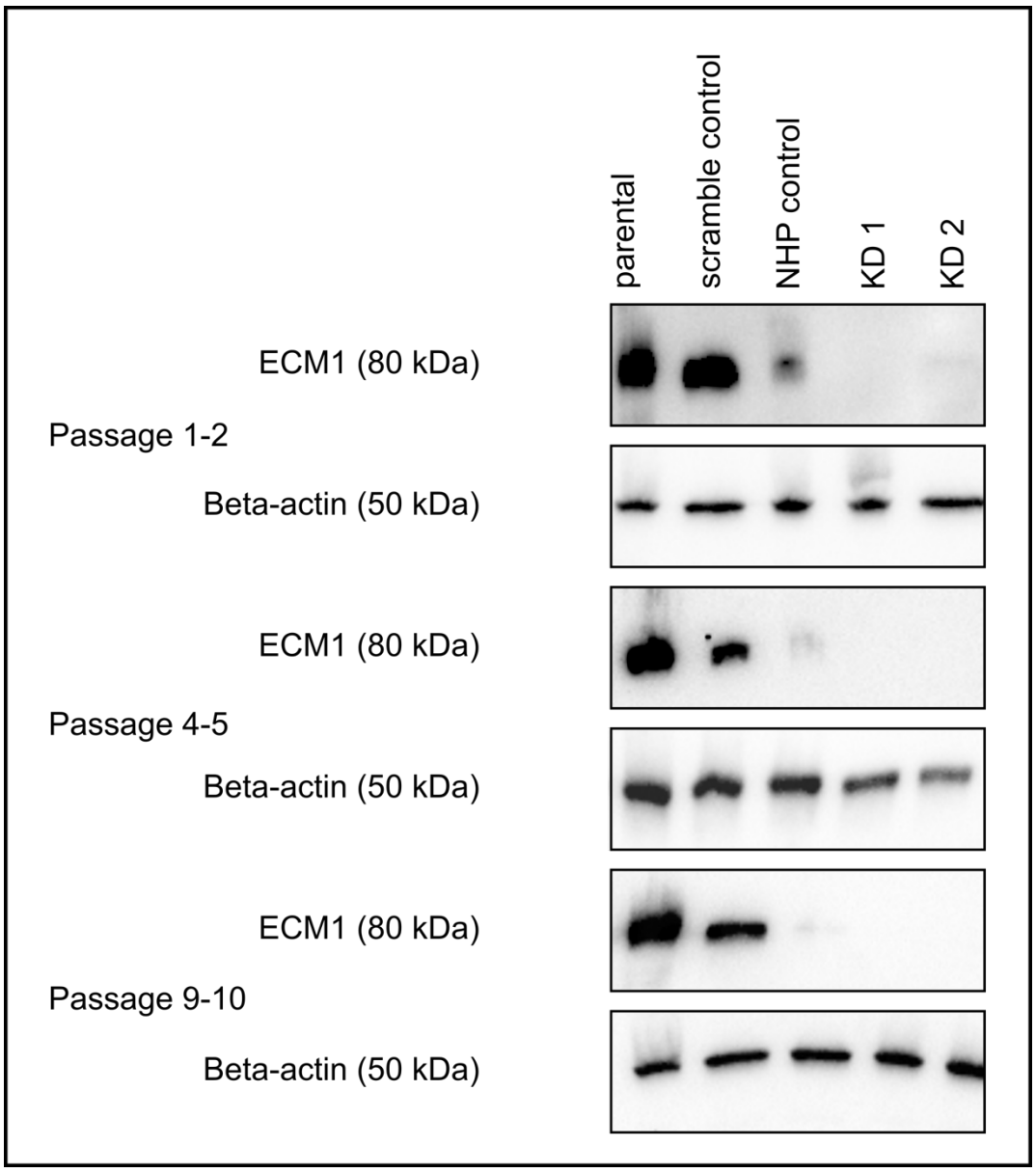

Western blot confirmation of knockdown of ECM1 at the protein level in LUCC4 over 10 passages.

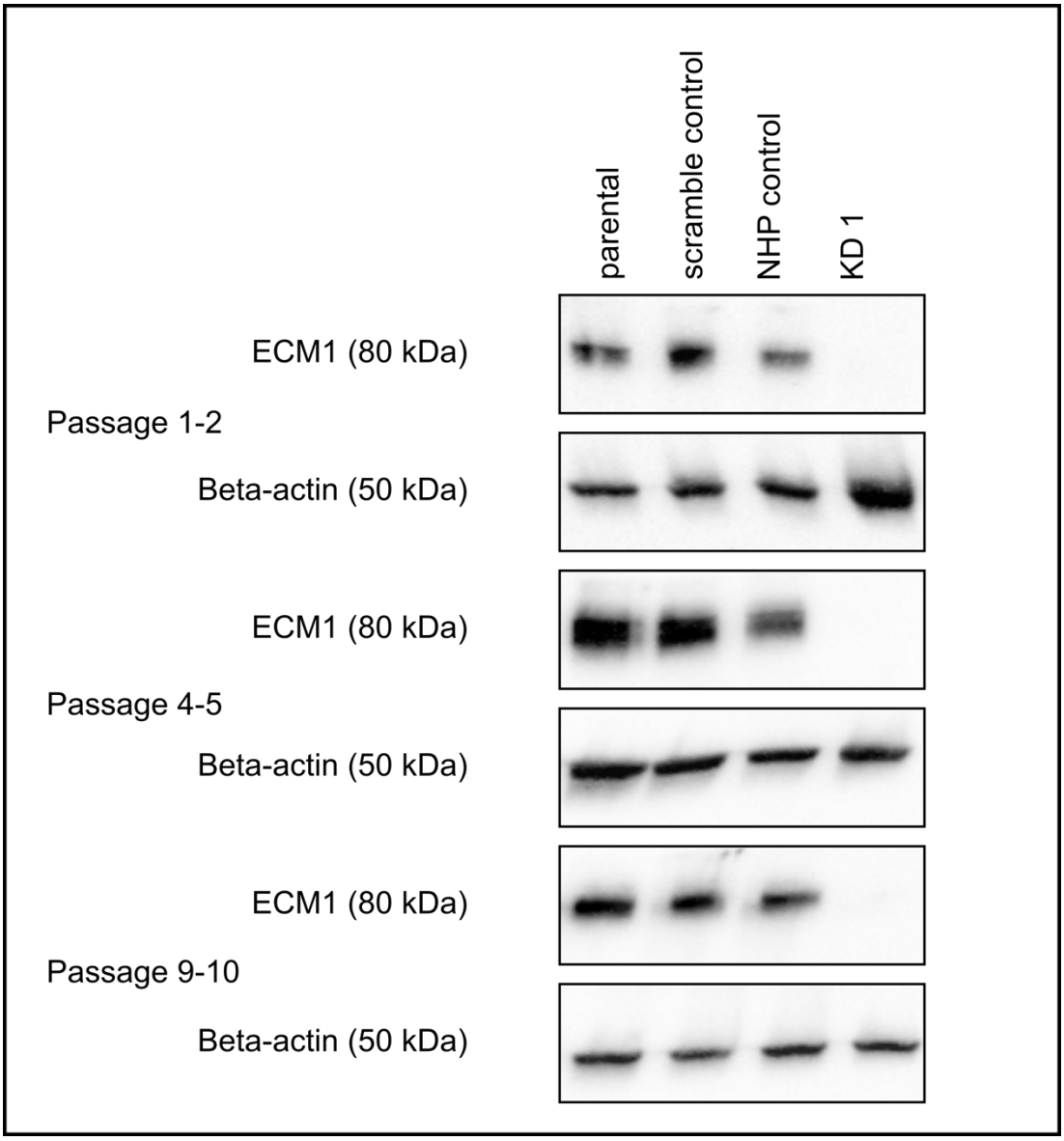

Western blot confirmation of knockdown of ECM1 at the protein level in HT-1197 over 10 passages.

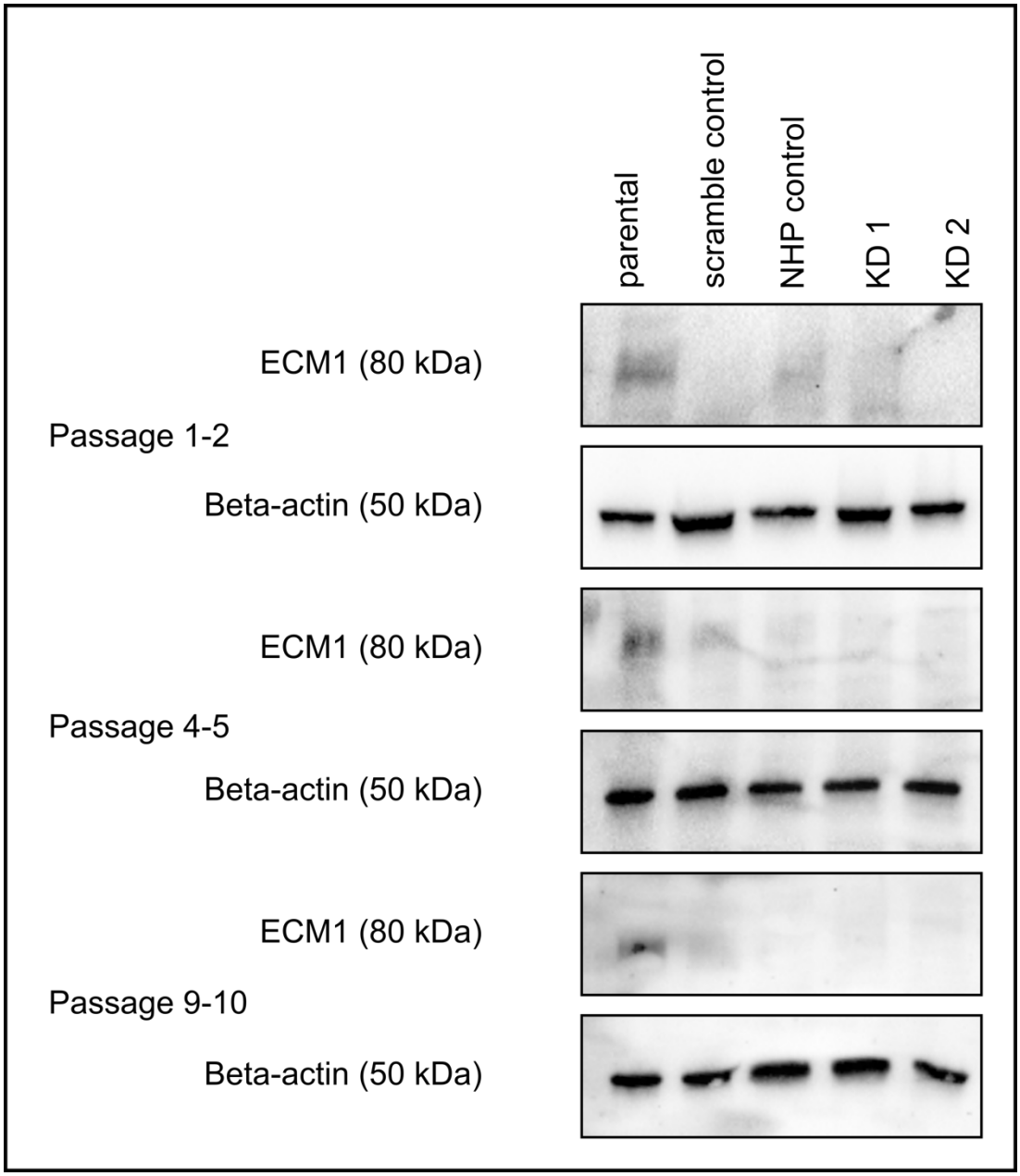

Western blot confirmation of knockdown of ECM1 at the protein level in 647V over 10 passages.

Appendix H - Wound healing assay with recombinant ECM1

In Chapter 4, wound healing assays were conducted using the HT-1376 KD1 cell line in combination with treatment with recombinant ECM1 at concentrations ranging from 100 ng/ml to 1 μg/ml. No statistical significance was observed between knockdown cells treated at any concentrations of recombinant ECM1, and the untreated knockdown at 24 h or 48 h. However, at the highest concentration of recombinant ECM1 treatment (1 μg/ml) resulted in a slight increase in wound healing although this was not statistically significantly different as compared to the scramble control. Treatment with a higher concentration (2 μg/ml) of recombinant ECM1 was also assessed in wound healing assays. **A)** Images were captured at 50x magnification at 0, 24 and 48 h for the HT-1376 scramble control cell line and ECM1 knockdown cell lines treated with two different concentrations of recombinant ECM1 (1 μg/ml and 2 μg/ml). Three replicate wells were treated at each concentration, and three images were taken per well for analysis. **B)** Statistical analysis of the percentage migration after 24 h was conducted using ordinary one-way ANOVA and Tukey's multiple comparisons test. This showed the knockdown cells to have a statistically significant slower wound healing rate after 24 h than the scramble control cells, as did the knockdown cells treated with 1 μg/ml and 2 μg/ml recombinant ECM1 ($p = 0.035$, 0.034, and 0.022 respectively). **C)** Knockdown cells also had a statistically significant slower wound healing rate than the scramble control after 48 h, as did the same cells treated with 1 μg/ml and 2 μg/ml recombinant ECM1 ($p < 0.0001$, < 0.0001, $= 0.0004$ respectively). (Key: * p = 0.05-0.01; ** p = 0.009-0.001; *** p = 0.0009-0.0001; **** p = <0.0001).

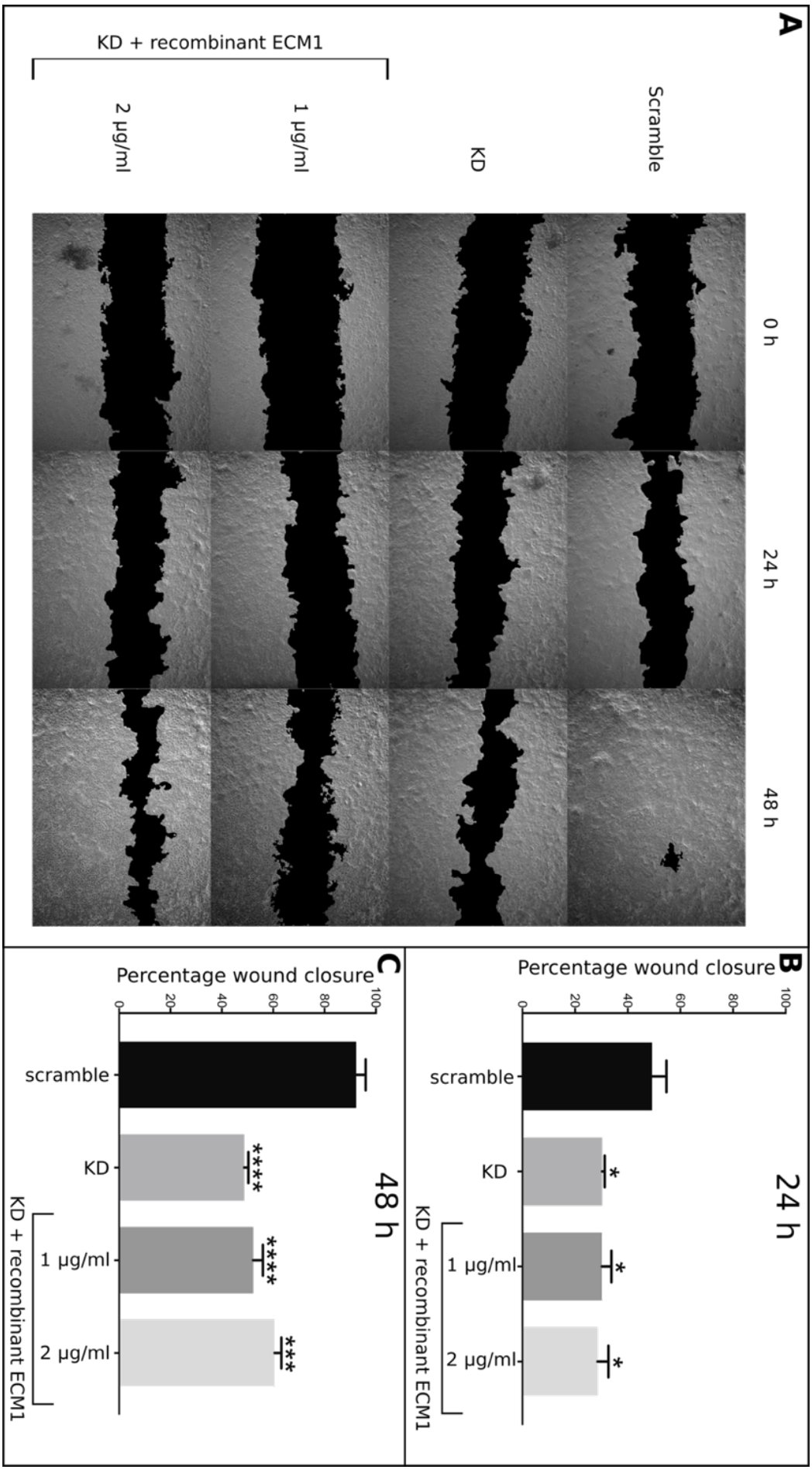
A
Scramble
KD
KD + recombinant ECM1
1 µg/ml
2 µg/ml
0 h
24 h
48 h
B
24 h
Percentage wound closure
scramble
KD
1 µg/ml
2 µg/ml
KD + recombinant ECM1
C
48 h
Percentage wound closure
scramble
KD
1 µg/ml
2 µg/ml
KD + recombinant ECM1

Appendix I - Co-immunoprecipitation of ECM1 and EGFR full blots

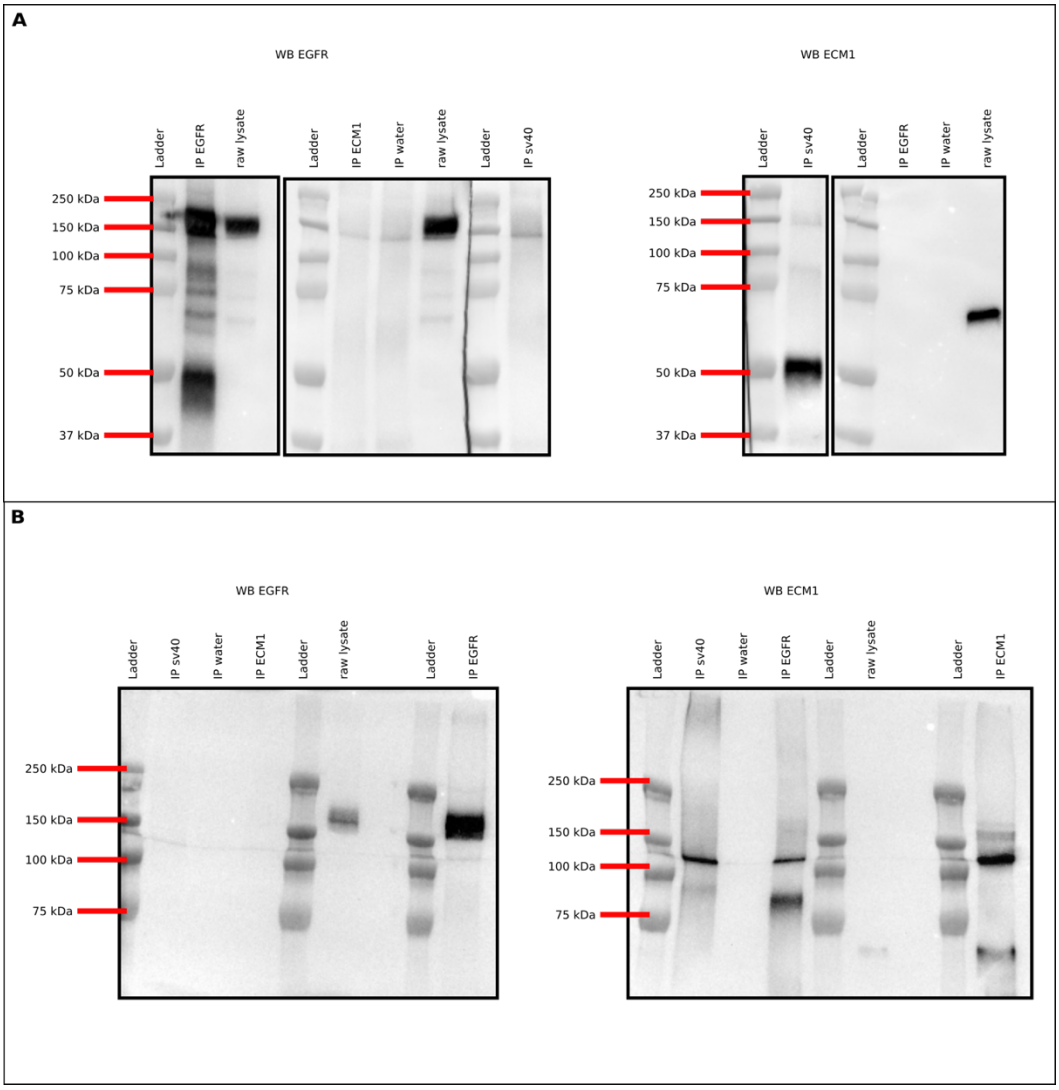

Full western blot images showing results from the co-immunoprecipitation of ECM1 and EGFR in HT-1376 and 647V cell lysates.

Total protein lysates harvested from the cell lines **A)** HT-1376 and **B)** 647V cell lines were used in co-immunoprecipitation with either anti-ECM1 or anti-EGFR antibodies and immunoprecipitation products were analysed by western blotting. Negative controls of water in place of antibody, or an Sv-40 T Ag antibody against a protein that does not interact with either ECM1 or EGFR were used. Blots were analysed using the ChemiDoc MP system.

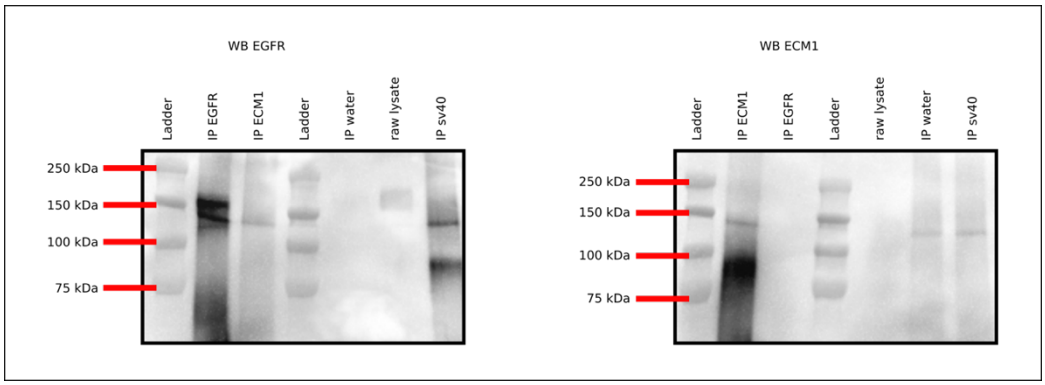

Full western blot images showing results from the co-immunoprecipitation of ECM1 and EGFR in HT-1376 cell lysates following pre-treatment with a crosslinker.

HT-1376 cells were incubated with the crosslinker DTSSP before lysis. Total protein lysates were used in co-immunoprecipitation with either anti-ECM1 or anti-EGFR antibodies and immunoprecipitation products were analysed by western blotting. Negative controls of water in place of antibody, or an Sv-40 T Ag antibody against a protein that does not interact with either ECM1 or EGFR were used. Blots were analysed using the ChemiDoc MP system.

Appendix J - Microarray analysis of HT1376 knockdown and scramble control lines

J.1 Analysis of RNA concentration and quality

The RNA ScreenTape System (Agilent) uses electrophoresis to separate RNA samples on microfabricated chips. Laser induced florescent detection is then used to detect separated RNA samples, and Bioanalyzer software (Agilent) is used to display details such as concentration in a sample information table. The software also generates an electropherogram for the visual assessment of the quality of the RNA sample. Using an algorithm developed from the assessment of over 1300 human, mouse, and rat RNA samples, the software also determines an RNA integrity number (RIN) to each sample which is a quantitative measurement of the quality of the RNA samples. This is based on a numbering system from 1- 10 with 10 being the most intact, and 1 being a highly degraded sample.

Well	RIN[e]	28S/18S (Height)	28S/18S (Area)	Conc. [ng/µl]	Sample Description	Alert	Observations	Total RNA Area	rRNA Area
A1	-	-	-	216	Ladder		Ladder	-	-
B1	9.1	2.1	2.8	213	HT1376 scramble 1			8.60	3.08
C1	9.5	2.0	3.1	124	HT1376 scramble 2			4.99	1.63
D1	9.5	2.0	2.8	201	HT1376 scramble 3			8.10	2.85
E1	9.8	1.9	3.0	189	HT1376 KD 1			7.65	2.79
F1	9.7	2.0	3.0	265	HT1376 KD 2			10.69	3.90
G1	10.0	2.0	3.1	183	HT1376 KD 3			7.39	2.73
H1	9.9	2.1	3.0	287	HT-1376 parental 1			11.60	4.34
A2	9.9	1.9	3.1	182	HT-1376 parental 2			7.33	2.72
B2	9.6	2.2	3.3	338	HT-1376 parental 3			13.66	5.09

A representative 2200 TapeStation (Agilent) sample information table.

The integrity of RNA lysates from HT-1376 scramble control, ECM1 KD, and parental cell lines was assessed and a sample information table was generated with the Agilent 2200 TapeStation system.

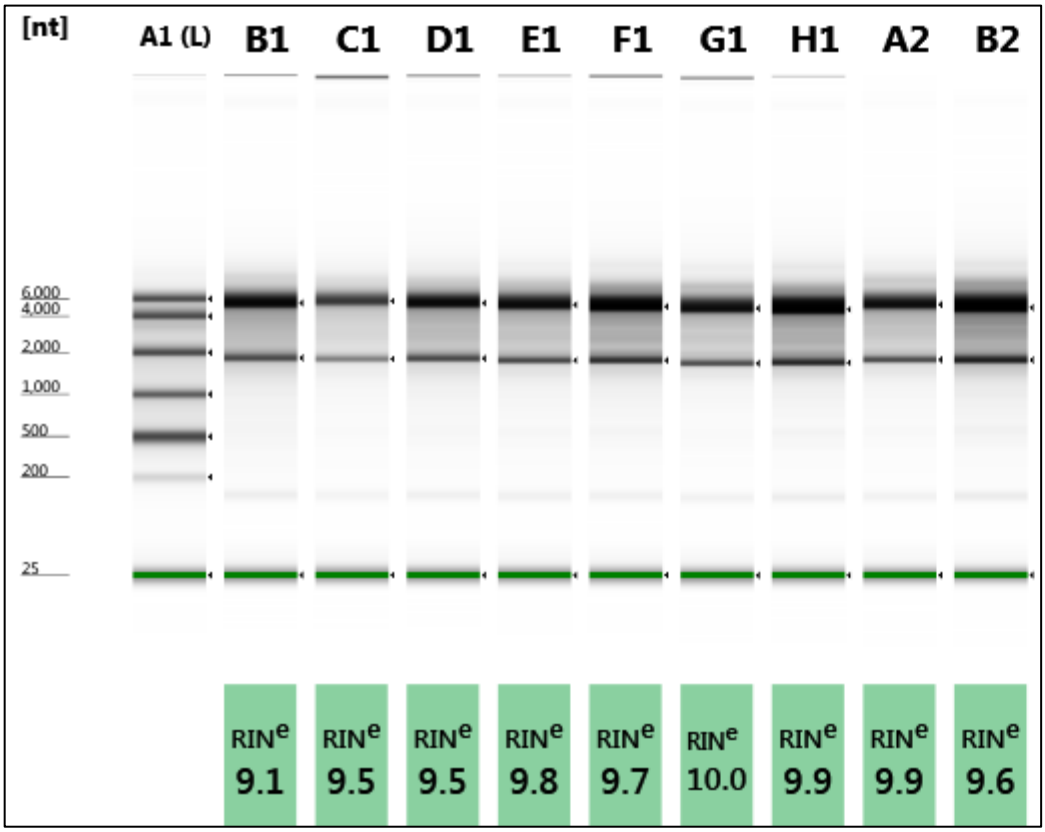

A representative 2200 TapeStation (Agilent) electropherogram.

The integrity of RNA lysates from HT-1376 scramble control, ECM1 KD, and parental cell lines was assessed and an electropherogram was generated with the Agilent 2200 TapeStation system. The automatically determined RIN values are also shown for each sample. Sample order is as indicated in the sample information Table (section J.1).

J.1.1 Quality control and normalisation of microarray transcriptome expression data

The following figures show the quality control data for the assessment of the raw data (CEL files) obtained from Affymetrix GeneChip HTA 2.0 transcriptome analysis of the HT-1376 ECM1 knockdown (KD) and scramble control cell lines. CEL files were imported into Affymetrix Expression Console™ version 1.4 in order to assess the quality of the RNA microarray data. Data was then normalised to enable comparison of gene expression across the samples. Three biological replicates were assessed for the knockdown and the control cell lines.

The area under the receiver operator curve was greater than or equal to 0.98 for all microarray samples, indicating a low false positive rate and high true positive rate for the microarray positive and negative controls.

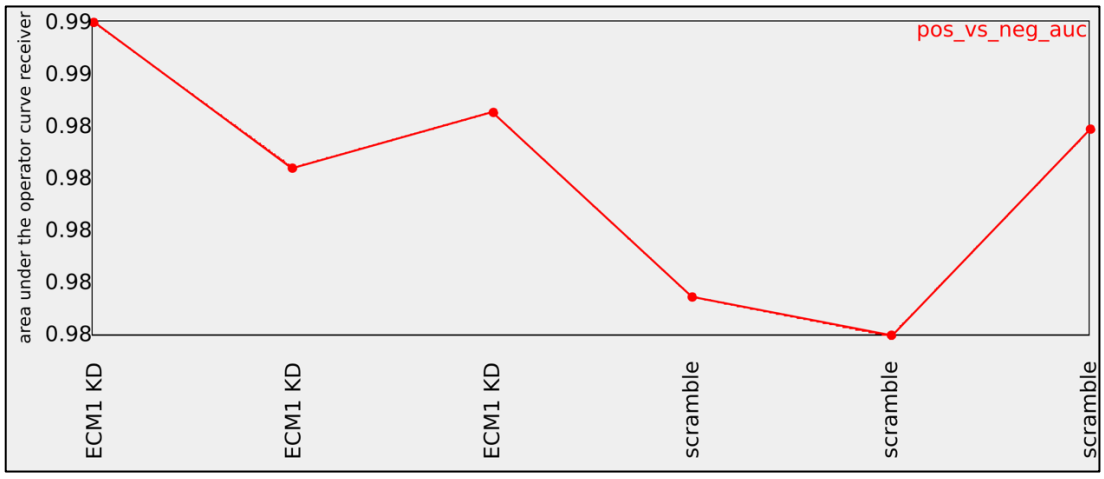

The area under the receiver operator curve.

The receiver operator curve plots the true positive rate against the false positive rate. Analysis of the area under the curve (AUC) was conducted in Affymetrix Expression Console™. The AUC gives an indication of how successfully the positive and negative microarray controls were identified, the closer the AUC is to 1, the more accurate the identification of the controls. For our samples the AUC was greater than or equal to 0.98 indicating a low false positive rate and high true positive rate.

The Eukaryotic hybridisation controls (spike controls) were detected with signal values from lowest to highest: bioB, bioC, bioD and cre. This matches the concentrations at which these controls were spiked into the hybridisation cocktail. Affymetrix state that bioC, bioD and cre should be present in every array sample and bioB should be present in a minimum of 70% of array samples. As the eukaryotic hybridisation controls are present in all our samples, this indicates successful hybridisation.

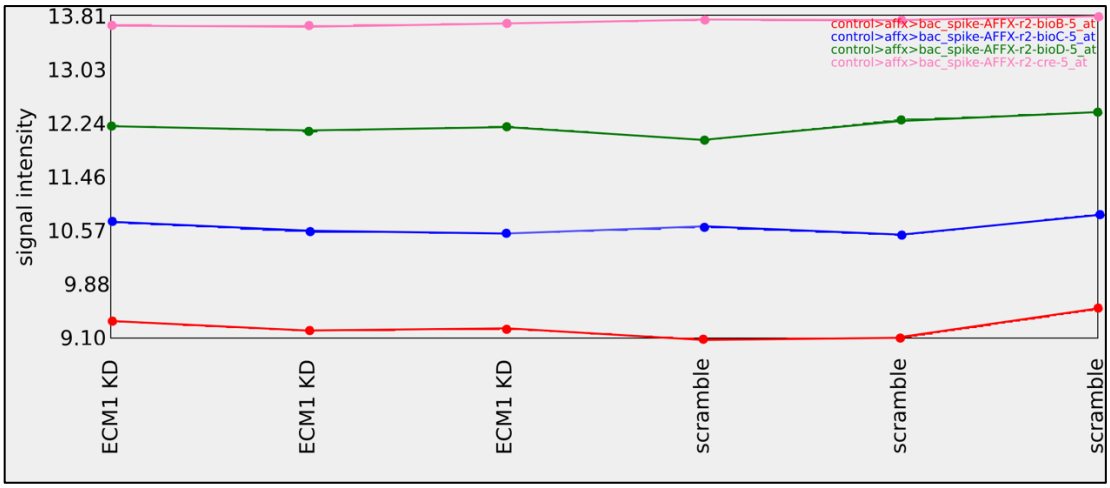

Eukaryotic hybridisation controls (spike controls).

Analysis of the spike controls was conducted in Affymetrix Expression Console™. The transcripts 'bioB', 'bioC' and 'bioD' take their sequence from genes of the E.coli biotin synthesis pathway, and the probe 'cre' takes its sequence form the bacteriophage P1 recombinase gene. As these are all non-eukaryotic genes, they are not expressed in human cells. These controls are spiked into the hybridisation control at different, known concentrations to enable signal alignment during image analysis.

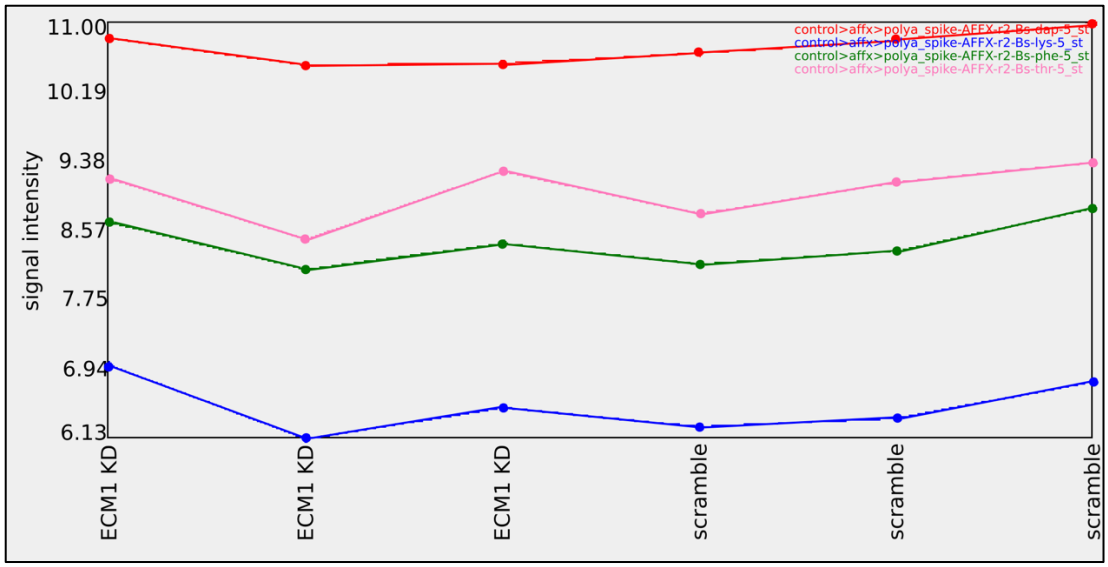

Array labelling controls.

Analysis of the labelling controls was conducted in Affymetrix Expression Console™. The transcripts 'lys', 'phe', 'thr' and 'dap' take their sequence from D. Subtilis genes. As these are all non-eukaryotic genes, they are not expressed in human cells. Different known concentrations of these transcripts were amplified and labelled with the assay samples to examine the labelling process.

Normalisation of the microarray data was conducted in the Affymetrix Expression Console™ version 1.4. As probe cell intensities are prior to normalisation, experimental variation such as that occurring during the fluorescent labelling of cDNA and hybridisation of cDNA to the microarray, means some differences in distributions may be expected. However, there was no significant variability between the probe cell intensity data of our microarray samples measured from CEL files prior to normalisation.

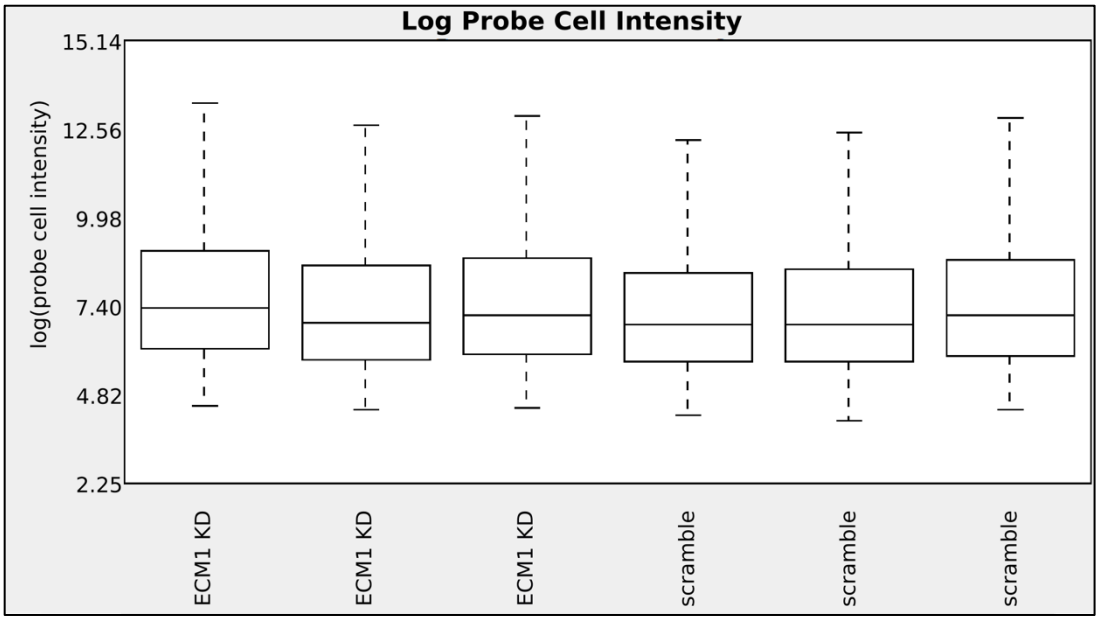

Log probe cell intensity.

The log probe cell intensity box plot was generated in Affymetrix Expression Console™ and shows the intensity of the signal from each array. No significant variations in median signal intensity were observed.

Signal Space Transformation-Robust Multichip Average (SST-RMA) normalisation was conducted using the raw data from the CEL files in order to adjust for the variability in probe cell intensity between microarray samples. This generated CHP files. SST removes significant fold-change compression and RMA minimises probe variance [326]. After normalisation, CHP file summarised probe set signal values have no variability compared to the probe cell intensity values of microarray samples measured from CEL files. This indicates that the data normalisation was successful and array samples can now be compared.

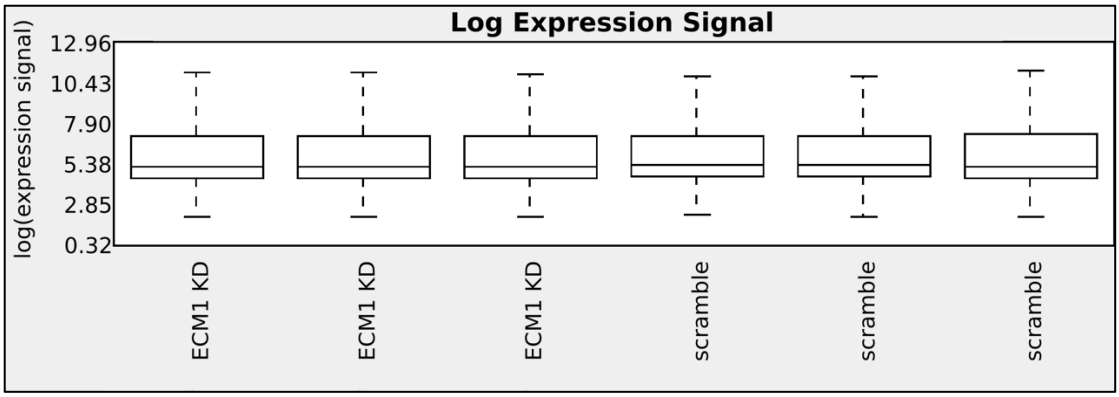

Log expression signal of CHP files generated from the CEL files through SST-RMA normalisation.

The box plot shows the signal intensity of each array following the SST-RMA normalisation conducted in Affymetrix Expression Console™. There are no differences in signal intensities between arrays indicating successful normalisation.

J.1.2 LIMMA analysis to detect differentially expressed genes

Microarray analysis using a whole genome transcript array was carried out to identify changes in gene expression induced by ECM1 knockdown in the HT-1376 cell line. Differential gene expression in HT-1376 ECM knockdown and scramble control cell lines was assessed using LIMMA analysis. Lists of the differentially expressed genes that were significantly upregulated and significantly downregulated.

A list of genes significantly upregulated in the HT-1376 ECM1 knockdown cell line compared to the scramble control .

ID	Gene Symbol	P-val	Fold Change
TC05001295.hg.1; TC05002968.hg.1	FYB	3.3E-03	2.01
TC05000125.hg.1	LINC01021	1.6E-05	2.01
TC14001144.hg.1	FERMT2	3.0E-04	2.02
TC17001937.hg.1	NPTX1	6.0E-03	2.02
TC12001772.hg.1; TC12002978.hg.1	LIN7A	9.8E-03	2.03
TC06002062.hg.1	MAN1A1	2.5E-02	2.04
TC05001676.hg.1	EPB41L4A	3.8E-06	2.05
TC07000095.hg.1	SCIN	2.2E-03	2.05
TC02002808.hg.1	EPHA4	1.4E-03	2.07
TC01002347.hg.1	ID3	8.6E-03	2.07
TC04000416.hg.1	PARM1	3.9E-03	2.08
TC01006291.hg.1	CFH	5.5E-06	2.09
TC10002924.hg.1	AKR1C1	8.0E-05	2.1
TC03000844.hg.1	ARHGEF26	6.0E-06	2.11
TC10000315.hg.1	ZNF488	1.8E-02	2.11
TC03002115.hg.1	FGF12	6.3E-05	2.12
TC19000781.hg.1	ZNF175	3.0E-04	2.12
TC07003061.hg.1	CDK6	4.0E-04	2.14
TC05002544.hg.1	PAM	4.8E-05	2.15
TC19002708.hg.1	PSG1	9.0E-04	2.16
TC15001335.hg.1	FBN1	1.9E-03	2.17
TC08000482.hg.1	RDH10	8.0E-03	2.17
TC05000262.hg.1	ZSWIM6	6.0E-04	2.19
TC17001801.hg.1	MIR5047	1.9E-03	2.2
TC12001170.hg.1; TC12002734.hg.1	SLC2A3	5.0E-04	2.22
TC05001641.hg.1	SLCO4C1	1.1E-03	2.26
TC02000041.hg.1	ID2	1.0E-04	2.32
TC13000577.hg.1	TRPC4	7.0E-04	2.32
TC21000060.hg.1	NCAM2	3.0E-04	2.35
TC02002482.hg.1	KCNH7	3.2E-05	2.37
TC01000892.hg.1	PALMD; MIR548AA1	5.7E-05	2.37
TC02004666.hg.1; TC02002474.hg.1	MXRA7	1.3E-02	2.39
TC04001344.hg.1	PLAC8	2.0E-04	2.39
TC17001757.hg.1	MIR4737	5.3E-03	2.41
TC04000548.hg.1	NPNT	1.3E-06	2.41
TC08001395.hg.1	DCAF4L2	1.0E-04	2.43
TC06000758.hg.1	SH3BGRL2	1.0E-04	2.44
TC02002606.hg.1; TC02004744.hg.1	TFPI	2.2E-05	2.47
TC09001211.hg.1	ALDH1A1	5.0E-04	2.53
TC02002083.hg.1	LOC654342	3.3E-03	2.55
TC11002242.hg.1	PDGFD	7.8E-05	2.56
TC02001874.hg.1; TC02004248.hg.1	LOC100129434	1.0E-04	2.58
TC12001804.hg.1	DCN	6.9E-06	2.65
TC03002430.hg.1	OR5H1	2.0E-04	2.68
TC03001512.hg.1	ID2B	2.0E-04	2.74
TC19001782.hg.1; TC19002560.hg.1	SIGLEC6	2.0E-04	2.95
TC0X000878.hg.1	ACE2	8.6E-07	3.05
TC05002512.hg.1	NR2F1	1.6E-05	3.08
TC07002499.hg.1	SERPINE1	1.4E-02	3.08
TC12000672.hg.1	ACSS3	9.9E-07	3.09
TC04001565.hg.1	PCDH18	6.9E-03	3.17
TC05002969.hg.1	DAB2	1.5E-05	3.21
TC07001355.hg.1	IGFBP3	1.4E-03	3.25
TC05001816.hg.1	SPOCK1	1.0E-04	3.42
TC04000369.hg.1; TC4_ctg9_hap1000001.hg.1	TMPRSS11E	3.8E-06	3.64
TC06000126.hg.1	ID4	2.8E-03	3.7
TC03000484.hg.1	OR5H14	3.0E-04	3.79
TC01000931.hg.1	FAM102B	1.3E-03	3.97
TC06000985.hg.1	ENPP1	7.4E-06	4.3
TC03001970.hg.1	BCHE	8.4E-06	4.38
TC04000478.hg.1; TC04002100.hg.1	SPP1	4.5E-05	4.42
TC04000638.hg.1	MIR2054	5.3E-03	4.51
TC02002747.hg.1	FN1	3.0E-04	4.61
TC08001248.hg.1	TOX	1.7E-05	5.28
TC10000621.hg.1	PAPSS2	5.0E-07	5.81
TC02002605.hg.1	CALCRL	4.0E-07	7.81
TC05001205.hg.1	CDH10	6.0E-06	8.86

ID	Gene Symbol	P-val	Fold Change								
TC20000341.hg.1	PI3	6.4E-03	-42.04	TC05000805.hg.1	SPINK5	2.3E-06	-4.33	TC01003932.hg.1	RNA5S13	8.0E-04	-3.15
TC12001532.hg.1	KRT1	2.7E-05	-20.7	TC04001753.hg.1	HPGD	1.0E-04	-4.22	TC01003933.hg.1	RNA5S14	8.0E-04	-3.15
TC19000266.hg.1	CASP14	1.0E-04	-13.98	TC17001472.hg.1	KRT10	1.0E-04	-4.04	TC01003934.hg.1	RNA5S15	8.0E-04	-3.15
TC12001525.hg.1	KRT6A	1.8E-05	-12.58	TC11001546.hg.1	ELF5	2.0E-04	-3.97	TC01003935.hg.1	RNA5S16	8.0E-04	-3.15
				TC01003255.hg.1; TC01005835.hg.1	SPRR2E	4.6E-03	-3.85	TC01003936.hg.1	RNA5S17	8.0E-04	-3.15
TC18001004.hg.1	SERPINB4; SERPINB3	1.0E-04	-10.25	TC19001765.hg.1	KLK7	3.6E-05	-3.8	TC01003921.hg.1	RNA5S2	8.0E-04	-3.15
TC12001524.hg.1	KRT6C	9.3E-06	-8.66	TC16001621.hg.1; TC16000589.hg.1	CALB2	3.6E-06	-3.65	TC01003922.hg.1	RNA5S3	8.0E-04	-3.15
TC18001005.hg.1	SERPINB3	2.0E-04	-8.25	TC19002457.hg.1	DMKN	1.4E-05	-3.61	TC01003923.hg.1	RNA5S4	8.0E-04	-3.15
TC19001444.hg.1	KRTDAP	2.0E-04	-7.45	TC15000602.hg.1	RNU5A-1	1.1E-02	-3.47	TC01003924.hg.1	RNA5S5	8.0E-04	-3.15
TC12001523.hg.1	KRT6B	1.4E-06	-7.03	TC01004000.hg.1	RNU5E-2P	4.1E-03	-3.39	TC01003925.hg.1	RNA5S6	8.0E-04	-3.15
TC01004752.hg.1; TC01001246.hg.1	SPRR1A	2.4E-03	-6.58	TC06001537.hg.1; TC6_cox_hap2000166.hg.1; TC6_cox_hap2000166.hg.1; TC6_mann_hap4000143.hg.1; TC6_mcf_hap5000143.hg.1; TC6_qbl_hap6000158.hg.1; TC6_ssto_hap7000138.hg.1	MIR4646	4.2E-02	-3.39	TC01003926.hg.1	RNA5S7	8.0E-04	-3.15
TC19001572.hg.1	CNFN	5.0E-04	-6.38	TC19001763.hg.1	KLK5	5.9E-06	-3.38	TC01003927.hg.1	RNA5S8	8.0E-04	-3.15
TC19001446.hg.1	SBSN	2.3E-05	-5.87	TC01001245.hg.1	SPRR4	8.3E-03	-3.31	TC01005831.hg.1; TC01003249.hg.1	LCE3D	4.8E-03	-3.1
TC12001536.hg.1	KRT4	1.0E-04	-5.29	TC01003920.hg.1	RNA5S1	8.0E-04	-3.15	TC02000767.hg.1	RNU4ATAC	1.1E-03	-2.97
TC03000630.hg.1	CSTA	1.4E-03	-4.77	TC01003929.hg.1	RNA5S10	8.0E-04	-3.15	TC12001453.hg.1	SNORA2C; MIR1291	8.0E-04	-2.96
TC01005830.hg.1; TC01005829.hg.1; TC01005828.hg.1; TC01003245.hg.1	FLG	7.0E-04	-4.65	TC01003930.hg.1	RNA5S11	8.0E-04	-3.15	TC01004746.hg.1; TC01001227.hg.1	CRCT1	1.3E-02	-2.96
TC12002888.hg.1; TC12001526.hg.1	KRT5	3.2E-06	-4.44	TC01003931.hg.1	RNA5S12	8.0E-04	-3.15	TC01001188.hg.1	ECM1	2.2E-05	-2.95

A list of significantly downregulated genes in the HT-1376 ECM1 knockdown cell line compared to the scramble control.

TC12002858.hg.1	VDR	5.0E-04	-2.95	TC6_mann_hap4000161.hg.1	HLA-DRB4; HLA-DRB1	4.7E-03	-2.29	TC11001418.hg.1	SNORD97	2.4E-03	-2.09
TC01001040.hg.1	HSD3B1	1.2E-05	-2.92	TC07001582.hg.1	STEAP4	2.3E-02	-2.28	TC06000779.hg.1	NT5E	1.3E-02	-2.08
TC01001251.hg.1	PRR9	1.2E-03	-2.76	TC19000705.hg.1	SULT2B1	1.3E-03	-2.27	TC01001248.hg.1	SPRR1B	1.3E-02	-2.08
TC09000736.hg.1	ASS1	4.5E-03	-2.74	TC01000160.hg.1	AADACL3	1.6E-03	-2.27	TC01003248.hg.1	LCE3E	1.1E-03	-2.07
TC11001376.hg.1	OR5P3	3.9E-02	-2.67	TC04002702.hg.1	TRPC3	1.8E-05	-2.25	TC01000821.hg.1	CLCA2	1.4E-02	-2.07
TC11000172.hg.1	SNORA23	7.3E-03	-2.57	TC12002040.hg.1	RNU4-1	1.9E-03	-2.25	TC16001156.hg.1	SNORA50A	4.0E-03	-2.06
TC10001589.hg.1	SNORA12	8.0E-03	-2.49	TC01000150.hg.1	RNU5E-1	8.5E-03	-2.24	TC02001528.hg.1	TMSB4XP2	9.0E-04	-2.05
TC19001764.hg.1	KLK6	3.0E-04	-2.46	TC09000687.hg.1	TMSB4XP4	8.3E-03	-2.23	TC03000509.hg.1	TMEM45A	2.0E-02	-2.05
TC0X000207.hg.1	MAOA	7.2E-03	-2.46	TC19001139.hg.1	MUC16	9.5E-03	-2.23	TC05000906.hg.1	CCNG1	9.3E-05	-2.04
TC17001474.hg.1	KRT23	8.4E-07	-2.41	TC18000127.hg.1	DSG3	1.4E-03	-2.22	TC01004449.hg.1	ROR1	3.4E-02	-2.04
TC12002039.hg.1	RNU4-2	7.6E-03	-2.41	TC18000231.hg.1	SERPINB2; SERPINB10	3.5E-02	-2.2	TC08000022.hg.1	AGPAT5	3.9E-05	-2.03
TC01001658.hg.1	PKP1	4.0E-04	-2.33	TC20000876.hg.1	SLPI	7.4E-03	-2.14	TC01000309.hg.1	GRHL3	9.0E-04	-2.03
TC05003313.hg.1	SPARC	5.0E-04	-2.33	TC11003505.hg.1	CASP1	3.8E-02	-2.13	TC08002306.hg.1	PLAT	2.4E-02	-2.03
TC06001518.hg.1; TC6_qbl_hap6000140.hg.1; TC6_cox_hap2000150.hg.1; TC6_dbb_hap3000139.hg.1	CDSN	6.5E-03	-2.33	TC16000456.hg.1	CAPNS2	4.3E-03	-2.11	TC03000846.hg.1	MME	2.2E-02	-2.02
TC01000757.hg.1	CTH	4.0E-04	-2.32	TC05001752.hg.1	FBN2	8.6E-03	-2.11	TC15002013.hg.1	TARSL2	2.0E-04	-2.01
TC15000603.hg.1	RNU5B-1	5.0E-04	-2.3	TC04002952.hg.1; TC04002953.hg.1	AREG	3.9E-02	-2.11	TC08002510.hg.1	MTSS1	5.0E-04	-2.01
TC07000144.hg.1	GPNMB	1.0E-02	-2.3	TC11003312.hg.1	MMP1	2.0E-04	-2.1	TC01002823.hg.1	LPAR3	4.1E-03	-2

Appendix K - List of suppliers

Agilent Technilogies LDA UK Limited, Life Sciences & Chemical Analysis Group, Lakeside, Cheadle Royal Business Park, Stockport, Cheshire SK8 3GR https://www.agilent.com/cs/agilent/en/contact-us/united-kingdom

Beckman Coulter, Oakley Court Kingsmead Business Park, Londn Road, High Wycombe, HP11 1JU
https://www.beckmancoulter.com/en/support/contact-us

Bethyl Laboratories, P.O. Box 850, Montgomery, Texas, USA, 77356
https://www.bethyl.com/Form/Contact

Bio-Rad Laboratories Ltd., The Junction, Station Road, Watford, Hertfordshire, WD17 1ET http://www.bio-rad.com/en-uk/contact-us

Cell Signalling Technology, Hamilton House, Mabledon Place, Lonson, WC1H 9BB https://www.cellsignal.co.uk/

Leica Biosystems, Larch House, Woodlands Business Park, Breckland, Linford Wood, Milton Keynes, MK14
6FG https://www.leicabiosystems.com/contact-us

New England Biolabs (NEB), 75/77 Knowl Piece, Wilbury Way, Hitchin, Hertfordshire, SG4 0TY https://www.neb.uk.com/support/customer-services

Promega, Delta House, Southampton Science Park, Southampton, SO16 7NS https://www.promega.co.uk/support/contact-promega

Qiagen, Skelton House, Lloyd St N, Manchester M15 6SH
https://www.qiagen.com/gb/about-us-old/contact

R&D Systems, 19 Barton Lane, Abingdon Science Park, Abingdon, OX14 3NB
https://www.rndsystems.com/support/contact-us

Santa Cruz Biotechnology, Bergheimer Strasse, 89-2, 69115, Heidelberg, Germany
https://www.scbt.com/scbt/customer-care/contact-us

Sigma-Aldrich, The Old Brickyard, New Road, Gillingham, Dorset, SP8 4XT
https://www.sigmaaldrich.com/united-kingdom/customer-service.html

Thermo Fisher Scientific, Fisher Science UK Ltd, Bishop Meadow Road, Loughborough, LE11 5RG https://www.fishersci.co.uk/gb/en/contact-us.html

References

1. Schafer, F. M., Algarrahi, K., Savarino, A., Yang, X., Seager, C., Franck, D., Costa, K., Liu, S., Logvinenko, T., Adam, R., Mauney, J. R. Mode of Surgical Injury Influences the Source of Urothelial Progenitors during Bladder Defect Repair. Stem Cell Reports. 2017;9(6):2005-17.

2. Epstein, J. I., Amin, M. B., Reuter, V. R., Mostofi, F. K. The World Health Organization/International Society of Urological Pathology consensus classification of urothelial (transitional cell) neoplasms of the urinary bladder. Bladder Consensus Conference Committee. Am J Surg Pathol. 1998;22(12):1435-48.

3. Dietrich, B., Srinivas, S. Urothelial carcinoma: the evolving landscape of immunotherapy for patients with advanced disease. Res Rep Urol. 2018;10:7-16.

4. Carneiro, B. A., Meeks, J. J., Kuzel, T. M., Scaranti, M., Abdulkadir, S. A., Giles, F. J. Emerging therapeutic targets in bladder cancer. Cancer Treat Rev. 2015;41(2):170-8.

5. NICE. Bladder cancer: diagnosis and management of bladder cancer: (c) NICE (2015) Bladder cancer: diagnosis and management of bladder cancer. BJU Int. 2017;120(6):755-65.

6. Cumberbatch, M. G. K., Jubber, I., Black, P. C., Esperto, F., Figueroa, J. D., Kamat, A. M., Kiemeney, L., Lotan, Y., Pang, K., Silverman, D. T., Znaor, A., Catto, J. W. F. Epidemiology of Bladder Cancer: A Systematic Review and Contemporary Update of Risk Factors in 2018. Eur Urol. 2018;74(6):784-95.

7. Cumberbatch, M. G., Cox, A., Teare, D., Catto, J. W. Contemporary Occupational Carcinogen Exposure and Bladder Cancer: A Systematic Review and Meta-analysis. JAMA Oncol. 2015;1(9):1282-90.

8. Cumberbatch, M. G., Rota, M., Catto, J. W., La Vecchia, C. The Role of Tobacco Smoke in Bladder and Kidney Carcinogenesis: A Comparison of Exposures and Meta-analysis of Incidence and Mortality Risks. Eur Urol. 2016;70(3):458-66.

9. Doll, R., Peto, R. The causes of cancer: quantitative estimates of avoidable risks of cancer in the United States today. J Natl Cancer Inst. 1981;66(6):1191-308.

10. Knowles, M. A., Hurst, C. D. Molecular biology of bladder cancer: new insights into pathogenesis and clinical diversity. Nat Rev Cancer. 2015;15(1):25-41.

11. Matulay, J. T., Kamat, A. M. Advances in risk stratification of bladder cancer to guide personalized medicine. F1000Res. 2018;7.

12. Eble, N., Sauter, G., Epstein, J., Sesterhennm, A. . World Health Organization Classification of Tumours. : IARC Press; 2004.

13. WHO. Histological Typing of Urinary Bladder Tumours. International Histological Classification of Tumours 10. 1973.
14. Aghaalikhani, N., Rashtchizadeh, N., Shadpour, P., Allameh, A., Mahmoodi, M. Cancer stem cells as a therapeutic target in bladder cancer. J Cell Physiol. 2018.
15. van Kessel, K. E., Zuiverloon, T. C., Alberts, A. R., Boormans, J. L., Zwarthoff, E. C. Targeted therapies in bladder cancer: an overview of in vivo research. Nat Rev Urol. 2015.
16. Brooks, N. A., O'Donnell, M. A. Treatment options in non-muscle-invasive bladder cancer after BCG failure. Indian J Urol. 2015;31(4):312-9.
17. Woldu, S. L., Bagrodia, A., Lotan, Y. Guideline of guidelines: non-muscle-invasive bladder cancer. BJU Int. 2017;119(3):371-80.
18. Denzinger, S., Fritsche, H. M., Otto, W., Blana, A., Wieland, W. F., Burger, M. Early versus deferred cystectomy for initial high-risk pT1G3 urothelial carcinoma of the bladder: do risk factors define feasibility of bladder-sparing approach? Eur Urol. 2008;53(1):146-52.
19. Tan, W. S., Lamb, B. W., Kelly, J. D. Complications of Radical Cystectomy and Orthotopic Reconstruction. Adv Urol. 2015;2015:323157.
20. Grayson, M. Bladder cancer. Nature. 2017;551(7679):S33.
21. Henrique, R., Nunes, S. P., Jeronimo, C. MSH2 Expression and Resistance to Cisplatin in Muscle-invasive Bladder Cancer: A Mix of Progress and Challenges. Eur Urol. 2018.
22. Tannock, I., Gospodarowicz, M., Connolly, J., Jewett, M. M-VAC (methotrexate, vinblastine, doxorubicin and cisplatin) chemotherapy for transitional cell carcinoma: the Princess Margaret Hospital experience. J Urol. 1989;142(2 Pt 1):289-92.
23. von der Maase, H., Hansen, S. W., Roberts, J. T., Dogliotti, L., Oliver, T., Moore, M. J., Bodrogi, I., Albers, P., Knuth, A., Lippert, C. M., Kerbrat, P., Sanchez Rovira, P., Wersall, P., Cleall, S. P., Roychowdhury, D. F., Tomlin, I., Visseren-Grul, C. M., Conte, P. F. Gemcitabine and cisplatin versus methotrexate, vinblastine, doxorubicin, and cisplatin in advanced or metastatic bladder cancer: results of a large, randomized, multinational, multicenter, phase III study. J Clin Oncol. 2000;18(17):3068-77.
24. Loehrer, P. J., Sr., Einhorn, L. H., Elson, P. J., Crawford, E. D., Kuebler, P., Tannock, I., Raghavan, D., Stuart-Harris, R., Sarosdy, M. F., Lowe, B. A., et al. A randomized comparison of cisplatin alone or in combination with methotrexate,

vinblastine, and doxorubicin in patients with metastatic urothelial carcinoma: a cooperative group study. J Clin Oncol. 1992;10(7):1066-73.

25. Kim, H. S., Seo, H. K. Immune checkpoint inhibitors for urothelial carcinoma. Investig Clin Urol. 2018;59(5):285-96.

26. Alfred Witjes, J., Lebret, T., Comperat, E. M., Cowan, N. C., De Santis, M., Bruins, H. M., Hernandez, V., Espinos, E. L., Dunn, J., Rouanne, M., Neuzillet, Y., Veskimae, E., van der Heijden, A. G., Gakis, G., Ribal, M. J. Updated 2016 EAU Guidelines on Muscle-invasive and Metastatic Bladder Cancer. Eur Urol. 2017;71(3):462-75.

27. Brown, S. D., Warren, R. L., Gibb, E. A., Martin, S. D., Spinelli, J. J., Nelson, B. H., Holt, R. A. Neo-antigens predicted by tumor genome meta-analysis correlate with increased patient survival. Genome Res. 2014;24(5):743-50.

28. Gopalakrishnan, D., Koshkin, V. S., Ornstein, M. C., Papatsoris, A., Grivas, P. Immune checkpoint inhibitors in urothelial cancer: recent updates and future outlook. Ther Clin Risk Manag. 2018;14:1019-40.

29. Rosser, C. J., Chamie, K., Rock, A., Ferguson, L., Wong H. C., . A study of intravesical bacillus Calmette-Guerin (BCG) in combination with ALT-803 in patients with non-muscle invasive bladder cancer. Journal of Clinical Oncology 2018;36(6).

30. Glaser, A. P., Fantini, D., Shilatifard, A., Schaeffer, E. M., Meeks, J. J. The evolving genomic landscape of urothelial carcinoma. Nat Rev Urol. 2017;14(4):215-29.

31. Hurst, C. D., Alder, O., Platt, F. M., Droop, A., Stead, L. F., Burns, J. E., Burghel, G. J., Jain, S., Klimczak, L. J., Lindsay, H., Roulson, J. A., Taylor, C. F., Thygesen, H., Cameron, A. J., Ridley, A. J., Mott, H. R., Gordenin, D. A., Knowles, M. A. Genomic Subtypes of Non-invasive Bladder Cancer with Distinct Metabolic Profile and Female Gender Bias in KDM6A Mutation Frequency. Cancer Cell. 2017;32(5):701-15 e7.

32. Robertson, A. G., Kim, J., Al-Ahmadie, H., Bellmunt, J., Guo, G., Cherniack, A. D., Hinoue, T., Laird, P. W., Hoadley, K. A., Akbani, R., Castro, M. A. A., Gibb, E. A., Kanchi, R. S., Gordenin, D. A., Shukla, S. A., Sanchez-Vega, F., Hansel, D. E., Czerniak, B. A., Reuter, V. E., Su, X., de Sa Carvalho, B., Chagas, V. S., Mungall, K. L., Sadeghi, S., Pedamallu, C. S., Lu, Y., Klimczak, L. J., Zhang, J., Choo, C., Ojesina, A. I., Bullman, S., Leraas, K. M., Lichtenberg, T. M., Wu, C. J., Schultz, N., Getz, G., Meyerson, M., Mills, G. B., McConkey, D. J., Network, T. R., Weinstein, J. N., Kwiatkowski, D. J., Lerner, S. P. Comprehensive Molecular Characterization of Muscle-Invasive Bladder Cancer. Cell. 2017;171(3):540-56 e25.

33. Hurst, C. D., Platt, F. M., Taylor, C. F., Knowles, M. A. Novel tumor subgroups of urothelial carcinoma of the bladder defined by integrated genomic analysis. Clin Cancer Res. 2012;18(21):5865-77.

34. Hurst, C. D., Tomlinson, D. C., Williams, S. V., Platt, F. M., Knowles, M. A. Inactivation of the Rb pathway and overexpression of both isoforms of E2F3 are obligate events in bladder tumours with 6p22 amplification. Oncogene. 2008;27(19):2716-27.

35. Blaveri, E., Brewer, J. L., Roydasgupta, R., Fridlyand, J., DeVries, S., Koppie, T., Pejavar, S., Mehta, K., Carroll, P., Simko, J. P., Waldman, F. M. Bladder cancer stage and outcome by array-based comparative genomic hybridization. Clin Cancer Res. 2005;11(19 Pt 1):7012-22.

36. Knowles, M. A., Habuchi, T., Kennedy, W., Cuthbert-Heavens, D. Mutation spectrum of the 9q34 tuberous sclerosis gene TSC1 in transitional cell carcinoma of the bladder. Cancer Res. 2003;63(22):7652-6.

37. Platt, F. M., Hurst, C. D., Taylor, C. F., Gregory, W. M., Harnden, P., Knowles, M. A. Spectrum of phosphatidylinositol 3-kinase pathway gene alterations in bladder cancer. Clin Cancer Res. 2009;15(19):6008-17.

38. di Martino, E., Tomlinson, D. C., Knowles, M. A. A Decade of FGF Receptor Research in Bladder Cancer: Past, Present, and Future Challenges. Adv Urol. 2012;2012:429213.

39. Guo, G., Sun, X., Chen, C., Wu, S., Huang, P., Li, Z., Dean, M., Huang, Y., Jia, W., Zhou, Q., Tang, A., Yang, Z., Li, X., Song, P., Zhao, X., Ye, R., Zhang, S., Lin, Z., Qi, M., Wan, S., Xie, L., Fan, F., Nickerson, M. L., Zou, X., Hu, X., Xing, L., Lv, Z., Mei, H., Gao, S., Liang, C., Gao, Z., Lu, J., Yu, Y., Liu, C., Li, L., Fang, X., Jiang, Z., Yang, J., Li, C., Zhao, X., Chen, J., Zhang, F., Lai, Y., Lin, Z., Zhou, F., Chen, H., Chan, H. C., Tsang, S., Theodorescu, D., Li, Y., Zhang, X., Wang, J., Yang, H., Gui, Y., Wang, J., Cai, Z. Whole-genome and whole-exome sequencing of bladder cancer identifies frequent alterations in genes involved in sister chromatid cohesion and segregation. Nat Genet. 2013;45(12):1459-63.

40. Williams, S. V., Hurst, C. D., Knowles, M. A. Oncogenic FGFR3 gene fusions in bladder cancer. Hum Mol Genet. 2013;22(4):795-803.

41. Jebar, A. H., Hurst, C. D., Tomlinson, D. C., Johnston, C., Taylor, C. F., Knowles, M. A. FGFR3 and Ras gene mutations are mutually exclusive genetic events in urothelial cell carcinoma. Oncogene. 2005;24(33):5218-25.

42. Knowles, M. A., Platt, F. M., Ross, R. L., Hurst, C. D. Phosphatidylinositol 3-kinase (PI3K) pathway activation in bladder cancer. Cancer Metastasis Rev. 2009;28(3-4):305-16.

43. Allory, Y., Beukers, W., Sagrera, A., Flandez, M., Marques, M., Marquez, M., van der Keur, K. A., Dyrskjot, L., Lurkin, I., Vermeij, M., Carrato, A., Lloreta, J., Lorente, J. A., Carrillo-de Santa Pau, E., Masius, R. G., Kogevinas, M., Steyerberg, E. W., van Tilborg, A. A., Abas, C., Orntoft, T. F., Zuiverloon, T. C., Malats, N., Zwarthoff, E. C., Real, F. X. Telomerase reverse transcriptase promoter mutations in bladder cancer: high frequency across stages, detection in urine, and lack of association with outcome. Eur Urol. 2014;65(2):360-6.

44. Hurst, C. D., Platt, F. M., Knowles, M. A. Comprehensive mutation analysis of the TERT promoter in bladder cancer and detection of mutations in voided urine. Eur Urol. 2014;65(2):367-9.

45. Huang, F. W., Hodis, E., Xu, M. J., Kryukov, G. V., Chin, L., Garraway, L. A. Highly recurrent TERT promoter mutations in human melanoma. Science. 2013;339(6122):957-9.

46. Lopez-Knowles, E., Hernandez, S., Kogevinas, M., Lloreta, J., Amoros, A., Tardon, A., Carrato, A., Kishore, S., Serra, C., Malats, N., Real, F. X., Investigators, E. S. The p53 pathway and outcome among patients with T1G3 bladder tumors. Clin Cancer Res. 2006;12(20 Pt 1):6029-36.

47. Cancer Genome Atlas Research Network. Comprehensive molecular characterization of urothelial bladder carcinoma. Nature. 2014;507(7492):315-22.

48. Kandoth, C., McLellan, M. D., Vandin, F., Ye, K., Niu, B., Lu, C., Xie, M., Zhang, Q., McMichael, J. F., Wyczalkowski, M. A., Leiserson, M. D. M., Miller, C. A., Welch, J. S., Walter, M. J., Wendl, M. C., Ley, T. J., Wilson, R. K., Raphael, B. J., Ding, L. Mutational landscape and significance across 12 major cancer types. Nature. 2013;502(7471):333-9.

49. Lawrence, M. S., Stojanov, P., Polak, P., Kryukov, G. V., Cibulskis, K., Sivachenko, A., Carter, S. L., Stewart, C., Mermel, C. H., Roberts, S. A., Kiezun, A., Hammerman, P. S., McKenna, A., Drier, Y., Zou, L., Ramos, A. H., Pugh, T. J., Stransky, N., Helman, E., Kim, J., Sougnez, C., Ambrogio, L., Nickerson, E., Shefler, E., Cortes, M. L., Auclair, D., Saksena, G., Voet, D., Noble, M., DiCara, D., Lin, P., Lichtenstein, L., Heiman, D. I., Fennell, T., Imielinski, M., Hernandez, B., Hodis, E., Baca, S., Dulak, A. M., Lohr, J., Landau, D. A., Wu, C. J., Melendez-Zajgla, J., Hidalgo-Miranda, A., Koren, A., McCarroll, S. A., Mora, J., Crompton, B., Onofrio, R., Parkin, M., Winckler, W., Ardlie, K., Gabriel, S. B., Roberts, C. W. M., Biegel, J. A., Stegmaier, K., Bass, A. J., Garraway, L. A., Meyerson, M., Golub, T. R., Gordenin, D. A., Sunyaev, S., Lander, E. S., Getz, G. Mutational heterogeneity in cancer and the search for new cancer-associated genes. Nature. 2013;499(7457):214-8.

50. Nordentoft, I., Lamy, P., Birkenkamp-Demtroder, K., Shumansky, K., Vang, S., Hornshoj, H., Juul, M., Villesen, P., Hedegaard, J., Roth, A., Thorsen, K., Hoyer, S., Borre, M., Reinert, T., Fristrup, N., Dyrskjot, L., Shah, S., Pedersen, J. S., Orntoft, T. F. Mutational context and diverse clonal development in early and late bladder cancer. Cell Rep. 2014;7(5):1649-63.

51. Pietzak, E. J., Bagrodia, A., Cha, E. K., Drill, E. N., Iyer, G., Isharwal, S., Ostrovnaya, I., Baez, P., Li, Q., Berger, M. F., Zehir, A., Schultz, N., Rosenberg, J. E., Bajorin, D. F., Dalbagni, G., Al-Ahmadie, H., Solit, D. B., Bochner, B. H. Next-generation Sequencing of Nonmuscle Invasive Bladder Cancer Reveals Potential Biomarkers and Rational Therapeutic Targets. Eur Urol. 2017;72(6):952-9.

52. Gui, Y., Guo, G., Huang, Y., Hu, X., Tang, A., Gao, S., Wu, R., Chen, C., Li, X., Zhou, L., He, M., Li, Z., Sun, X., Jia, W., Chen, J., Yang, S., Zhou, F., Zhao, X., Wan, S., Ye, R., Liang, C., Liu, Z., Huang, P., Liu, C., Jiang, H., Wang, Y., Zheng, H., Sun, L., Liu, X., Jiang, Z., Feng, D., Chen, J., Wu, S., Zou, J., Zhang, Z., Yang, R., Zhao, J., Xu, C., Yin, W., Guan, Z., Ye, J., Zhang, H., Li, J., Kristiansen, K., Nickerson, M. L., Theodorescu, D., Li, Y., Zhang, X., Li, S., Wang, J., Yang, H., Wang, J., Cai, Z. Frequent mutations of chromatin remodeling genes in transitional cell carcinoma of the bladder. Nat Genet. 2011;43(9):875-8.

53. Tomlinson, D. C., Baldo, O., Harnden, P., Knowles, M. A. FGFR3 protein expression and its relationship to mutation status and prognostic variables in bladder cancer. J Pathol. 2007;213(1):91-8.

54. Tomlinson, D. C., Lamont, F. R., Shnyder, S. D., Knowles, M. A. Fibroblast growth factor receptor 1 promotes proliferation and survival via activation of the mitogen-activated protein kinase pathway in bladder cancer. Cancer Res. 2009;69(11):4613-20.

55. Hashmi, A. A., Hussain, Z. F., Irfan, M., Khan, E. Y., Faridi, N., Naqvi, H., Khan, A., Edhi, M. M. Prognostic significance of epidermal growth factor receptor (EGFR) over expression in urothelial carcinoma of urinary bladder. BMC Urol. 2018;18(1):59.

56. Sriplakich, S., Jahnson, S., Karlsson, M. G. Epidermal growth factor receptor expression: predictive value for the outcome after cystectomy for bladder cancer? BJU Int. 1999;83(4):498-503.

57. Cardillo, M. R., Castagna, G., Memeo, L., De Bernardinis, E., Di Silverio, F. Epidermal growth factor receptor, MUC-1 and MUC-2 in bladder cancer. J Exp Clin Cancer Res. 2000;19(2):225-33.

58. Li, W., Wang, Y., Tan, S., Rao, Q., Zhu, T., Huang, G., Li, Z., Liu, G. Overexpression of Epidermal Growth Factor Receptor (EGFR) and HER-2 in

Bladder Carcinoma and Its Association with Patients' Clinical Features. Med Sci Monit. 2018;24:7178-85.

59. Mansour, A. M., Abdelrahim, M., Laymon, M., Elsherbeeny, M., Sultan, M., Shokeir, A., Mosbah, A., Abol-Enein, H., Awadalla, A., Cho, E., Sairam, V., Park, T. D., Shahid, M., Kim, J. Epidermal growth factor expression as a predictor of chemotherapeutic resistance in muscle-invasive bladder cancer. BMC Urol. 2018;18(1):100.

60. Hass, R., Jennek, S., Yang, Y., Friedrich, K. c-Met expression and activity in urogenital cancers - novel aspects of signal transduction and medical implications. Cell Commun Signal. 2017;15(1):10.

61. Kuijjer, M. L., Paulson, J. N., Salzman, P., Ding, W., Quackenbush, J. Cancer subtype identification using somatic mutation data. Br J Cancer. 2018;118(11):1492-501.

62. Cancer Genome Atlas Research Network. Integrated genomic analyses of ovarian carcinoma. Nature. 2011;474(7353):609-15.

63. Cancer Genome Atlas Network. Comprehensive molecular portraits of human breast tumours. Nature. 2012;490(7418):61-70.

64. Noushmehr, H., Weisenberger, D. J., Diefes, K., Phillips, H. S., Pujara, K., Berman, B. P., Pan, F., Pelloski, C. E., Sulman, E. P., Bhat, K. P., Verhaak, R. G., Hoadley, K. A., Hayes, D. N., Perou, C. M., Schmidt, H. K., Ding, L., Wilson, R. K., Van Den Berg, D., Shen, H., Bengtsson, H., Neuvial, P., Cope, L. M., Buckley, J., Herman, J. G., Baylin, S. B., Laird, P. W., Aldape, K., Cancer Genome Atlas Research, N. Identification of a CpG island methylator phenotype that defines a distinct subgroup of glioma. Cancer Cell. 2010;17(5):510-22.

65. Verhaak, R. G., Hoadley, K. A., Purdom, E., Wang, V., Qi, Y., Wilkerson, M. D., Miller, C. R., Ding, L., Golub, T., Mesirov, J. P., Alexe, G., Lawrence, M., O'Kelly, M., Tamayo, P., Weir, B. A., Gabriel, S., Winckler, W., Gupta, S., Jakkula, L., Feiler, H. S., Hodgson, J. G., James, C. D., Sarkaria, J. N., Brennan, C., Kahn, A., Spellman, P. T., Wilson, R. K., Speed, T. P., Gray, J. W., Meyerson, M., Getz, G., Perou, C. M., Hayes, D. N., Cancer Genome Atlas Research, N. Integrated genomic analysis identifies clinically relevant subtypes of glioblastoma characterized by abnormalities in PDGFRA, IDH1, EGFR, and NF1. Cancer Cell. 2010;17(1):98-110.

66. Zhao, L., Lee, V. H. F., Ng, M. K., Yan, H., Bijlsma, M. F. Molecular subtyping of cancer: current status and moving toward clinical applications. Brief Bioinform. 2018.

67. Bailey, P., Chang, D. K., Nones, K., Johns, A. L., Patch, A. M., Gingras, M. C., Miller, D. K., Christ, A. N., Bruxner, T. J., Quinn, M. C., Nourse, C., Murtaugh, L. C., Harliwong, I., Idrisoglu, S., Manning, S., Nourbakhsh, E., Wani, S., Fink, L., Holmes, O., Chin, V., Anderson, M. J., Kazakoff, S., Leonard, C., Newell, F., Waddell, N., Wood, S., Xu, Q., Wilson, P. J., Cloonan, N., Kassahn, K. S., Taylor, D., Quek, K., Robertson, A., Pantano, L., Mincarelli, L., Sanchez, L. N., Evers, L., Wu, J., Pinese, M., Cowley, M. J., Jones, M. D., Colvin, E. K., Nagrial, A. M., Humphrey, E. S., Chantrill, L. A., Mawson, A., Humphris, J., Chou, A., Pajic, M., Scarlett, C. J., Pinho, A. V., Giry-Laterriere, M., Rooman, I., Samra, J. S., Kench, J. G., Lovell, J. A., Merrett, N. D., Toon, C. W., Epari, K., Nguyen, N. Q., Barbour, A., Zeps, N., Moran-Jones, K., Jamieson, N. B., Graham, J. S., Duthie, F., Oien, K., Hair, J., Grutzmann, R., Maitra, A., Iacobuzio-Donahue, C. A., Wolfgang, C. L., Morgan, R. A., Lawlor, R. T., Corbo, V., Bassi, C., Rusev, B., Capelli, P., Salvia, R., Tortora, G., Mukhopadhyay, D., Petersen, G. M., Australian Pancreatic Cancer Genome, I., Munzy, D. M., Fisher, W. E., Karim, S. A., Eshleman, J. R., Hruban, R. H., Pilarsky, C., Morton, J. P., Sansom, O. J., Scarpa, A., Musgrove, E. A., Bailey, U. M., Hofmann, O., Sutherland, R. L., Wheeler, D. A., Gill, A. J., Gibbs, R. A., Pearson, J. V., Waddell, N., Biankin, A. V., Grimmond, S. M. Genomic analyses identify molecular subtypes of pancreatic cancer. Nature. 2016;531(7592):47-52.

68. Collisson, E. A., Sadanandam, A., Olson, P., Gibb, W. J., Truitt, M., Gu, S., Cooc, J., Weinkle, J., Kim, G. E., Jakkula, L., Feiler, H. S., Ko, A. H., Olshen, A. B., Danenberg, K. L., Tempero, M. A., Spellman, P. T., Hanahan, D., Gray, J. W. Subtypes of pancreatic ductal adenocarcinoma and their differing responses to therapy. Nat Med. 2011;17(4):500-3.

69. Cejalvo, J. M., Martinez de Duenas, E., Galvan, P., Garcia-Recio, S., Burgues Gasion, O., Pare, L., Antolin, S., Martinello, R., Blancas, I., Adamo, B., Guerrero-Zotano, A., Munoz, M., Nuciforo, P., Vidal, M., Perez, R. M., Chacon Lopez-Muniz, J. I., Caballero, R., Peg, V., Carrasco, E., Rojo, F., Perou, C. M., Cortes, J., Adamo, V., Albanell, J., Gomis, R. R., Lluch, A., Prat, A. Intrinsic Subtypes and Gene Expression Profiles in Primary and Metastatic Breast Cancer. Cancer Res. 2017;77(9):2213-21.

70. Cejalvo, J. M., Pascual, T., Fernandez-Martinez, A., Braso-Maristany, F., Gomis, R. R., Perou, C. M., Munoz, M., Prat, A. Clinical implications of the non-luminal intrinsic subtypes in hormone receptor-positive breast cancer. Cancer Treat Rev. 2018;67:63-70.

71. Lindgren, D., Frigyesi, A., Gudjonsson, S., Sjödahl, G., Hallden, C., Chebil, G., Veerla, S., Ryden, T., Mansson, W., Liedberg, F., Hoglund, M. Combined gene

expression and genomic profiling define two intrinsic molecular subtypes of urothelial carcinoma and gene signatures for molecular grading and outcome. Cancer Res. 2010;70(9):3463-72.

72. Sjödahl, G., Lauss, M., Lovgren, K., Chebil, G., Gudjonsson, S., Veerla, S., Patschan, O., Aine, M., Ferno, M., Ringner, M., Mansson, W., Liedberg, F., Lindgren, D., Hoglund, M. A molecular taxonomy for urothelial carcinoma. Clin Cancer Res. 2012;18(12):3377-86.

73. Sjödahl, G., Eriksson, P., Liedberg, F., Hoglund, M. Molecular classification of urothelial carcinoma: global mRNA classification versus tumour-cell phenotype classification. J Pathol. 2017;242(1):113-25.

74. Damrauer, J. S., Hoadley, K. A., Chism, D. D., Fan, C., Tiganelli, C. J., Wobker, S. E., Yeh, J. J., Milowsky, M. I., Iyer, G., Parker, J. S., Kim, W. Y. Intrinsic subtypes of high-grade bladder cancer reflect the hallmarks of breast cancer biology. Proc Natl Acad Sci U S A. 2014;111(8):3110-5.

75. Choi, W., Porten, S., Kim, S., Willis, D., Plimack, E. R., Hoffman-Censits, J., Roth, B., Cheng, T., Tran, M., Lee, I. L., Melquist, J., Bondaruk, J., Majewski, T., Zhang, S., Pretzsch, S., Baggerly, K., Siefker-Radtke, A., Czerniak, B., Dinney, C. P., McConkey, D. J. Identification of distinct basal and luminal subtypes of muscle-invasive bladder cancer with different sensitivities to frontline chemotherapy. Cancer Cell. 2014;25(2):152-65.

76. Seiler, R., Ashab, H. A. D., Erho, N., van Rhijn, B. W. G., Winters, B., Douglas, J., Van Kessel, K. E., Fransen van de Putte, E. E., Sommerlad, M., Wang, N. Q., Choeurng, V., Gibb, E. A., Palmer-Aronsten, B., Lam, L. L., Buerki, C., Davicioni, E., Sjödahl, G., Kardos, J., Hoadley, K. A., Lerner, S. P., McConkey, D. J., Choi, W., Kim, W. Y., Kiss, B., Thalmann, G. N., Todenhofer, T., Crabb, S. J., North, S., Zwarthoff, E. C., Boormans, J. L., Wright, J., Dall'Era, M., van der Heijden, M. S., Black, P. C. Impact of Molecular Subtypes in Muscle-invasive Bladder Cancer on Predicting Response and Survival after Neoadjuvant Chemotherapy. Eur Urol. 2017;72(4):544-54.

77. Cheetham, P. J., Petrylak, D. P. New Agents for the Treatment of Advanced Bladder Cancer. Oncology (Williston Park). 2016;30(6):571-9, 88.

78. Ho, P. L., Kurtova, A., Chan, K. S. Normal and neoplastic urothelial stem cells: getting to the root of the problem. Nat Rev Urol. 2012;9(10):583-94.

79. Rosenberg, J. E., Hoffman-Censits, J., Powles, T., van der Heijden, M. S., Balar, A. V., Necchi, A., Dawson, N., O'Donnell, P. H., Balmanoukian, A., Loriot, Y., Srinivas, S., Retz, M. M., Grivas, P., Joseph, R. W., Galsky, M. D., Fleming, M. T., Petrylak, D. P., Perez-Gracia, J. L., Burris, H. A., Castellano, D., Canil, C.,

Bellmunt, J., Bajorin, D., Nickles, D., Bourgon, R., Frampton, G. M., Cui, N., Mariathasan, S., Abidoye, O., Fine, G. D., Dreicer, R. Atezolizumab in patients with locally advanced and metastatic urothelial carcinoma who have progressed following treatment with platinum-based chemotherapy: a single-arm, multicentre, phase 2 trial. Lancet. 2016;387(10031):1909-20.

80. Lawrence, M. S., Stojanov, P., Mermel, C. H., Robinson, J. T., Garraway, L. A., Golub, T. R., Meyerson, M., Gabriel, S. B., Lander, E. S., Getz, G. Discovery and saturation analysis of cancer genes across 21 tumour types. Nature. 2014;505(7484):495-501.

81. Tan, T. Z., Rouanne, M., Tan, K. T., Huang, R. Y., Thiery, J. P. Molecular Subtypes of Urothelial Bladder Cancer: Results from a Meta-cohort Analysis of 2411 Tumors. Eur Urol. 2018.

82. Hedegaard, J., Lamy, P., Nordentoft, I., Algaba, F., Hoyer, S., Ulhoi, B. P., Vang, S., Reinert, T., Hermann, G. G., Mogensen, K., Thomsen, M. B. H., Nielsen, M. M., Marquez, M., Segersten, U., Aine, M., Hoglund, M., Birkenkamp-Demtroder, K., Fristrup, N., Borre, M., Hartmann, A., Stohr, R., Wach, S., Keck, B., Seitz, A. K., Nawroth, R., Maurer, T., Tulic, C., Simic, T., Junker, K., Horstmann, M., Harving, N., Petersen, A. C., Calle, M. L., Steyerberg, E. W., Beukers, W., van Kessel, K. E. M., Jensen, J. B., Pedersen, J. S., Malmstrom, P. U., Malats, N., Real, F. X., Zwarthoff, E. C., Orntoft, T. F., Dyrskjot, L. Comprehensive Transcriptional Analysis of Early-Stage Urothelial Carcinoma. Cancer Cell. 2016;30(1):27-42.

83. Earl, J., Rico, D., Carrillo-de-Santa-Pau, E., Rodriguez-Santiago, B., Mendez-Pertuz, M., Auer, H., Gomez, G., Grossman, H. B., Pisano, D. G., Schulz, W. A., Perez-Jurado, L. A., Carrato, A., Theodorescu, D., Chanock, S., Valencia, A., Real, F. X. The UBC-40 Urothelial Bladder Cancer cell line index: a genomic resource for functional studies. BMC Genomics. 2015;16:403.

84. Eriksson, P., Sjodahl, G. Re: Tuan Zea Tan, Mathieu Rouanne, Kien Thiam Tan, Ruby Yun-Ju Huang, Jean-Paul Thiery. Molecular Subtypes of Urothelial Bladder Cancer: Results from a Meta-cohort Analysis of 2411 Tumors. Eur Urol. In press. https://doi.org/10.1016/j.eururo.2018.08.027. Eur Urol. 2018.

85. Mo, Q., Nikolos, F., Chen, F., Tramel, Z., Lee, Y. C., Hayashi, K., Xiao, J., Shen, J., Chan, K. S. Prognostic Power of a Tumor Differentiation Gene Signature for Bladder Urothelial Carcinomas. J Natl Cancer Inst. 2018;110(5):448-59.

86. Rebouissou, S., Bernard-Pierrot, I., de Reynies, A., Lepage, M. L., Krucker, C., Chapeaublanc, E., Herault, A., Kamoun, A., Caillault, A., Letouze, E., Elarouci, N., Neuzillet, Y., Denoux, Y., Molinie, V., Vordos, D., Laplanche, A., Maille, P., Soyeux, P., Ofualuka, K., Reyal, F., Biton, A., Sibony, M., Paoletti, X., Southgate,

J., Benhamou, S., Lebret, T., Allory, Y., Radvanyi, F. EGFR as a potential therapeutic target for a subset of muscle-invasive bladder cancers presenting a basal-like phenotype. Sci Transl Med. 2014;6(244):244ra91.

87. Marzouka, N. A., Eriksson, P., Rovira, C., Liedberg, F., Sjödahl, G., Hoglund, M. A validation and extended description of the Lund taxonomy for urothelial carcinoma using the TCGA cohort. Sci Rep. 2018;8(1):3737.

88. Nickerson, M. L., Witte, N., Im, K. M., Turan, S., Owens, C., Misner, K., Tsang, S. X., Cai, Z., Wu, S., Dean, M., Costello, J. C., Theodorescu, D. Molecular analysis of urothelial cancer cell lines for modeling tumor biology and drug response. Oncogene. 2017;36(1):35-46.

89. Goodspeed, A., Jean, A., Theodorescu, D., Costello, J. C. A Gene Expression Signature Predicts Bladder Cancer Cell Line Sensitivity to EGFR Inhibition. Bladder Cancer. 2018;4(3):269-82.

90. Sercu, S., Zhang, L., Merregaert, J. The extracellular matrix protein 1: its molecular interaction and implication in tumor progression. Cancer Invest. 2008;26(4):375-84.

91. Mathieu, E., Meheus, L., Raymackers, J., Merregaert, J. Characterization of the osteogenic stromal cell line MN7: identification of secreted MN7 proteins using two-dimensional polyacrylamide gel electrophoresis, western blotting, and microsequencing. J Bone Miner Res. 1994;9(6):903-13.

92. Smits, P., Ni, J., Feng, P., Wauters, J., Van Hul, W., Boutaibi, M. E., Dillon, P. J., Merregaert, J. The human extracellular matrix gene 1 (ECM1): genomic structure, cDNA cloning, expression pattern, and chromosomal localization. Genomics. 1997;45(3):487-95.

93. Han, Z., Ni, J., Smits, P., Underhill, C. B., Xie, B., Chen, Y., Liu, N., Tylzanowski, P., Parmelee, D., Feng, P., Ding, I., Gao, F., Gentz, R., Huylebroeck, D., Merregaert, J., Zhang, L. Extracellular matrix protein 1 (ECM1) has angiogenic properties and is expressed by breast tumor cells. FASEB J. 2001;15(6):988-94.

94. Mongiat, M., Fu, J., Oldershaw, R., Greenhalgh, R., Gown, A. M., Iozzo, R. V. Perlecan protein core interacts with extracellular matrix protein 1 (ECM1), a glycoprotein involved in bone formation and angiogenesis. J Biol Chem. 2003;278(19):17491-9.

95. Deckers, M. M., Smits, P., Karperien, M., Ni, J., Tylzanowski, P., Feng, P., Parmelee, D., Zhang, J., Bouffard, E., Gentz, R., Lowik, C. W., Merregaert, J. Recombinant human extracellular matrix protein 1 inhibits alkaline phosphatase activity and mineralization of mouse embryonic metatarsals in vitro. Bone. 2001;28(1):14-20.

96. Wang, L., Yu, J., Ni, J., Xu, X. M., Wang, J., Ning, H., Pei, X. F., Chen, J., Yang, S., Underhill, C. B., Liu, L., Liekens, J., Merregaert, J., Zhang, L. Extracellular matrix protein 1 (ECM1) is over-expressed in malignant epithelial tumors. Cancer Lett. 2003;200(1):57-67.

97. Bhalerao, J., Tylzanowski, P., Filie, J. D., Kozak, C. A., Merregaert, J. Molecular cloning, characterization, and genetic mapping of the cDNA coding for a novel secretory protein of mouse. Demonstration of alternative splicing in skin and cartilage. J Biol Chem. 1995;270(27):16385-94.

98. Godin, R. E., Urry, L. A., Ernst, S. G. Alternative splicing of the Endo16 transcript produces differentially expressed mRNAs during sea urchin gastrulation. Dev Biol. 1996;179(1):148-59.

99. Fujimoto, N., Terlizzi, J., Aho, S., Brittingham, R., Fertala, A., Oyama, N., McGrath, J. A., Uitto, J. Extracellular matrix protein 1 inhibits the activity of matrix metalloproteinase 9 through high-affinity protein/protein interactions. Exp Dermatol. 2006;15(4):300-7.

100. Sercu, S., Poumay, Y., Herphelin, F., Liekens, J., Beek, L., Zwijsen, A., Wessagowit, V., Huylebroeck, D., McGrath, J. A., Merregaert, J. Functional redundancy of extracellular matrix protein 1 in epidermal differentiation. Br J Dermatol. 2007;157(4):771-5.

101. Mirancea, N., Hausser, I., Metze, D., Stark, H. J., Boukamp, P., Breitkreutz, D. Junctional basement membrane anomalies of skin and mucosa in lipoid proteinosis (hyalinosis cutis et mucosae). J Dermatol Sci. 2007;45(3):175-85.

102. Kong, L., Tian, Q., Guo, F., Mucignat, M. T., Perris, R., Sercu, S., Merregaert, J., Di Cesare, P. E., Liu, C. J. Interaction between cartilage oligomeric matrix protein and extracellular matrix protein 1 mediates endochondral bone growth. Matrix Biol. 2010;29(4):276-86.

103. Chan, I. The role of extracellular matrix protein 1 in human skin. Clin Exp Dermatol. 2004;29(1):52-6.

104. Kong, L., Zhao, Y. P., Tian, Q. Y., Feng, J. Q., Kobayashi, T., Merregaert, J., Liu, C. J. Extracellular matrix protein 1, a direct targeting molecule of parathyroid hormone-related peptide, negatively regulates chondrogenesis and endochondral ossification via associating with progranulin growth factor. FASEB J. 2016;30(8):2741-54.

105. Smits, P., Poumay, Y., Karperien, M., Tylzanowski, P., Wauters, J., Huylebroeck, D., Ponec, M., Merregaert, J. Differentiation-dependent alternative splicing and expression of the extracellular matrix protein 1 gene in human keratinocytes. J Invest Dermatol. 2000;114(4):718-24.

106. Horev, L., Potikha, T., Ayalon, S., Molho-Pessach, V., Ingber, A., Gany, M. A., Edin, B. S., Glaser, B., Zlotogorski, A. A novel splice-site mutation in ECM-1 gene in a consanguineous family with lipoid proteinosis. Exp Dermatol. 2005;14(12):891-7.

107. Oyama, N., Merregaert J. The Extracellular Matrix Protein 1 (ECM1) in Skin Biology: An Update for the Pleiotropic Action The Open Dermatology Journal. 2013;7:29-41.

108. Hamada, T., Wessagowit, V., South, A. P., Ashton, G. H., Chan, I., Oyama, N., Siriwattana, A., Jewhasuchin, P., Charuwichitratana, S., Thappa, D. M., Jeevankumar, B., Lenane, P., Krafchik, B., Kulthanan, K., Shimizu, H., Kaya, T. I., Erdal, M. E., Paradisi, M., Paller, A. S., Seishima, M., Hashimoto, T., McGrath, J. A. Extracellular matrix protein 1 gene (ECM1) mutations in lipoid proteinosis and genotype-phenotype correlation. J Invest Dermatol. 2003;120(3):345-50.

109. Hamada, T., McLean, W. H., Ramsay, M., Ashton, G. H., Nanda, A., Jenkins, T., Edelstein, I., South, A. P., Bleck, O., Wessagowit, V., Mallipeddi, R., Orchard, G. E., Wan, H., Dopping-Hepenstal, P. J., Mellerio, J. E., Whittock, N. V., Munro, C. S., van Steensel, M. A., Steijlen, P. M., Ni, J., Zhang, L., Hashimoto, T., Eady, R. A., McGrath, J. A. Lipoid proteinosis maps to 1q21 and is caused by mutations in the extracellular matrix protein 1 gene (ECM1). Hum Mol Genet. 2002;11(7):833-40.

110. Omrani, H. G., Tajdini, M., Ghelichnia, B., Hosseini, S. M., Tafakhori, A., Rahimian, E., Aghamollaii, V. Should we think of Urbach-Wiethe disease in refractory epilepsy? Case report and review of the literature. J Neurol Sci. 2012;320(1-2):149-52.

111. Chan, I., Liu, L., Hamada, T., Sethuraman, G., McGrath, J. A. The molecular basis of lipoid proteinosis: mutations in extracellular matrix protein 1. Exp Dermatol. 2007;16(11):881-90.

112. Oyama, N., Chan, I., Neill, S. M., South, A. P., Wojnarowska, F., Kawakami, Y., D'Cruz, D., Mepani, K., Hughes, G. J., Bhogal, B. S., Kaneko, F., Black, M. M., McGrath, J. A. Development of antigen-specific ELISA for circulating autoantibodies to extracellular matrix protein 1 in lichen sclerosus. J Clin Invest. 2004;113(11):1550-9.

113. Adali, G., Ersoy Tunali, N., Yorulmaz, E., Tiryakioglu, N. O., Mungan, S. G., Ulasoglu, C., Yilmaz Enc, F., Tuncer, I. Extracellular matrix protein 1 gene rs3737240 single nucleotide polymorphism is associated with ulcerative colitis in Turkish patients. Turk J Gastroenterol. 2017;28(4):254-9.

114. Gomez-Contreras, P., Ramiro-Diaz, J. M., Sierra, A., Stipp, C., Domann, F. E., Weigel, R. J., Lal, G. Extracellular matrix 1 (ECM1) regulates the actin cytoskeletal architecture of aggressive breast cancer cells in part via S100A4 and Rho-family GTPases. Clin Exp Metastasis. 2017;34(1):37-49.

115. Lal, G., Padmanabha, L., Nicholson, R., Smith, B. J., Zhang, L., Howe, J. R., Robinson, R. A., O'Dorisio, M. S. ECM1 expression in thyroid tumors--a comparison of real-time RT-PCR and IHC. J Surg Res. 2008;149(1):62-8.

116. Lal, G., Hashimi, S., Smith, B. J., Lynch, C. F., Zhang, L., Robinson, R. A., Weigel, R. J. Extracellular matrix 1 (ECM1) expression is a novel prognostic marker for poor long-term survival in breast cancer: a Hospital-based Cohort Study in Iowa. Ann Surg Oncol. 2009;16(8):2280-7.

117. Lal, G., Contreras, P. G., Kulak, M., Woodfield, G., Bair, T., Domann, F. E., Weigel, R. J. Human Melanoma cells over-express extracellular matrix 1 (ECM1) which is regulated by TFAP2C. PLoS One. 2013;8(9):e73953.

118. Chen, H., Jia, W. D., Li, J. S., Wang, W., Xu, G. L., Ma, J. L., Ren, W. H., Ge, Y. S., Yu, J. H., Liu, W. B., Zhang, C. H., Wang, Y. C. Extracellular matrix protein 1, a novel prognostic factor, is associated with metastatic potential of hepatocellular carcinoma. Med Oncol. 2011;28 Suppl 1:S318-25.

119. Gu, M., Guan, J., Zhao, L., Ni, K., Li, X., Han, Z. Correlation of ECM1 expression level with the pathogenesis and metastasis of laryngeal carcinoma. Int J Clin Exp Pathol. 2013;6(6):1132-7.

120. Lee, K. M., Nam, K., Oh, S., Lim, J., Kim, R. K., Shim, D., Choi, J. H., Lee, S. J., Yu, J. H., Lee, J. W., Ahn, S. H., Shin, I. ECM1 regulates tumor metastasis and CSC-like property through stabilization of beta-catenin. Oncogene. 2015.

121. Wu, Q. W., She, H. Q., Liang, J., Huang, Y. F., Yang, Q. M., Yang, Q. L., Zhang, Z. M. Expression and clinical significance of extracellular matrix protein 1 and vascular endothelial growth factor-C in lymphatic metastasis of human breast cancer. BMC Cancer. 2012;12:47.

122. Lee, K. M., Nam, K., Oh, S., Lim, J., Kim, Y. P., Lee, J. W., Yu, J. H., Ahn, S. H., Kim, S. B., Noh, D. Y., Lee, T., Shin, I. Extracellular matrix protein 1 regulates cell proliferation and trastuzumab resistance through activation of epidermal growth factor signaling. Breast Cancer Res. 2014;16(6):479.

123. Colquhoun, A. J., Mellon, J. K. Epidermal growth factor receptor and bladder cancer. Postgrad Med J. 2002;78(924):584-9.

124. Tzahar, E., Waterman, H., Chen, X., Levkowitz, G., Karunagaran, D., Lavi, S., Ratzkin, B. J., Yarden, Y. A hierarchical network of interreceptor interactions

determines signal transduction by Neu differentiation factor/neuregulin and epidermal growth factor. Mol Cell Biol. 1996;16(10):5276-87.
125. Seshacharyulu, P., Ponnusamy, M. P., Haridas, D., Jain, M., Ganti, A. K., Batra, S. K. Targeting the EGFR signaling pathway in cancer therapy. Expert Opin Ther Targets. 2012;16(1):15-31.
126. Wang, M., Yuang-Chi Chang, A. Molecular mechanism of action and potential biomarkers of growth inhibition of synergistic combination of afatinib and dasatinib against gefitinib-resistant non-small cell lung cancer cells. Oncotarget. 2018;9(23):16533-46.
127. Pellat, A., Vaquero, J., Fouassier, L. Role of ErbB/HER family of receptor tyrosine kinases in cholangiocyte biology. Hepatology. 2017.
128. Ko, B., Paucar, D., Halmos, B. EGFR T790M: revealing the secrets of a gatekeeper. Lung Cancer (Auckl). 2017;8:147-59.
129. Ljuslinder, I., Melin, B., Henriksson, M. L., Oberg, A., Palmqvist, R. Increased epidermal growth factor receptor expression at the invasive margin is a negative prognostic factor in colorectal cancer. Int J Cancer. 2011;128(9):2031-7.
130. Ohsaki, Y., Tanno, S., Fujita, Y., Toyoshima, E., Fujiuchi, S., Nishigaki, Y., Ishida, S., Nagase, A., Miyokawa, N., Hirata, S., Kikuchi, K. Epidermal growth factor receptor expression correlates with poor prognosis in non-small cell lung cancer patients with p53 overexpression. Oncol Rep. 2000;7(3):603-7.
131. Sainsbury, J. R., Farndon, J. R., Needham, G. K., Malcolm, A. J., Harris, A. L. Epidermal-growth-factor receptor status as predictor of early recurrence of and death from breast cancer. Lancet. 1987;1(8547):1398-402.
132. Rosenkranz, A. A., Slastnikova, T. A., Karmakova, T. A., Vorontsova, M. S., Morozova, N. B., Petriev, V. M., Abrosimov, A. S., Khramtsov, Y. V., Lupanova, T. N., Ulasov, A. V., Yakubovskaya, R. I., Georgiev, G. P., Sobolev, A. S. Antitumor Activity of Auger Electron Emitter (111)In Delivered by Modular Nanotransporter for Treatment of Bladder Cancer With EGFR Overexpression. Front Pharmacol. 2018;9:1331.
133. Abbosh, P. H., McConkey, D. J., Plimack, E. R. Targeting Signaling Transduction Pathways in Bladder Cancer. Curr Oncol Rep. 2015;17(12):58.
134. Shah, J. B., McConkey, D. J., Dinney, C. P. New strategies in muscle-invasive bladder cancer: on the road to personalized medicine. Clin Cancer Res. 2011;17(9):2608-12.
135. Gonul, II, Cakir, A., Sozen, S. Immunohistochemical expression profiles of MUC1 and MUC2 mucins in urothelial tumors of bladder. Indian J Pathol Microbiol. 2018;61(3):350-5.

136. Hollingsworth, M. A., Swanson, B. J. Mucins in cancer: protection and control of the cell surface. Nat Rev Cancer. 2004;4(1):45-60.
137. Walsh, M. D., Hohn, B. G., Thong, W., Devine, P. L., Gardiner, R. A., Samaratunga, M. L., McGuckin, M. A. Mucin expression by transitional cell carcinomas of the bladder. Br J Urol. 1994;73(3):256-62.
138. Li, Y., Liu, D., Chen, D., Kharbanda, S., Kufe, D. Human DF3/MUC1 carcinoma-associated protein functions as an oncogene. Oncogene. 2003;22(38):6107-10.
139. Lau, S. K., Weiss, L. M., Chu, P. G. Differential expression of MUC1, MUC2, and MUC5AC in carcinomas of various sites: an immunohistochemical study. Am J Clin Pathol. 2004;122(1):61-9.
140. Bafna, S., Kaur, S., Batra, S. K. Membrane-bound mucins: the mechanistic basis for alterations in the growth and survival of cancer cells. Oncogene. 2010;29(20):2893-904.
141. Kaur, S., Momi, N., Chakraborty, S., Wagner, D. G., Horn, A. J., Lele, S. M., Theodorescu, D., Batra, S. K. Altered expression of transmembrane mucins, MUC1 and MUC4, in bladder cancer: pathological implications in diagnosis. PLoS One. 2014;9(3):e92742.
142. Patriarca, C., Colombo, P., Pio Taronna, A., Wesseling, J., Franchi, G., Guddo, F., Naspro, R., Macchi, R. M., Giunta, P., Di Pasquale, M., Parente, M., Arizzi, C., Roncalli, M., Campo, B. Cell discohesion and multifocality of carcinoma in situ of the bladder: new insight from the adhesion molecule profile (e-cadherin, Ep-CAM, and MUC1). Int J Surg Pathol. 2009;17(2):99-106.
143. Abd Elazeez, T. A., El-Balshy Ael, L., Khalil, M. M., El-Tabye, M. M., Abdul-Halim, H. Prognostic significance of P27 (Kip 1) and MUC1 in papillary transitional cell carcinoma of the urinary bladder. Urol Ann. 2011;3(1):8-13.
144. Merlin, J., Stechly, L., de Beauce, S., Monte, D., Leteurtre, E., van Seuningen, I., Huet, G., Pigny, P. Galectin-3 regulates MUC1 and EGFR cellular distribution and EGFR downstream pathways in pancreatic cancer cells. Oncogene. 2011;30(22):2514-25.
145. Neeraja, D., Engel, B. J., Carson, D. D. Activated EGFR stimulates MUC1 expression in human uterine and pancreatic cancer cell lines. J Cell Biochem. 2013;114(10):2314-22.
146. Untergasser A, C. I., Koressaar T, Ye J, Faircloth BC, Remm M, Rozen SG. Primer3 - new capabilities and interfaces. Nucleic Acids Research. 2012;40(15):e115.

147. Bertani, G. Lysogeny at mid-twentieth century: P1, P2, and other experimental systems. J Bacteriol. 2004;186(3):595-600.
148. Mariathasan, S., Turley, S. J., Nickles, D., Castiglioni, A., Yuen, K., Wang, Y., Kadel, E. E., III, Koeppen, H., Astarita, J. L., Cubas, R., Jhunjhunwala, S., Banchereau, R., Yang, Y., Guan, Y., Chalouni, C., Ziai, J., Senbabaoglu, Y., Santoro, S., Sheinson, D., Hung, J., Giltnane, J. M., Pierce, A. A., Mesh, K., Lianoglou, S., Riegler, J., Carano, R. A. D., Eriksson, P., Hoglund, M., Somarriba, L., Halligan, D. L., van der Heijden, M. S., Loriot, Y., Rosenberg, J. E., Fong, L., Mellman, I., Chen, D. S., Green, M., Derleth, C., Fine, G. D., Hegde, P. S., Bourgon, R., Powles, T. TGFbeta attenuates tumour response to PD-L1 blockade by contributing to exclusion of T cells. Nature. 2018;554(7693):544-8.
149. Reich, M., Liefeld, T., Gould, J., Lerner, J., Tamayo, P., Mesirov, J. P. GenePattern 2.0. Nat Genet. 2006;38(5):500-1.
150. Brunet, J. P., Tamayo, P., Golub, T. R., Mesirov, J. P. Metagenes and molecular pattern discovery using matrix factorization. Proc Natl Acad Sci U S A. 2004;101(12):4164-9.
151. Saeed, A. I., Sharov, V., White, J., Li, J., Liang, W., Bhagabati, N., Braisted, J., Klapa, M., Currier, T., Thiagarajan, M., Sturn, A., Snuffin, M., Rezantsev, A., Popov, D., Ryltsov, A., Kostukovich, E., Borisovsky, I., Liu, Z., Vinsavich, A., Trush, V., Quackenbush, J. TM4: a free, open-source system for microarray data management and analysis. Biotechniques. 2003;34(2):374-8.
152. Wu, Q., Li, X., Yang, H., Lu, C., You, J., Zhang, Z. Extracellular matrix protein 1 is correlated to carcinogenesis and lymphatic metastasis of human gastric cancer. World J Surg Oncol. 2014;12:132.
153. Uematsu, S., Goto, Y., Suzuki, T., Sasazawa, Y., Dohmae, N., Simizu, S. N-Glycosylation of extracellular matrix protein 1 (ECM1) regulates its secretion, which is unrelated to lipoid proteinosis. FEBS Open Bio. 2014;4:879-85.
154. Kim, J., Akbani, R., Creighton, C. J., Lerner, S. P., Weinstein, J. N., Getz, G., Kwiatkowski, D. J. Invasive Bladder Cancer: Genomic Insights and Therapeutic Promise. Clin Cancer Res. 2015;21(20):4514-24.
155. Chalise, P., Fridley, B. L. Integrative clustering of multi-level 'omic data based on non-negative matrix factorization algorithm. PLoS One. 2017;12(5):e0176278.
156. Frigyesi, A., Hoglund, M. Non-negative matrix factorization for the analysis of complex gene expression data: identification of clinically relevant tumor subtypes. Cancer Inform. 2008;6:275-92.

157. Wang, H. M., Hsiao, C. L., Hsieh, A. R., Lin, Y. C., Fann, C. S. Constructing endophenotypes of complex diseases using non-negative matrix factorization and adjusted rand index. PLoS One. 2012;7(7):e40996.
158. Kebebew, E., Peng, M., Reiff, E., Duh, Q. Y., Clark, O. H., McMillan, A. ECM1 and TMPRSS4 are diagnostic markers of malignant thyroid neoplasms and improve the accuracy of fine needle aspiration biopsy. Ann Surg. 2005;242(3):353-61; discussion 61-3.
159. Morey, J. S., Ryan, J. C., Van Dolah, F. M. Microarray validation: factors influencing correlation between oligonucleotide microarrays and real-time PCR. Biol Proced Online. 2006;8:175-93.
160. Mantione, K. J., Kream, R. M., Kuzelova, H., Ptacek, R., Raboch, J., Samuel, J. M., Stefano, G. B. Comparing bioinformatic gene expression profiling methods: microarray and RNA-Seq. Med Sci Monit Basic Res. 2014;20:138-42.
161. Ivell, R., Teerds, K., Hoffman, G. E. Proper application of antibodies for immunohistochemical detection: antibody crimes and how to prevent them. Endocrinology. 2014;155(3):676-87.
162. Chen, H., Jia, W., Li, J. ECM1 promotes migration and invasion of hepatocellular carcinoma by inducing epithelial-mesenchymal transition. World J Surg Oncol. 2016;14(1):195.
163. Sercu, S., Oyama, N., Merregaert, J. Importance of Extracellular Matrix Protein 1 (ECM1) in Maintaining the Functional Integrity of the Human Skin. The Open Dermatology Journal. 2009;3(1):44-51.
164. Siroy, A., Abdul-Karim, F. W., Miedler, J., Fong, N., Fu, P., Gilmore, H., Baar, J. MUC1 is expressed at high frequency in early-stage basal-like triple-negative breast cancer. Hum Pathol. 2013;44(10):2159-66.
165. Creaney, J., Segal, A., Sterrett, G., Platten, M. A., Baker, E., Murch, A. R., Nowak, A. K., Robinson, B. W., Millward, M. J. Overexpression and altered glycosylation of MUC1 in malignant mesothelioma. Br J Cancer. 2008;98(9):1562-9.
166. Kirschenbaum, A., Itzkowitz, S. H., Wang, J. P., Yao, S., Eliashvili, M., Levine, A. C. MUC1 Expression in Prostate Carcinoma: Correlation with Grade and Stage. Mol Urol. 1999;3(3):163-8.
167. Horm, T. M., Schroeder, J. A. MUC1 and metastatic cancer: expression, function and therapeutic targeting. Cell Adh Migr. 2013;7(2):187-98.
168. Hammel, I., Lagunoff, D., Galli, S. J. Regulation of secretory granule size by the precise generation and fusion of unit granules. J Cell Mol Med. 2010;14(7):1904-16.

169. Sercu, S., Zhang, M., Oyama, N., Hansen, U., Ghalbzouri, A. E., Jun, G., Geentjens, K., Zhang, L., Merregaert, J. H. Interaction of extracellular matrix protein 1 with extracellular matrix components: ECM1 is a basement membrane protein of the skin. J Invest Dermatol. 2008;128(6):1397-408.
170. Li, Z., Zhang, Y., Liu, Z., Wu, X., Zheng, Y., Tao, Z., Mao, K., Wang, J., Lin, G., Tian, L., Ji, Y., Qin, M., Sun, S., Zhu, X., Sun, B. ECM1 controls T(H)2 cell egress from lymph nodes through re-expression of S1P(1). Nat Immunol. 2011;12(2):178-85.
171. Ly, T., Ahmad, Y., Shlien, A., Soroka, D., Mills, A., Emanuele, M. J., Stratton, M. R., Lamond, A. I. A proteomic chronology of gene expression through the cell cycle in human myeloid leukemia cells. Elife. 2014;3:e01630.
172. Evans, K., Albanetti, T., Venkat, R., Schoner, R., Savery, J., Miro-Quesada, G., Rajan, B., Groves, C. Assurance of monoclonality in one round of cloning through cell sorting for single cell deposition coupled with high resolution cell imaging. Biotechnol Prog. 2015;31(5):1172-8.
173. Khan, G. N., Kim, E. J., Shin, T. S., Lee, S. H. Heterogeneous Cell Types in Single-cell-derived Clones of MCF7 and MDA-MB-231 Cells. Anticancer Res. 2017;37(5):2343-54.
174. Wang, R., Jin, C., Hu, X. Evidence of drug-response heterogeneity rapidly generated from a single cancer cell. Oncotarget. 2017;8(25):41113-24.
175. Li, W., Olivier, M. Current analysis platforms and methods for detecting copy number variation. Physiol Genomics. 2013;45(1):1-16.
176. Eriksson, P., Aine, M., Sjödahl, G., Staaf, J., Lindgren, D., Hoglund, M. Detailed Analysis of Focal Chromosome Arm 1q and 6p Amplifications in Urothelial Carcinoma Reveals Complex Genomic Events on 1q, and SOX4 as a Possible Auxiliary Target on 6p. PLoS One. 2013;8(6):e67222.
177. Ling, X. H., Chen, Z. Y., Luo, H. W., Liu, Z. Z., Liang, Y. K., Chen, G. X., Jiang, F. N., Zhong, W. D. BCL9, a coactivator for Wnt/beta-catenin transcription, is targeted by miR-30c and is associated with prostate cancer progression. Oncol Lett. 2016;11(3):2001-8.
178. Cui, J., Placzek, W. J. Post-Transcriptional Regulation of Anti-Apoptotic BCL2 Family Members. Int J Mol Sci. 2018;19(1).
179. Sherry S T, W. M. H., Kholodov M, Baker J, Phan L, Smigielski E M, Sirotkin K. dbSNP: the NCBI Database of Genetic Variation. Nucleic Acids Res. 2001;29(1):308 - 11.
180. Ahmad, S., Lam, T. B., N'Dow, J. Significance of MUC1 in bladder cancer. BJU Int. 2015;115(1):161-2.

181. Xiong, G. P., Zhang, J. X., Gu, S. P., Wu, Y. B., Liu, J. F. Overexpression of ECM1 contributes to migration and invasion in cholangiocarcinoma cell. Neoplasma. 2012;59(4):409-15.

182. Sjödahl, G., Lovgren, K., Lauss, M., Patschan, O., Gudjonsson, S., Chebil, G., Aine, M., Eriksson, P., Mansson, W., Lindgren, D., Ferno, M., Liedberg, F., Hoglund, M. Toward a molecular pathologic classification of urothelial carcinoma. Am J Pathol. 2013;183(3):681-91.

183. National Center for Biotechnology Information (NCBI). Nucleotide [Internet] Bethesda (MD) National Library of Medicine (US); 1988 [cited 2016]. Available from: https://www.ncbi.nlm.nih.gov/nucleotide/.

184. Enache, M., Simionescu, C. E., Stepan, A. EGFR and Her2/neu immunoexpression in papillary urothelial bladder carcinomas. Rom J Morphol Embryol. 2013;54(1):137-41.

185. Gao, J., Aksoy, B. A., Dogrusoz, U., Dresdner, G., Gross, B., Sumer, S. O., Sun, Y., Jacobsen, A., Sinha, R., Larsson, E., Cerami, E., Sander, C., Schultz, N. Integrative analysis of complex cancer genomics and clinical profiles using the cBioPortal. Sci Signal. 2013;6(269):pl1.

186. Cerami, E., Gao, J., Dogrusoz, U., Gross, B. E., Sumer, S. O., Aksoy, B. A., Jacobsen, A., Byrne, C. J., Heuer, M. L., Larsson, E., Antipin, Y., Reva, B., Goldberg, A. P., Sander, C., Schultz, N. The cBio cancer genomics portal: an open platform for exploring multidimensional cancer genomics data. Cancer Discov. 2012;2(5):401-4.

187. Karantza, V. Keratins in health and cancer: more than mere epithelial cell markers. Oncogene. 2011;30(2):127-38.

188. Knosel, T., Emde, V., Schluns, K., Schlag, P. M., Dietel, M., Petersen, I. Cytokeratin profiles identify diagnostic signatures in colorectal cancer using multiplex analysis of tissue microarrays. Cell Oncol. 2006;28(4):167-75.

189. Ricciardelli, C., Lokman, N. A., Pyragius, C. E., Ween, M. P., Macpherson, A. M., Ruszkiewicz, A., Hoffmann, P., Oehler, M. K. Keratin 5 overexpression is associated with serous ovarian cancer recurrence and chemotherapy resistance. Oncotarget. 2017;8(11):17819-32.

190. Slusser-Nore, A., Garrett, S. H., Zhou, X. D., Sens, D. A., Sens, M. A., Somji, S. The expression of keratin 6 is regulated by the activation of the ERK1/2 pathway in arsenite transformed human urothelial cells. Toxicol Appl Pharmacol. 2017;331:41-53.

191. Kramer, C., Klasmeyer, K., Bojar, H., Schulz, W. A., Ackermann, R., Grimm, M. O. Heparin-binding epidermal growth factor-like growth factor isoforms and

epidermal growth factor receptor/ErbB1 expression in bladder cancer and their relation to clinical outcome. Cancer. 2007;109(10):2016-24.

192. Sato, M., Narita, T., Kawakami-Kimura, N., Higashiyama, S., Taniguchi, N., Akiyama, S., Hashimoto, T., Manabe, T., Kannagi, R. Increased expression of integrins by heparin-binding EGF like growth factor in human esophageal cancer cells. Cancer Lett. 1996;102(1-2):183-91.

193. Ito, Y., Takeda, T., Higashiyama, S., Noguchi, S., Matsuura, N. Expression of heparin-binding epidermal growth factor-like growth factor in breast carcinoma. Breast Cancer Res Treat. 2001;67(1):81-5.

194. Miyamoto, S., Hirata, M., Yamazaki, A., Kageyama, T., Hasuwa, H., Mizushima, H., Tanaka, Y., Yagi, H., Sonoda, K., Kai, M., Kanoh, H., Nakano, H., Mekada, E. Heparin-binding EGF-like growth factor is a promising target for ovarian cancer therapy. Cancer Res. 2004;64(16):5720-7.

195. Ongusaha, P. P., Kwak, J. C., Zwible, A. J., Macip, S., Higashiyama, S., Taniguchi, N., Fang, L., Lee, S. W. HB-EGF is a potent inducer of tumor growth and angiogenesis. Cancer Res. 2004;64(15):5283-90.

196. Adam, R. M., Danciu, T., McLellan, D. L., Borer, J. G., Lin, J., Zurakowski, D., Weinstein, M. H., Rajjayabun, P. H., Mellon, J. K., Freeman, M. R. A nuclear form of the heparin-binding epidermal growth factor-like growth factor precursor is a feature of aggressive transitional cell carcinoma. Cancer Res. 2003;63(2):484-90.

197. Stoll, S. W., Rittie, L., Johnson, J. L., Elder, J. T. Heparin-binding EGF-like growth factor promotes epithelial-mesenchymal transition in human keratinocytes. J Invest Dermatol. 2012;132(9):2148-57.

198. Fife, C. M., McCarroll, J. A., Kavallaris, M. Movers and shakers: cell cytoskeleton in cancer metastasis. Br J Pharmacol. 2014;171(24):5507-23.

199. Witjes, J. A., Comperat, E., Cowan, N. C., De Santis, M., Gakis, G., Lebret, T., Ribal, M. J., Van der Heijden, A. G., Sherif, A., European Association of, U. EAU guidelines on muscle-invasive and metastatic bladder cancer: summary of the 2013 guidelines. Eur Urol. 2014;65(4):778-92.

200. Ohishi, T., Koga, F., Migita, T. Bladder Cancer Stem-Like Cells: Their Origin and Therapeutic Perspectives. Int J Mol Sci. 2015;17(1).

201. Ikushima, H., Todo, T., Ino, Y., Takahashi, M., Saito, N., Miyazawa, K., Miyazono, K. Glioma-initiating cells retain their tumorigenicity through integration of the Sox axis and Oct4 protein. J Biol Chem. 2011;286(48):41434-41.

202. Chan, K. S., Espinosa, I., Chao, M., Wong, D., Ailles, L., Diehn, M., Gill, H., Presti, J., Jr., Chang, H. Y., van de Rijn, M., Shortliffe, L., Weissman, I. L. Identification, molecular characterization, clinical prognosis, and therapeutic

targeting of human bladder tumor-initiating cells. Proc Natl Acad Sci U S A. 2009;106(33):14016-21.

203. Kampf, C., Olsson, I., Ryberg, U., Sjostedt, E., Ponten, F. Production of tissue microarrays, immunohistochemistry staining and digitalization within the human protein atlas. J Vis Exp. 2012(63).

204. Hughes, O. D., Bishop, M. C., Perkins, A. C., Wastie, M. L., Denton, G., Price, M. R., Frier, M., Denley, H., Rutherford, R., Schubiger, P. A. Targeting superficial bladder cancer by the intravesical administration of copper-67-labeled anti-MUC1 mucin monoclonal antibody C595. J Clin Oncol. 2000;18(2):363-70.

205. Stojnev, S., Ristic-Petrovic, A., Velickovic, L. J., Krstic, M., Bogdanovic, D., Khanh do, T., Ristic, A., Conic, I., Stefanovic, V. Prognostic significance of mucin expression in urothelial bladder cancer. Int J Clin Exp Pathol. 2014;7(8):4945-58.

206. Nielsen, T. O., Borre, M., Nexo, E., Sorensen, B. S. Co-expression of HER3 and MUC1 is associated with a favourable prognosis in patients with bladder cancer. BJU Int. 2015;115(1):163-5.

207. O'Keefe, E. P. siRNAs and shRNAs: Tools for Protein Knockdown by Gene Silencing. Labome. 2013;3:197.

208. Stewart, S. A., Dykxhoorn, D. M., Palliser, D., Mizuno, H., Yu, E. Y., An, D. S., Sabatini, D. M., Chen, I. S., Hahn, W. C., Sharp, P. A., Weinberg, R. A., Novina, C. D. Lentivirus-delivered stable gene silencing by RNAi in primary cells. RNA. 2003;9(4):493-501.

209. Climente-Gonzalez, H., Porta-Pardo, E., Godzik, A., Eyras, E. The Functional Impact of Alternative Splicing in Cancer. Cell Rep. 2017;20(9):2215-26.

210. Ye, H., Yu, X., Xia, J., Tang, X., Tang, L., Chen, F. MiR-486-3p targeting ECM1 represses cell proliferation and metastasis in cervical cancer. Biomed Pharmacother. 2016;80:109-14.

211. Hulkower, K. I., Herber, R. L. Cell migration and invasion assays as tools for drug discovery. Pharmaceutics. 2011;3(1):107-24.

212. Zhao, L. Bench Tips: Measuring Cell Migration: Biocompare; 2014 [29th August 2018]. Available from: https://www.biocompare.com/Bench-Tips/170254-Measuring-Cell-Migration/.

213. Menyhart, O., Harami-Papp, H., Sukumar, S., Schafer, R., Magnani, L., de Barrios, O., Gyorffy, B. Guidelines for the selection of functional assays to evaluate the hallmarks of cancer. Biochim Biophys Acta. 2016;1866(2):300-19.

214. Hemaprabha, E. Chemical Crosslinking of Proteins: A Review. Journal of Pharmaceutical and Scientific Innovation. 2012;1(1):5.

215. Mooso, B. A., Vinall, R. L., Mudryj, M., Yap, S. A., deVere White, R. W., Ghosh, P. M. The role of EGFR family inhibitors in muscle invasive bladder cancer: a review of clinical data and molecular evidence. J Urol. 2015;193(1):19-29.
216. Philips, G. K., Halabi, S., Sanford, B. L., Bajorin, D., Small, E. J., Cancer, Leukemia Group, B. A phase II trial of cisplatin (C), gemcitabine (G) and gefitinib for advanced urothelial tract carcinoma: results of Cancer and Leukemia Group B (CALGB) 90102. Ann Oncol. 2009;20(6):1074-9.
217. Petrylak, D. P., Tangen, C. M., Van Veldhuizen, P. J., Jr., Goodwin, J. W., Twardowski, P. W., Atkins, J. N., Kakhil, S. R., Lange, M. K., Mansukhani, M., Crawford, E. D. Results of the Southwest Oncology Group phase II evaluation (study S0031) of ZD1839 for advanced transitional cell carcinoma of the urothelium. BJU Int. 2010;105(3):317-21.
218. Hardy, S. A., Mabotuwana, N. S., Murtha, L. A., Coulter, B., Sanchez-Bezanilla, S., Al-Omary, M. S., Senanayake, T., Loering, S., Starkey, M., Lee, R. J., Rainer, P. P., Hansbro, P. M., Boyle, A. J. Novel role of extracellular matrix protein 1 (ECM1) in cardiac aging and myocardial infarction. PLoS One. 2019;14(2):e0212230.
219. Kohno, M., Pouyssegur, J. Targeting the ERK signaling pathway in cancer therapy. Ann Med. 2006;38(3):200-11.
220. Yang, W. L., Wang, J., Chan, C. H., Lee, S. W., Campos, A. D., Lamothe, B., Hur, L., Grabiner, B. C., Lin, X., Darnay, B. G., Lin, H. K. The E3 ligase TRAF6 regulates Akt ubiquitination and activation. Science. 2009;325(5944):1134-8.
221. Fan, C. D., Lum, M. A., Xu, C., Black, J. D., Wang, X. Ubiquitin-dependent regulation of phospho-AKT dynamics by the ubiquitin E3 ligase, NEDD4-1, in the insulin-like growth factor-1 response. J Biol Chem. 2013;288(3):1674-84.
222. Wang, G., Long, J., Gao, Y., Zhang, W., Han, F., Xu, C., Sun, L., Yang, S. C., Lan, J., Hou, Z., Cai, Z., Jin, G., Hsu, C. C., Wang, Y. H., Hu, J., Chen, T. Y., Li, H., Lee, M. G., Lin, H. K. SETDB1-mediated methylation of Akt promotes its K63-linked ubiquitination and activation leading to tumorigenesis. Nat Cell Biol. 2019;21(2):214-25.
223. Zhao, X., Qu, J., Hui, Y., Zhang, H., Sun, Y., Liu, X., Zhao, X., Zhao, Z., Yang, Q., Wang, F., Zhang, S. Clinicopathological and prognostic significance of c-Met overexpression in breast cancer. Oncotarget. 2017;8(34):56758-67.
224. Awad, M. M., Oxnard, G. R., Jackman, D. M., Savukoski, D. O., Hall, D., Shivdasani, P., Heng, J. C., Dahlberg, S. E., Janne, P. A., Verma, S., Christensen, J., Hammerman, P. S., Sholl, L. M. MET Exon 14 Mutations in Non-Small-Cell Lung

Cancer Are Associated With Advanced Age and Stage-Dependent MET Genomic Amplification and c-Met Overexpression. J Clin Oncol. 2016;34(7):721-30.
225. Chu, J. S., Ge, F. J., Zhang, B., Wang, Y., Silvestris, N., Liu, L. J., Zhao, C. H., Lin, L., Brunetti, A. E., Fu, Y. L., Wang, J., Paradiso, A., Xu, J. M. Expression and prognostic value of VEGFR-2, PDGFR-beta, and c-Met in advanced hepatocellular carcinoma. J Exp Clin Cancer Res. 2013;32:16.
226. Shintani, T., Kusuhara, Y., Daizumoto, K., Dondoo, T. O., Yamamoto, H., Mori, H., Fukawa, T., Nakatsuji, H., Fukumori, T., Takahashi, M., Kanayama, H. The Involvement of Hepatocyte Growth Factor-MET-Matrix Metalloproteinase 1 Signaling in Bladder Cancer Invasiveness and Proliferation. Effect of the MET Inhibitor, Cabozantinib (XL184), on Bladder Cancer Cells. Urology. 2017;101:169 e7- e13.
227. Weller, M. G. Quality Issues of Research Antibodies. Anal Chem Insights. 2016;11:21-7.
228. Liu, Z. Q., Mahmood, T., Yang, P. C. Western blot: technique, theory and trouble shooting. N Am J Med Sci. 2014;6(3):160.
229. Mahmood, T., Yang, P. C. Western blot: technique, theory, and trouble shooting. N Am J Med Sci. 2012;4(9):429-34.
230. Gassmann, M., Grenacher, B., Rohde, B., Vogel, J. Quantifying Western blots: pitfalls of densitometry. Electrophoresis. 2009;30(11):1845-55.
231. Janes, K. A. An analysis of critical factors for quantitative immunoblotting. Sci Signal. 2015;8(371):rs2.
232. Neuzillet, Y., Chapeaublanc, E., Krucker, C., De Koning, L., Lebret, T., Radvanyi, F., Bernard-Pierrot, I. IGF1R activation and the in vitro antiproliferative efficacy of IGF1R inhibitor are inversely correlated with IGFBP5 expression in bladder cancer. BMC Cancer. 2017;17(1):636.
233. Sun, H. Z., Wu, S. F., Tu, Z. H. Blockage of IGF-1R signaling sensitizes urinary bladder cancer cells to mitomycin-mediated cytotoxicity. Cell Res. 2001;11(2):107-15.
234. Vigneri, R., Goldfine, I. D., Frittitta, L. Insulin, insulin receptors, and cancer. J Endocrinol Invest. 2016;39(12):1365-76.
235. Parks, M. M., Kurylo, C. M., Dass, R. A., Bojmar, L., Lyden, D., Vincent, C. T., Blanchard, S. C. Variant ribosomal RNA alleles are conserved and exhibit tissue-specific expression. Sci Adv. 2018;4(2):eaao0665.
236. Gibbons, J. G., Branco, A. T., Godinho, S. A., Yu, S., Lemos, B. Concerted copy number variation balances ribosomal DNA dosage in human and mouse genomes. Proc Natl Acad Sci U S A. 2015;112(8):2485-90.

237. Wang, M., Lemos, B. Ribosomal DNA copy number amplification and loss in human cancers is linked to tumor genetic context, nucleolus activity, and proliferation. PLoS Genet. 2017;13(9):e1006994.
238. Valvezan, A. J., Turner, M., Belaid, A., Lam, H. C., Miller, S. K., McNamara, M. C., Baglini, C., Housden, B. E., Perrimon, N., Kwiatkowski, D. J., Asara, J. M., Henske, E. P., Manning, B. D. mTORC1 Couples Nucleotide Synthesis to Nucleotide Demand Resulting in a Targetable Metabolic Vulnerability. Cancer Cell. 2017;32(5):624-38 e5.
239. Wu, B., Cao, X., Liang, X., Zhang, X., Zhang, W., Sun, G., Wang, D. Epigenetic regulation of Elf5 is associated with epithelial-mesenchymal transition in urothelial cancer. PLoS One. 2015;10(1):e0117510.
240. Luk, I. Y., Reehorst, C. M., Mariadason, J. M. ELF3, ELF5, EHF and SPDEF Transcription Factors in Tissue Homeostasis and Cancer. Molecules. 2018;23(9).
241. Tummala, R., Sinha, S. Differentiation-specific transcriptional regulation of the ESE-2 gene by a novel keratinocyte-restricted factor. J Cell Biochem. 2006;97(4):766-81.
242. Kalyuga, M., Gallego-Ortega, D., Lee, H. J., Roden, D. L., Cowley, M. J., Caldon, C. E., Stone, A., Allerdice, S. L., Valdes-Mora, F., Launchbury, R., Statham, A. L., Armstrong, N., Alles, M. C., Young, A., Egger, A., Au, W., Piggin, C. L., Evans, C. J., Ledger, A., Brummer, T., Oakes, S. R., Kaplan, W., Gee, J. M., Nicholson, R. I., Sutherland, R. L., Swarbrick, A., Naylor, M. J., Clark, S. J., Carroll, J. S., Ormandy, C. J. ELF5 suppresses estrogen sensitivity and underpins the acquisition of antiestrogen resistance in luminal breast cancer. PLoS Biol. 2012;10(12):e1001461.
243. Wee, P., Wang, Z. Epidermal Growth Factor Receptor Cell Proliferation Signaling Pathways. Cancers (Basel). 2017;9(5).
244. Singh, B., Carpenter, G., Coffey, R. J. EGF receptor ligands: recent advances. F1000Res. 2016;5.
245. Berasain, C., Avila, M. A. Amphiregulin. Semin Cell Dev Biol. 2014;28:31-41.
246. Roepstorff, K., Grandal, M. V., Henriksen, L., Knudsen, S. L., Lerdrup, M., Grovdal, L., Willumsen, B. M., van Deurs, B. Differential effects of EGFR ligands on endocytic sorting of the receptor. Traffic. 2009;10(8):1115-27.
247. Stern, K. A., Place, T. L., Lill, N. L. EGF and amphiregulin differentially regulate Cbl recruitment to endosomes and EGF receptor fate. Biochem J. 2008;410(3):585-94.

248. Baldys, A., Gooz, M., Morinelli, T. A., Lee, M. H., Raymond, J. R., Jr., Luttrell, L. M., Raymond, J. R., Sr. Essential role of c-Cbl in amphiregulin-induced recycling and signaling of the endogenous epidermal growth factor receptor. Biochemistry. 2009;48(7):1462-73.
249. Shin, H. S., Lee, H. J., Nishida, M., Lee, M. S., Tamura, R., Yamashita, S., Matsuzawa, Y., Lee, I. K., Koh, G. Y. Betacellulin and amphiregulin induce upregulation of cyclin D1 and DNA synthesis activity through differential signaling pathways in vascular smooth muscle cells. Circ Res. 2003;93(4):302-10.
250. van Helden, E. J., Menke-van der Houven van Oordt, C. W., Heymans, M. W., Ket, J. C. F., van den Oord, R., Verheul, H. M. W. Optimal use of anti-EGFR monoclonal antibodies for patients with advanced colorectal cancer: a meta-analysis. Cancer Metastasis Rev. 2017;36(2):395-406.
251. Blaszczak, W., Barczak, W., Wegner, A., Golusinski, W., Suchorska, W. M. Clinical value of monoclonal antibodies and tyrosine kinase inhibitors in the treatment of head and neck squamous cell carcinoma. Med Oncol. 2017;34(4):60.
252. Uitdehaag, J. C. M., Verkaar, F., Alwan, H., de Man, J., Buijsman, R. C., Zaman, G. J. R. A guide to picking the most selective kinase inhibitor tool compounds for pharmacological validation of drug targets. Brit J Pharmacol. 2012;166(3):858-76.
253. Yewale, C., Baradia, D., Vhora, I., Patil, S., Misra, A. Epidermal growth factor receptor targeting in cancer: a review of trends and strategies. Biomaterials. 2013;34(34):8690-707.
254. Jiang, J., Greulich, H., Janne, P. A., Sellers, W. R., Meyerson, M., Griffin, J. D. Epidermal growth factor-independent transformation of Ba/F3 cells with cancer-derived epidermal growth factor receptor mutants induces gefitinib-sensitive cell cycle progression. Cancer Res. 2005;65(19):8968-74.
255. Pruthi, R. S., Nielsen, M., Heathcote, S., Wallen, E. M., Rathmell, W. K., Godley, P., Whang, Y., Fielding, J., Schultz, H., Grigson, G., Smith, A., Kim, W. A phase II trial of neoadjuvant erlotinib in patients with muscle-invasive bladder cancer undergoing radical cystectomy: clinical and pathological results. BJU Int. 2010;106(3):349-54.
256. Ikeda, R., Vermeulen, L. C., Lau, E., Jiang, Z., Kavanaugh, S. M., Yamada, K., Kolesar, J. M. Isolation and characterization of erlotinib-resistant human non-small cell lung cancer A549 cells. Oncol Lett. 2011;2(1):91-4.
257. Mo, H. N., Liu, P. Targeting MET in cancer therapy. Chronic Dis Transl Med. 2017;3(3):148-53.

258. Munshi, N., Jeay, S., Li, Y., Chen, C. R., France, D. S., Ashwell, M. A., Hill, J., Moussa, M. M., Leggett, D. S., Li, C. J. ARQ 197, a novel and selective inhibitor of the human c-Met receptor tyrosine kinase with antitumor activity. Mol Cancer Ther. 2010;9(6):1544-53.

259. Yap, T. A., Olmos, D., Brunetto, A. T., Tunariu, N., Barriuso, J., Riisnaes, R., Pope, L., Clark, J., Futreal, A., Germuska, M., Collins, D., deSouza, N. M., Leach, M. O., Savage, R. E., Waghorne, C., Chai, F., Garmey, E., Schwartz, B., Kaye, S. B., de Bono, J. S. Phase I trial of a selective c-MET inhibitor ARQ 197 incorporating proof of mechanism pharmacodynamic studies. J Clin Oncol. 2011;29(10):1271-9.

260. Zaman, S., Shentu, S., Yang, J., He, J., Orlowski, R. Z., Stellrecht, C. M., Gandhi, V. Targeting the pro-survival protein MET with tivantinib (ARQ 197) inhibits growth of multiple myeloma cells. Neoplasia. 2015;17(3):289-300.

261. Basilico, C., Pennacchietti, S., Vigna, E., Chiriaco, C., Arena, S., Bardelli, A., Valdembri, D., Serini, G., Michieli, P. Tivantinib (ARQ197) displays cytotoxic activity that is independent of its ability to bind MET. Clin Cancer Res. 2013;19(9):2381-92.

262. Aoyama, A., Katayama, R., Oh-Hara, T., Sato, S., Okuno, Y., Fujita, N. Tivantinib (ARQ 197) exhibits antitumor activity by directly interacting with tubulin and overcomes ABC transporter-mediated drug resistance. Mol Cancer Ther. 2014;13(12):2978-90.

263. Engelman, J. A., Zejnullahu, K., Mitsudomi, T., Song, Y., Hyland, C., Park, J. O., Lindeman, N., Gale, C. M., Zhao, X., Christensen, J., Kosaka, T., Holmes, A. J., Rogers, A. M., Cappuzzo, F., Mok, T., Lee, C., Johnson, B. E., Cantley, L. C., Janne, P. A. MET amplification leads to gefitinib resistance in lung cancer by activating ERBB3 signaling. Science. 2007;316(5827):1039-43.

264. Qi, J., McTigue, M. A., Rogers, A., Lifshits, E., Christensen, J. G., Janne, P. A., Engelman, J. A. Multiple mutations and bypass mechanisms can contribute to development of acquired resistance to MET inhibitors. Cancer Res. 2011;71(3):1081-91.

265. Bachleitner-Hofmann, T., Sun, M., Chen, C., Tang, L., Song, L., Zeng, Z., Shah, M., Christensen, J., Rosen, N., Solit D., Weiser, M. Stimulation of epidermal growth factor (EGFR) or HER-3 mediates resistance to MET tyrosine kinase inhibition in MET-amplified gastric cancer cells. Cancer Resarch. 2008;68(9).

266. Rajagopal, C., Harikumar, K. B. The Origin and Functions of Exosomes in Cancer. Front Oncol. 2018;8:66.

267. Liu, Y. R., Ortiz-Bonilla, C. J., Lee, Y. F. Extracellular Vesicles in Bladder Cancer: Biomarkers and Beyond. Int J Mol Sci. 2018;19(9).

268. Fontana, S., Saieva, L., Taverna, S., Alessandro, R. Contribution of proteomics to understanding the role of tumor-derived exosomes in cancer progression: state of the art and new perspectives. Proteomics. 2013;13(10-11):1581-94.
269. Zhang, J. M., Wu, X. H., Zhang, Y., Xia, Y. G., Luo, C. L. [Exosomes derived form bladder transitional cell carcinoma cells induce CTL cytotoxicity in vitro]. Zhonghua Zhong Liu Za Zhi. 2009;31(10):738-41.
270. Perl, A., Hanczko, R., Telarico, T., Oaks, Z., Landas, S. Oxidative stress, inflammation and carcinogenesis are controlled through the pentose phosphate pathway by transaldolase. Trends Mol Med. 2011;17(7):395-403.
271. Andreu, Z., Otta Oshiro, R., Redruello, A., Lopez-Martin, S., Gutierrez-Vazquez, C., Morato, E., Marina, A. I., Olivier Gomez, C., Yanez-Mo, M. Extracellular vesicles as a source for non-invasive biomarkers in bladder cancer progression. Eur J Pharm Sci. 2017;98:70-9.
272. Lee, J., McKinney, K. Q., Pavlopoulos, A. J., Niu, M., Kang, J. W., Oh, J. W., Kim, K. P., Hwang, S. Altered Proteome of Extracellular Vesicles Derived from Bladder Cancer Patients Urine. Mol Cells. 2018;41(3):179-87.
273. Welton, J. L., Khanna, S., Giles, P. J., Brennan, P., Brewis, I. A., Staffurth, J., Mason, M. D., Clayton, A. Proteomics analysis of bladder cancer exosomes. Mol Cell Proteomics. 2010;9(6):1324-38.
274. Kang, H., Kim, W., Yun, S. The role of the tumor microenvironment in bladder cancer development and progression. Translational Cancer research 2017;6(4).
275. Lorusso, G., Ruegg, C. The tumor microenvironment and its contribution to tumor evolution toward metastasis. Histochem Cell Biol. 2008;130(6):1091-103.
276. Koontongkaew, S. The tumor microenvironment contribution to development, growth, invasion and metastasis of head and neck squamous cell carcinomas. J Cancer. 2013;4(1):66-83.
277. Weber, C. E., Kuo, P. C. The tumor microenvironment. Surg Oncol. 2012;21(3):172-7.
278. Kufe, D. W. Mucins in cancer: function, prognosis and therapy. Nat Rev Cancer. 2009;9(12):874-85.
279. Gendler, S. J. MUC1, the renaissance molecule. J Mammary Gland Biol Neoplasia. 2001;6(3):339-53.
280. Kumar, P., Lindberg, L., Thirkill, T., Ji, J., Martsching, L., Douglas G., . The MUC1 Extracellular Domain Subunit Is Found in Nuclear Speckles and Associates with Spliceosomes. PLOS ONE. 2012;7(10).

281. Oppizzi, M. L., Akhavan, A., Singh, M., Fata, J. E., Muschler, J. L. Nuclear translocation of beta-dystroglycan reveals a distinctive trafficking pattern of autoproteolyzed mucins. Traffic. 2008;9(12):2063-72.
282. Sterlacci, W., Fiegl, M., Veits, L., Tzankov, A. Diagnostic and prognostic impact of mucin 1-6 expression in non-small cell lung cancer. Indian J Pathol Microbiol. 2018;61(2):187-91.
283. Bitler, B. G., Goverdhan, A., Schroeder, J. A. MUC1 regulates nuclear localization and function of the epidermal growth factor receptor. J Cell Sci. 2010;123(Pt 10):1716-23.
284. Sahraei, M., Roy, L. D., Curry, J. M., Teresa, T. L., Nath, S., Besmer, D., Kidiyoor, A., Dalia, R., Gendler, S. J., Mukherjee, P. MUC1 regulates PDGFA expression during pancreatic cancer progression. Oncogene. 2012;31(47):4935-45.
285. Ellisen, L. A wound-healing program is hijacked to promote cancer metastasis. Journal of Experimental Medicine. 2017;214(10):2813.
286. Oliveira-Ferrer, L., Legler, K., Milde-Langosch, K. Role of protein glycosylation in cancer metastasis. Semin Cancer Biol. 2017;44:141-52.
287. Pastar, I., Stojadinovic, O., Yin, N. C., Ramirez, H., Nusbaum, A. G., Sawaya, A., Patel, S. B., Khalid, L., Isseroff, R. R., Tomic-Canic, M. Epithelialization in Wound Healing: A Comprehensive Review. Adv Wound Care (New Rochelle). 2014;3(7):445-64.
288. Armstrong, D. G., Jude, E. B. The role of matrix metalloproteinases in wound healing. J Am Podiatr Med Assoc. 2002;92(1):12-8.
289. Stefanini, A. C., da Cunha, B. R., Henrique, T., Tajara, E. H. Involvement of Kallikrein-Related Peptidases in Normal and Pathologic Processes. Dis Markers. 2015;2015:946572.
290. Blum, W., Pecze, L., Felley-Bosco, E., Schwaller, B. Overexpression or absence of calretinin in mouse primary mesothelial cells inversely affects proliferation and cell migration. Respir Res. 2015;16:153.
291. Bindels, E. M., van der Kwast, T. H., Izadifar, V., Chopin, D. K., de Boer, W. I. Functions of epidermal growth factor-like growth factors during human urothelial reepithelialization in vitro and the role of erbB2. Urol Res. 2002;30(4):240-7.
292. Carpenter, G., Cohen, S. Epidermal growth factor. J Biol Chem. 1990;265(14):7709-12.
293. Liu, F., Yang, X., Geng, M., Huang, M. Targeting ERK, an Achilles' Heel of the MAPK pathway, in cancer therapy. Acta Pharm Sin B. 2018;8(4):552-62.
294. Samatar, A. A., Poulikakos, P. I. Targeting RAS-ERK signalling in cancer: promises and challenges. Nat Rev Drug Discov. 2014;13(12):928-42.

295. Zhang, X., Ma, L., Qi, J., Shan, H., Yu, W., Gu, Y. MAPK/ERK signaling pathway-induced hyper-O-GlcNAcylation enhances cancer malignancy. Mol Cell Biochem. 2015;410(1-2):101-10.

296. Germann, U. A., Furey, B. F., Markland, W., Hoover, R. R., Aronov, A. M., Roix, J. J., Hale, M., Boucher, D. M., Sorrell, D. A., Martinez-Botella, G., Fitzgibbon, M., Shapiro, P., Wick, M. J., Samadani, R., Meshaw, K., Groover, A., DeCrescenzo, G., Namchuk, M., Emery, C. M., Saha, S., Welsch, D. J. Targeting the MAPK Signaling Pathway in Cancer: Promising Preclinical Activity with the Novel Selective ERK1/2 Inhibitor BVD-523 (Ulixertinib). Mol Cancer Ther. 2017;16(11):2351-63.

297. Blake, J. F., Burkard, M., Chan, J., Chen, H., Chou, K. J., Diaz, D., Dudley, D. A., Gaudino, J. J., Gould, S. E., Grina, J., Hunsaker, T., Liu, L., Martinson, M., Moreno, D., Mueller, L., Orr, C., Pacheco, P., Qin, A., Rasor, K., Ren, L., Robarge, K., Shahidi-Latham, S., Stults, J., Sullivan, F., Wang, W., Yin, J., Zhou, A., Belvin, M., Merchant, M., Moffat, J., Schwarz, J. B. Discovery of (S)-1-(1-(4-Chloro-3-fluorophenyl)-2-hydroxyethyl)-4-(2-((1-methyl-1H-pyrazol-5-y l)amino)pyrimidin-4-yl)pyridin-2(1H)-one (GDC-0994), an Extracellular Signal-Regulated Kinase 1/2 (ERK1/2) Inhibitor in Early Clinical Development. J Med Chem. 2016;59(12):5650-60.

298. Mattmann, M. E., Stoops, S. L., Lindsley, C. W. Inhibition of Akt with small molecules and biologics: historical perspective and current status of the patent landscape. Expert Opin Ther Pat. 2011;21(9):1309-38.

299. Nitulescu, G. M., Margina, D., Juzenas, P., Peng, Q., Olaru, O. T., Saloustros, E., Fenga, C., Spandidos, D., Libra, M., Tsatsakis, A. M. Akt inhibitors in cancer treatment: The long journey from drug discovery to clinical use (Review). Int J Oncol. 2016;48(3):869-85.

300. Elliott, A. Y., Bronson, D. L., Cervenka, J., Stein, N., Fraley, E. E. Properties of cell lines established from transitional cell cancers of the human urinary tract. Cancer Res. 1977;37(5):1279-89.

301. Elliott, A. Y., Cleveland, P., Cervenka, J., Castro, A. E., Stein, N., Hakala, T. R., Fraley, E. E. Characterization of a cell line from human transitional cell cancer of the urinary tract. J Natl Cancer Inst. 1974;53(5):1341-9.

302. Fogh, J. Cultivation, characterization, and identification of human tumor cells with emphasis on kidney, testis, and bladder tumors. Natl Cancer Inst Monogr. 1978(49):5-9.

303. Elliott, A. Y., Bronson, D. L., Stein, N., Fraley, E. E. In vitro cultivation of epithelial cells derived from tumors of the human urinary tract. Cancer Res. 1976;36(2 Pt 1):365-9.

304. Yeager, T. R., DeVries, S., Jarrard, D. F., Kao, C., Nakada, S. Y., Moon, T. D., Bruskewitz, R., Stadler, W. M., Meisner, L. F., Gilchrist, K. W., Newton, M. A., Waldman, F. M., Reznikoff, C. A. Overcoming cellular senescence in human cancer pathogenesis. Genes Dev. 1998;12(2):163-74.

305. Sarkar, S., Julicher, K. P., Burger, M. S., Della Valle, V., Larsen, C. J., Yeager, T. R., Grossman, T. B., Nickells, R. W., Protzel, C., Jarrard, D. F., Reznikoff, C. A. Different combinations of genetic/epigenetic alterations inactivate the p53 and pRb pathways in invasive human bladder cancers. Cancer Res. 2000;60(14):3862-71.

306. Pratsinis, H., Saetta, A., Gagos, S., Davaris, P. Isolation and characterization of a novel bladder cancer cell line: inhibition by epidermal growth factor. In Vitro Cell Dev Biol Anim. 1998;34(9):722-8.

307. Tzeng, C. C., Liu, H. S., Li, C., Jin, Y. T., Chen, R. M., Yang, W. H., Lin, J. S. Characterization of two urothelium cancer cell lines derived from a blackfoot disease endemic area in Taiwan. Anticancer Res. 1996;16(4A):1797-804.

308. Cattan, N., Rochet, N., Mazeau, C., Zanghellini, E., Mari, B., Chauzy, C., Stora de Novion, H., Amiel, J., Lagrange, J. L., Rossi, B., Gioanni, J. Establishment of two new human bladder carcinoma cell lines, CAL 29 and CAL 185. Comparative study of cell scattering and epithelial to mesenchyme transition induced by growth factors. Br J Cancer. 2001;85(9):1412-7.

309. Williams, S. V., Sibley, K. D., Davies, A. M., Nishiyama, H., Hornigold, N., Coulter, J., Kennedy, W. J., Skilleter, A., Habuchi, T., Knowles, M. A. Molecular genetic analysis of chromosome 9 candidate tumor-suppressor loci in bladder cancer cell lines. Genes Chromosomes Cancer. 2002;34(1):86-96.

310. Rasheed, S., Gardner, M. B., Rongey, R. W., Nelson-Rees, W. A., Arnstein, P. Human bladder carcinoma: characterization of two new tumor cell lines and search for tumor viruses. J Natl Cancer Inst. 1977;58(4):881-90.

311. O'Toole, C., Price, Z. H., Ohnuki, Y., Unsgaard, B. Ultrastructure, karyology and immunology of a cell line originated from a human transitional-cell carcinoma. Br J Cancer. 1978;38(1):64-76.

312. Morita, T., Shinohara, N., Honma, M., Tokue, A. Establishment and characterization of a new cell line from human bladder cancer (JMSU1). Urol Res. 1995;23(3):143-9.

313. Tachibana, M., Miyakawa, A., Tazaki, H., Nakamura, K., Kubo, A., Hata, J., Nishi, T., Amano, Y. Autocrine growth of transitional cell carcinoma of the bladder induced by granulocyte-colony stimulating factor. Cancer Res. 1995;55(15):3438-43.

314. Lin, C. W., Lin, J. C., Prout, G. R., Jr. Establishment and characterization of four human bladder tumor cell lines and sublines with different degrees of malignancy. Cancer Res. 1985;45(10):5070-9.
315. Marshall, C. J., Franks, L. M., Carbonell, A. W. Markers of neoplastic transformation in epithelial cell lines derived from human carcinomas. J Natl Cancer Inst. 1977;58(6):1743-51.
316. Rigby, C. C., Franks, L. M. A human tissue culture cell line from a transitional cell tumour of the urinary bladder: growth, chromosone pattern and ultrastructure. Br J Cancer. 1970;24(4):746-54.
317. O'Toole, C., Nayak, S., Price, Z., Gilbert, W. H., Waisman, J. A cell line (SCABER) derived from squamous cell carcinoma of the human urinary bladder. Int J Cancer. 1976;17(6):707-14.
318. Paulie, S., Hansson, Y., Lundblad, M. L., Perlmann, P. Lectins as probes for identification of tumor-associated antigens on urothelial and colonic carcinoma cell lines. Int J Cancer. 1983;31(3):297-303.
319. Kyriazis, A. A., Kyriazis, A. P., McCombs, W. B., 3rd, Peterson, W. D., Jr. Morphological, biological, and biochemical characteristics of human bladder transitional cell carcinomas grown in tissue culture and in nude mice. Cancer Res. 1984;44(9):3997-4005.
320. Bubenik, J., Baresova, M., Viklicky, V., Jakoubkova, J., Sainerova, H., Donner, J. Established cell line of urinary bladder carcinoma (T24) containing tumour-specific antigen. Int J Cancer. 1973;11(3):765-73.
321. Nayak, S. K., O'Toole, C., Price, Z. H. A cell line from an anaplastic transitional cell carcinoma of human urinary bladder. Br J Cancer. 1977;35(2):142-51.
322. Bruch, J., Wohr, G., Bruderlein, S., Barbi, G., Wolter, H., Dixkens, C., Mattfeldt, T., Moller, P., Paiss, T., Hautmann, R., Vogel, W., Hameister, H. Detailed marker chromosome analysis in cell line U-BLC1, established from transitional-cell carcinoma of the bladder. Int J Cancer. 1999;80(6):903-10.
323. Grossman, H. B., Wedemeyer, G., Ren, L., Wilson, G. N., Cox, B. Improved growth of human urothelial carcinoma cell cultures. J Urol. 1986;136(4):953-9.
324. Williams, R. D. Human urologic cancer cell lines. Invest Urol. 1980;17(5):359-63.
325. National Center for Biotechnology Information (NCBI). Protein [Internet] Bethesda (MD) National Library of Medicine (US); 1988 [cited 2016]. Available from: https://www.ncbi.nlm.nih.gov/nucleotide/.

326. Irizarry, R. A., Hobbs, B., Collin, F., Beazer-Barclay, Y. D., Antonellis, K. J., Scherf, U., Speed, T. P. Exploration, normalization, and summaries of high density oligonucleotide array probe level data. Biostatistics. 2003;4(2):249-64.